

Characterization of Oil and Gas Reservoir Heterogeneity

Final Report

By

N. Tyler, M. D. Barton, D. G. Bebout,  
R. S. Fisher, J. D. Grigsby, E. Guevara, M. Holtz,  
C. Kerans, H. S. Nance, and R. A. Levey

October 1992

Work Performed Under Contract No. DE-FG22-89BC14403

Prepared for  
U.S. Department of Energy  
Assistant Secretary for Fossil Energy

Chandra Nautiyal, Project Manager  
Bartlesville Project Office  
P. O. Box 1398  
Bartlesville, OK 74005

Prepared by  
Bureau of Economic Geology  
The University of Texas at Austin  
Austin, TX 78713-7508

## CONTENTS

ABSTRACT .....	1
<b>CHAPTER I: INTRODUCTION</b>	
Noel Tyler .....	2
OBJECTIVES.....	4
APPLICABILITY OF OUTCROP STUDIES TO THE SUBSURFACE: DATA PORTABILITY .....	5
<b>CHAPTER II: OUTCROP DELINEATION OF CARBONATE SAND BODY DISTRIBUTION IN A SEQUENCE-STRATIGRAPHIC FRAMEWORK</b>	
Charles Kerans .....	7
INTRODUCTION.....	7
Sequence Stratigraphy in Reservoir Studies .....	8
<b>OUTCROP SEQUENCE-STRATIGRAPHIC FRAMEWORK OF THE GRAYBURG FORMATION— IMPLICATIONS FOR SUBSURFACE RESERVOIR CHARACTERIZATION.....</b>	<b>9</b>
Regional Framework of the Grayburg Outcrop in the Guadalupe Mountains.....	18
Development of a Sequence-Stratigraphic Framework.....	18
<i>San Andres/Grayburg Sequence Boundary</i> .....	20
<i>Lowstand/Transgressive Systems Tract (LTST)</i> .....	23
<i>Maximum Flooding Surface</i> .....	23
<i>Highstand Systems Tract</i> .....	24
<i>Grayburg/Queen Sequence Boundary</i> .....	30
REGIONAL RESERVOIR ARCHITECTURE WITHIN A SEQUENCE FRAMEWORK.....	30
Reservoir-Scale Parasequence Framework .....	32
<b>CHAPTER III: FACIES ARCHITECTURE AND INTERNAL GEOMETRY OF A MIXED SILICICLASTIC-CARBONATE DEPOSITIONAL SEQUENCE: GRAYBURG FORMATION, STONE CANYON, NEW MEXICO</b>	
H. S. Nance.....	40
INTRODUCTION.....	40
Geologic Setting and Sequence Stratigraphy of the Grayburg in Stone Canyon.....	43
Methods .....	48

RESULTS .....	49
SPATIAL DISTRIBUTION OF DEPOSITIONAL AND DIAGENETIC FACIES IN PARASEQUENCE SC23 .....	61
PARASEQUENCE-SCALE VARIATION IN POROSITY AND PERMEABILITY STRUCTURE.....	71
CONCLUSIONS .....	87
<b>CHAPTER IV: APPLICATION OF THE OUTCROP MODEL TO THE NORTH FOSTER GRAYBURG UNIT</b>	
Don G. Bebout .....	89
INTRODUCTION.....	89
Geological Setting.....	92
Grayburg Sequence Stratigraphy at North Foster.....	95
San Andres/Grayburg Sequence Boundary .....	95
Lowstand/Transgressive Systems Tract (LTST).....	102
Maximum Flooding Surface.....	103
Highstand Systems Tract.....	103
Diagenesis.....	109
Porosity and Permeability Distribution.....	110
RESERVOIR EXPLOITATION APPROACHES .....	111
IMPLICATIONS OF OUTCROP ANALOG METHODOLOGY FOR IMPROVED RESERVOIR DESCRIPTION AT NORTH FOSTER GRAYBURG UNIT.....	114
<b>CHAPTER V: RESOURCE ASSESSMENT OF NONASSOCIATED GAS PRODUCTION IN FLUVIAL-DOMINATED DELTAIC RESERVOIRS, TEXAS</b>	
Mark Holtz.....	117
INTRODUCTION.....	117
DISTRIBUTION OF TEXAS GAS PRODUCTION BY GEOLOGIC DEPOSITIONAL SYSTEM.....	117
Classification of Depositional Systems.....	117
Clastic Depositional Systems.....	117
Carbonate Depositional Systems.....	118
Distribution of Cumulative Production Sorted by Depositional System.....	118

PRODUCTION, DISCOVERY, DEPTH, AND TRAP CHARACTERISTICS OF FLUVIAL-DELTAIC RESERVOIRS.....	118
Tertiary Texas Gulf Coast .....	120
Wilcox Fluvial-Deltaic Gas Reservoirs .....	120
Frio Fluvial-Deltaic Gas Reservoirs.....	124
Yegua Fluvial-Deltaic Gas Reservoirs.....	124
Vicksburg Fluvial-Deltaic Gas Reservoirs.....	125
Miocene Fluvial-Deltaic Gas Reservoirs.....	126
Cretaceous East Texas Basin.....	126
Travis Peak Fluvial-Deltaic Gas Reservoirs .....	126
Upper Cretaceous Group Fluvial-Deltaic Gas Reservoirs.....	127
Pennsylvanian North-Central Texas and Texas Panhandle .....	127
ASSESSMENT OF THE REMAINING RESOURCES IN WILCOX FLUVIAL-DELTAIC GAS RESERVOIRS.....	128
Methodology of Gas-in-Place Calculation .....	128
Remaining Gas Resource.....	131
<b>CHAPTER VI: QUANTIFICATION OF FLOW UNIT AND BOUNDING ELEMENT PROPERTIES AND GEOMETRIES, FERRON SANDSTONE, UTAH: IMPLICATIONS FOR HETEROGENEITY IN GULF COAST TERTIARY DELTAIC RESERVOIRS</b>	
R. Stephen Fisher, Noel Tyler, and Mark D. Barton.....	134
INTRODUCTION.....	134
Study Area .....	135
Approach.....	135
RESULTS.....	138
Architecture of Unit 5 Ferron Sandstones.....	138
Delta-Front Sandstones.....	138
Distributary-Channel and Associated Sandstones.....	140
<i>Basal channels</i> .....	140
<i>Laterally migrating distributary channels</i> .....	142

<i>Late-stage distributary channels</i> .....	144
Bounding Element Hierarchy .....	146
Petrography of Unit 5 Ferron Sandstones.....	147
PERMEABILITY STRUCTURE OF UNIT 5 FERRON SANDSTONES.....	150
Permeability Characteristics of Facies and Stratal Types .....	150
Small-Scale Permeability Structure .....	155
Spatial Correlation of Permeability.....	157
Permeability Correlation Using Vertical Profiles.....	157
Permeability Correlation Using Variograms.....	157
CONCLUSIONS .....	165
<b>CHAPTER VII: OUTCROP-CONSTRAINED DELINEATION OF STRATIGRAPHIC ARCHITECTURE AND RESERVOIR PROPERTIES OF WILCOX GROUP DELTAIC DEPOSITS, LAKE CREEK FIELD, TEXAS</b>	
Edgar H. Guevara, Jeffrey D. Grigsby, and Raymond A. Levey .....	169
INTRODUCTION.....	169
DEPOSITIONAL ENVIRONMENTS OF THE G SANDSTONE .....	173
Vertical and Areal Facies Development.....	173
Shelf/Interdistributary Bay/Prodelta Mud Facies.....	176
Delta-Front Facies .....	176
Distributary-Channel Facies.....	178
Delta-Plain Facies .....	184
Transgressive, Delta-Destructional Facies .....	184
STRATIGRAPHIC ARCHITECTURE OF THE G SANDSTONE.....	184
Vertical and Areal Facies Development.....	184
Styles of Between-Well Heterogeneity .....	186
RESERVOIR COMPOSITION AND QUALITY .....	187
IMPLICATIONS FOR GAS RESERVE GROWTH IN WILCOX DELTAIC RESERVOIRS .....	190
CONCLUSIONS .....	191

## CHAPTER VIII: CONCLUSION

Noel Tyler .....	192
RESERVOIR ARCHITECTURAL CONTROLS ON UNRECOVERED MOVABLE OIL—THE APPLICATION OF PREDICTIVE GEOLOGY .....	194
ADVANCED SECONDARY RECOVERY—A NEW APPROACH TO ADVANCED RECOVERY .....	197
CONCLUSION—TRANSLATION FROM RESOURCE TO RESERVES.....	202
ACKNOWLEDGMENTS .....	203
REFERENCES.....	205

### Figures

II-1. Simplified geologic map of the central Guadalupe Mountains.....	12
II-2. Simplified geologic map of central Guadalupe Mountains showing measured sections used in figures II-4, II-6, and II-8 through II-12, and approximate position of Grayburg shelf margin .....	13
II-3. Chronostratigraphic chart of Guadalupian (Permian) units of the greater Permian Basin .....	14
II-4. Stratigraphic framework of Grayburg Formation .....	15
II-5. Grayburg paleogeography of the Permian Basin showing position of oil fields having greater than 10 million barrels cumulative production.....	17
II-6. Sequence-stratigraphic framework of the Grayburg Formation in the Shattuck Valley area.....	19
II-7. Relationship of platform margin geometry to application of sequence-stratigraphic terminology.....	21
II-8. Distribution of fenestral/tepee facies within Grayburg parasequence framework.....	25
II-9. Distribution of ooid grainstone facies within Grayburg parasequence framework.....	26
II-10. Distribution of ooid-peloid packstone facies within Grayburg parasequence framework.....	27
II-11. Distribution of fusulinid-peloid packstone facies within Grayburg parasequence framework.....	28
II-12. Distribution of sandstone facies within Grayburg parasequence framework.....	29
II-13. Dimensional data for the five generalized Grayburg facies in terms of average thickness and maximum dip-oriented dimension.....	35

II-14.	Simplified profile of the Grayburg highstand systems tract as exposed in the Guadalupe Mountains .....	36
III-1.	Topographic contour map of Stone Canyon study area, Eddy County, New Mexico.....	44
III-2.	Photomosaic showing northern and southern walls of Stone Canyon .....	45
III-3.	West-East stratigraphic cross section of uppermost Grayburg Formation, northern wall of Stone Canyon.....	46
III-4.	East-West stratigraphic cross section of uppermost Grayburg Formation, southern wall of Stone Canyon .....	47
III-5.	Outcrop features, Grayburg Formation of Stone Canyon.....	50
III-6.	Facies photomicrographs from SC 23.....	53
III-7.	West-East cross section of SC 23, sections 8 to 3 .....	56
III-8.	Photomicrographs of rocks associated with zones of suspected meteoric diagenesis.....	66
III-9.	Photomicrographs of basal quartz-bearing beds of SC 24.....	70
III-10.	Porosity frequency polygons for facies identified from samples recovered from SC 23 and mapped on figure III-5.....	72
III-11.	Computer-generated contour map of porosity distribution, SC 23.....	74
III-12.	Computer-generated contour map of permeability distribution, SC 23.....	78
III-13.	Computer-generated contour maps of porosity and permeability distribution, SC 23/grid-section 8, cement-occluded ooid-peloid dolograin/packstone.....	79
III-14.	Computer-generated contour maps of porosity and permeability distribution, SC 23/grid-section 3, fossiliferous peloid dolograine.....	80
III-15.	Cross plots of log porosity against log permeability with regression lines for more permeable facies in SC 23.....	81
IV-1.	Index map of the Permian Basin showing the location of the ARCO North Foster unit on the eastern side of the Central Basin Platform, Ector County.....	90
IV-2.	Stratigraphic section of the Paleozoic strata of the Central Basin Platform/Midland Basin showing relative distribution of produced oil.....	91
IV-3.	Well-location map of the study area showing location of the ARCO North Foster, Cities Service Johnson Grayburg, and Conoco Johnson units, and location of cross section A-A'.....	93
IV-4.	Structure map contoured on top of the Grayburg Formation.....	94

IV-5.	Generalized dip cross section A–A' across the ARCO North Foster and Conoco Johnson units showing the sequence-stratigraphic units of the Grayburg Formation and occurrence of the fusulinid-wackestone facies.....	97
IV-6.	Generalized dip cross section A–A' across the ARCO North Foster and Conoco Johnson units showing the occurrence of the siltstone and silty dolostone facies.....	98
IV-7.	Generalized dip cross section A–A' across the ARCO North Foster and Conoco Johnson units showing the occurrence of the grainstone facies.....	99
IV-8.	Generalized dip cross section A–A' across the ARCO North Foster and Conoco Johnson units showing the occurrence of the diagenetically altered dolostone facies.....	100
IV-9.	Generalized dip cross section A–A' across the ARCO North Foster and Conoco Johnson units showing the occurrence of the tidal-flat facies.....	101
IV-10.	Isopach map of the FG correlation unit.....	105
IV-11.	Isopach map of the EF correlation unit.....	106
IV-12.	Isopach map of the DE correlation unit.....	107
IV-13.	Rate of oil production from wells in the ARCO North Foster unit.....	112
V-1.	Cumulative nonassociated gas production in Texas.....	119
V-2.	Distribution of gas-productive fluvial-dominated deltaic plays.....	121
V-3.	The cumulative production of fluvial-deltaic reservoirs by region in Texas.....	122
V-4.	The distribution of Tertiary cumulative fluvial-dominated deltaic gas production by formation in the Texas Gulf Coast.....	123
V-5.	Current status of the gas resource in Wilcox fluvial-deltaic reservoirs displaying the breakdown of the 18.56 Tcf original gas in place.....	132
VI-1.	Location map of measured sections in Muddy Creek and Picture Flats canyons.....	136
VI-2.	Vertical profile through typical delta-front and distributary-channel sandstones showing vertical changes in depositional environment, lithofacies, permeability, and gamma-ray response.....	139
VI-3.	Cross section of outcrop panel, South Muddy Creek window, showing geometry of major facies and bounding elements, and permeability profiles at each measured section.....	143
VI-4.	Plot of apparent width and thickness dimensions of distributary-channel and tidal-channel sandstones.....	145
VI-5.	Trilinear plots of Ferron unit 5 sandstone compositions.....	148

VI-6.	Facies cumulative-frequency plot for Ferron unit 5 sandstones from South Muddy Creek and Picture Flats.....	152
VI-7.	Stratal-type cumulative-frequency plot for Ferron unit 5 sandstones from South Muddy Creek.....	154
VI-8.	Kriged permeability structure of distributary-channel sandstones as indicated by a 40-ft <sup>2</sup> sample grid with measurements at 2-ft intervals.....	156
VI-9.	Horizontal semivariograms for permeability measurements on the 40-ft <sup>2</sup> grid classified by stratal type.....	159
VI-10.	Horizontal variogram structure of laterally migrating distributary channel and geologic interpretation.....	161
VI-11.	Vertical variogram structure from laterally migrating distributary channel and geologic interpretation.....	162
VI-12.	Horizontal variogram structure of late-stage distributary channel and geologic interpretation.....	163
VI-13.	Vertical variogram structure of late-stage distributary channel and geologic interpretation.....	164
VII-1.	Location map of the Lake Creek unit in the Wilcox WX-1 gas play.....	170
VII-2.	Schematic depositional dip-oriented cross section through the central Texas Gulf Coast Basin, illustrating the relative position of major sand depocenters.....	171
VII-3.	Structure map showing the top of G-1 across the Lake Creek unit.....	172
VII-4.	Type well log showing the oil reservoirs at the top and gas and condensate reservoirs in the lower stratigraphic intervals of the Wilcox Group in the Lake Creek unit.....	174
VII-5.	Spontaneous potential gamma-ray-resistivity log of the Mobil LCU-36 well showing oil-gas reservoirs and underlying gas-condensate reservoirs of the Wilcox Group in the Lake Creek unit.....	175
VII-6.	Well log showing subdivisions of the G sandstone and core graph and petrophysical data of cores of the G sandstone in the LCU-48 well, Lake Creek unit, Montgomery County.....	177
VII-7.	Facies map of the G-4 lower interval illustrating the lowest parasequence in the G sandstone.....	179
VII-8.	Facies map illustrating the G-4 middle interval in the G sandstone.....	180
VII-9.	Facies map illustrating the G-2 lower interval in the G sandstone.....	181
VII-10.	Facies map illustrating the G-2 upper interval in the G sandstone.....	182

VII-11.	Facies map of the G-1 interval illustrating the uppermost parasequence in the G sandstone.....	183
VII-12.	Depositional strike-oriented cross section A–A’ showing the four parasequences in the G sandstone interval across the Lake Creek unit.....	188
VIII-1.	Schematic fluvial-dominated delta drilled on 40-acre spacing.....	193
VIII-2.	Advanced secondary recovery strategies applied to a hypothetical fluvial-dominated delta to tap uncontacted compartments and to optimize injection profiles to waterflood zones bypassed by the flood.....	201

### Tables

II-1.	Sequence-stratigraphic terminology and relevance to reservoir development.....	10
II-2.	Attributes and environments of standard Grayburg facies types.....	34
III-1.	Results of porosity and permeability analyses, Stone Canyon, Grayburg Formation, parasequence SC 23 .....	76
IV-1.	Character and interpretation of Grayburg facies at North Foster.....	96
VI-1.	Apparent dimensions of distributary-channel macroforms in amalgamated Ferron unit 5 distributary-channel sand bodies.....	141
VI-2.	Statistical characterization by depositional classification and scale.....	151
VIII-1.	Heterogeneity matrix wherein depositional systems are classified according to vertical and lateral heterogeneity.....	196
VIII-2.	Projected recovery efficiency, residency of unrecovered mobile oil, and appropriate recovery strategies, as a function of reservoir heterogeneity, to target remaining mobile-oil saturations .....	198

## ABSTRACT

Ultimate recovery from Texas oil reservoirs at current technological and development levels is projected to be 36 percent of the oil in place. Thus, of the 165 billion barrels (Bbbl) of oil discovered statewide, 106 Bbbl will remain in existing reservoirs after recovery of proved reserves. This remaining resource is composed of residual oil (71 Bbbl) and mobile oil (35 Bbbl). The remaining mobile oil is conventionally recoverable but is prevented from migrating to the well bore by intrareservoir seals or bounding surfaces.

Reservoir architecture, the internal fabric or structure of reservoirs, governs paths of fluid migration during oil and gas production. Reservoir architecture is, in turn, the product of the depositional and diagenetic processes responsible for the origin of the reservoir. If an understanding of the origin of the reservoir is developed, reservoir architecture, and therefore the paths of fluid migration, becomes predictable. Thus, with a greater understanding of the fabric of the reservoir and its inherent control on the paths of fluid flow, we can more efficiently design and implement advanced recovery strategies.

Research described in this report addresses the internal architecture of two specific reservoir types: restricted-platform carbonates and fluvial-deltaic sandstones. Together, these two reservoir types contain more than two-thirds of the unrecovered mobile oil remaining in Texas. The approach followed in this study was to develop a strong understanding of the styles of heterogeneity of these reservoir types based on a detailed outcrop description and a translation of these findings into optimized recovery strategies in select subsurface analogs. Research targeted Grayburg Formation restricted-platform carbonate outcrops along the Algerita Escarpment and in Stone Canyon in southeastern New Mexico and Ferron deltaic sandstones in central Utah as analogs for the North Foster (Grayburg) and Lake Creek (Wilcox) units, respectively. In both settings, sequence-stratigraphic style profoundly influenced between-well architectural fabric and permeability structure.

Reservoirs can be characterized according to varying degrees of lateral and vertical heterogeneity. For example, the distributaries of fluvial-dominated deltas display a high degree of lateral heterogeneity; in contrast, the delta front has very low lateral heterogeneity but a moderate degree of vertical heterogeneity. Highly stratified restricted-platform carbonate reservoirs in the Permian Basin contrast with Gulf Coast strandplain sandstones that are relatively simple in vertical character.

It is concluded that reservoirs of different depositional origins can therefore be categorized into a "heterogeneity matrix" based on varying intensity of vertical and lateral heterogeneity. The utility of the matrix is that it allows prediction of the nature and location of remaining mobile oil. Highly stratified reservoirs such as the Grayburg, for example, will contain a large proportion of vertically bypassed oil; thus, an appropriate recovery strategy will be waterflood optimization and profile modification. Laterally heterogeneous reservoirs such as deltaic distributary systems would benefit from targeted infill drilling (possibly with horizontal wells) and improved areal sweep efficiency. Potential for advanced recovery of remaining mobile oil through heterogeneity-based advanced secondary recovery strategies in Texas is projected to be an incremental 16 Bbbl. In the Lower 48 States this target may be as much as 45 Bbbl at low to moderate oil prices over the near- to mid-term.

## CHAPTER I: INTRODUCTION

Noel Tyler

Internal architecture of reservoirs provides a fundamental control on the paths of reservoir drainage, oil and gas recovery efficiency, and ultimately on the volumes of conventionally recoverable hydrocarbons left in the reservoir at abandonment. Efficient recovery of hydrocarbons is thus dependent on advanced understanding of reservoir anatomy and the spatial distribution of the petrophysical attributes that govern fluid flow. The predictability of reservoir and intrareservoir seal properties composes the crux of this report, which addresses the spatial distribution of permeability in deltaic sandstone and restricted platform carbonate reservoirs—reservoir classes that collectively account for 65 percent of the estimated ultimate recovery from Texas oil reservoirs. On the basis of similar depositional and diagenetic histories, we have selected the Cretaceous Ferron delta system in central Utah as an analog for the prolific Gulf Coast deltaic reservoirs. This report also discusses outcrop and subsurface characterization of the Permian Grayburg Formation of West Texas and New Mexico as a type example of restricted platform carbonate reservoirs in the Permian Basin.

Reservoir architecture, the internal fabric or structure of reservoirs, governs paths of fluid migration during oil and gas production. Reservoir architecture is, in turn, the product of the depositional and diagenetic processes that cause the reservoir to form. Therefore, if an understanding of the origin of the reservoir is developed, reservoir architecture and the paths of fluid migration become predictable. Thus, with greater understanding of the anatomy of the reservoir and its inherent control on the paths of fluid flow, we can more efficiently target remaining, conventionally recoverable, hydrocarbons that are prevented from migrating to the well bore by intrareservoir seals or bounding surfaces. Furthermore, advanced recovery strategies that account for the internal compartmentalization of the reservoir can be designed and implemented.

Research discussed in this report addresses the controls of sequence stratigraphy on sedimentary architecture and permeability structure and how this permeability structure affects oil and gas mobility under reservoir conditions. The approach was to establish the depositional architecture and diagenetic modification of reservoir equivalents within the context of a well-defined sequence-stratigraphic framework and then to determine how these factors affect the spatial distribution of permeability. The steps involved in this characterization of heterogeneity are the determination of sequence-stratigraphic histories of the targeted formations, delineation of facies architecture, delineation of the position, continuity, and causes of both permeable zones and barriers to oil and gas flow, and establishment of predictable permeability trends common to fluvial-deltaic sandstones and restricted platform carbonates. Ultimately, the goal is to translate this understanding of outcrop architecture to a reservoir model that can be used to test hypotheses concerning the most efficient methods for recovery of incremental oil and gas reserves in heterogeneous, compartmented reservoirs.

## OBJECTIVES

This study had multiple objectives that were divided into seven subtasks as follows: (1) Defining the expected distribution of carbonate sand bar facies in the Grayburg Formation on a regional or sequence scale in the outcrop. (2) Characterizing external geometries and internal heterogeneities of productive sandbar facies on the basis of detailed outcrop studies at both the systems-tract scale and the intraparasequence scale. (3) Conducting geological and engineering characterization studies of flow-unit structure using reservoir data from a selected reservoir. The North Foster Grayburg unit was targeted for detailed analysis on the basis of the quality of available data and on operator cooperation. (4) Developing exploitation approaches and infill drilling strategies for advanced recovery of remaining hydrocarbons. (5) Determining which genetic reservoir types are most amenable to advanced gas recovery. (6) Undertaking detailed characterization of reservoir types identified in subtask 5 to develop strategies for

advanced recovery. (7) Testing, if possible, the approaches developed in subtask 6 in a selected field analog.

Subtasks 1 through 4 were performed to determine the effects of heterogeneity on oil recovery in carbonate reservoirs. Results of these subtasks are presented in chapters 2 through 4 of this report as follows. Chapter 2 describes the outcrop sequence-stratigraphic framework of the Grayburg Formation and implications for reservoir characterization. Chapter 3 describes interwell-scale reservoir heterogeneity in the Grayburg highstand systems tract of the Stone Canyon area. In chapter 4 the Grayburg reservoir in the North Foster/Johnson units, eastern margin of the Central Basin Platform, is described, and implications for subsurface sequence-guided advanced recovery approaches are discussed. Subtasks 5 through 7 were developed to address the effects of sandstone reservoir heterogeneity on gas production and recovery efficiencies. Chapter 5 presents results of the analysis of gas reservoir recovery and reasons for targeting deltaic reservoirs for advanced gas recovery. Chapter 6 addresses results of outcrop characterization of the selected reservoir analog for Gulf Coast deltaic reservoirs, and chapter 7 discusses the transfer of advanced recovery approaches to the subsurface in this critical reservoir type.

#### APPLICABILITY OF OUTCROP STUDIES TO THE SUBSURFACE: DATA PORTABILITY

Reservoir characterization from outcrop studies allows the continuous sampling necessary for a more detailed reservoir description than is available from subsurface data alone. In addition to being able to rigorously map geometric attributes of component facies in two (and locally three) dimensions, outcrop characterization allows ready access for high-resolution field minipermeametry. Field minipermeametry uses a portable minipermeameter to transform the rate of flow of nitrogen through a carefully prepared outcrop surface, together with attendant drop in pressure, into permeability. This was the fundamental approach used in this study, as

discussed in chapters 2 and 6. An obvious limitation of surface studies is the transfer, that is, portability, of outcrop permeability values to the subsurface. Several studies have demonstrated the portability of outcrop observations to the subsurface (Stalkup and Ebanks, 1986; Goggin, 1988; Kittridge, 1988; Chandler and others, 1989). In general, it has been found that the mean of the permeability measurements is not portable. However, distribution type, coefficient of variation, and correlation measures are portable between outcrop and subsurface. In particular, Stalkup and Ebanks (1986) investigated permeability of sandstones in the Ferron study area. They compared outcrop with subsurface rocks of the same stratigraphic interval in a nearby well and found that permeability contrast among lithofacies is greater in the subsurface than in the outcrops. They attributed this to the effects of surface weathering. However, they also found that the vertical arrangement of statistically different permeabilities is preserved in the two situations, indicating the portability of outcrop data to core.

Several recent studies have shown that sedimentary facies exert an important control on permeability distribution in clastic rocks (Weber, 1982; Stalkup and Ebanks, 1986; Jones and others, 1987; Dreyer and others, 1990). The most influential variables influencing permeability are grain size, grain sorting, mineralogy, fabric, and degree of cementation (Dreyer and others, 1990). Thus, based on the results of these earlier studies, the approach we followed was to relate permeability measurements at the outcrop to quantification of these same variables. Permeability variation on the outcrop was then compared with rock-property variation to establish discrete permeability groups for specific depositional systems and settings. This information provided the basis for assigning values and distributions of petrophysical properties to reservoir models of sandstones from similar depositional systems and settings.

CHAPTER II: OUTCROP DELINEATION OF CARBONATE  
SAND BODY DISTRIBUTION IN A SEQUENCE-  
STRATIGRAPHIC FRAMEWORK

Charles Kerans

INTRODUCTION

Analyses of oil and gas production trends (in terms of reserve additions and reservoir volumetrics) by industry, government, and applied academic groups have revealed an extensive remaining hydrocarbon potential in existing reservoirs in the lower 48 states, particularly in the Permian Basin (Tyler and others, 1984; Fisher and Finley, 1986a; Fisher, 1987; Tyler and Banta, 1989). This potential has sparked renewed interest in developing advanced reservoir descriptions and models aimed at recovering this substantial low- to intermediate-cost resource. A central element in improving reservoir models is the ability to predict the continuity of reservoir flow units between well bores. A variety of emerging technologies such as downhole seismic and horizontal drilling indicate better deterministic characterization of the interwell area and its flow characteristics in the future. In the nearterm, however, economic constraints dictate that reservoir geologists and engineers rely on maximizing existing subsurface data to develop improved reservoir models.

The role of outcrop studies in improving reservoir heterogeneity models has been recognized by numerous groups as a means of developing conceptual and geostatistical approaches to modeling interwell heterogeneity (Goggin and others, 1986; Stalkup and Ebanks, 1986; Sharma and others, 1989; Lewis, 1988; Ravenne and others, 1989; Tyler and others, 1991). Outcrop studies will continue to play a central role in improving reservoir models because they enable both the deterministic and geostatistic characterization of patterns of

geologic facies and their related petrophysical properties at scales comparable to the interwell area of subsurface reservoirs.

The demands for carbonate outcrop studies for reservoir modeling are particularly great because little is known about the geometry and lateral and vertical distribution of carbonate reservoir facies at the interwell scale. Comparison of existing carbonate reservoir descriptions with state-of-the-art sandstone reservoir models highlights this discrepancy (compare Bebout and others, 1987 and Kerans, 1988, with Galloway and Cheng, 1985 and Tyler and Ambrose, 1986).

Studies of sandstone reservoirs by Ravenne and others (1989), Tyler and others (1991), and numerous other workers have delineated petrophysically significant reservoir facies such as channel, levee, crevasse splay, as well as the equally important shale flow barriers, using gamma-ray, SP, and resistivity wireline tools. In contrast, the well-log signatures of carbonate reservoir strata are less diagnostic and thus generally limit stratigraphic framework studies to those areas with extensive core control. Also, the greater susceptibility of carbonate sediments to diagenetic overprints typically obscures or masks the relationship between depositional and petrophysical facies, making construction of flow unit models more complex. Outcrop studies of carbonate reservoirs perhaps provide the best opportunity to document the true facies architecture of carbonate depositional facies and their relationship to petrophysically defined flow units.

### Sequence Stratigraphy in Reservoir Studies

Equally important for improved characterization of reservoir flow unit structure and delineation of the remaining resource is the application of sequence-stratigraphic concepts at both the sequence scale, for reservoir framework construction, and the parasequence scale, for providing improved packaging of strata into genetically and petrophysically significant units at the interwell scale. Sequence stratigraphy (Vail, 1987; Van Wagoner and others, 1988) evolved

largely as a tool for exploration in frontier basins and unexplored parts of mature basins. Only more recently has it become recognized as a fundamental conceptual tool in reservoir characterization (Van Wagoner and others, 1990; Kerans and others, 1991). In this study of Grayburg sandbar facies, we established the sequence-stratigraphic framework of the formation through development of a detailed outcrop model that can be tested through subsurface correlation and core description. Basic sequence-stratigraphic terms and their implication for reservoir geologists are given in table II-1.

## OUTCROP SEQUENCE-STRATIGRAPHIC FRAMEWORK OF THE GRAYBURG FORMATION—IMPLICATIONS FOR SUBSURFACE RESERVOIR CHARACTERIZATION

This discussion consists of a general introduction to the Grayburg Formation, development of a sequence-stratigraphic framework for the Grayburg Formation in its outcrop area (figs. II-1 and II-2), application of the outcrop sequence framework to the regional characterization of Grayburg reservoirs in the subsurface (and in particular carbonate sandbar facies production), and definition of the parasequence-scale framework of the Grayburg Formation outcrop and its contained facies tracts.

The Grayburg Formation is a major player within the open/restricted dolomitized carbonate platform plays of the Permian Basin, having 16 reservoirs that have produced more than 10 million barrels (MMbbl). The Grayburg, the lowest unit of the Artesia Group, is Permian (Middle Guadalupian) in age (fig. II-3). It is a mixed clastic/carbonate unit that records predominantly shallow-shelf sedimentation in lowstand, transgressive, and highstand systems tracts and represents a single third-order sequence of 1- to 5-m.y. duration (fig. II-4). Grayburg carbonates rimmed the Delaware and Midland Basins along the Northwestern, Northern, and Eastern Shelves, the Ozona Arch, and the Central Basin Platform. Producing reservoirs are

Table II-I. Sequence-stratigraphic terminology and relevance to reservoir development.

Term		Definition	Reservoir Application
Sequence stratigraphy		Study of rock relationships within a chronostratigraphic framework of repetitive, genetically related strata bounded by surfaces of erosion or nondeposition, or their correlative conformities	Reservoir framework
Sequence	S	Relatively conformable succession of genetically related strata bounded by unconformities and their correlative conformities	Total reservoir interval
Parasequence	ps	Relatively conformable succession of genetically related and generally progradational beds and bed sets bounded above and below by marine flooding surfaces and their correlative surfaces	Basic reservoir mapping unit; can be closely related to flow units
Marine flooding surface	FS	Surface that separates older strata below from younger above, across which there is evidence of abrupt increase in water depth	Potentially critical as intrareservoir flow barriers
Depositional system		3-D assemblage of lithofacies	Classic style of geologic reservoir description, ex. delta
Systems tract	ST	Linkage of contemporaneous DS's, in sequence recognize three systems tracts: lowstand (or shelf margin if type 2 sequence), transgressive, and highstand	Recognition of systems tract within sequence lends predictability to vertical and lateral trends of reservoir strata
Lowstand ST	LST	Basal ST of sequence, rests on type 1 unconformity surface or correl. conformity, basin-restricted geometry	Typical submarine fan reservoirs, ex. Spraberry, Midland Basin, also basinal carbonate debris, Bone Spring, Penn. debris complexes, Cretaceous Poza Rica of Mexico
Shelf margin ST	SMST	Basal ST of type 2 sequence, developed atop and seaward of old shelf margin	May represent separate shingled reservoir zone within overall progradational sequence set
Transgressive ST	TST	Middle ST of either type 1 or type 2 sequence, separated from LST/SMST by transgressive surface, deposited during sea-level rise with component sediments overlapping underlying sequence boundary	Retrogradational package, can form separated reservoir draped by condensed section deposits, ex., Holt (lower San Andres) reservoirs at North Cowden, Penwell
Transgressive surface	TS	First significant marine-flooding surface across the precursor shelf	Used to separate TST and LST
Downlap surface	DLS	Marine flooding surface onto which the toes of clinoforms of overlying highstand tract downlap	
Maximum flooding surface	MFS	Downlap surface	Key seismically resolvable mapping surface, typically separates distinctly different reservoir styles

Table II-I (cont.)

Term		Definition	Reservoir Application
Condensed section	CS	Starved sediment deposit at DS	Can serve as source bed and/or intrasequence reservoir seal
Highstand ST	HST	Widespread uppermost ST of sequence containing aggradational and/or progradational parasequence sets, onlapping sequence boundary (SB) toward shelf and downlapping TST or LST basinward in clinoformal geometry, and capped by type 1 or type 2	Contains high-energy shoal-type reservoir strata

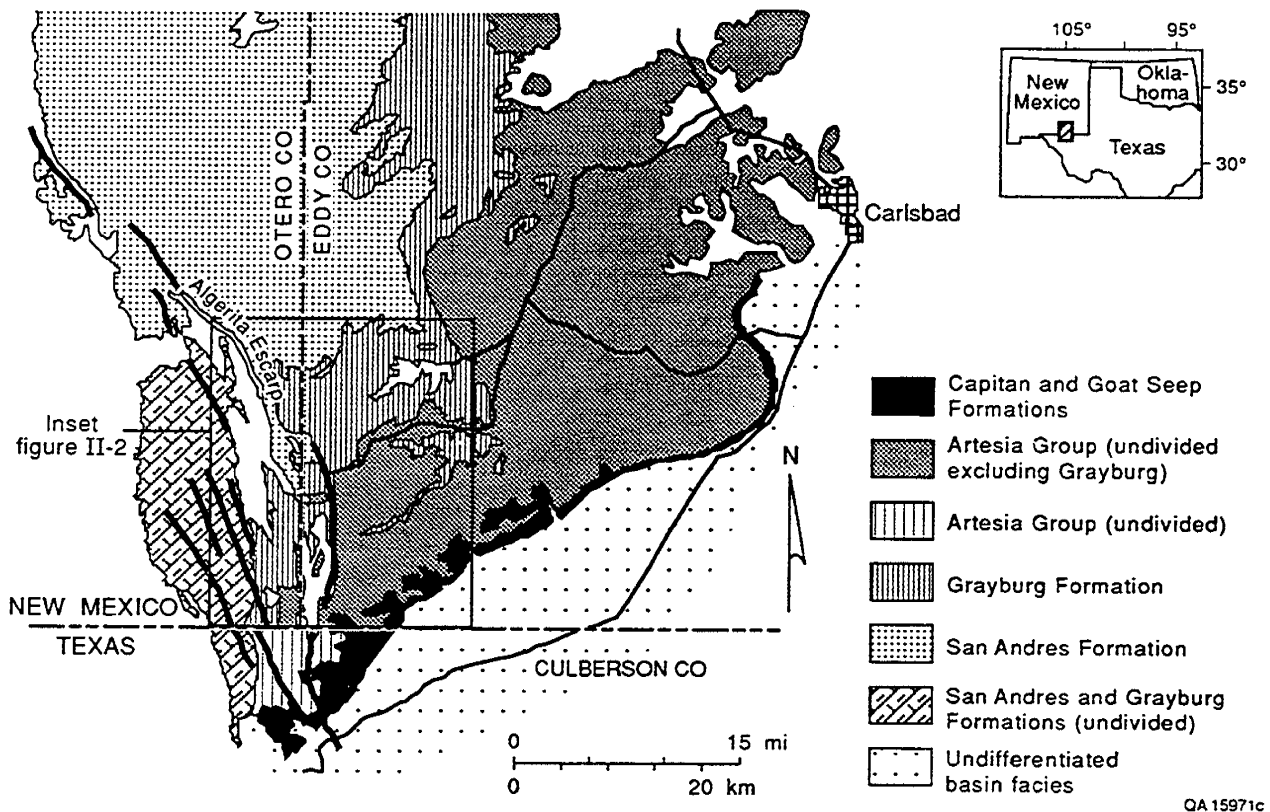


Figure II-1. Simplified geologic map of the central Guadalupe Mountains (after Hayes, 1964). Outlined area marks position of inset map of figure II-2.

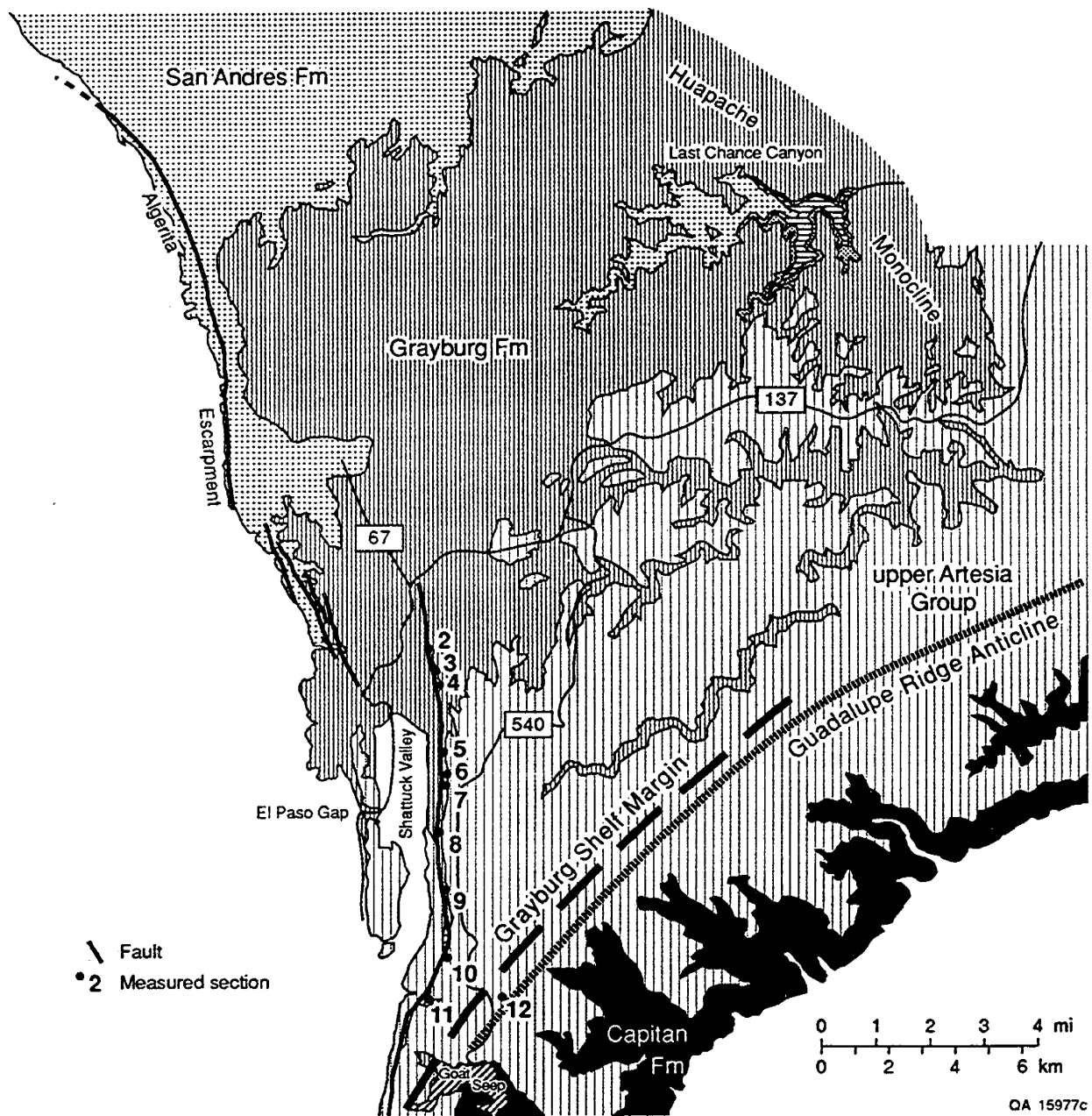
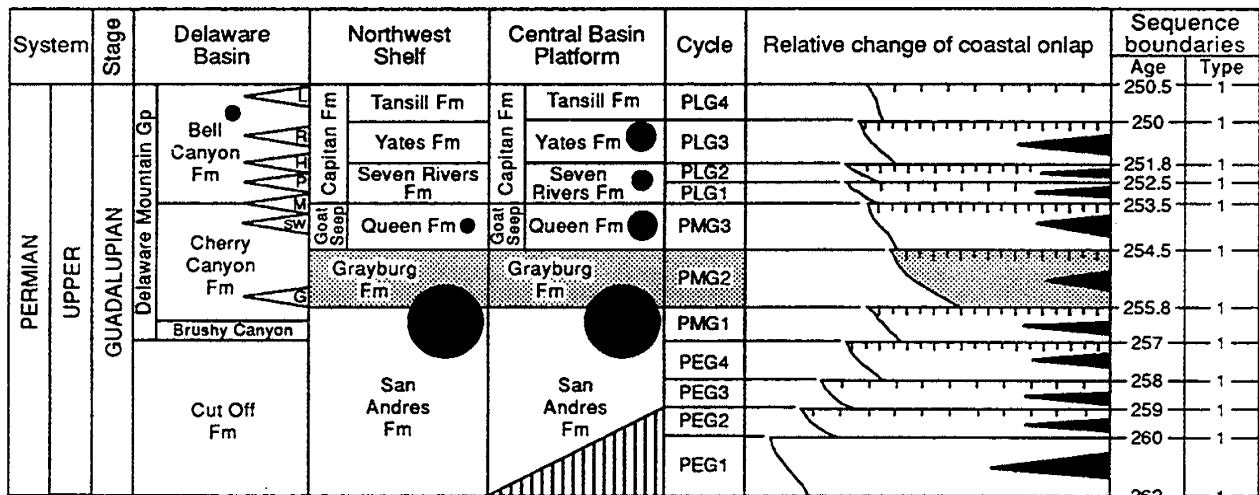
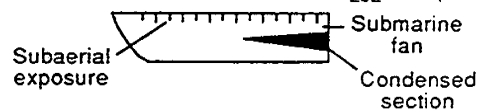


Figure II-2. Simplified geologic map of central Guadalupe Mountains (after Hayes, 1964) showing measured sections used in figures II-4, II-6, and II-8 through II-12, and approximate position of Grayburg shelf margin. The Guadalupe Ridge anticline may be a surface reflection of differential compaction over this margin.



Carbonate tongues within the Delaware Mountain Gp: G = Getaway, SW = South Wells, M = Manzanita, P = Pinery, H = Hegler, R = Rader, L = Lamar



● Relative importance as a producing unit; based on Galloway and others (1983)

Modified from Galloway and others (1983); Ross & Ross (1987)

QA 15984c

Figure II-3. Chronostratigraphic chart of Guadalupian (Permian) units of the greater Permian Basin, compiled from Galloway and others (1983) and Ross and Ross (1987).

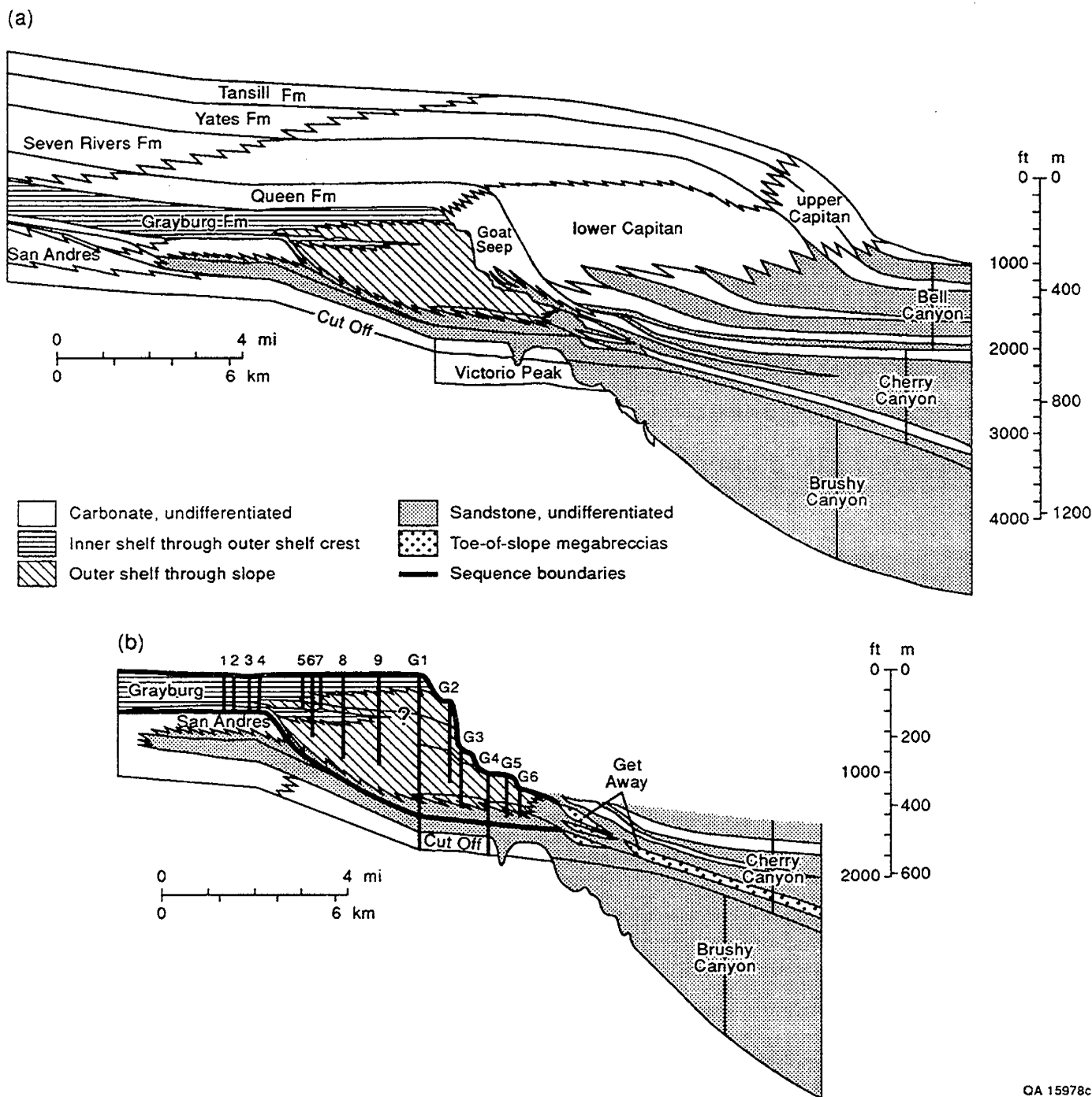


Figure II-4. Stratigraphic framework of Grayburg Formation showing (a) its relationship to other Guadalupian platforms, and (b) a more detailed view of the Grayburg platform using measured sections and stratigraphic relationships of Franseen and others (1989) for the Western Escarpment (G1-G6) and Shattuck Valley sections of this study (1-9). Cross section in (a) was compiled by W. Fitchen from various sources.

concentrated along the eastern margin of the Central Basin Platform but also occur along the rimming shelves (fig. II-5).

The Grayburg Formation as exposed in the Guadalupe Mountains (figs. II-1 and II-2) defines the northwestern rim of the Delaware Basin during Grayburg time, but precise definition of the Grayburg shelf edge in outcrop has proved difficult because of massive erosion and truncation marking the Grayburg/Queen sequence boundary (fig. II-4b) (Fekete and others, 1986, Franseen and others, 1989).

Guadalupian-aged Grayburg strata exposed in the Guadalupe Mountains compose a mixed siliciclastic-carbonate third-order depositional sequence (terminology of Mitchum and others, 1977) deposited on the Northwestern Shelf of the Delaware Basin. Dickey (1940) defined the Grayburg Formation type section in the Cecil H. Lockhart Root Permit No. 2 well from the Grayburg-Jackson field in Eddy County, New Mexico. Since that time several authors have variously defined its boundaries in outcrop, sometimes including the Grayburg in the Queen Formation (Skinner, 1946) or including within the Grayburg uppermost San Andres strata (Boyd, 1958; Moran, 1962). Tait and others (1962) collected the Grayburg with other post-San Andres strata of the Guadalupian Series (Queen, Seven Rivers, Yates, and Tansill Formations) into the Artesia Group, referring to the outcrop belt near Artesia, eastern New Mexico. As mapped by Hayes and Adams (1962) and Hayes (1964), the Grayburg Formation in the Algerita Escarpment/Shattuck Valley study area comprises an interval of interbedded siliciclastic and carbonate rocks overlying, locally unconformably, the carbonate-dominated San Andres Formation. The Grayburg underlies the siliciclastic-rich Queen Formation from which it is separated by a "locally conspicuous sandstone" (Hayes, 1964) that is "thicker than any of those in the Grayburg" (Hayes and Adams, 1962). The most recent field studies have shown that conspicuous karsted surfaces (sequence boundaries) occur at the top and base of the Grayburg Formation in the southern and central Guadalupe Mountains (Fekete and others, 1986; Kerans and Nance, 1991). The Grayburg interval on the Central Basin Platform is lithologically similar

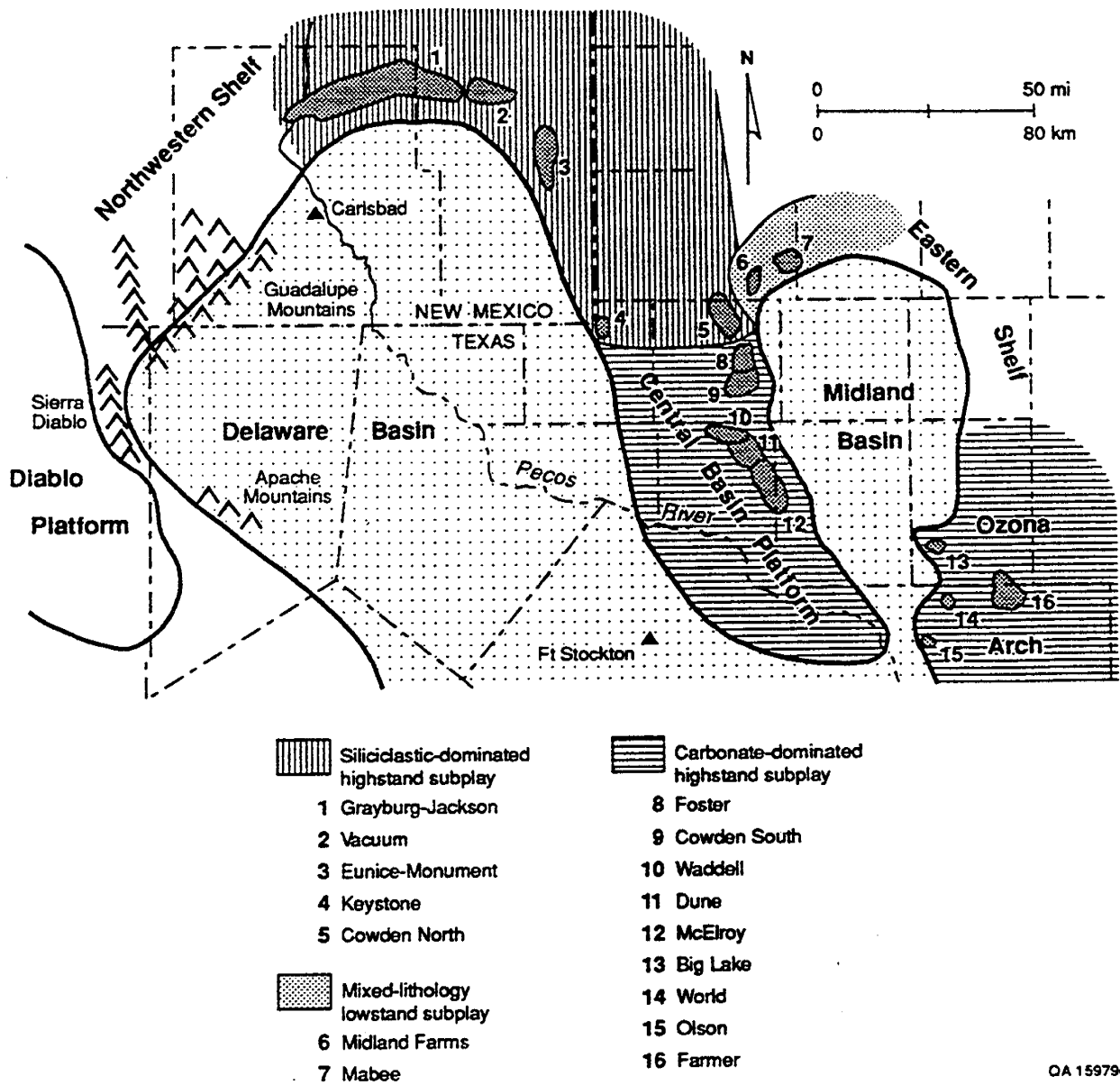


Figure II-5. Grayburg paleogeography of the Permian Basin showing position of oil fields having greater than 10 million barrels cumulative production. Modified from Ward and others (1987).

except that siliciclastics are represented by siltstone beds on the platform rather than by fine-grained sandstone, as on the Northwestern Shelf of the Delaware Basin (chapter IV).

Previous studies of Grayburg reservoirs include those of Longacre (1980), Harris and others (1984), and Bebout and others (1987). Studies of the Grayburg Formation in the Guadalupe Mountains outcrops include early regional work by Lang (1937), King (1948), and Newell and others (1953), as well as more specific mapping studies by Boyd (1958) in the Brokeoff Mountains and Algerita Escarpment areas, and by Hayes (1959, 1964), who covered the central and northern Guadalupe exclusive of the Brokeoff Mountains. The surface type locality of the Grayburg was defined for the Sitting Bull Falls area by Moran (1954). The Grayburg of the Last Chance Canyon area was also treated in a general depositional/diagenetic analysis by Naiman (1982) and in a regional sequence-stratigraphic synthesis by Sarg and Lehmann (1986). Basin margin relationships and erosional history of the Grayburg along the western escarpment of the Guadalupe was reported by Fekete and others (1986).

Grayburg carbonates are pervasively dolomitized in the Guadalupe Mountains outcrop belt and in the subsurface, and all descriptions of carbonates should be assumed to be dolomite.

## Regional Framework of the Grayburg Outcrop in the Guadalupe Mountains

### Development of a Sequence-Stratigraphic Framework

The sequence-stratigraphic framework of the Grayburg as used for this study is shown in figures II-4 and II-6. This interpretation suggests that the Grayburg varies markedly in thickness, from 260 ft on top of the underlying San Andres platform to more than 1,000 ft as accommodation space increases seaward of the terminal San Andres margin as exposed on the Western Escarpment. This interpretation is consistent with terminology of Franseen and others (1989) but differs from that of Sarg and Lehmann (1986), who considered the lower Grayburg as mapped on the Western Escarpment by Franseen and others (1989) to be equivalent to the upper San Andres of Last Chance Canyon.

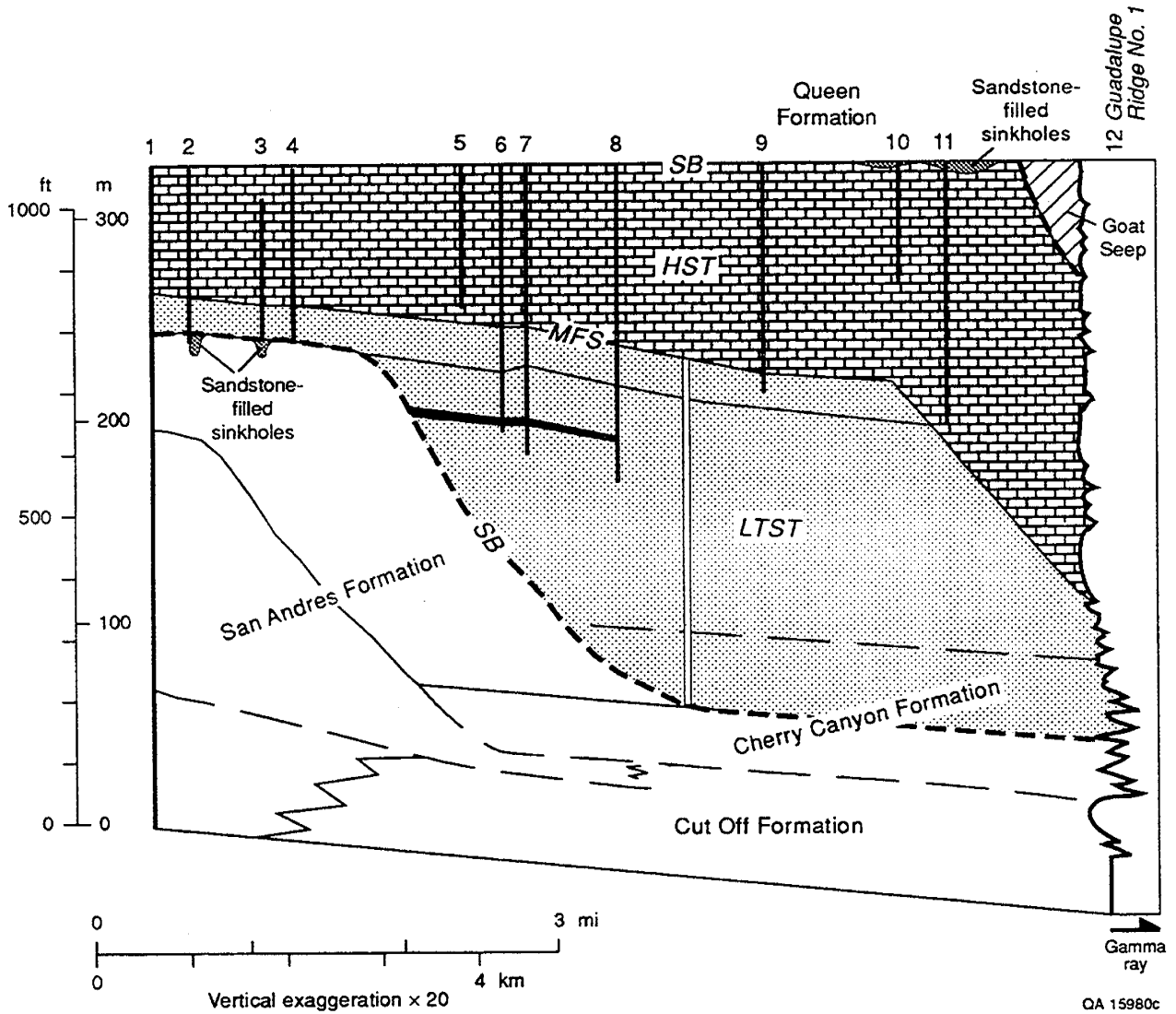


Figure II-6. Sequence-stratigraphic framework of the Grayburg Formation in the Shattuck Valley area. The blackened unit near the base of sections 6 and 7 is a crossbedded sand-rich ooid grainstone documenting the downward shift in coastal onlap of the Grayburg LTST onto the San Andres. The geometry of the San Andres sequence boundary downdip of section 4 is not constrained.

Application of existing sequence-stratigraphic and systems-tract terminology to the Grayburg sequence in outcrop is complicated by (1) a lack of critical exposures showing the relationship between the terminal San Andres shelf margin and the onlapping Grayburg, and (2) the long-term (third-order) topographic fall of the San Andres toplap position as that platform prograded in a series of high-oblique clinoforms. In an ideal case, where the platform top of the underlying sequence is nearly level, onlap by the succeeding sequence occurs topographically below the terminal platform margin of the underlying sequence. This makes recognition of a type 1 sequence and its associated lowstand and transgressive systems tracts unambiguous (fig. II-7a).

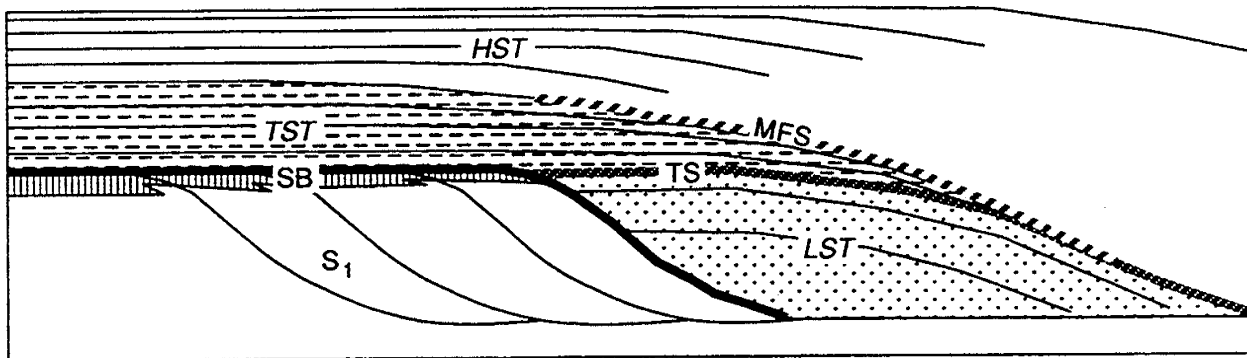
Where decreasing accommodation space during the third-order sea-level fall has resulted in a basin-sloping toplap surface/sequence boundary, it is possible to observe onlap relationships above the terminal shelf margin that can be confused with onlap below the terminal shelf edge. Because recognizing onlap relative to the terminal shelf margin is required to distinguish type 1 from type 2 sequence boundaries and lowstand prograding wedge from shelf-margin wedge, delineation of the terminal shelf margin is important (fig. II-7).

For the Grayburg outcrop it has not yet been possible to define the terminal shelf margin, although the critical exposures may be present along Cutoff Ridge in the Brokeoff Mountains. Thus, until relationships at the terminal San Andres shelf margin are resolved, all deposits beneath the maximum flooding surface will be grouped together as lowstand through transgressive systems tracts (LTST) (fig. II-6).

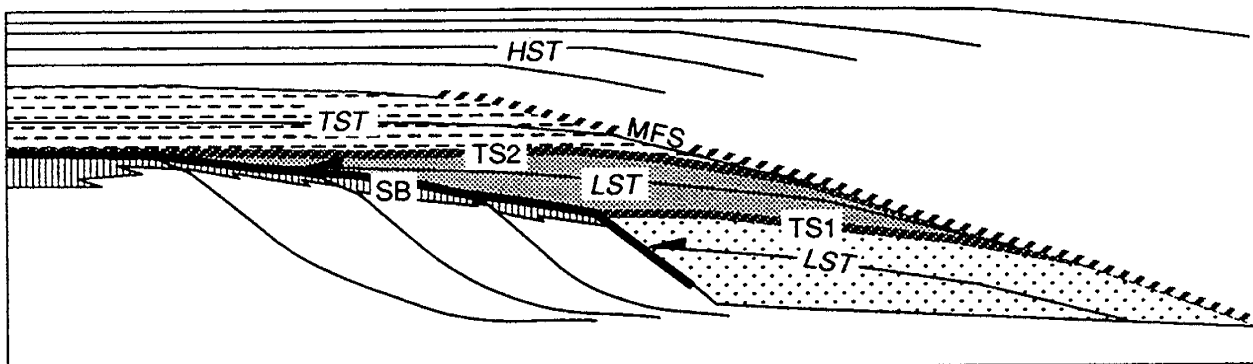
#### *San Andres/Grayburg Sequence Boundary*

The basal Grayburg Formation sequence boundary with the San Andres Formation is variably expressed across the shelf-slope paleotopography of the San Andres Formation. In the most basinward outcrops of Last Chance Canyon near its entrance (fig. II-2), the basal Grayburg sequence boundary is a clean, sharp contact with relatively shallow-water sandstones of the

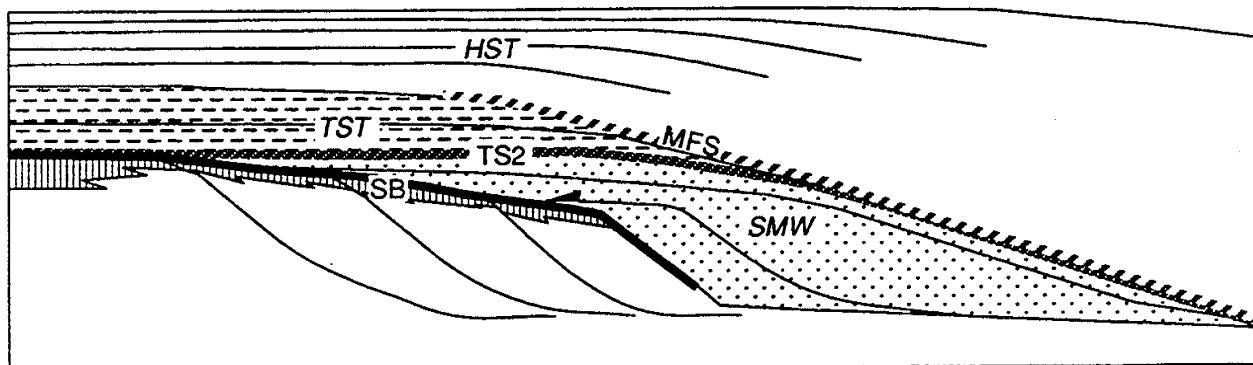
(a)  $S_1$  toplap surface flat



(b)  $S_1$  toplap surface falls basinward, onlap below terminal shelf margin



(c)  $S_1$  toplap surface falls basinward, onlap above terminal shelf margin



Outer shelf facies



Slope facies

OA 15981c

Figure II-7. Relationship of platform margin geometry to application of sequence-stratigraphic terminology. See text for discussion.

uppermost Grayburg Formation lowstand systems tract resting on subtidal packstones of the San Andres. Rare sand-filled cracks (grikes) in the San Andres provide evidence for subaerial exposure. Moving up Last Chance Canyon in a paleolandward direction (westward), small breccia-filled pockets and sinkholes several feet deep lend more convincing evidence for subaerial exposure at this contact. A minimum estimate for the downward shift in relative sea level here is 50 ft, based on onlap geometries documented by Sonnenfeld (1991).

To the west, in the Algerita Escarpment area a thin preserved Grayburg section rests on peritidal San Andres dolostones with sharp erosional contact. Locally along this contact a 0- to 3-ft-thick basal lithoclast pebble conglomerate and minor regolith are preserved (sections B and C, fig. II-2). The San Andres-Grayburg sequence boundary on the northern Shattuck Valley wall, just downdip of the Algerita Escarpment outcrops, displays solution dolines cut 30 ft deep into fenestral dolostones of the San Andres Formation (section 2, figs. II-2 and II-6). These dolines, filled with massive sandstone, and are overlain by basal Grayburg Formation sandstones that show no collapse into the dolines and are texturally and mineralogically identical to doline-fill sandstones. These relationships indicate a pre-Grayburg origin for the dolines. A minimum estimate for downward shift in coastal onlap associated with the dolines is again 50 ft, taken from the vadose karst profile in this area.

In section 4 (figs. II-2 and II-6) the basal sequence boundary is 30 ft lower than at section 2 and is developed on subtidal skeletal grainstones instead of on tidal-flat facies. Calcification of the grainstones here persists for 30 ft beneath the unconformity. Above the unconformity is a 15-ft-thick granule-pebble conglomerate that thins to less than 1 ft at section 2. These relationships suggest that the sequence boundary is developed on a seaward slope that is projected below the base of measured sections, further south on the Shattuck Valley wall (fig. II-6). The occurrence of crossbedded sand-rich ooid grainstone within the Grayburg Formation lowstand wedge and 115 ft below the top of the karsted San Andres platform suggests that the magnitude of relative sea-level fall is closer to 115 ft and possibly as much as 200 ft (measured section 6, fig. II-6).

### *Lowstand/Transgressive Systems Tract (LTST)*

Using the framework shown in figure II-4, the seaward part of the LTST is exposed only on the Western Escarpment in the Blue Ridge/Bush Mountain area, where it is approximately 800 ft thick and interfingers with the underlying Cherry Canyon sandstone in a toe-of-slope position (Franseen and others, 1989). Only the uppermost part is truncated by the major basin-bounding Grayburg/Queen sequence boundary (Fekete and others, 1986, Franseen and others, 1989).

Shattuck Valley sections contain only the uppermost 150 ft of the LTST (fig. II-6). Here the LTST is made up of at least 10 parasequences, dominated by fusulinid-peloid packstone to dolomitic sandstone parasequences succeeded upward by those with crossbedded sand-rich ooid-peloid grainstones and rare fenestral wackestones of the uppermost LTST (sections 5 through 7, fig. II-6). In more updip parts of the LTST (sections 1 through 4, fig. II-6) parasequences contain only peloid packstone to fenestral wackestone facies. In Last Chance Canyon the LTST is considered to be that section beneath the ooid-shoal complexes (see below), which approximates maximum flooding in this area. Here sand-based, peloid packstone capped parasequences are largely of shallow subtidal origin, having only one of the parasequences aggrading to tidal-flat conditions where observed near the interpreted terminal San Andres shelf margin.

### *Maximum Flooding Surface*

Maximum flooding is represented in the Shattuck Valley area by a single fusulinid-peloid packstone-based parasequence in sections 1 through 4, which can be traced seaward through sections 5 through 8 with confidence. Downlap onto this surface cannot be observed in the Shattuck Valley area because the limited accommodation space on the platform top did not allow development of clinoforms. In Last Chance Canyon this surface is interpreted to lie at or

near the top of a set of stacked ooid grainstone capped parasequences in the middle of the section. These grainstones appear to mark the most seaward facies tract in this area, and their vertical stacking indicates moderate to high accommodation space associated with transgression.

### *Highstand Systems Tract*

On the Western Escarpment the upper 450 ft of section is inferred to be highstand, assuming a position of the maximum flooding surface not far above the top of the lowstand systems tract oolitic sandstones. This assumption, as well as other inferences concerning the Grayburg on the Western Escarpment, is drawn from the discussion by Franseen and others (1989) of their G-1 section. Lack of knowledge of the direct correlation between this area and the remainder of the Grayburg outcrops in the Guadalupes must limit the confidence of this lithostratigraphic correlation.

Most of the Grayburg outcrop in the Algerita/Shattuck Valley area and in the Last Chance Canyon area (where the outcrop reference section of the Grayburg Formation is described [Moran, 1954]) is within the highstand systems tract (fig. II-6). The exposed part of the highstand systems tract varies in thickness from 220 ft in the northern Shattuck to at least 400 ft in the southern Shattuck Valley, and is 250 ft thick in the downdip (eastern) part of Last Chance Canyon.

The excellent exposures of the Shattuck Valley area permit detailed examination of lateral facies changes within parasequences, as well as the stacking pattern of these parasequences within the sequence framework (figs. II-8 through II-12). Discussion of lateral facies associations and the relation to subsurface reservoir development are presented later in this chapter in the section on parasequence framework of the outcrop model.

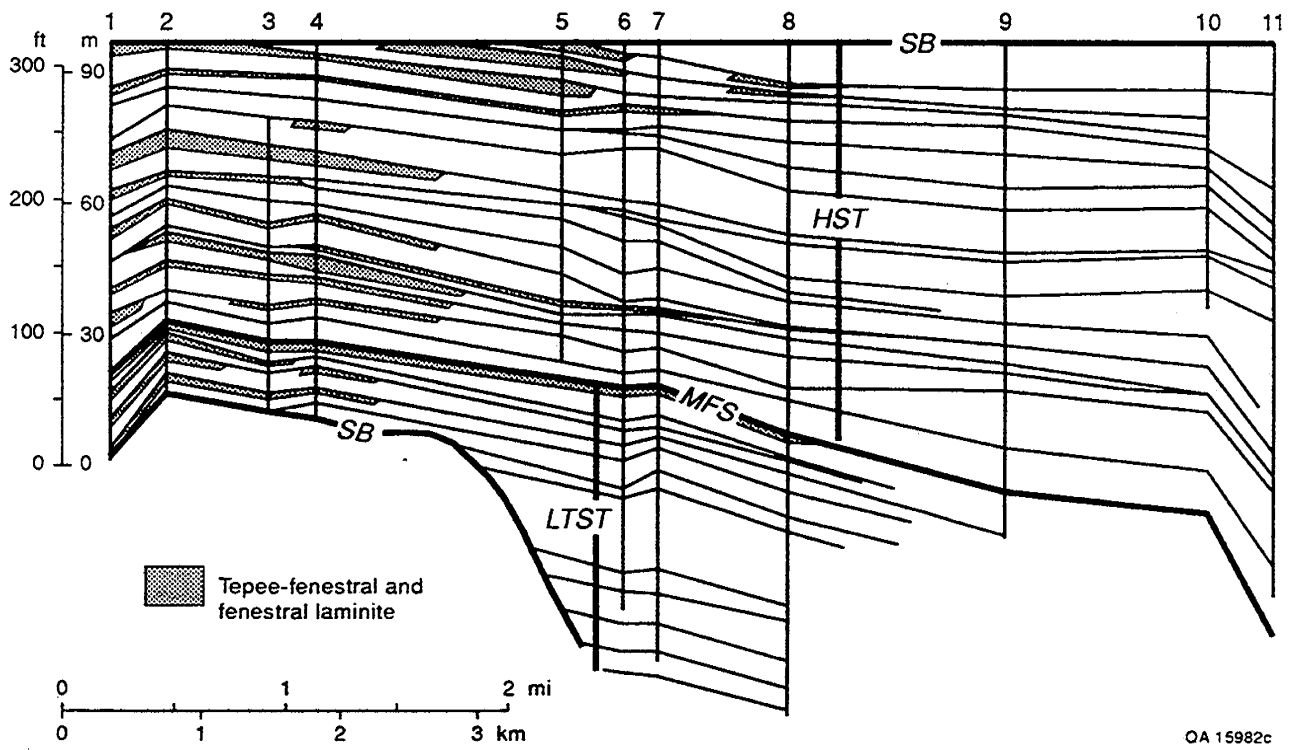


Figure II-8. Distribution of fenestral/tepee facies within Grayburg parasequence framework. Note the restriction of this facies to the updip portions of the cross section.

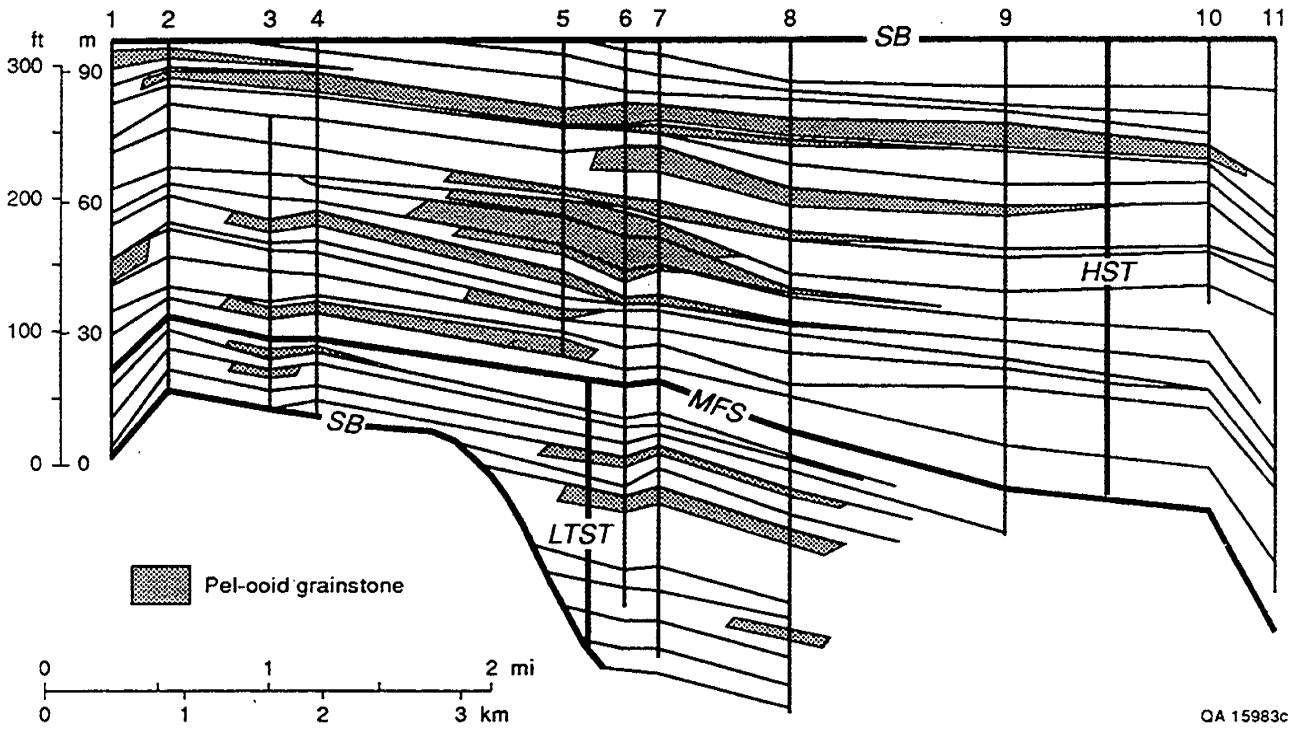
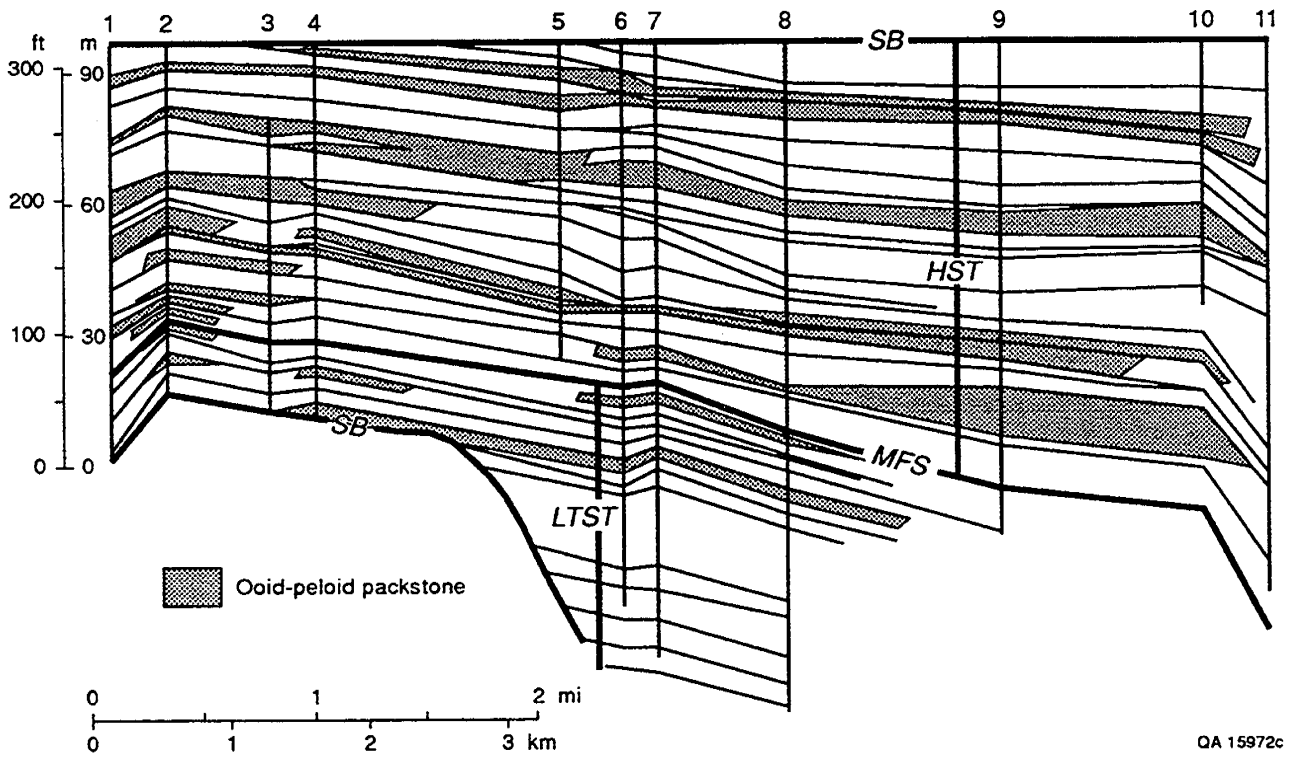
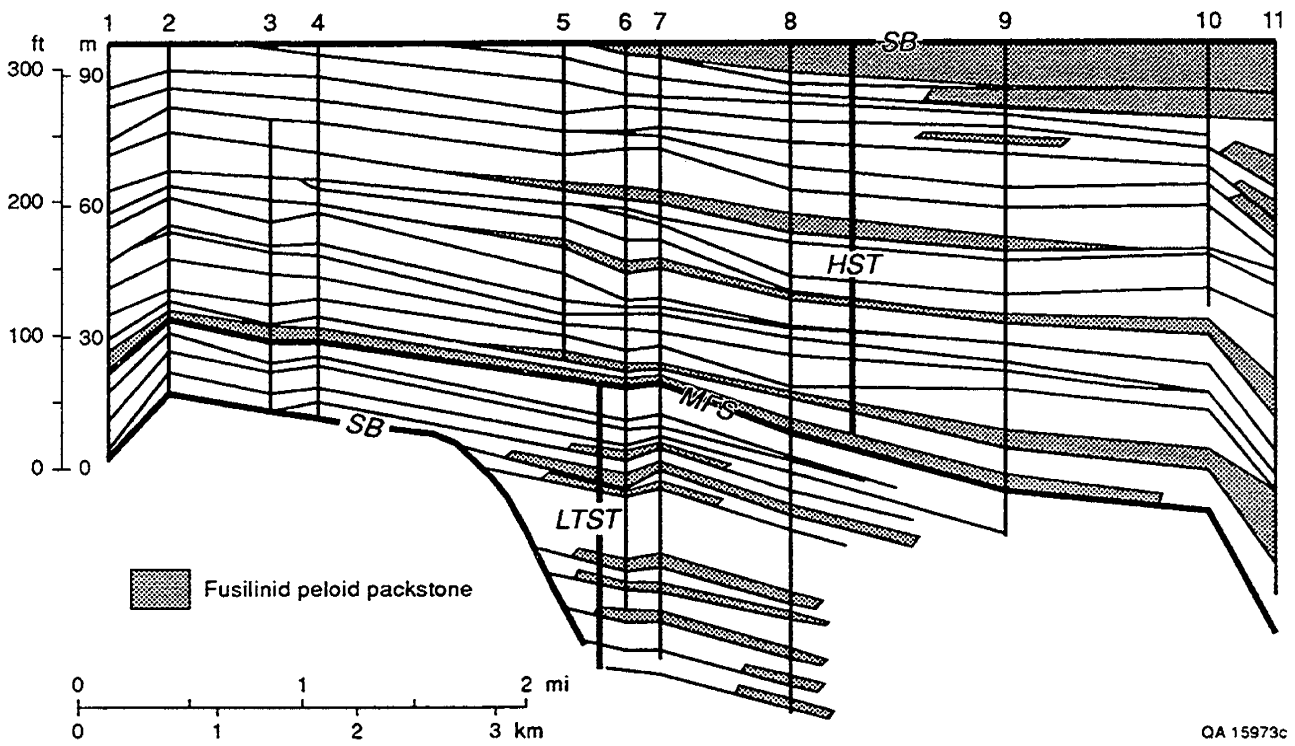


Figure II-9. Distribution of ooid grainstone facies within Grayburg parasequence framework. Note the position of thickest grainstone development coinciding approximately with the projected terminal San Andres shelf margin.



QA 15972c

Figure II-10. Distribution of ooid-peloid packstone facies within Grayburg parasequence framework.



QA 15973c

Figure II-11. Distribution of fusulinid-peloid packstone facies within Grayburg parasequence framework.

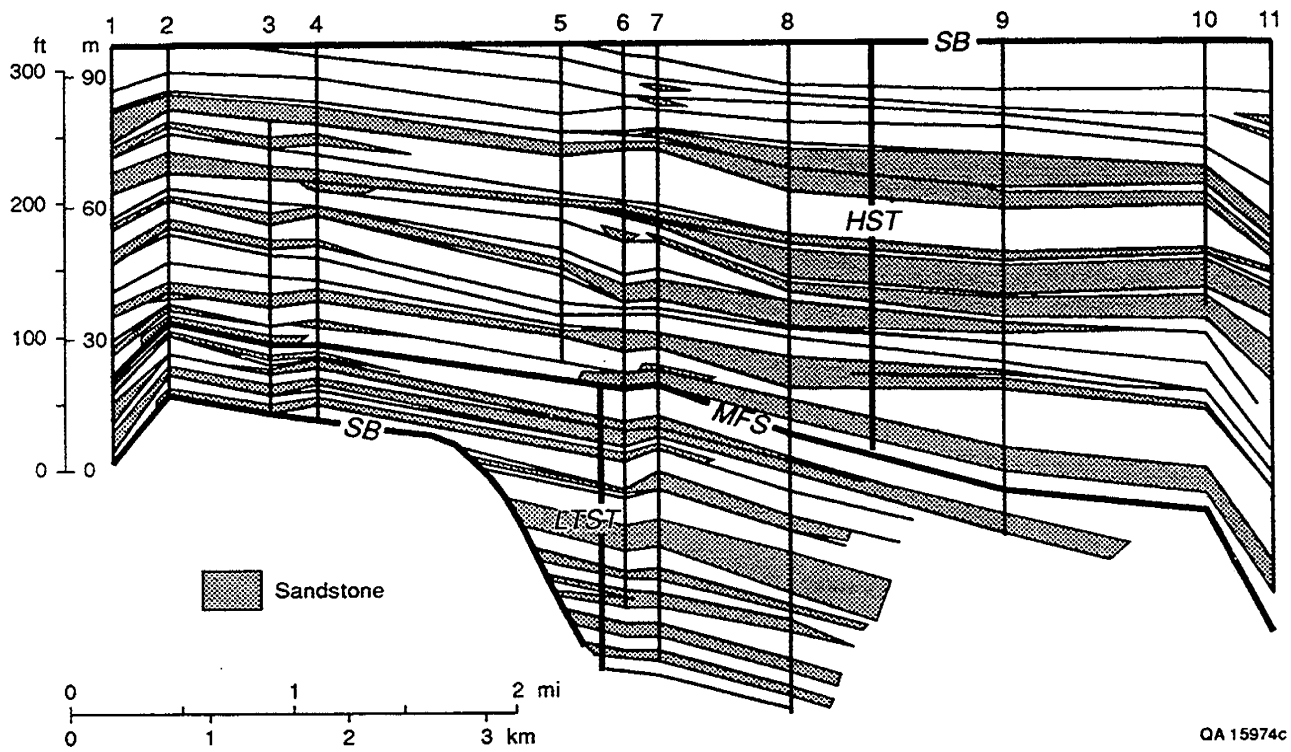


Figure II-12. Distribution of sandstone facies within Grayburg parasequence framework.

### *Grayburg/Queen Sequence Boundary*

The base of the Queen Formation as it overlies the Grayburg Formation is defined by Hayes (1964) as the base of a locally conspicuous sandstone. In the Shattuck Valley area the Grayburg-Queen contact of Hayes (1964) corresponds to a genetically significant karst surface interpreted here to be correlative with the erosion surface mapped between these units on the Western Escarpment (fig. II-4 of Franseen and others, 1989). Karst is only locally developed, however, and cannot be used on a regional basis to recognize this surface. It is considered likely that the Grayburg/Queen sequence boundary is variably mapped in areas lacking unequivocal karst or continuous outcrops linked to the contact.

### REGIONAL RESERVOIR ARCHITECTURE WITHIN A SEQUENCE FRAMEWORK

Development of a simple three-part classification for Grayburg reservoirs is now possible using knowledge of the outcrop sequence framework and basic information concerning dominant productive lithology and position relative to the postulated shelf margin of these reservoirs. This classification includes (1) highstand carbonate sandbar subplay, (2) mixed highstand siliciclastic and carbonate sandbar subplay, and (3) lowstand mixed clastic/oolitic subplay (fig. II-5). A spectrum of intermediate reservoirs exists within the highstand systems tract subplays, but the general pattern is for production from sandstone/siltstone to dominate on the Northwest Shelf and northernmost Central Basin Platform, whereas highstand carbonate production dominates from just south of the North Cowden Grayburg to McElroy (fig. II-5). Lowstand carbonate production is attributed to a discrete family of Grayburg reservoirs situated immediately east of the Central Basin Platform in southeastern Andrews County. The dominant reservoirs in this subplay are Mabee and Midland Farms, but Midland Farms East and other minor production reservoirs are also ascribed to this trend.

Reservoirs of the siliciclastic subplay contain very fine sandstone to siltstone beds ranging from 1 to 25 ft thick that have a variety of degrees of continuity. These sands commonly

appear to amalgamate and then split within the same reservoir, making mapping difficult. The relative importance of siliciclastic production from the Grayburg of the Northwest Shelf is consistent with the source of siliciclastic detritus coming off the Pedernal Uplift to the north and west of the Guadalupe Mountains. This increase in sand content in the Grayburg highstand systems tract is particularly apparent if one compares the importance of sandstone in the Guadalupe outcrop study (fig. II-12) with that described from the North Foster Grayburg unit, a member of the carbonate-dominated highstand subplay situated on the eastern side of the Central Basin Platform.

The carbonate-dominated highstand subplay includes Johnson, North Foster, Cowden South, Waddell, Dune, and McElroy fields (Longacre, 1980; Harris and others, 1984; Bebout and others, 1987). The Big Lake, Farmer, Olson, and World reservoirs on the Ozona Arch are also tentatively included in this subplay, but regional correlation by D. G. Bebout (personal communication) suggests that they may be equivalent to the Queen Formation of the Central Basin Platform. The highstand tract of the carbonate-dominated highstand subplay is characterized by thin (5 to 25 ft) peritidal parasequences of peloid packstone/grainstone that pass off-platform into fusulinid-bearing peloid packstone/grain-dominated packstone. Siliciclastics are 1- to 2-ft thick, burrowed to ripple-laminated siltstone. Carbonate grainstone to grain-dominated packstone is the most important reservoir facies in this subplay, and a common trend toward increased production on the seaward margin of these reservoirs appears to reflect enhanced porosity and permeability associated with late-diagenetic leaching (see chapter IV).

The lowstand mixed lithology subplay is not as well represented, with Midland Farms and Mabee reservoirs (Friedman and others, 1990) being the only two examples having produced more than 10 MMbbl. Eastern parts of the Means San Andres unit are also considered to be genetically within this subplay. In the discussion of the outcrop sequence model, it was demonstrated that a substantial part of the Grayburg Formation was deposited in a lowstand prograding wedge below and basinward of the terminal San Andres Formation ramp margin.

Without pertinent reflection seismic data, it is difficult to definitively document the lowstand character of Mabee or Midland Farms reservoirs, but well logs and structure maps show that these reservoirs are situated below the terminal San Andres shelf margin. It is interesting to note that both reservoirs also have a high proportion of oolitic grainstone not seen in highstand systems tracts of either San Andres or Grayburg affinity. In addition, both show gradational contact below with siliciclastics of basinal affinity, in contrast to Grayburg reservoirs of the Central Basin platform that rest atop subaerially exposed San Andres lithologies (see discussion of North Foster, chapter IV). Finally, these reservoirs are only partially dolomitized, in contrast to their pervasively dolomitized counterparts on the Central Basin Platform and Eastern Shelf. Absence of pervasive dolomitization is most likely related to the isolation of these lowstand strata from regional reflux systems of the highstand platforms.

The selective development of this high-energy facies tract within the lowstand prograding wedge probably represents focused wave/current energy on the narrow lowstand platform that developed directly exposed to the relatively deep water of the Midland Basin. Better definition of the Grayburg lowstand subplay awaits publication of additional data on these reservoirs, but it is clear that significant differences exist and can best be explained by analogy with a lowstand prograding complex.

#### Reservoir-Scale Parasequence Framework

Ongoing outcrop and subsurface description and modeling of San Andres reservoir facies (Kerans and others, 1991; Lucia and others, 1991; Senger and others, 1991) have demonstrated that fluid-flow patterns in subsurface reservoirs are controlled in part by the vertical and lateral distribution of rock-fabric facies within a stacked assemblage of upward-coarsening parasequences. A second key conclusion of the studies cited above is that permeability structure within a rock-fabric facies of a single parasequence typically demonstrates a homogeneously heterogeneous pattern and that this pattern can be represented effectively

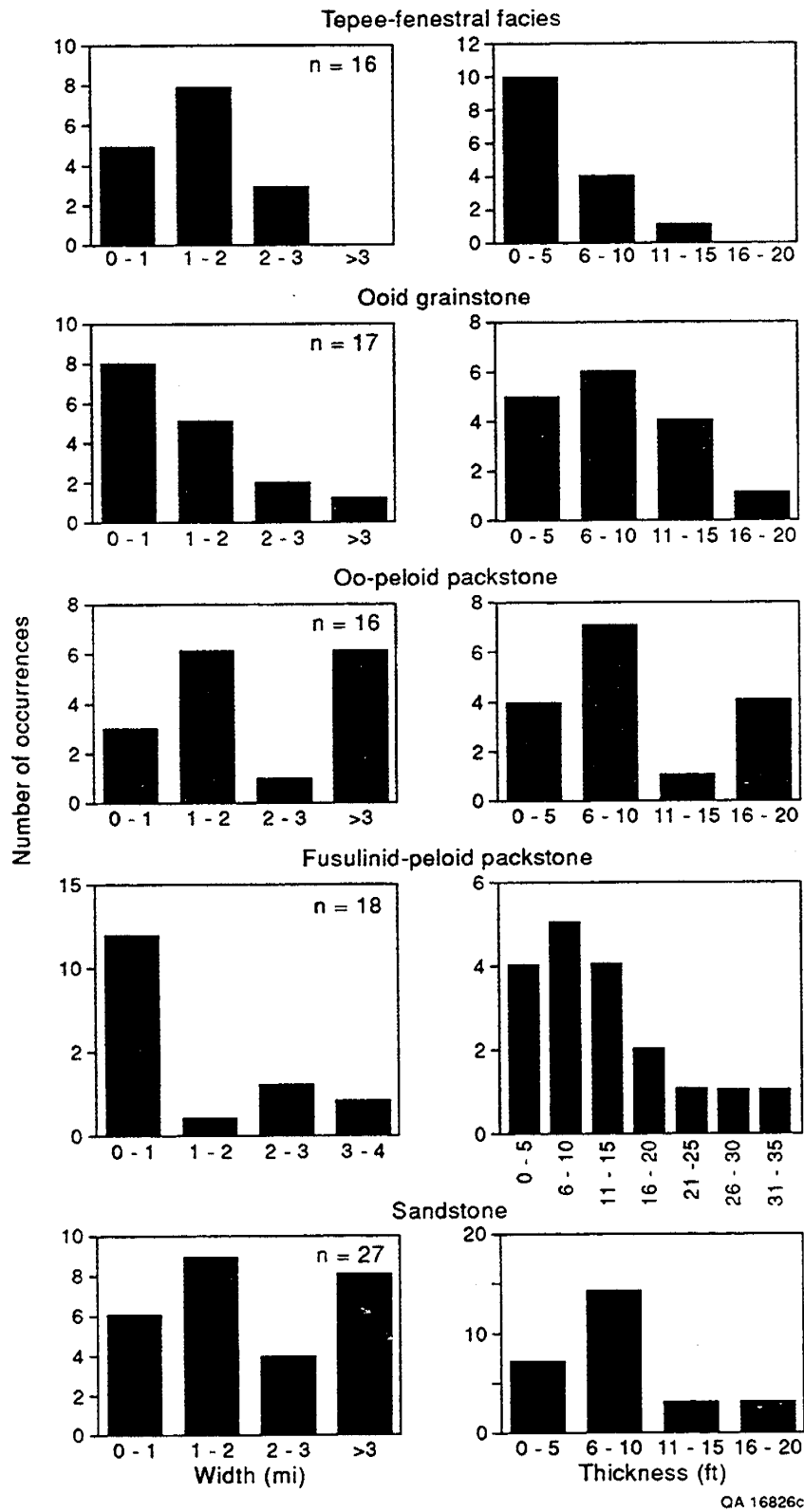
through a geometric mean of the permeability measurements within that facies. The significance of this observation is that if standard dimensional statistics could be generated for rock-fabric facies elements, then stochastic models of carbonate reservoir architecture comparable to those now being generated for siliciclastic reservoirs (Haldorsen and Damsleth, 1990) could be developed. Until now, however, such dimensional data was not available for carbonate facies because of the absence of detailed description and because of the complexities inherent in carbonate facies analysis, where the overprint of depositional fabrics by diagenetic processes can mask critical relationships. The data set presented here represents one of the few attempts to map in detail carbonate parasequences and their internal facies heterogeneity as they cross through different facies tracts in a landward to seaward profile.

Cross sections showing the distribution of facies in the parasequence framework (1) outline the platform-scale facies tracts and their dimensions, (2) demonstrate the progradational nature of the highstand tract and aggradational to retrogradational nature of the LTST, (3) provide dimensional data on individual facies for use in modeling exercises (fig. II-13), and (4) demonstrate the potential internal complexities of the highstand parasequence sets with their internal onlap, toplap and erosional truncation. Facies characteristics are summarized in table II-2, and the distribution of facies across the Shattuck profile is shown in figures II-8 through II-12. These facies distributions define four broad facies tracts in which the highstand tract is arranged in a progradational parasequence set (fig. II-14).

The inner shelf is predominantly low-energy mixed siliciclastics and mud-dominated carbonates that extend landward for an undefined distance. The inner-shelf crest is that part of the shelf that witnessed repeated subaerial exposure and development of fenestral and tepee-fenestral facies. This facies tract is 2 mi wide and prograded 1 mi seaward during the highstand deposition. The outer-shelf crest facies tract is outlined by a 1.5-mi-wide seaward-stepping zone dominated by ooid grainstone shoals. The cross section of these grainstones (fig. II-9) shows the

Table II-2. Attributes and environments of standard Grayburg facies types.

FACIES	STRUCTURES	ALLOCHEMS	DIMENSIONS thickness (ft), dip width (mi)	ENVIRONMENT	WATER DEPTH RANGE (ft)
sandstone, crossbedded	small-medium- scale trough cross- strat., ripple lam.	rare fusulinids	1-20, 0-5	inner-shelf crest, outer-shelf crest	0-25
sandstone, massive	massive		as above, not separated	inner shelf-outer shelf	0-100
fusulinid-peloid packstone	massive, vertically burrowed	fusulinids, pelmatzoa, peloids, sand	1-35, 0-5	outer shelf	25-100
peloid packstone	massive	peloids w/minor composite grains, pisolites, ooids, sand, pelmatzoa	as below, not separated	inner shelf to outer shelf	0-100
oid-peloid packstone	massive to bioturbated	peloids, ooids, pelmatzoa, brachiopods, algae	1-20, 0-4	shelf crest to inner-outer shelf	0-100
pel-oid grainstone	crossbedded	ooids, peloids, w/minor pelmatzoa and algae	1-20, 0-3	outer shelf crest	0-25
peloid wackestone/ mudstone	massive, faint parallel lamination	peloids		inner shelf,shelf crest flooding	0-30
fenestral laminite	fenestrae, smooth algal laminae	pisolites, rip-ups, peloids, ooids	1-15, 0-2.5	inner-shelf crest	0 - +3
tepee-fenestral	fenestrae, tepees, sheet cracks, internal sediments	pisolites, peloids	as above, not separated	inner-shelf crest	0 - +3



QA 16826c

Figure II-13. Dimensional data for the five generalized Grayburg facies in terms of average thickness (ft) and maximum dip-oriented dimension (mi).

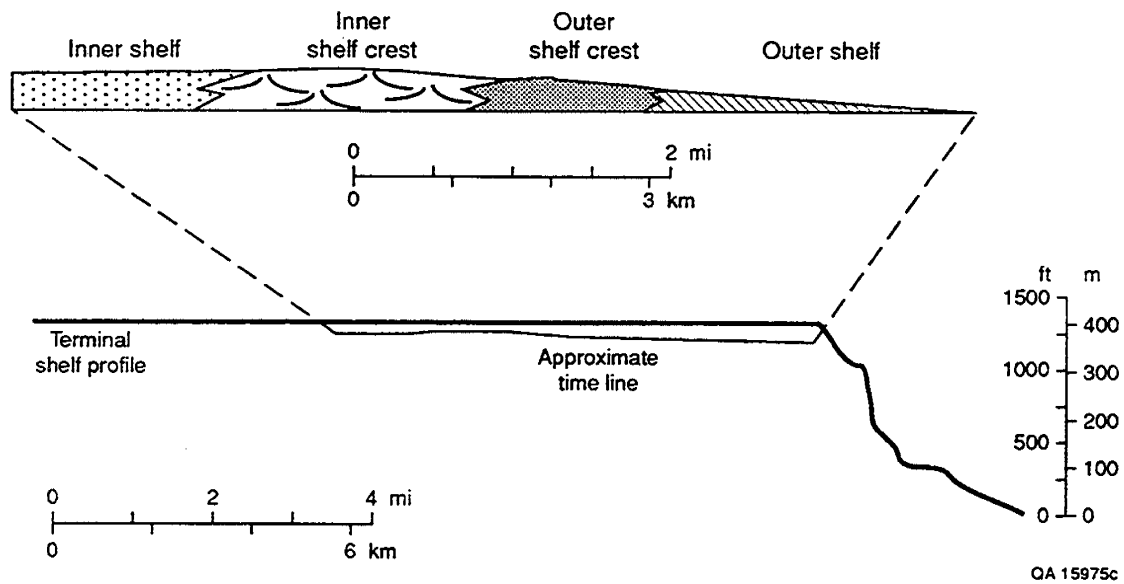


Figure II-14. Simplified profile of the Grayburg highstand systems tract as exposed in the Guadalupe Mountains. Generalized water depths for the profile are 0 to 10 ft for the inner shelf, 0 to +3 ft for the inner shelf crest, 0 to 25 ft for the outer-shelf crest, and 25 to 100? ft for the outer shelf.

progradational character of the Grayburg highstand systems tract. The outer shelf is that part of the profile seaward of the outer-ramp crest out to the shelf-slope break (not exposed in Grayburg highstand outcrops) that is characterized by the ooid-peloid packstone and fusulinid-peloid packstone facies.

In addition to providing a clear picture of retrogradation, aggradation, and progradation of the Grayburg sequence, the parasequence framework provides a means of determining the geometry and dimensions of carbonate facies. These dimensional data (fig. II-13) are best collected within the higher resolution of the parasequence framework because this minimizes effects of averaging data across time lines. Although small in number, these data represent the starting point for developing a set of standard carbonate facies dimensional data for use in reservoir and stratigraphic modeling.

Particularly relevant for the carbonate sandbar facies, the focus of this report, are the histograms and cross sections of the ooid grainstone and ooid-peloid packstone facies. The ooid grainstone element of each parasequence represents the preserved active grainstone complex of that parasequence. Many of these grainstones have relatively high porosity and permeability, but others may be cemented tight by anhydrite (in the subsurface) or dolomite (see chapter III) and thus act as flow barriers.

The ooid grainstones, which can be distinguished in cores by the presence of cross-stratification and absence of mud matrix, have the greatest thickness to width ratios, or essentially have minimal dip continuity. Some ooid grainstones decrease from 20 ft thick to pinch out in less than 2,000 ft in a dip direction but most grainstone bodies mapping were continuous for greater than 2,000 ft (fig. II-9). Although no data exist for strike-parallel continuity of these grainstones, analogy with modern settings (Ball, 1967; Harris, 1979) suggests that equal or greater discontinuity may be encountered, such as occurs in ooid tidal bar belts.

Ooid-peloid packstone facies are as important, if not more important, in producing Grayburg reservoirs of the carbonate highstand type (Longacre, 1980; Harris and others, 1984; Bebout and others, 1987; and chapter IV of this report). These facies are recognized in core by

their massive appearance, grain-rich character, and paucity of bioclastic material. They are interpreted to represent reworked material derived from active ooid sand bars, and their dimensions reflect this, being thinner and more tabular in external geometry than the ooid grainstones. Although porosity and permeability are generally less than that of the ooid grainstones, the greater continuity (typically greater than 3,000 ft) suggests better interwell connectedness in the subsurface.

Sandstone geometry within the outcrop parasequence framework from the Shattuck escarpment is also very instructive for reservoir characterization in reservoirs of the siliciclastic-dominated highstand subplay (fig. II-5). Sandstone facies analysis in shelf reservoirs of the Grayburg or throughout the Guadalupian can be complicated by the narrow range in grain size and absence of sedimentary structures in these deposits. Grain size limitation is a result of eolian reworking prior to final deposition, whereas the absence of sedimentary structures is caused by extensive bioturbation as sandstones are transgressed.

Two different size populations of sandstones appear on the cross section and histograms (figs. II-12 and II-13). Those sandstones deposited in the inner-shelf through outer-shelf crest parts of the highstand systems tract (fig. II-14) are discontinuous on the scale of hundreds of feet and are relatively thin. Sandstones in the inner- and outer-shelf crest positions are commonly channel-form, filling topography between thicks in grainstone bars. Again, strike variability (not investigated in this study because of lack of outcrop) may produce a high degree of lateral variability in sandstone geometry. In the outer-shelf position, sandstones become thicker and more continuous in a dip profile (fig. II-12), and it is anticipated that this continuity is comparable in strike-oriented profiles.

Recognizing these different sandstone types can be instrumental in constructing a reservoir architecture, particularly in reservoirs of the siliciclastic-dominated highstand type. The massive homogeneous character of these sandstones would limit the ability to predict sandstone geometry on the basis of core or log descriptions. However, recognition of position

in the carbonate shelf profile should prove a powerful tool for predicting sandstone geometry, as shown in this discussion.

CHAPTER III: FACIES ARCHITECTURE AND INTERNAL GEOMETRY  
OF A MIXED SILICICLASTIC-CARBONATE DEPOSITIONAL SEQUENCE:  
GRAYBURG FORMATION, STONE CANYON, NEW MEXICO

H. S. Nance

INTRODUCTION

Analyzing the architecture of reservoirs situated in carbonate platform strata traditionally involves defining and correlating stratigraphic "zones" on the basis of the occurrence of similar well-log responses at several wells. In the Permian Basin, gamma-ray logs with sonic, formation density, or neutron logs are most often used to define zones. In a reservoir, however, no direct data are available on lithologic and petrophysical properties between wells. Outcrop investigations in carbonate terranes have shown that stratigraphic zones are characterized by complex associations of different rock types having varying geometries and petrophysical properties that change over short distances relative to well spacing in oil fields. Such changes profoundly affect fluid flow and, thus, the producibility of hydrocarbons. The internal complexity of these zones is typically beyond the resolution of well-log or surface-based reflection seismic data. In spite of this limitation, calculations of interwell rock properties are made by assuming that lithologic and petrophysical characteristics between wells are gradational.

Low recovery efficiency arises when lithologic variability between wells limits primary and secondary (water flooding) production of oil (Bebout and others, 1987). Much, if not most, of the oil is trapped in less permeable rocks or uncontacted compartments, whereas primary production and subsequent flooding tends to sweep the more permeable rocks. Continued flooding results in repeated sweeping of the same flow paths, resulting in an increase in water/oil ratios over time. Isolated oil-rich compartments between wells may remain untapped

and unswept. Our knowledge concerning lateral continuity of reservoir-quality facies, petrophysical properties, and the nature and geometries of compartments is inadequate to optimize production efficiency.

Strata deposited in specific carbonate depositional environments (for example, inner shelf, outer shelf, slope, and so forth) are composed and organized in different, but generally predictable, ways. The challenge for petroleum geologists and engineers is to identify from typical subsurface data sets correlatable, thus mappable, geologic units characterized by predictable facies distributions and petrophysical attributes. This investigation is based on the premise that outcrop observations of facies, with their geometries and petrophysical properties, can be adapted to hydrocarbon reservoirs developed in similar depositional settings in the Permian Basin.

Other studies (chapter II) have identified the upward-shoaling depositional cycle, or parasequence (term of Van Wagoner and others, 1988), as the fundamental cyclic genetic unit composing the Grayburg depositional sequence. Parasequences have generally predictable internal architectures comprising both reservoir-quality and nonreservoir-quality rocks. Each parasequence records sedimentary filling of space created by combined effects of eustatic sea-level rise and subsidence. Parasequences comprise genetically related rock types (facies) whose properties and geometries depend on their geographic positions in the original depositional environment. A host of conditions controls component facies compositions and geometries, including climate, dominant wind directions, rates of relative sea-level change, availability of terrigenous sediments, topography inherited from previous depositional events, and postdepositional processes of erosion and diagenesis.

As defined by Van Wagoner and others (1988), parasequences are bounded above and below by marine-flooding surfaces that represent periods of nondeposition. This means that parasequences are asymmetric; each parasequence records rapid deepening followed by relatively gradual shallowing of the depositional environment as accommodation space (volume created by combined effects of eustatic sea-level change and benthic subsidence) is filled

essentially to sea level, then followed by a nondepositional period before abrupt deepening (marine transgression), leading to deposition of the next parasequence. Strictly defined, a parasequence contains no record of gradual return to deeper marine conditions at its top. As will be shown, most Grayburg depositional cycles observed in Stone Canyon accurately fit the definition of parasequence. Platform strata in other Guadalupian depositional sequences in the Permian Basin, including the petroliferous San Andres, Queen, and Yates Formations (Guadalupian), as well as sequences in the Leonardian Series, are dominated by this asymmetrical packaging.

Our studies also place outcropping Grayburg strata in a sequence-stratigraphic framework that organizes sets of parasequences into sea level-lowstand (LST), transgressive (TST), and highstand (HST) depositional systems tracts (chapter II). A systems tract comprises several similarly composed parasequences in which specific sedimentary facies in succeeding cycles are stacked in patterns caused by relative sea-level changes. For example, a given facies (for example, shoal grainstones) might occur progressively seaward in succeeding parasequences if relative sea level is static or falling (=HST). Organization of sets of parasequences into systems tracts is based upon these facies-stacking patterns (Van Wagoner, 1985).

Consequently, strata with comparable reservoir quality are generally stacked in patterns that indicate their positions in the sequence-stratigraphic framework. Specific facies within the LST and the TST tend to backstep, that is, occur progressively more upslope depositionally through succeeding parasequences. Within the HST specific facies tend to prograde, that is, step basinward, upward through the section. These principles provide petroleum geologists a predictive tool with which to target drilling once the position of a reservoir within the sequence-stratigraphic framework is determined.

The investigation reported here was designed to establish continuity of component depositional and diagenetic facies in Grayburg parasequences previously identified (as discussed in chapter II) as well as continuity of their petrophysical properties over typical interwell distances (<2,000-ft lateral separation). The subjects of this study are reservoir-analogous

parasequences developed in an inner-shelf crest setting comprising mixed siliciclastic-carbonate marine strata deposited in shallow subtidal, intertidal, and supratidal environments.

### Geologic Setting and Sequence Stratigraphy of the Grayburg in Stone Canyon

The Grayburg Formation in Stone Canyon (fig. III-1) is 310- to 325-ft thick, comprising interbedded dolomitic sandstones and dolostones (figs. III-2 through III-4). The underlying San Andres Formation is not exposed in Stone Canyon but outcrops nearby to the north and east, where its karst-modified surface unconformably underlies basal sandstone beds of the Grayburg Formation. It is impossible to trace the lowermost Grayburg beds out of Stone Canyon, but similarities in thickness between the Stone Canyon section and other Grayburg sections nearby, where the contact with the San Andres is exposed, suggest that the San Andres is about 10 ft below the canyon floor.

The Grayburg Formation unconformably underlies 80 ft of Queen Formation dolostone and siliciclastics in Stone Canyon. The top of the Grayburg Formation is a karst-modified surface that is correlated to similar surfaces developed on top of the Grayburg exposed on the Shattuck Valley wall to the east and in nearby canyons to the north on Algerita Escarpment.

The occurrence of regionally extensive karst-modified surfaces (sequence boundaries) at both the top and base of the Grayburg Formation qualify it as a probable "type 1 depositional sequence" in the terminology of sequence-stratigraphic analysis (Van Wagoner and others, 1988; Kerans and Nance, 1991). Considered within a sequence-stratigraphic framework, the Grayburg Formation comprises LST and TST deposits (collectively abbreviated as the LTST) and HST deposits. The Grayburg LTST comprises generally aggradational and backstepping facies-stacking patterns developed in response to relative sea-level rising; the HST comprises seaward-stepping, progradational facies-stacking patterns developed during stillstands and fall of relative sea level.

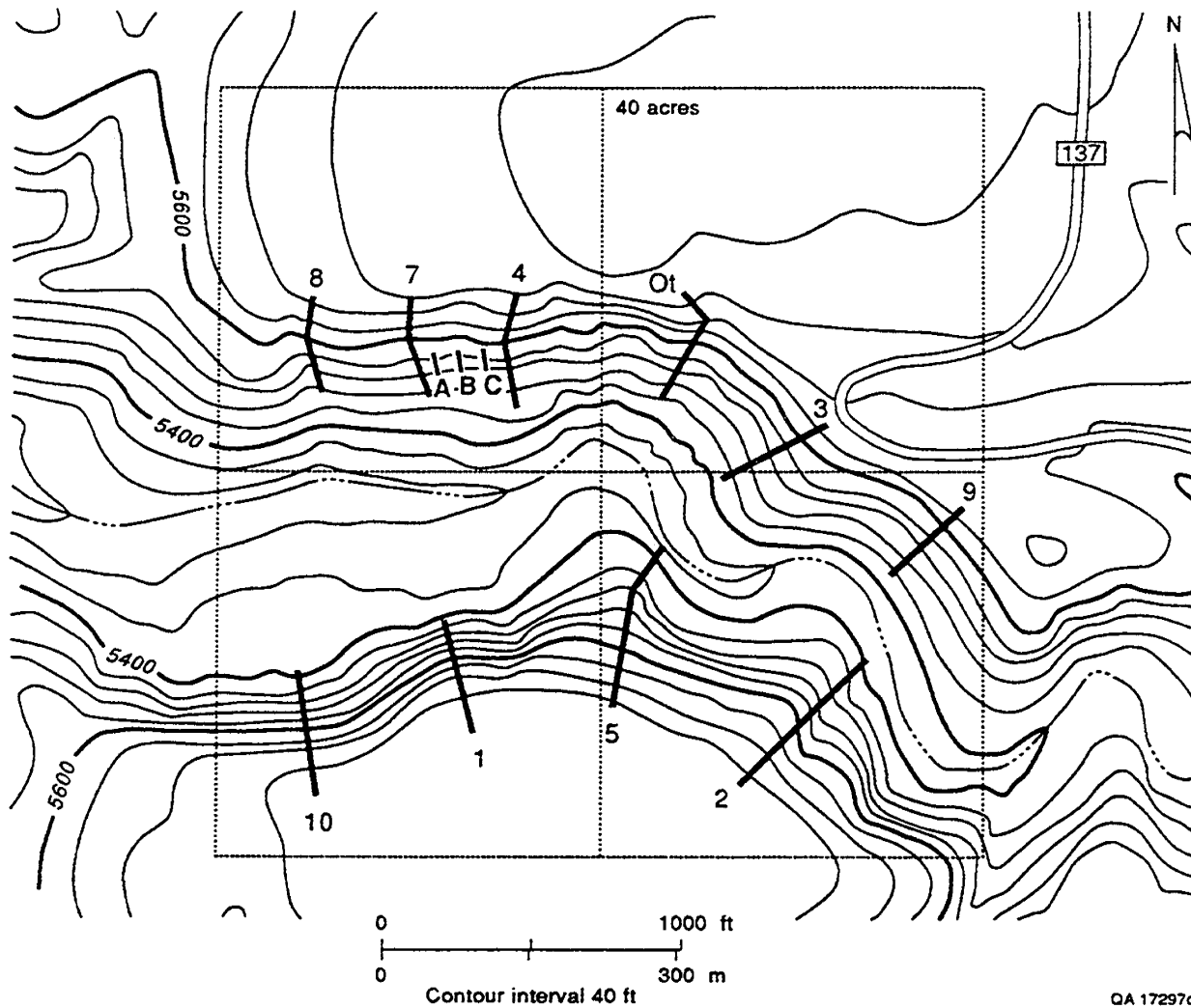
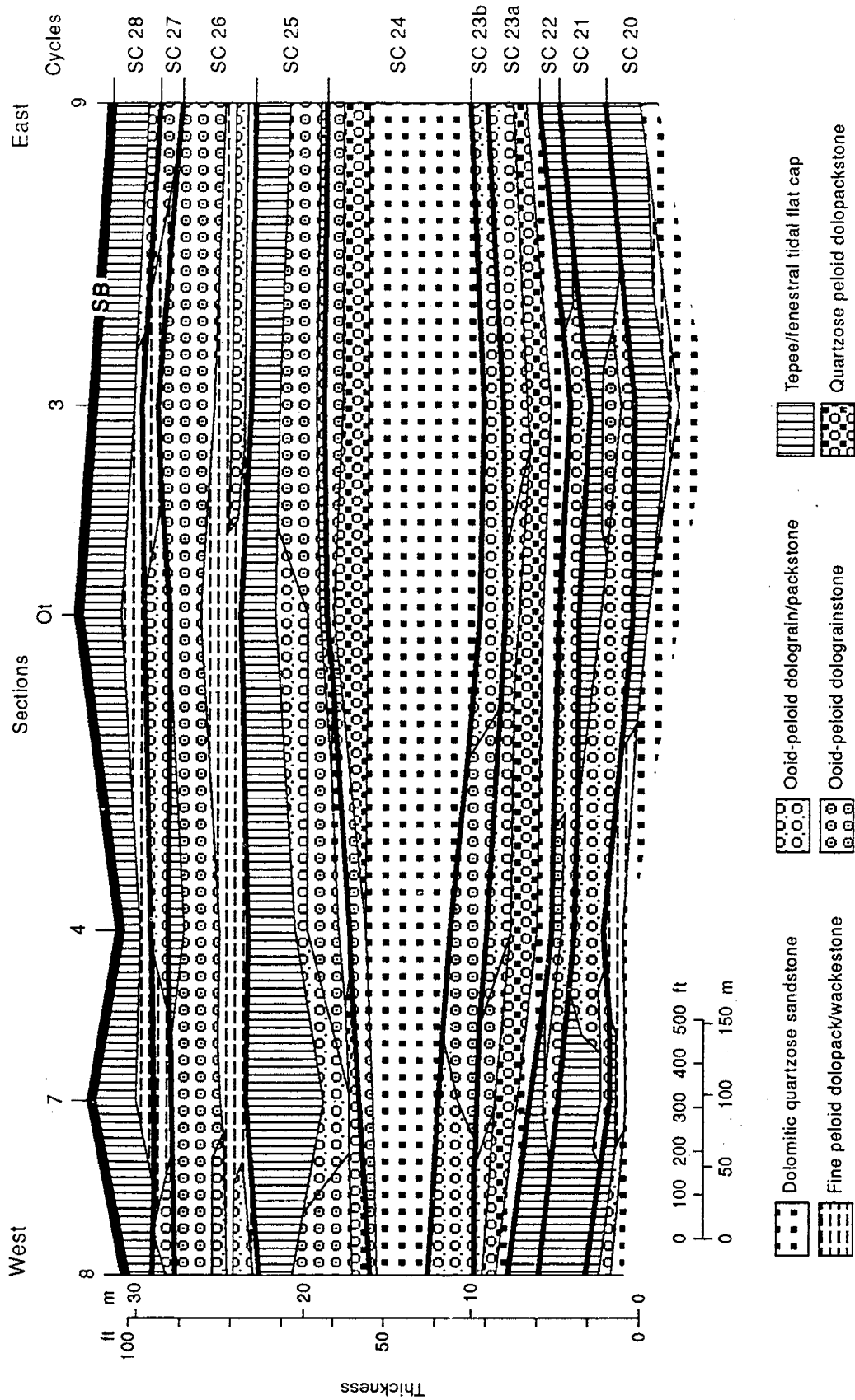


Figure III-1. Topographic contour map of Stone Canyon study area, Eddy County, New Mexico (El Paso Gap Quadrangle, Sec. 19, T 25S, R 21 E) with overlay representing 160 acres to illustrate scale of study area compared with typical oil field well spacing. Also shown are locations of measured sections. Sections A, B, and C are detailed sections through SC 23.



Figure III-2. Photomosaic, looking west from Hwy 137, showing northern (right) and southern (left) walls of Stone Canyon. Arrows indicate (SB) Grayburg/Queen sequence boundary (also visible in foreground), (23) base of parasequence SC 23 (subject of detailed study), and (24) base of channelized sandstone, SC 24. Perpendicular distance between uppermost canyon walls is approximately 1,200 ft. Photo taken from Grayburg-Queen sequence boundary at section 3.



OA 17304c

Figure III-3. West-East stratigraphic cross section of uppermost Grayburg Formation, northern wall of Stone Canyon. Shown are locations of measured sections, generalized facies, parasequence boundaries (thin lines), and Grayburg/Queen sequence boundary (SB, thick line). Subdivision of parasequence SC 23 into SC 23a and SC 23b based upon figure III-7.

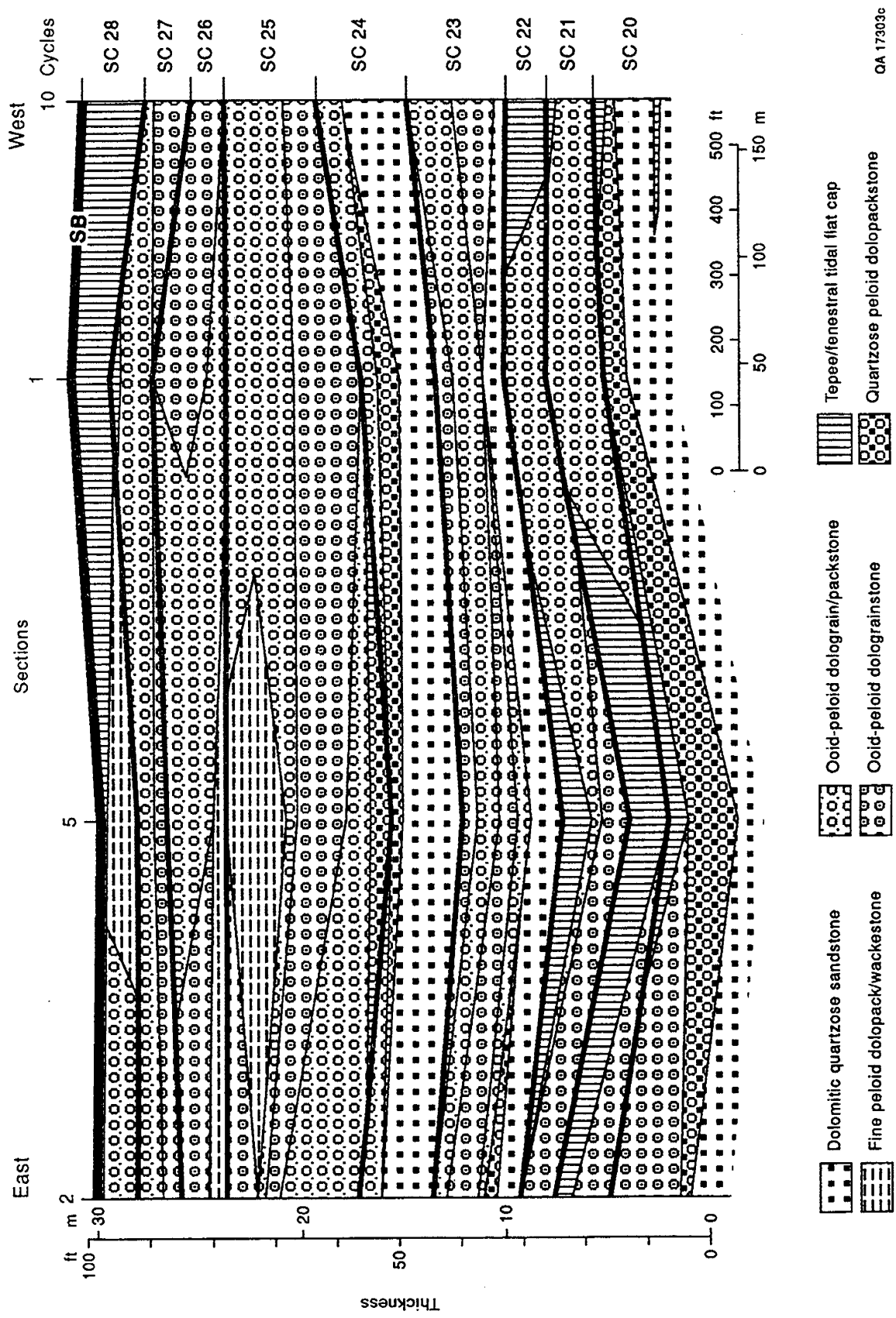


Figure III-4. East-West stratigraphic cross section of uppermost Grayburg Formation, southern wall of Stone Canyon. Shown are locations of measured sections, generalized facies, parasequence boundaries (thin lines), and Grayburg/Queen sequence boundary (SB, thick line). Note relatively thin basal sandstone in SC 24 compared with that in figure III-3.

Within the HST occurs a stack of seaward-stepping shallow water to emergent fenestral-laminated and tepee-structured tidal-flat deposits. Tidal-flat strata are most abundant in the updip parts of the Grayburg study area, including Stone Canyon, and represent the paleotopographically highest parts of the marine inner shelf. The area where these facies are prevalent is called the inner-shelf crest (chapter II). Sandwiched between these generally impermeable tidal-flat deposits are permeable reservoir-quality and less permeable nonreservoir-quality facies. It is within the inner-shelf crest strata at Stone Canyon that detailed studies of parasequence character and facies distributions have proceeded.

### Methods

The basis of this investigation is that relationships between depositional and diagenetic facies and their petrophysical and geometric properties observed in the field can be applied, with reservoir-specific modifications, to hydrocarbon reservoirs developed in similar depositional settings on the Central Basin Platform and shelves that rim the Permian Basin. Methods of outcrop analysis include identification and mapping of individual parasequences from measurement and geologic description of 11 vertical sections including both walls of Stone Canyon (figs. III-1 through III-4). Sections were correlated by tracing beds in the field and on photographs taken of the canyon walls. Where exposures were poor, measured sections were correlated with laterally extensive sandstone marker beds.

Following a general stratigraphic survey a single, representative parasequence was sampled intensively to define more precisely facies types and their distributions and to quantify petrophysical parameters relevant to reservoir analysis, namely porosity and permeability. Within this parasequence about 245 one-inch core plugs were collected from vertical sections along the northern wall of the canyon. Additional samples were collected from grids established in specific facies. Oriented samples were obtained with a portable drill that consisted of a small gasoline-powered chain-saw drive coupled with a one-inch-diameter, water-irrigated, diamond-

studded core barrel. Porosity and permeability analyses were conducted on all samples by Rotary Engineers Laboratory, Midland, Texas. Thin sections of 116 samples were produced for petrographic examination.

Terminology used herein to classify carbonate-dominated rocks follows that of Dunham (1962). Dunham's terms including the following:

- (a) Grainstone—consists entirely of sand-sized or larger ( $\geq 0.0625$  mm) allochems; in grain-to-grain contact (grain-supported) and is free of finer material (mud);
- (b) packstone—grain-supported but with a measurable quantity of mud occurring in pores between allochems;
- (c) Wackestone—allochems are abundant but are suspended in a mud matrix;
- (d) Mudstone—dominated by mud with relatively few allochems present.

Terms are combined when precise classification is not possible. For example, grainstone/packstone describes a rock that is grain supported but whose mud content is not determined. All Grayburg carbonate rock in Stone Canyon has been dolomitized, therefore the prefix "dolo" is added to Dunham's original terms (for example, dolograinstone).

Data developed from engineering analyses and geologic descriptions were mapped and various graphic plots of petrophysical data were produced to illustrate facies/petrophysical relationships.

## RESULTS

The Grayburg Formation at Stone Canyon comprises beds of dolomitic sandstone, quartzose dolostone, and a variety of relatively pure dolostone facies (figs. III-5 through III-7) organized into at least 28 upward-shallowing cycles, or parasequences. Parasequences of the LTST and HST are separated from each other by the maximum flooding surface (MFS). The MFS is at the base of a 6-ft-thick fusulinid dolopackstone bed, the only one in Stone Canyon. This bed (fig. III-5C) occurs within parasequence SC 7, about 80 ft above the canyon floor. The bed is correlated to a



Figure III-5. Outcrop features, Grayburg Formation of Stone Canyon. A. Sandstone-dominated parasequence SC 2 overlying dolostone tidal-flat bed of SC 1. Heavy line marks boundary between SC 1 and SC 2. Lower two sandstone beds are planar- to cross-laminated, lens cap (center) rests in burrowed interval; upper beds are ripple- to cryptogally laminated tidal-flat deposits. B. Ooid-peloid dolograinstone lateral accretion beds (inclined), deposited as subtidal to intertidal bar overlain by flat-lying, fenestraly laminated tidal-flat beds, SC 10. Five-foot staff for scale. C. Fusulinid-peloid packstone bed near maximum flooding surface (MFS). Ball-point pen cap for scale. D. Parasequence SC 23 at section Ot with basal massive to cross-laminated dolomitic quartz sandstone overlain by flaggy, quartzose peloid dolopackstone, in turn overlain by fossiliferous peloid dolopackstone. Upper surface is erosional unconformity between SC 23 and SC 24. E. Multidirectionally cross-laminated ooid peloid dolograinstone on bar crest of SC 23, section 4. Sotol plant is approximately 1.5 ft high. F. Tepee-structured dolopackstone at top of Grayburg. Six-foot stalk for scale. G. Laminated dolopack/wackestone at top of Grayburg. These beds correlate with tepee-structured beds about 200 ft along canyon wall in both directions. H. Karst pockets in darker colored Grayburg rock filled with lighter colored Queen dolomudstone, Grayburg/Queen sequence boundary. Lens cap for scale.

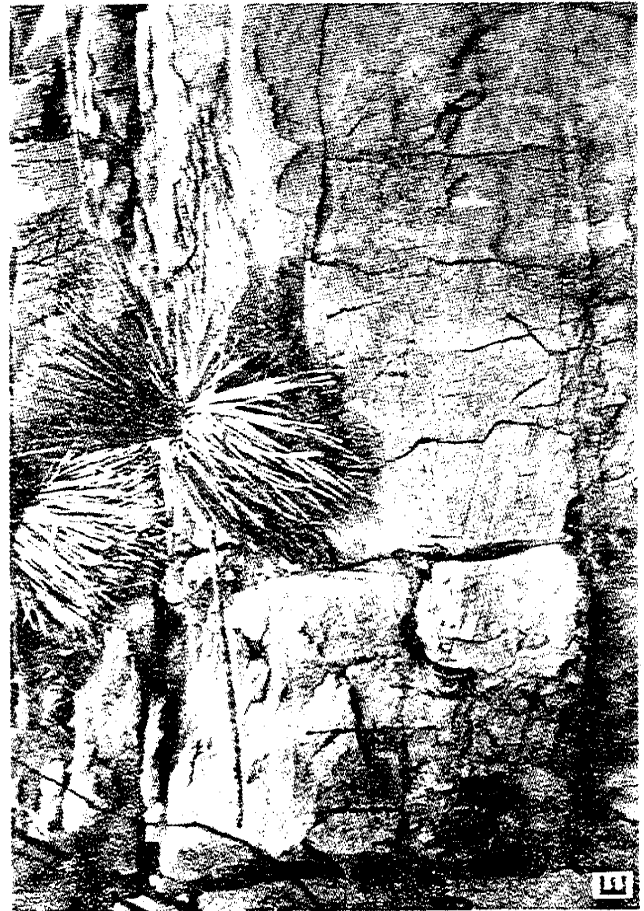
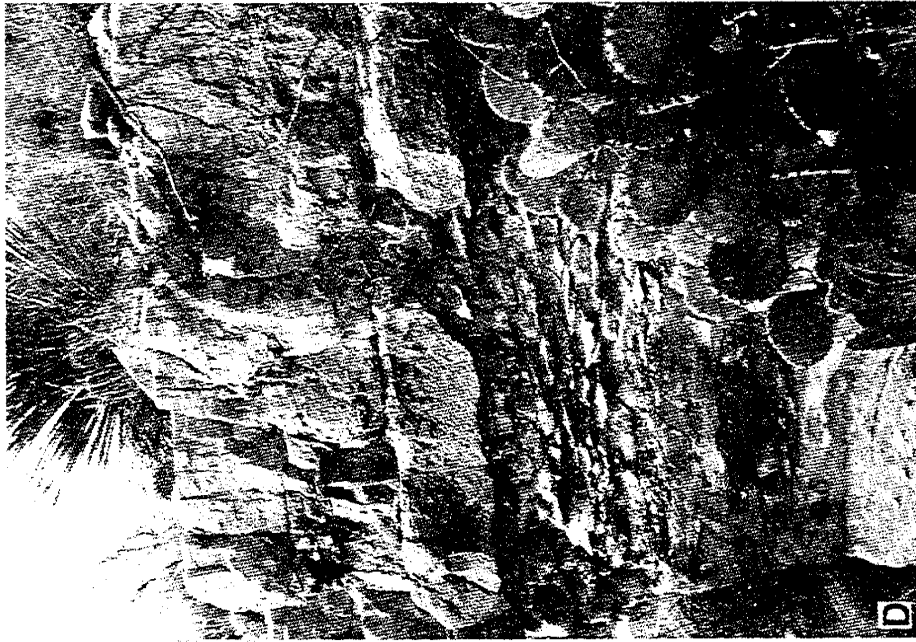


Figure III-5 (cont.)

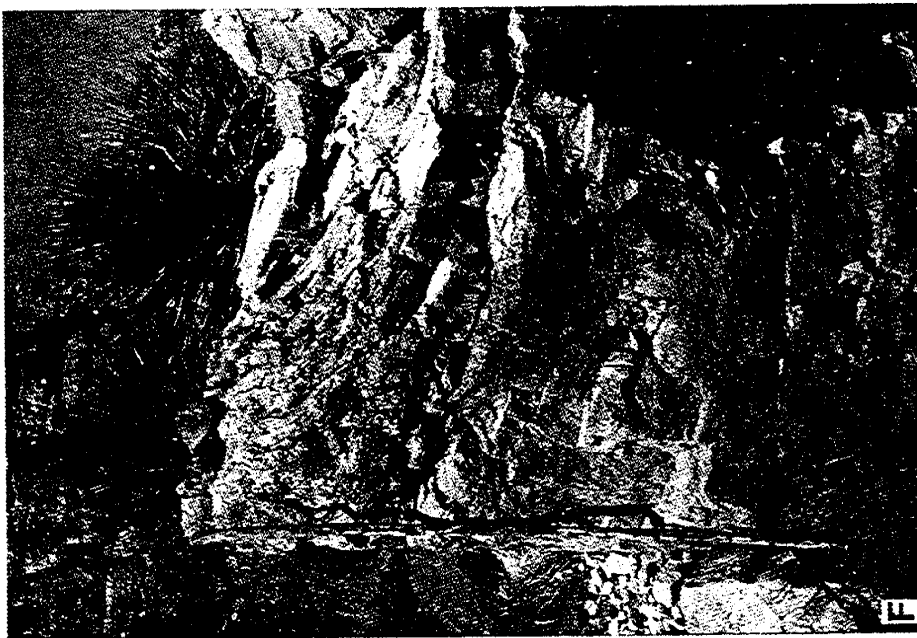


Figure III-5 (cont.)

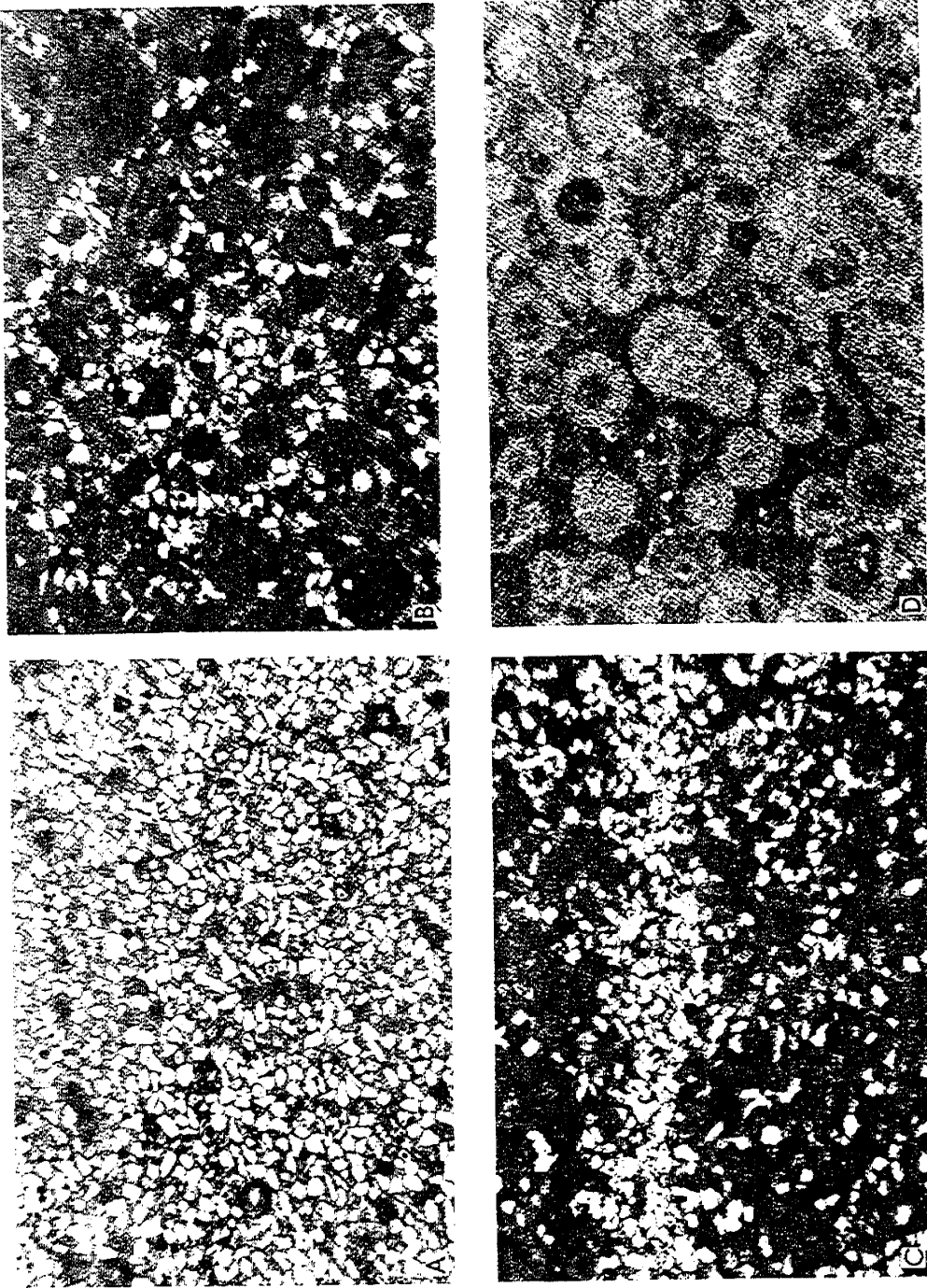


Figure III-6. Facies photomicrographs, A-I are from SC 23. A. Dolomitic quartz sandstone, sample 8-1; rectangular pores result from dissolution of feldspar. B. Quartzose peloid dolopackstone, completely bioturbated, sample 3-4. C. Quartzose peloid dolopackstone, sample 3-8; preservation of sand laminae indicates incomplete bioturbation. D. Cement-occluded compacted ooid-peloid dolopackstone, sample 7B-18. This facies is similar to ooid-peloid dolopackstone except that little intergranular pore space is preserved. E. Compacted, crossbedded ooid-peloid dolopackstone, sample 4-16, with intergranular pores and some well-preserved ooid cortices. F. Fossiliferous peloid dolopackstone, sample 3 (3, 5). G. Fossiliferous peloid dolopackstone, sample 3-16. H. Fine peloid dolopack/grainstone, sample 7B-20. I. Ooid-peloid dolopackstone with some quartz nuclei, sample 7B-12. J. Very fine peloid dolowacke/packstone, SC 26. K. Silty fusulinid-peloid packstone near maximum flooding surface, SC 7. L. Cement-occluded lithoclastic peloid dolopackstone from fenestrally laminated tidal-flat bed, SC 23. Note fine detail preserved in algal(?) laminations around larger grains. Some grains are in penetrative intersection with others in D, E, and I, showing porosity-reducing effects of chemical (pressure-solution) compaction. All photomicrographs represent approximately 4 mm across.

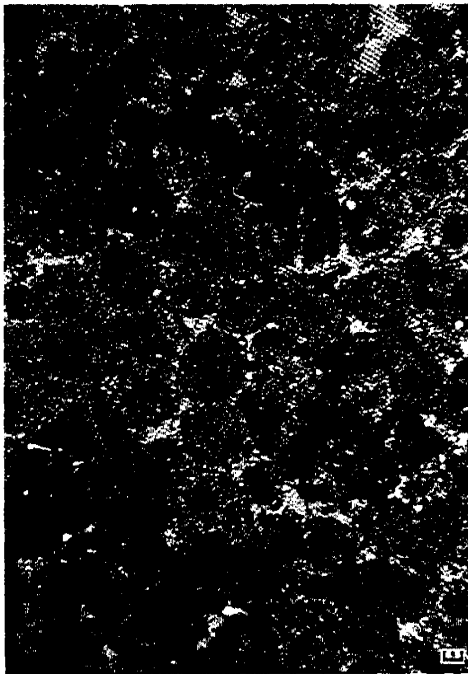
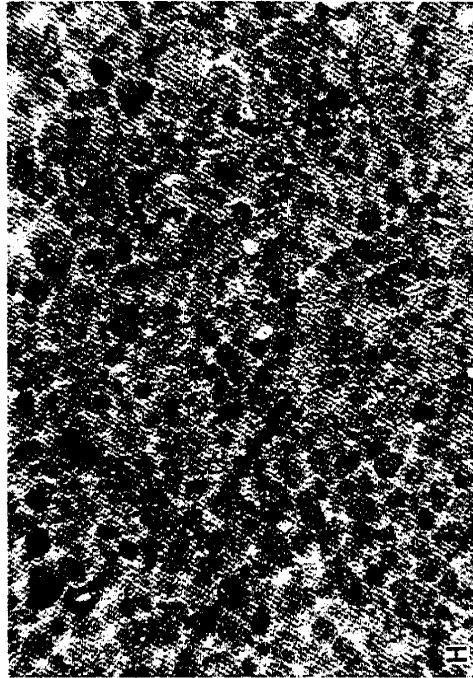


Figure III-6 (cont.)

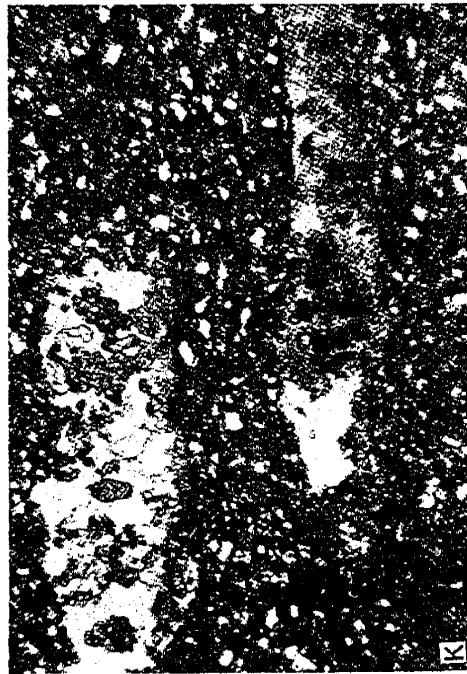
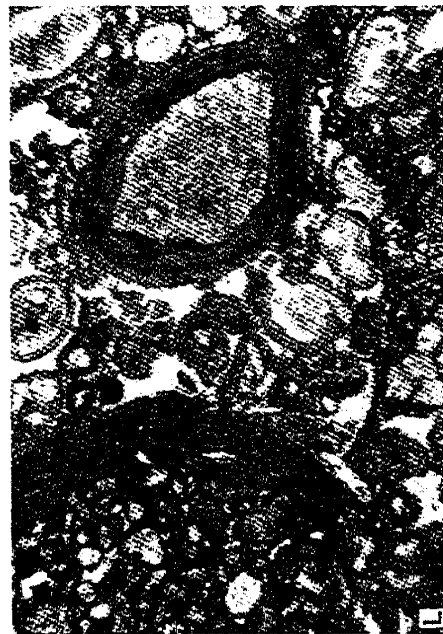


Figure III-6 (cont.)

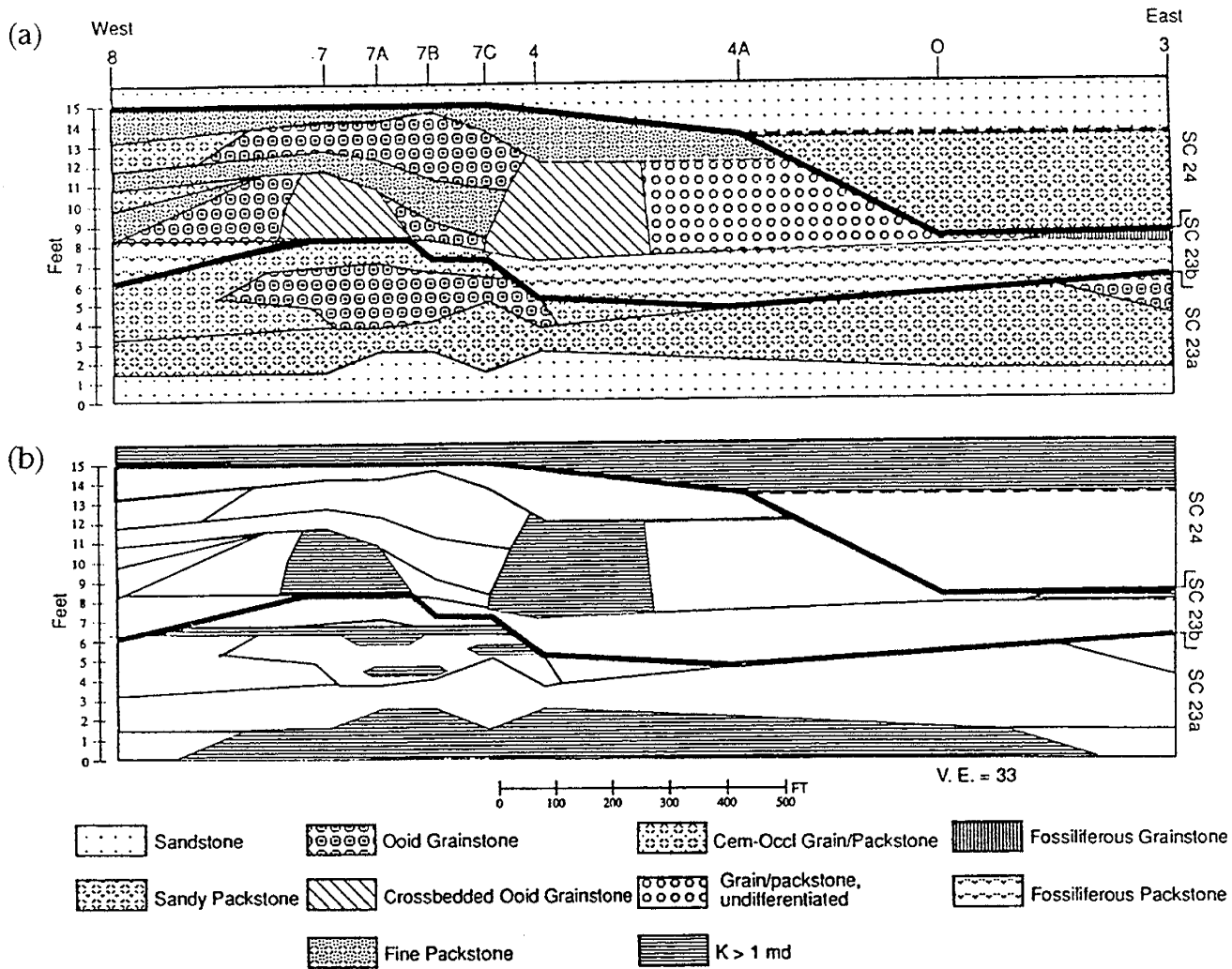


Figure III-7. A. West-East cross section of SC 23, sections 8 to 3. Shown are locations of sample sections, facies, and parasequence boundaries. Section 4A used for measurement of total section thickness only. Boundary between SC 23 and SC 24 is erosional. B. Distribution of permeability values > 0.1 md. Polygons are boundaries of facies depicted in III-7A.

similar bed on the Shattuck Valley wall (chapter II). The MFS is either within or at one of the bounding surfaces of this bed because (1) fusulinid dolopackstone is the deepest water deposit in Stone Canyon and deep water had to be present before deposition of the unit and (2) shallow-water sand-bearing-quartz rocks occur immediately above it.

Parasequences have three styles of lithologic associations, each showing compositions and sedimentary features that indicate shallowing conditions: (1) dolomitic sandstone throughout (for example, SC 2; fig. III-5A), (2) dolomitic sandstone grading up to dolostone (for example, SC 23; fig. III-5D), and (3) relatively pure dolostone throughout (for example, SC 26 through 28; uppermost Grayburg Formation in cliffs shown in fig. III-2). Each of these cycle types consists of a basal transgressive facies composed of dolomitic sandstone (figs. III-6A and III-7A) or a relatively nonporous and impermeable carbonate facies (figs. III-6B, III-6C, III-6D, and III-6J) overlain by generally coarser grained carbonate facies. Locally, dolograinstone occurs at some cycle bases (for example, SC 3 and SC 5). At each location these facies developed sequentially, as sediment-water accommodation space was filled.

Most Stone Canyon parasequences are capped locally by tidal-flat deposits characterized by fenestral and tepee-structured lamination (figs. III-5A, III-5B, and III-5F). Tidal-flat caps indicate that final development of the parasequence occurred at or slightly above sea level and reflect coastal emergence or low-relief-island development. Where tidal-flat deposits extend vertically through several parasequences (figs. III-3 and III-4), they are interpreted to record the persistent location of islands during deposition of these cycles. In these cases, areas with elevated topography on tidal flats developed during deposition of a parasequence became locations for continued tidal-flat development during deposition of the next parasequence.

Fenestrally laminated carbonate and tepee structures are laterally discontinuous in Stone Canyon parasequences. Along the length of the Stone Canyon study area, tepee-structured beds capping individual parasequences pass into fenestrally laminated beds and then into laminated fine-grained packstone beds several times (fig. III-5G). In a reservoir analysis, correlations between cored wells based on presence of similar tidal-flat facies could lead to

miscorrelations, incorrect reconstruction of parasequences, and therefore incorrect reconstruction of reservoir architecture.

Somewhat more sandstone occurs in parasequences of the LTST than in those of the HST. Much sand probably bypassed an exposed Stone Canyon area during high-frequency sea-level lowstands, although some was probably stored in thin transient eolian sand deposits developed on the exposed shelf. In Palo Duro Basin, essentially an extension of the North and Northwest Shelves during Guadalupian time, erg development during Grayburg sea-level lowstands has been documented (Nance, 1988). Well-sorted sandstone in Stone Canyon cycles has no sedimentary features diagnostic of eolian deposition, and most of it is mixed with carbonate peloids of marine origin. Therefore, these deposits are interpreted to record trapping and marine reworking of eolian sand during transgression.

A greater relative abundance of pure carbonate cycles in the HST than in the LTST is possibly due to the landward migration (onlap), inherent in lowstand and transgressive system tracts, of similar depositional facies within succeeding parasequences. At some point fifth-order (parasequence-scale) sea-level fall is insufficient to allow sand to be transported basinward to locations where sand was deposited in underlying parasequences. This general pattern is interrupted by the occasional sea-level fall of greater than average magnitude where sandstone depositional environments are reestablished in downslope areas.

Alternatively, the preferential deposition of sandstone in parasequences of the LTST may reflect conditions whereby HST sand was stored further up depositional slope because drops in relative sea level were of lower magnitude or shorter duration than those during LTST deposition. This hypothesis may be supported by relations seen between cycle SC 23 and immediately overlying SC 24 (figs. III-1 and III-7A). In this interval deep erosion of one parasequence is followed by abundant sand accumulation in the base of the next overlying parasequence. This pattern suggests longer exposure time for the eroded parasequence, which may reflect a larger than average (for Stone Canyon) magnitude and duration of relative sea-level fall. SC 23 ranges from 15 ft thick at the western end of the outcrop at section 8 to about

9 ft thick in the eastern parts of the outcrop at section Ot. Although the uneven thickness of SC 23 also reflects bar-crest topography, it mainly records erosion during sea-level lowstand preceding SC 24 deposition. Depth of erosional truncation is greater for SC 23 than for any other cycle in Stone Canyon. The thickest dolomitic sandstone interval found in the HST at Stone Canyon (approximately 17 ft) occurs in the base of SC 24, just above the most truncated part of SC 23 between sections Ot and 3, and suggests infilling of the erosional topography by SC 24 sand. On the southern canyon wall, SC 24 sandstone thickness is comparatively uniform and thin, ranging from 5 to 10 ft thick. The sandstone thickness distribution suggests deposition in an erosional channel with a southeast trend. This trend probably lies approximately along paleoslope. It is possible that the erosional unconformity on SC 23 is a fourth-order sequence boundary within the third-order HST.

Quartz sandstone beds are the most laterally extensive of Grayburg facies in the canyon, and many can be correlated to the Grayburg section exposed on the Shattuck Valley wall (chapter II). The widespread distribution of much of the sandstone in Stone Canyon records the trapping of eolian sand along a transgressing shore zone. During the preceding sea-level lowstand, shelf-bypassed sand was deposited in a sea in which the shoreline was located at a more downslope position. Erg deposits stored on the shelf during sea-level lowstand were reworked by shallow marine processes during transgression. These processes produced regionally extensive sheetlike sand deposits.

Sandstone beds in other arid mixed siliciclastic-carbonate settings may have similar histories and geometries, thus making the best marker beds for correlation between wells in reservoirs. Sandstone beds in the Grayburg-equivalent Eunice Monument South unit, located on the northwest corner of the Central Basin Platform, have been used recently to define the cycle-scale framework of that reservoir (Lindsay, 1991). In some Grayburg reservoirs (for example, Cowden North in Ector and Andrews Counties), sandstones are not only good correlation markers but produce hydrocarbons as well (Galloway and others, 1983). Gamma-ray logs are

useful in distinguishing siliciclastic-dominated from carbonate-dominated strata in hydrocarbon reservoirs.

Specific carbonate facies, however, are generally autochthonous, developing in response to interplay between water depths, current energies, and geographic position relative to nearby depositional topography. Therefore, specific carbonate facies are more limited in geographical extent and are generally inferior markers over typical interwell distances.

Sampling of various facies in Stone Canyon indicate that the best porosity and permeability values occur in dolomitic sandstone beds at the bases of sandstone-dolostone cycles and in porous ooid-bearing and fossil-bearing dolograins (figs. III-6A, III-6E, and III-6F) usually positioned within middle parts of parasequences. Lower porosity and permeability values generally occur within cement-occluded dolograins and dolopackstones (figs. III-6B, III-6C, III-6D, III-6G, III-6H, III-6J, and III-6L). Tidal-flat caps (figs. III-5B and III-5F), whatever their textural composition, are typically impermeable because vadose cements are preferentially precipitated in pore throats during subaerial exposure attendant high-frequency sea-level lowstands. In the subsurface pores are often occluded with sulfates precipitated from hypersaline brines produced during late sea-level highstand by evaporation of restricted lagoons that developed in topographic lows behind tidal flats, emergent shoals, and reefs. Ancient examples of such lagoons include the Lower Cretaceous Ferry Lake Anhydrite of East Texas (Loucks and Longman, 1985) and the Upper Jurassic Buckner evaporite member of the Smackover Formation (Moore and others, 1988) illustrate this type of paleogeography. In Stone Canyon pure dolostone parasequences, the basal interval is usually an impermeable dolowackestone or dolopackstone (figs. III-6C and III-6J). These relationships result in relatively porous and permeable facies of individual parasequences being isolated vertically from one another by intervening impermeable facies. The lateral continuity of permeable facies is also limited. Porous and permeable dolomitic quartz sandstones change laterally into relatively impermeable quartzose dolopackstones; dolograins change laterally to cement-occluded grainstones or packstones, usually over distances shorter than typical interwell spacing.

SPATIAL DISTRIBUTION OF DEPOSITIONAL AND DIAGENETIC FACIES  
IN PARASEQUENCE SC 23

A sampling program was designed to determine the characteristics and dimensions of depositional and diagenetic facies in a single representative parasequence (SC 23) (figs. III-2, III-3, III-5D and III-7) to gain insight into the internal complexities of parasequences developed in inner-shelf crest settings. Parasequence SC 23 was chosen for its variety of facies representative of most Stone Canyon cycles, easy access, and manageable size. Brief points will be made in the following sections about comparisons between Stone Canyon rocks and those seen in some reservoirs and about applicability of the findings of this study to reservoir analysis.

Samples were collected from SC 23 at 6-inch intervals along vertical sections on the northern wall of Stone Canyon that were spaced 90 ft to 900 ft laterally (fig. III-1). To investigate petrophysical variability over smaller distances, two rectangular grids with 2-inch sample spacing were established in two different facies occurring respectively toward the top of SC 23 at the east (section 3) and west (section 8) ends of the detail study area.

Rock types identified from SC 23 include both depositional and combined depositional/diagenetic facies, although the division between the two general categories is not well defined. Depositional facies include dolomitic quartz sandstone, quartzose peloid dolopackstone, cement-occluded ooid-peloid dolograinstone/packstone, ooid-peloid dolograinstone, fossiliferous peloid dolopackstone and dolograinstone, and fine-grained peloid dolograinstone/packstone (figs. III-6A through III-6I and III-7). Ooid-peloid dolograinstones are further divided between those occurring on bar crests characterized by relatively higher intergranular porosity and those underlying and flanking bar crests characterized by significantly lower porosity. Combined depositional/diagenetic facies include cement-occluded ooid-peloid dolograin/packstone and possible leached facies, the most notable of which includes both oo-moldic peloidal dolograinstone and cement-occluded ooid-peloid

dolograinstone/packstone that occurs at the top of SC 23a (fig. III-7A). The less porous dolograinstone is transitional in fabric between the bar-crest dolograinstone and the cement-occluded dolograinstone/packstone. Facies names in the following sections will be abbreviated:

- (a) dolomitic quartz sandstone = sandstone,
- (b) quartzose peloid dolopackstone = sandy packstone,
- (c) ooid peloid dolograinstone = ooid grainstone,
- (d) fine grained peloid dolopackstone/grainstone = fine pack/grainstone,
- (e) fossiliferous peloid dolopackstone = fossiliferous packstone,
- (f) fossiliferous peloid dolograinstone = fossiliferous grainstone,
- (g) cement-occluded ooid peloid dolopackstone/grainstone = cement-occluded grain/packstone, and
- (h) oo-moldic peloid dolograinstone/packstone = moldic grain/packstone.

The detailed facies cross section of SC 23 (fig. III-7) shows a basal massive to crossbedded, well-sorted fine-grained sandstone (figs. III-5D and III-6A). The sandstone has numerous molds that resulted from dissolution of feldspar grains. The original sediment was subarkosic (feldspar-bearing), reflecting its ultimate source in the granitic highlands of the Pedernal Uplift that extended from central to south-central New Mexico. The sands are probably recycled from other sandstones because the granite massif was buried beneath terrigenous sediments earlier in the Permian (Ross and Ross, 1986). Prior to final deposition by marine processes, Grayburg sand probably spent much of its history in an arid eolian depositional environment. Evidence for this is its excellent size sorting and the preservation of feldspar grains that would have degraded relatively quickly in a humid environment. In the Palo Duro Basin area located upslope of the North and Northwestern Shelves, Grayburg sandstone has been observed that has wind-ripple laminations and textural qualities characteristic of deposition on eolian dunes and eolian sand sheets (Nance, 1988).

Although the SC 23 sandstone extends along the entire length of the canyon's northern wall, it becomes more dolomitic toward the west (section 8) and east (section 3) ends of the study area. Consequently, it becomes less porous and permeable in those positions.

Siliciclastics observed in Stone Canyon parasequences are similar to those observed in Grayburg-equivalent Eunice Monument South Unit in that both are sandstone with porosity enhancement caused by feldspar dissolution (Lindsay, 1991). In the North Foster field, a study of which accompanies this report (chapter IV), siltstone represents the siliciclastic component of parasequences. Notably, feldspar-dissolution-enhanced porosity was also observed there.

The SC 23 sandstone is overlain by massive, moderately sorted sandy packstone (figs. III-6B and III-6C). Sand content decreases upward in this facies and reflects a transition from siliciclastic-dominated to carbonate-dominated deposition. Decrease of siliciclastic influx resulted from repetitive marine transgression and trapping of terrigenous sediments progressively up depositional slope. Overall lack of bedding in the packstone resulted from bioturbation, where sand deposited intermittently in thin layers (fig. III-6C) was churned in with carbonate peloids. The flaggy appearance of the packstone probably results from pressure solution. The sandy packstone is laterally continuous along the canyon wall for the entire length (1,900 ft) of the detailed study area, although locally it is significantly less quartzose (for example, in section 8).

Relatively pure dolostones immediately overlie sandy packstone facies (figs. III-5D and III-7). These dolostones comprise five distinct facies: (1) cement-occluded grain/packstone (fig. III-6D), (2) ooid grainstone (fig. III-6E), (3) fossiliferous grainstone (fig. III-6F), (4) fossiliferous packstone (fig. III-6G), and (5) fine packstone (fig. III-6H).

The cement-occluded grain/packstone and the ooid grainstone record deposition on and around a carbonate bar crest (fig. III-7). The ooid grainstones preferentially occur on the crossbedded bar crests (figs. III-6E, III-7). These rocks are distinguished by excellent grain sorting and relatively well preserved intergranular porosity. Ooids mostly range from 0.4 to

0.6 mm in diameter (medium- to coarse-sized sand). Ooid nuclei include peloids of uncertain origin, quartz sand grains (fig. III-6I), and fossil fragments.

Ooid cortices (accretion rings) are well preserved in many examples (fig. III-6E), suggesting microscale alteration (neomorphism) to calcite and dolomite of the original mineral species (aragonite or Mg-calcite). Neomorphic processes are most common in vadose (Pingitore, 1976) or burial diagenetic environments where chemical near-equilibrium is maintained between carbonate species and slow-moving or stationary diagenetic fluids. When there is vadose neomorphism, the slow-moving water is in the form of a thin film of capillary water surrounding grains (Pingitore, 1982).

Distribution of compactional fabrics suggests that some SC 23 carbonate transformations occurred in a vadose zone, whereas others occurred in a meteoric phreatic zone. Chemical compaction (pressure solution) is indicated by penetrative intersections of grains observed in the ooid-peloid rocks (figs. III-6D, III-6E, and III-6I). Pressure solution, in addition to mechanical packing and dewatering (mainly in rocks dominated by mud-sized particles), is a major process by which carbonate rocks are compacted (Wanless, 1979; Shinn and Robbin, 1983). Pore-sized reduction in chemically compacted rock is caused not only by grain-sized reduction but also by the probable reprecipitation of dissolved carbonate in nearby pores (Dunnington, 1954). Compaction fabrics in SC 23 are systematically distributed in rocks around a zone of above-average permeability (to be discussed under the section on porosity and permeability). Examples from rocks above the zone show more evidence of pressure-solution (figs. III-6D and III-6E) than rocks within the zone (figs. III-8A through III-8C), or rocks below it (fig. III-8E). In Jurassic Smackover oolites of Louisiana (Humphrey and others, 1986) and Arkansas (Wagner and Mathews, 1982), porous, relatively uncompacted oolites were overlain and underlain by chemically compacted oolites. These contrasting fabrics were interpreted to result from preferential early mineral stabilization by meteoric-phreatic diagenesis of the relatively uncompacted interval. Rocks in the vadose zone were not stabilized because they were not exposed sufficiently to chemically aggressive diagenetic fluids, whereas rocks in the marine-

phreatic zone were not stabilized because they were bathed in waters compositionally similar to those which they had formed. The authors of the Smackover studies interpreted the establishment of a floating meteoric lens (meteoric-phreatic zone) during sea-level lowstand that effected stabilization of the sediments within it. Because pressure solution is enhanced in chemically metastable carbonate sediments, those rocks in the vadose- and marine-phreatic zones were preferentially compacted and cemented. Isotopic studies were used to support the interpretations of meteoric diagenesis in Smackover oolites, but such analyses were beyond the scope of this investigation.

Postdepositional transformations of the original carbonate species, including pervasive dolomitization, make it difficult to determine if the cement-occluded grain/packstone facies originally included intergranular mud of sufficient quantity to classify it as packstone. In many examples pores of a grainstone probably have been filled with cement precipitated from through-going carbonate-supersaturated fluids. The local occurrence of crossbedding in the cement-occluded grain/packstone facies suggests that some of these rocks were originally similar to the more porous rocks herein classified as ooid grainstones.

The lateral dimensions of the bar-crest grainstone facies of SC 23 is about 300 ft on the north wall of Stone Canyon (fig. III-7). The cement-occluded grain/packstone facies does not pinch out within the canyon study area; thus, only a minimum length of about 2,000 ft can be given. Without a sufficiently extensive three-dimensional view of parasequences, it is impossible to know solid geometries of facies (for example, bar crests could be elongate into the plane of the canyon wall). Along the Shattuck Valley wall 2 miles to the east, several crossbedded ooid grainstones measure 1 to 3 mi along apparent dip (Kerans and Nance, 1991).

The fossiliferous packstone facies is interpreted to onlap the SC 23a bar crest from the east and west (fig. III-7). This interpretation is based on the distribution of core-plug data, but no actual onlap surface was observed in outcrop; therefore, it is possible that fossiliferous facies interfinger with ooidic facies. However, the similarity of samples taken over such a close-spaced interval (6 inches) supports the interpretation that no ooid-peloid facies occur within the

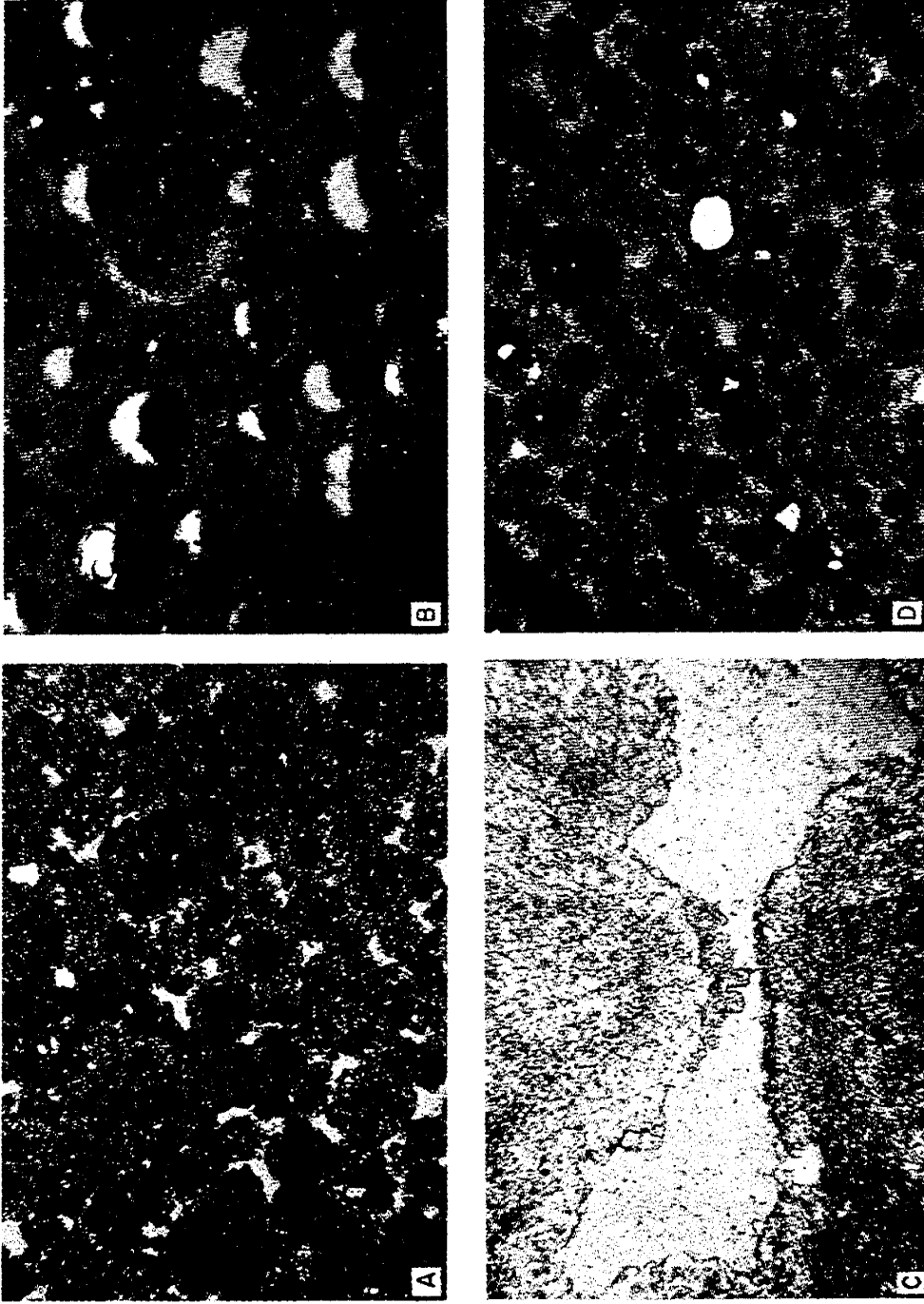


Figure III-8. Photomicrographs of rocks associated with zones of suspected meteoric diagenesis. A-E are from SC 23. A. Ooid-peloid dolograins (sample 7A-12), with 16.12-md permeability. B. Uncompacted cement-occluded ooid-peloid dolograins with geopedal oo-moldic fabric, probably resulting from meteoric diagenesis (sample 7-12). C. Cement-occluded ooid-peloid dolograins with microstalactitic cements on upper surfaces of vugs, 0.59-md permeability (sample 7-13). D. Little-compacted ooid-peloid dolograins with isopachous cements and intergranular porosity (sample 7-10). E. Ooid-peloid dolopackstone with pore after sulfate and oo-moldic geopedal fabric, SC 26, section 8. F. Fossiliferous peloid dolopackstone with fossil molds and pendulous cements (arrow), 59 md permeability, SC 25, section 3. Photomicrographs (except D) represent approximately 4 mm across; D is approximately 1 mm across.

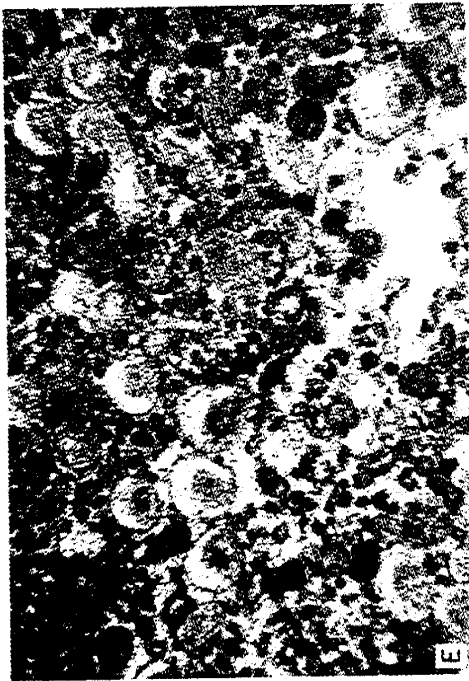


Figure III-8 (cont.)

interval mapped as fossiliferous packstone. Given the interpretation of onlap of the bar crest by the fossiliferous packstone, the relief presently displayed by the underlying bar crest is about 3 ft. This is a minimum figure for the original depositional relief because the grainstones have been compacted, as will be shown. The presence of fossils in this facies contrasts with the faunally barren facies that composes the rest of the parasequence and suggests deposition during a marine transgression. Its absence at the apex of the bar crest may reflect erosion associated with current energies attendant development of the overlying bar or with infilling of topographic lows around an emergent bar crest by the fossiliferous facies. The occurrence within SC 23 of a transgressive facies suggests that SC 23 consists of two cycles. The lower cycle (SC 23a) has a sandstone at its base, whereas the upper cycle (SC 23b) has a carbonate (fossiliferous packstone or grainstone) base.

At the east end of the outcrop study area, the fossiliferous packstone changes to fossiliferous grainstone (fig. III-7). This facies change includes accompanying changes in porosity and permeability and provides a lateral pinch-out into the packstone of the more permeable qualities of the fossiliferous grainstone facies. This will be further discussed later in the report.

Fine packstone occurs as two distinct intervals in SC 23b (fig. III-7). These are probably lower energy shoal-flank deposits that filled in depositional topography inherited from the grainstone-bar forms. Their thickness patterns and the structure on their bases defines the underlying bar crests. Based upon this interpretation the two bar crests of SC 23b presently have post-compaction relief of about 3 ft each over a minimum distance of 900 ft (fig. III-7), about the same relief as that of the the bar crest in SC 23a. The position of these fine-grained, tight packstones overlapping more porous and permeable grainstones provides potential seals against vertical migration of hydrocarbons stored in the grainstones. The reoccurrence of ooid grain/packstone deposits on top of the fine packstone in SC 23b may indicate a depositional break following deposition of the lower half of SC 23b. The dashed boundary in figure III-7 suggests this possibility. Similar to the interpretation of SC 23a that was based on the

occurrence of fossiliferous facies, the reactivation of shoal crest deposition in the upper part of SC 23b may reflect the presence of an additional cycle. Whatever the cause, the results are small (3 ft thick by 900 ft wide in outcrop) potential stratigraphic traps comprising lenses of ooid grainstone separated from each other by intervening thin (1 to 2 ft thick); fine-grained packstone beds.

Erosion at the top of SC 23 created differential topography that affected facies distributions in overlying SC 24. Not only the thickness of SC 24 sandstone but also its composition appears affected by precedent erosional topography developed on SC 23. Upon the paleotopographically higher terrain in the west, the basal sandstone is cross-laminated, well sorted, and contains no peloids (spherical coated grains of uncertain marine origin [fig. III-9A]). In the erosional trough to the east, however, the basal deposit is a massive to planar-laminated, moderately sorted, quartzose peloid dolopackstone (fig. III-9B). This compositional difference reflects changing depositional conditions related to water deepening during SC 24 transgression. Although the initial transgressive deposits in the trough may have been current-laminated quartz sand, upon marine deepening a carbonate depositional environment was established with burrowing organisms that churned carbonate components with the quartz sand. Current energies on the higher area may have been too high, thus incompatible with development of large coated carbonate grains or population by organisms. As discussed in the following section, petrophysical properties are significantly more favorable to fluid flow in quartz sandstone than in quartzose peloid packstone. Therefore, topography that locally affects sandstone facies distributions consequently affects distribution of petrophysical properties pertinent to potential hydrocarbon productivity of the sandstone.

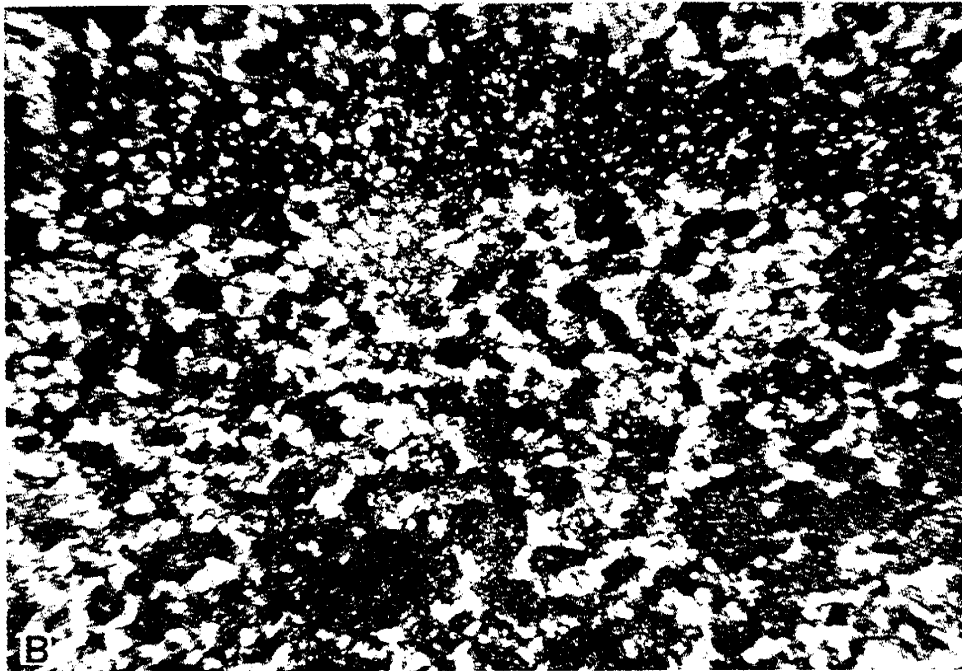
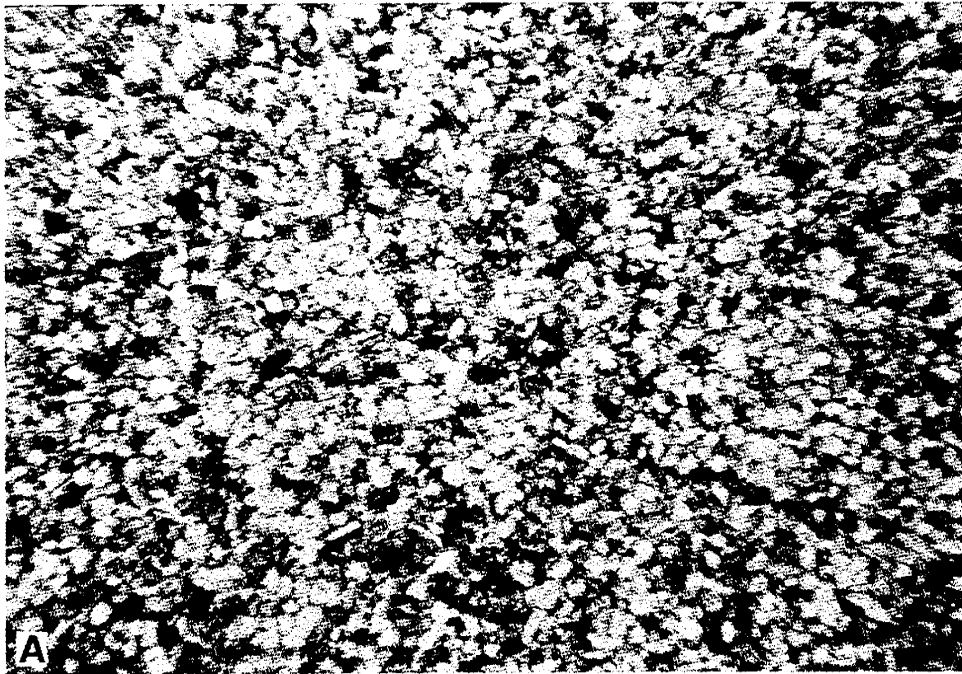


Figure III-9. Photomicrographs of basal quartz-bearing beds of SC 24. A. Dolomitic fine-grained quartz sandstone deposited on paleotopographic high of erosional unconformity on SC 23. B. Quartzose peloid dolopackstone deposited in erosional trough on SC 23. Photomicrographs represent approximately 4 mm across.

PARASEQUENCE-SCALE VARIATION  
IN POROSITY AND PERMEABILITY STRUCTURE

Overall, SC 23 is composed of rocks distinguished by low porosity and low permeability. The range of porosity values is limited to 14 percent or less (fig. III-10). Porosity values greater than or equal to 9 percent characterize only 3 percent of the samples and are all in sandstone. Most of the porosity values  $\leq 2$  percent are in fine packstone. Samples with porosity values of 3 to 8 percent are divided among the sandy packstone, fossiliferous grainstone, ooid grainstone, cement-occluded grain/packstone, and fossiliferous packstone (in order of decreasing average porosity). Permeability values range between less than 0.01 md to 30 md. Only 17 percent of the 245 samples recovered from SC 23 have  $k \geq 1.0$  md. Rocks with permeabilities below 0.1 md are defined as "tight" (Finley, 1984).

Much of the original depositional porosity has been reduced by compaction and carbonate cementation. Some cement was probably precipitated from seawater soon after deposition. Other cements were probably precipitated from solutions charged with carbonate acquired from dissolution (including pressure solution) of marine cements and depositional particles (ooids, peloids, and fossils) (figs. III-6D, III-6E, III-8B, III-8F, and III-8G) under meteoric or mixed meteoric-marine conditions developed when the shoal emerged during sea-level drop. All carbonate components of SC 23, as well as the rest of the Grayburg carbonate rocks in Stone Canyon, have been dolomitized. Dolomitization episodes probably provided additional cement as well as transforming calcitic species already present. In spite of these considerations, there remain significant differences in the petrophysical properties of the several facies identified in SC 23, most of which directly reflect primary depositional and syndepositional diagenetic features. By emphasizing these differences and the causal depositional and diagenetic processes, observations made on outcrop can be applied readily to reservoirs formed in similar environments.

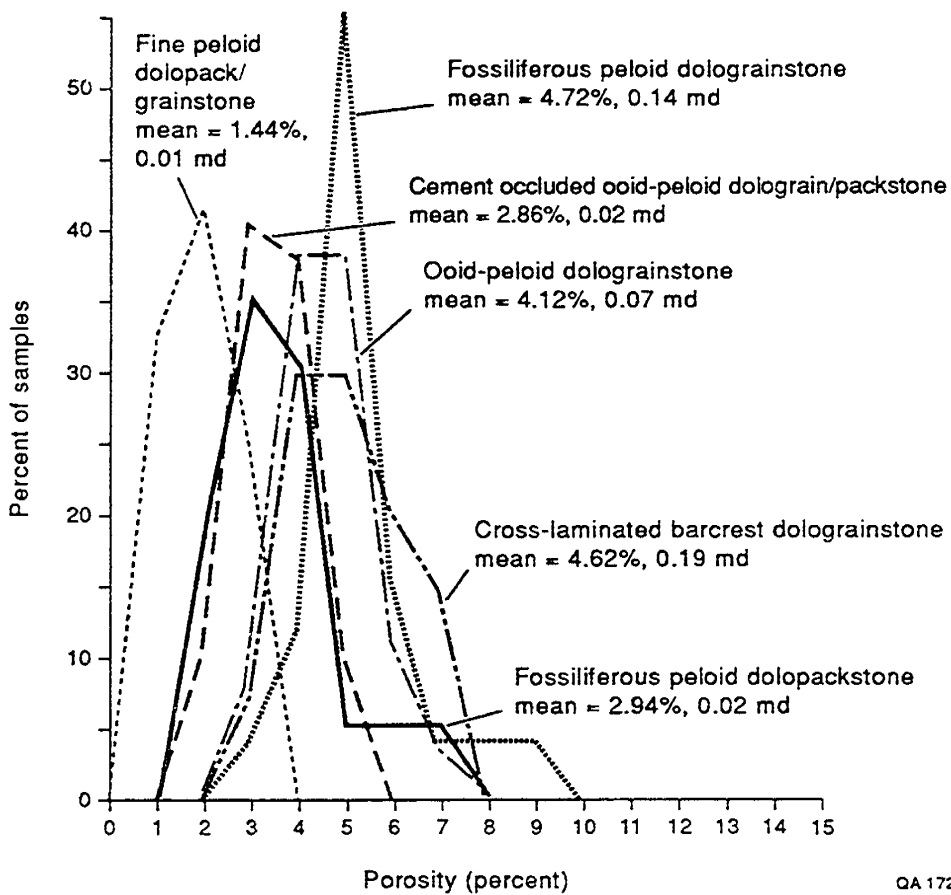
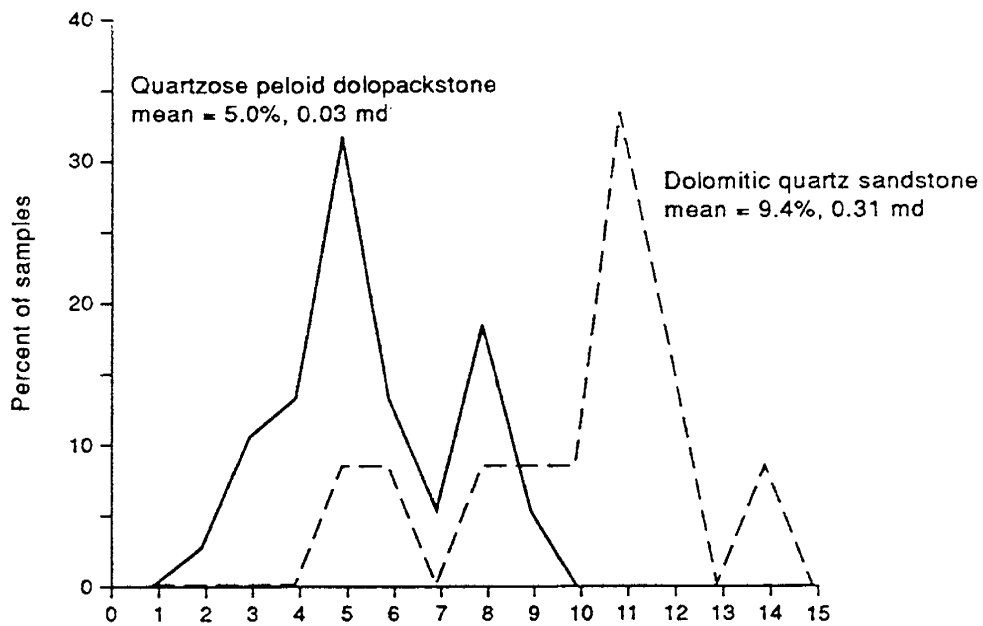


Figure III-10. Porosity frequency polygons for facies identified from samples recovered from SC 23 and mapped on figure III-5. Also indicated are arithmetic-mean porosities and geometric-mean permeabilities for each facies.

The most obvious porosity in quartz-bearing facies lies in the rectangular molds developed from leaching of feldspar (fig. III-6A), whereas well-developed but irregularly distributed intergranular porosity characterizes the ooid and fossiliferous grainstones (figs. III-6E and III-6F). Intergranular porosity is reduced in cement-occluded facies and fine packstones. The better porosities occur in the sandstone (avg. 9.4 percent), sandy packstone (avg. 5.0 percent), fossiliferous grainstone (avg. 4.7 percent), and in the ooid grainstone (avg. 4.1 percent). Lowest porosities occur in fossiliferous packstones (avg. 2.94 percent), cement-occluded grain/packstone (avg. 2.86 percent) and fine packstones (avg. 1.44 percent).

Although the range of porosity values in SC 23 samples is small, a significant relationship exists between facies types and porosity. Figure III-11 is a computer-generated deterministic contour map based on porosity values, without regard to facies types. By using porosity-value cutoffs selected from facies/porosity relationships (fig. III-10), the essential facies structure of SC 23 is captured, especially distribution of the sandstone ( $\geq 9$  percent porosity), fine packstone ( $\leq 2$  percent porosity), and more porous parts of the ooid grainstone facies ( $> 4$  percent porosity). Overlap of higher porosity values within the cement-occluded grain/packstone with lower values in the sandy packstone prevents defining the boundaries between these two facies on the basis of porosity values alone. Similarly, overlapping porosity values of ooid grainstones and cement-occluded grain/packstone prevent use of porosity values to delineate the boundaries between those facies. However, because the sandstone facies is the most volumetrically significant reservoir-quality unit, and because the fine packstones form seals over the next most volumetrically significant reservoir-quality rock (ooid grainstone), the ability to differentiate these by criteria displayed on geophysical porosity logs should be helpful.

The maximum permeabilities occur in samples recovered from fossiliferous grainstone (29.5 md) and from cross-laminated ooid grainstone (16 md). Although quite permeable, the fossiliferous grainstones were relatively insignificant volumetrically in the study area. The remaining 37 samples with  $k \geq 0.1$  md have permeabilities less than 10 md. Of these remaining samples, 29 occur in cross-laminated ooid grainstone facies and 8 occur in samples recovered

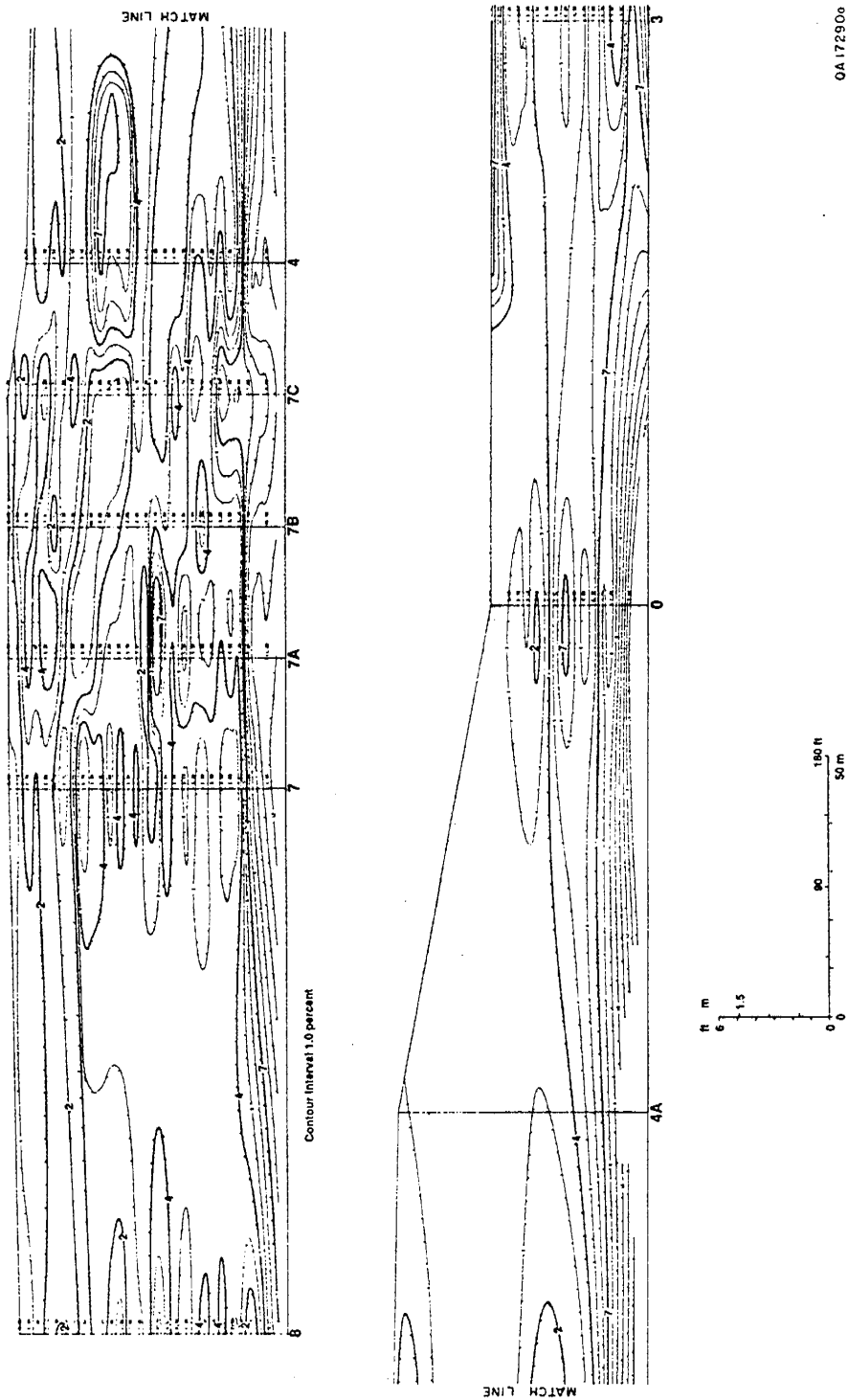


Figure III-11. Computer-generated contour map of porosity distribution, SC 23. Zones defined by values greater than 7 percent in lowest part of diagram generally encompass the dolomitic quartz sandstone facies; values of 4 to 5 percent generally encompass more porous ooid dolograins facies; values of greater than 7 percent at top of section 3 is fossiliferous peloid dolograins; values less than 2 percent encompass fine peloid dolopack/grainstone. Values posted along right sides of vertical section lines correspond to sample points.

from the sandstone facies. Sandstone is unique among SC 23 facies in that it has permeability values consistently above 0.1 md across the outcrop study area, although it does not have the highest permeability values. Volumetrically less significant oo-moldic grain/packstones (four samples) all have permeabilities above 0.1 md and are at the same elevation across at least 400 ft of continuous outcrop, more of which will be discussed below. Lastly, fine packstone, cement-occluded grain/packstone, and sandy packstones are practically impermeable.

On the basis of average values calculated from petrophysical analyses, facies identified in SC 23 fall into the following order of decreasing permeability (table III-1):

- (1) oo-mold-bearing grain/packstone (stratiform permeability zone; 4.25 md);
- (2) sandstone (0.31 md);
- (3) cross-laminated ooid grainstone (0.19 md);
- (4) fossiliferous grainstone (0.14 md);
- (5) massive ooid grainstone (0.07 md);
- (6) sandy packstone (0.03 md);
- (7) fossiliferous packstone (0.02 md);
- (8) cement-occluded ooid grain/packstone (0.02 md);
- (9) fine pack/grainstone (0.01 md).

Samples were also collected from the several Grayburg parasequences overlying SC 23. Most of the above facies were present in those cycles as well. In those samples the highest permeabilities occurred in a thin zone (2 inches thick) of fossiliferous pack/grainstone in SC 24 (54 md) (fig. III-8G) and in cross-laminated sandstone in SC 24 (4.43 md) (fig. III-9A). The next most permeable facies was cross-laminated ooid grainstone in SC 24 (0.14–1.72 md). Packstones and wackestones had very low permeabilities of 0.01 to 0.03 md. On the basis of sampling from Stone Canyon, the most porous and permeable facies are sandstones, fossiliferous grainstones, and cross-laminated (bar-crest) grainstones. The thin dimension (6 inches to 1 ft thick) of the permeable stratiform oo-mold-bearing facies disqualifies them as potentially significant reservoir

Table III-I. Results of porosity and permeability analyses,  
 Stone Canyon, Grayburg Formation, Parasequence SC 23.

Facies	Mean porosity (%)	Mean permeability (md)
Dolomitic quartz sandstone	9.40	0.31
Quartzose peloid dolopackstone	5.00	0.03
Fossiliferous peloid dolograinstone	4.72	0.14
Ooid peloid dolograinstone	4.12	0.07
Fossiliferous peloid dolopackstone	2.94	0.02
Cement-occluded ooid peloid dolograin/packstone	2.86	0.02
Fine peloid dolopack/grainstone	1.44	0.01

rocks, although similar facies could complicate parasequence architecture and reservoir recovery efficiency by acting as intraparasequence thief zones or as seals if occluded by sulfate.

Figures III-7B and III-12 are based on distribution of permeability values. Figure III-7B shows permeabilities related to facies mapped in figure III-7A, whereas figure III-12 is purely deterministic. In these illustrations permeability values  $\geq 0.1$  md are emphasized because lower values characterize nonreservoir-quality (tight) rock. Features captured in this diagram include the permeable sandstones (including the base of SC 24), the more permeable parts of the bar-crest ooid grainstones, the fossiliferous grainstones at the cycle top at section 3, and the solution-affected grain/packstone zone across the bar crest in SC 23a.

The results of closely spaced sampling on rectangular grids are depicted in figures III-13 and III-14. Samples collected at section 8 (fig. III-13) are from cement-occluded grain/packstone. Porosity values range only between 2.3 and 3.8 percent, and the possible measurement errors inherent in porosity/permeability analysis may well be greater than the variation shown on the map; that is, there is little significant porosity variation indicated by the data. Permeability values for these same samples, however, range over several orders of magnitude and the map has a bull's-eye pattern common in other Guadalupian carbonate facies sampled in the area (Kittridge, 1988; Hinrichs and others, 1986; Kerans and others, 1991). Samples with significant permeabilities (0.5 md and 1.0 md, in this case) occur no more than 2 inches from samples without significant permeabilities. Clearly, there is no close correlation between porosity and permeability values in this facies or in most of the other facies, a situation that complicates prediction of permeabilities from porosity-log responses in reservoirs. Porosity/permeability relationships will be further discussed below.

Fossiliferous grainstone facies were sampled on a grid established at the top of SC 23 near section 3 (fig. III-14). The resulting porosity and permeability maps contrast with those produced for the cement-occluded packstone in three ways. First, the porosity and permeability values are significantly higher for the fossiliferous packstone. Second, there is a correlation between permeability and porosity in these data (fig. III-15C) in that all samples

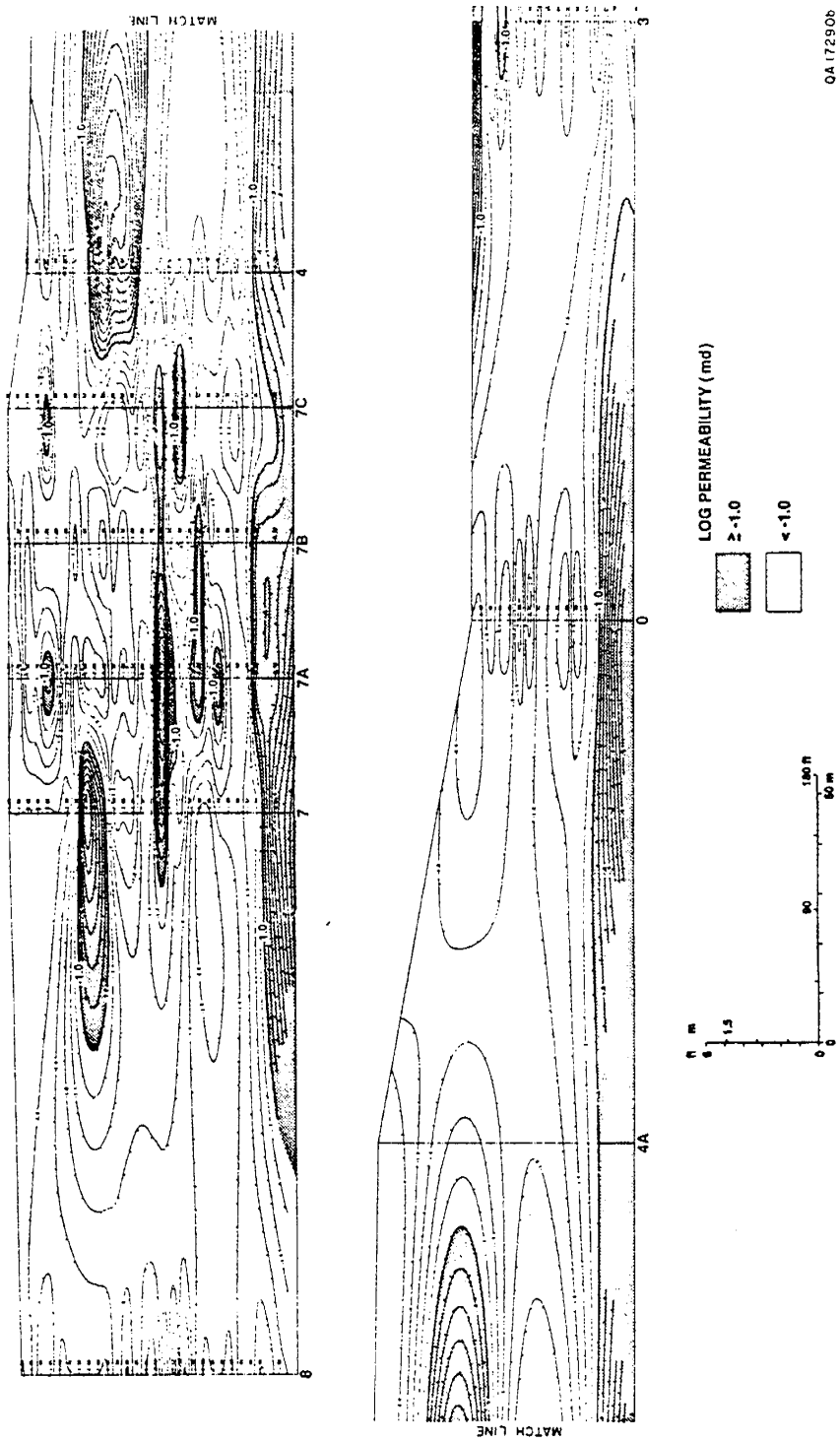


Figure III-12. Computer-generated contour map of permeability distribution, SC 23. Highlighted are zones including values greater than 0.1 md. Permeability is most laterally continuous in dolomitic quartz sandstone and in thin zone at top of SC 23a (see text). Highlighted zone between sections Ot and 3 is in fossiliferous peloid dolostone.

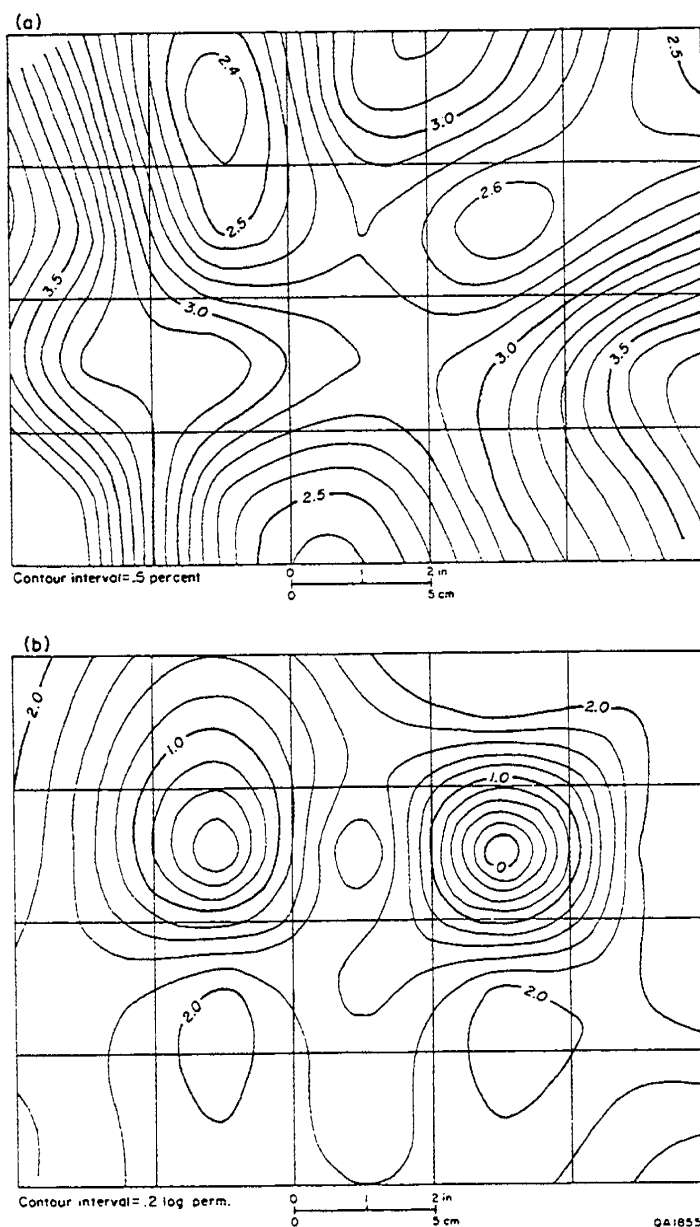


Figure III-13. Computer-generated contour maps of (a) porosity and (b) permeability distribution, SC 23/grid-section 8, cement-occluded ooid-peloid dolograins/packstone. Permeability distribution is a bull's-eye pattern, where samples differing in permeability by orders of magnitude occur in adjacent locations. Permeability values show little relation to porosity. Data points are at center of each grid block. Grid blocks are 2-inch squares.

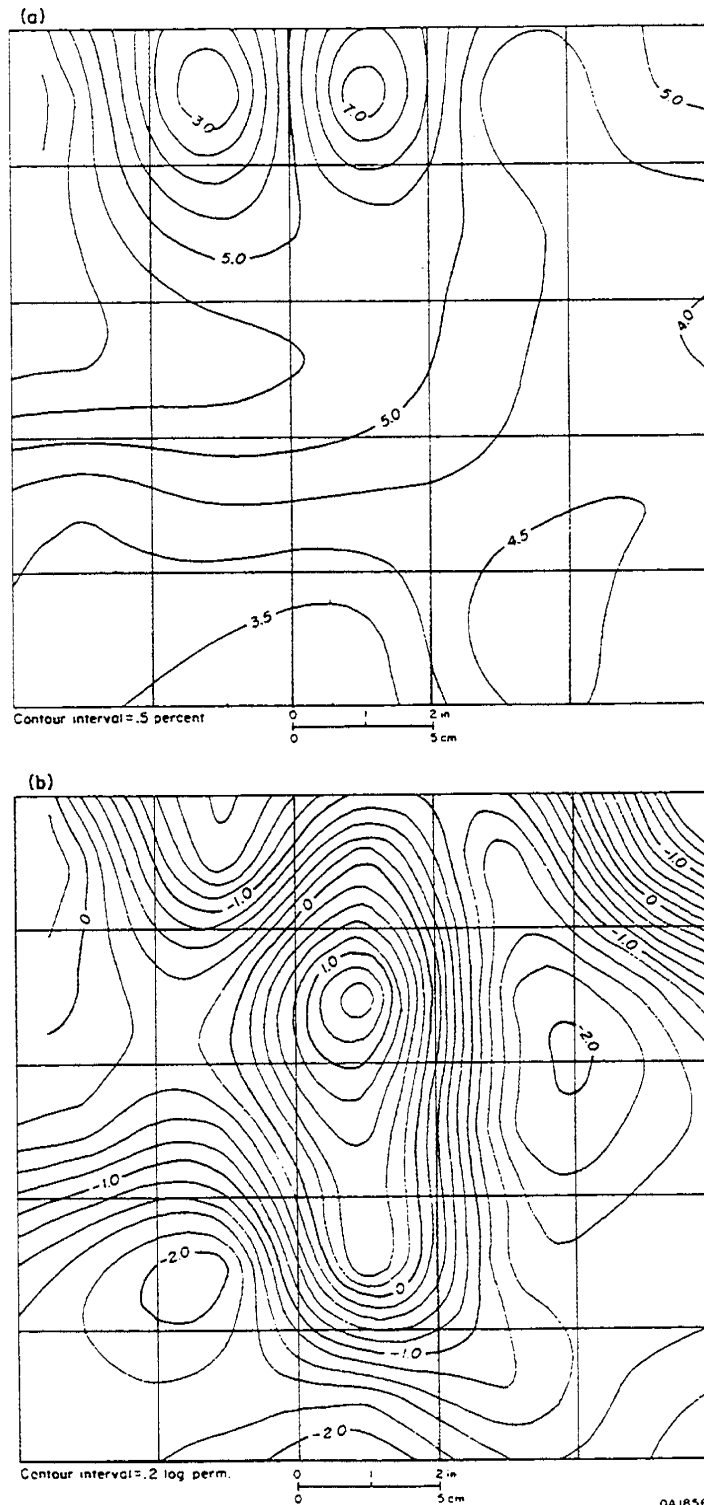


Figure III-14. Computer-generated contour maps of (a) porosity and (b) permeability distribution, SC 23/grid-section 3, fossiliferous peloid dolograins. Unlike cement-occluded ooid-peloid dolograins/packstone, there is a trend in this facies of samples with higher and lower permeability values to be separated by samples with intermediate values. Higher permeability values are generally associated with higher porosity values. These samples compose most of the data set for the porosity/permeability cross plot in figure III-15c. Data points are at center of each grid block. Grid blocks are 2-inch squares.

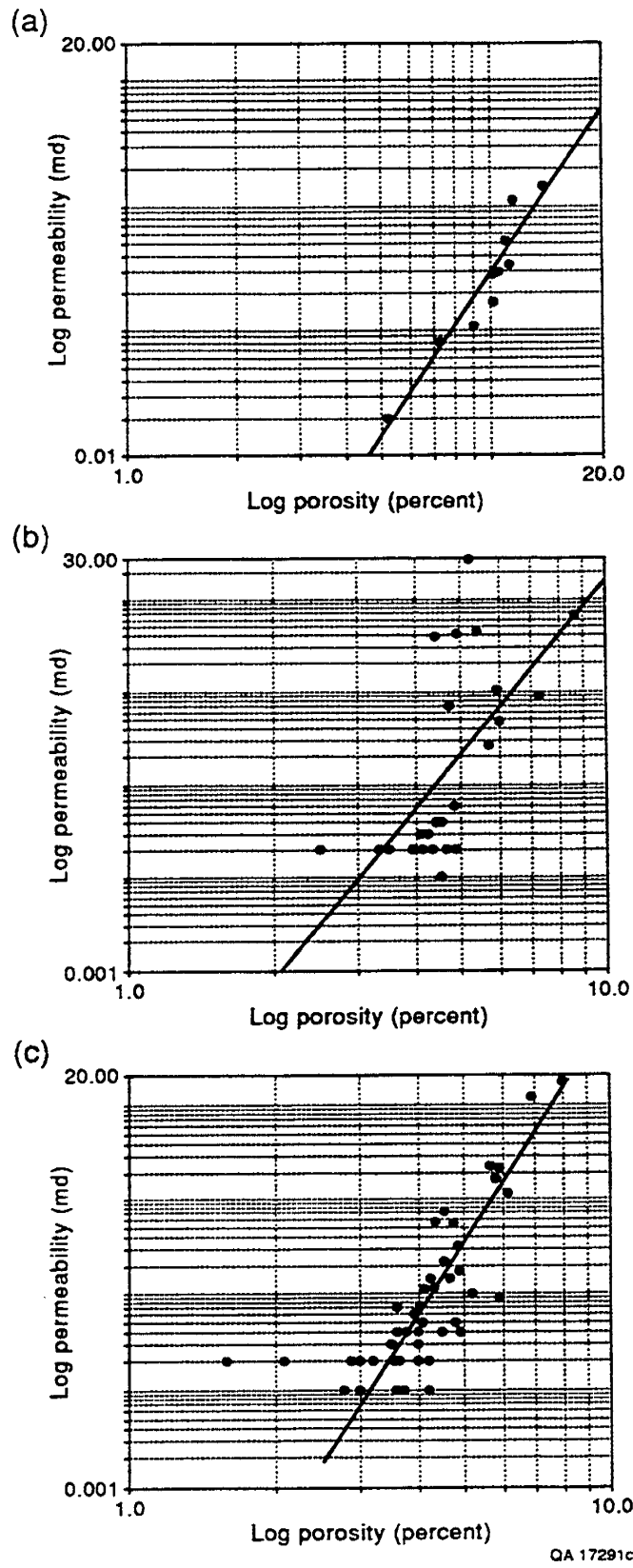


Figure III-15. Cross plots of log porosity against log permeability with regression lines for more permeable facies in SC 23. (a) dolomitic quartz sandstone, (b) ooid-peloid dolograinstone, and (c) fossiliferous peloid dolograinstone.

with permeabilities  $\geq 0.1$  md have at least 4.4 percent porosity. Sixty percent of the samples with porosities  $\geq 4.4$  percent have  $k \geq 0.1$  md and 80 percent of samples with porosities  $\geq 4.7$  percent have  $k \geq 0.1$  md. Third, highest and lowest permeability values on the fossiliferous grainstone grid are separated by intermediate permeability values. These patterns suggest that there is a through-going pathway of significant permeability in the fossiliferous grainstone facies that is not present in the cement-occluded grain/packstone.

The change from relatively impermeable rocks with less than 4.4 percent porosity to significantly permeable rocks at greater than 4.4 percent porosity probably results from preferential precipitation of a small volume of cement in pore throats of lower permeability samples. Pore throats are bottlenecks to flow, and small occlusions at those points profoundly affect permeability without greatly affecting porosity volume.

These results suggest that in an ideally analogous reservoir, the best reservoir-quality rock would be sandstones, followed by fossiliferous grainstones and bar-crest ooid grainstones. However, many Guadalupian-aged reservoirs in the Permian Basin are characterized by calcium sulfate (gypsum and anhydrite) emplacement within carbonate facies whose porosities immediately following carbonate deposition were high. Several examples of this phenomena in reservoirs located on the Central Basin Platform of Texas include Dune field in Crane County (Bebout and others, 1987), East Penwell San Andres Unit in Ector County (Major and others, 1990), and Jordan field in Ector and Crane Counties (Major and Holtz, 1989). Sulfate reduces porosity and permeability in these rocks. Some evidence was observed in this study that indicated former presence of sulfate (fig. III-8F), and it is possible that soluble sulfate components were leached from outcropping rocks during Tertiary uplift. Given the overall low porosity of Grayburg rocks in Stone Canyon, however, the original sulfate content would have been low. Nonetheless, even if the most porous and permeable facies observed on outcrop are modified by postdepositional sulfate emplacement in the subsurface, knowledge of distributions and geometries of all the component facies can augment recovery strategies.

Figure III-15 depicts the porosity/permeability relationships for sandstone, ooid grainstone, and fossiliferous grainstone samples from SC 23. The sandstone plot shows fairly strong correlation between permeability and porosity (intergranular and moldic), whereas the ooid grainstone (mainly intergranular porosity) plot shows considerable scatter around a regression line. In spite of the scatter, crossplots for ooid and fossiliferous grainstones show significant dependence of permeability on porosity for a carbonate rock. These results are typical in that carbonate rocks generally show scattered distributions on such plots, and sandstone permeability is generally more predictable from porosity than is carbonate permeability (Archie, 1952).

A feature of potential importance is defined by five samples with permeabilities greater than 0.1 md that were recovered from similar elevations above the base of SC 23 at four separate sections (sections 7, 7A, 7B, and 7C; figs. III-7 and III-12). These samples have permeabilities one to two orders of magnitude higher than the samples immediately above or below. The consistent elevation along which these samples were collected suggest the presence of a continuous stratiform zone of significant permeability.

Thin sections of these higher permeability rocks show the occurrence of intergranular pores larger than those seen in lower permeability samples (fig. III-8A). Also, presence of partial molds after ooids (fig. III-8B) indicate selective dissolution of more soluble cortices of the ooids. Pendulous (microstalactitic) vadose cements are also present (figs. III-8C and III-8D), indicating precipitation in the vadose zone.

Additionally, the possible permeability zone is positioned across the paleotopographically high bar-crest in SC 23a and occurs in both ooid grainstone and cement-occluded grain/packstone facies. It does not cross into the onlapping transgressive fossil packstone, however, and this may indicate that its formation predated transgression that led to deposition of SC 23b. However, it is also possible that development of the permeable zone postdated deposition of the fossiliferous packstone and textural qualities of the packstone facies prohibited formation of enhanced permeability.

The distribution of cement types found in samples above and below the permeability zone gives clues to its genesis. Below the zone many of the ooids and peloids have isopachous-rimming cements and relatively even distribution of intergranular cements, whereas little isopachous cement is found in samples above this zone, with blocky dolomite cement (probably derived from pressure solution of nearby grains) or pore space being present instead. Cement distribution is marginally patchier in the samples above the zone than below it, although this pattern is not well developed. In a modern Bahamian ooid shoal investigated by Halley and Harris (1979), meteoric diagenetic cements were found to be more evenly distributed around ooid grains below the water table than above it, and the overall appearance of cementation was more patchy in oolite residing above the meteoric water table (vadose zone) than below it. This reflects conditions whereby grains in the meteoric phreatic zone are completely submerged in diagenetic fluids and grains in the generally unsaturated vadose zone are bathed in transient fluids that are nonuniformly distributed. The preferential distribution of pressure- solution- compaction fabrics (discussed earlier) in rocks above the permeability zone tend also to support a meteoric phreatic diagenetic environment for rocks with isopachous cements.

Preferential distribution of oo-moldic fabrics, isopachous cements, and compactional fabrics around an interpreted thin zone of continuous permeability suggests that diagenesis associated with a meteoric water table may have caused dissolution of relatively soluble carbonate components along a thin (<1 ft) horizontal interval. Waters in the (uppermost) part of the phreatic zone (beneath but proximal to the water table) are generally the most chemically aggressive because they are charged with carbon dioxide acquired from the atmosphere (which extends down through the vadose zone) and soils (Moore, 1989).

This meteoric water table may have been established during a sea-level lowstand that occurred after SC 23a bar-crest deposition but prior to deposition of the immediately overlying SC 23b bar, the base of which is the transgressive fossil packstone that is not characterized by the anomalous permeability streak. Budd and Vacher (1991) developed criteria from which the maximum thickness of a floating meteoric lens beneath an island could be calculated. Although

facies types and diagenetically modified hydraulic paleoconductivity affect the calculations, the authors established that maximum lens thickness varied mainly between 1 and 2 percent of the island width. Assuming an island width for SC 23a of about 600 ft (the distance between points of intersection of the permeability zone with the bar flank [fig. III-7B]), the meteoric-lens thickness would have been between 6 and 12 ft beneath the bar crest. Given 1.5 ft between the base of the permeability zone and the compacted bar crest, a minimum of 1.5 ft of sea-level fall is required at the end of SC 23a deposition. There is no tidal-flat facies on the SC 23a bar crest, however, so sea level was probably several feet above it prior to the fall that established a meteoric lens. A fall of at least 3 ft is probably more reasonable. The positioning of the water table was probably rapid and short lived, as suggested by the thin geometry of the anomalous permeability zone and by the lack of abundant grain dissolution. Conditions conducive to development of these features are most likely achieved during a stillstand of lowered sea level because a much broader zone would have been affected if permeability-enhancing processes operated during the entire sea-level history of SC 23a.

Other samples recovered from Stone Canyon show similar evidence of meteoric diagenesis. Ooid-moldic grainstone was sampled from SC 26 just beneath tidal-flat facies at section 8 (fig. III-8F), but this sample was not especially permeable. However, fossil-moldic grain/packstone was recovered from SC 25, also just beneath tidal-flat facies at section 3 (fig. III-8G). The SC 25 sample has the highest permeability (59 md) of any sample recovered from Stone Canyon and was recovered from a 2-inch-thick stratiform zone that is laterally continuous for at least several meters along the outcrop; however, its total lateral dimension was not determined. This sample has well-developed dark-toned microstalactitic cements adjacent to fossil molds, indicating that vadose dissolution caused at least one generation of molds. The pendulous cements are enclosed in a later generation of light-toned cement that almost completely occludes primary intergranular pore spaces but its geometry suggests that it may be a second generation of vadose cement. The greatest volume of visible pores are molds; however, micrite envelopes on the fossil molds appear intact and interconnection between molds was not observed. This suggests

that molds may be insufficiently interconnected to form the pore network that composes most of the effective porosity of the sample. Another population of pores is observed to intersect the darker pendulous cements in places and, along with intercrystalline porosity, may compose the effective porosity in this sample. Further study is required to determine if permeability in this sample is caused by water-table-related processes or the presence of chemically metastable grain types (fossils).

An alternative process for development of the anomalous streak of above-average permeability in SC 23 is also suggested by figure III-8F, a photomicrograph of ooid-moldic grainstone that was sampled from SC 26. Here a large pore is shown that may have resulted from dissolution of formerly occurring calcium sulfate (anhydrite or gypsum). Although such large pores were not seen in SC 23 samples or in the fossil-moldic sample recovered from SC 25, many of the intergranular pores seen in samples such as shown in figure III-8A could have been filled with anhydrite during postdepositional carbonate cementation. A combination of porefilling and replacement by sulfate would have both preserved and enhanced original depositional porosity. During lowered sea level a back-barrier lagoon may have been established with an attendant hypersaline water table established within the emergent bar crest. Precipitation of evaporite minerals within primary depositional pores along the water table could have protected them against subsequent occlusion by carbonate cements suffered by overlying and underlying rocks. Leaching of a few unstable grains (ooid molds) could reflect dissolution attendant a thin ephemeral mixing zone of saline and meteoric water, although vadose processes are still considered more likely, given the presence of microstalactitic cements that indicate water-unsaturated conditions. Leaching of the evaporites would probably have occurred during Tertiary basin-and-range uplift but would probably survive in the subsurface if not exposed to sulfate-undersaturated water.

The presence of a laterally continuous thin zone of relatively high permeability has relevance to secondary recovery programs. Fluids used in flood operations would tend to flow disproportionately through such a pipe thus reducing sweep efficiency in the surrounding

stratigraphic section. Given that some of the better reservoir-quality rock may be in the bar crests of inner-shelf crest shoals, a pipe, or "thief zone," developed through bar crests could cause considerable bypass. Alternatively, a similar zone could become or remain filled with impermeable sulfate minerals in the subsurface and act as a barrier to vertical flow, thus forming a seal.

## CONCLUSIONS

Results from the general survey and detailed investigation of the Grayburg Formation in Stone Canyon have significant implications for development and secondary recovery programs involving hydrocarbon reservoirs developed in inner-shelf crest parts of mixed siliciclastic-carbonate reservoirs.

1. The organization of facies composing potential reservoir units conforms to a parasequence framework and thus the facies distribution is predictable.
2. Sandstones are laterally continuous at interwell distances and make good marker beds for correlation between wells in mixed siliciclastic-carbonate reservoirs, while specific carbonate facies are discontinuous and are poorer candidates for markers.
3. Reservoir-quality strata will be vertically enveloped by significantly less porous and permeable strata, generally at parasequence boundaries comprising transgressive tight packstone/wackestone or tight tidal-flat facies.
4. Reservoir-quality facies are likely to pinch out into nonreservoir facies within typical interwell distances of 650 ft (10 acres) to 1,320 ft (40 acres).
5. In mixed siliciclastic-carbonate reservoirs of the northern Central Basin Platform and in the fringing shelves of the Permian Basin, the better reservoir facies will be laterally continuous sandstones and fossiliferous grainstones and discontinuous bar-crest grainstones. Favorable petrophysical qualities of these same facies may be degraded in a reservoir containing abundant sulfate.

6. Primary depositional porosity may be preferentially preserved in grainstones mineralogically stabilized by early meteoric phreatic diagenesis during high-frequency sea-level lowstand episodes. Porosity and permeability in rocks not so stabilized prior to burial may be reduced by chemical compaction and reprecipitation in pores of carbonate mobilized by pressure-solution.
7. Thin high-permeability zones may be developed laterally through individual parasequences due to meteoric diagenesis along a water table associated with stillstands at lowered high-frequency sea levels. Alternatively, occlusion of primary depositional porosity by evaporites could have protected pores from carbonate cementation seen in overlying and underlying rocks. In a reservoir, similar zones could act as thief zones if effective pore spaces are not mineralogically occluded, or as barriers to vertical flow if occluded with sulfates.
8. Facies may be characterized and differentiated petrophysically by averaging porosity and permeability analyses performed within each facies. Given development of a facies-succession model and determination of porosity/permeability relationships on the basis of reservoir core analysis, averaged porosity values taken from geophysical porosity logs might be used to calculate permeabilities for various facies. These calculated permeability values can be used to generate simulations of reservoir fluid flow.
9. In a mixed siliciclastic-carbonate reservoir certain key facies may be identified with well-log data. Gamma-ray logs may be useful to differentiate siliciclastic-dominated from relatively pure carbonate strata; porosity logs may be useful in discriminating relatively porous carbonate strata from less porous, generally finer grained rocks.

CHAPTER IV: APPLICATION OF THE OUTCROP MODEL  
TO THE NORTH FOSTER GRAYBURG UNIT

Don G. Bebout

INTRODUCTION

The North Foster and Johnson Grayburg units are located in the northern part of the Foster and southern part of the Johnson Fields, respectively, in Ector County (fig. IV-1). These fields are part of the San Andres/Grayburg Carbonate (South Central Basin Platform) play, along with 17 other major San Andres and Grayburg reservoirs; the total cumulative production from reservoirs in this play through 1983 was 2.4 billion barrels (Bbbl). The Foster field produced 220 million barrels (MMbbl) and the Johnson field produced 24 MMbbl through 1983. Production is from the Guadalupian Grayburg Formation (fig. IV-2).

The ARCO North Foster unit was selected to serve as the subsurface setting for application of the Grayburg outcrop study results of sequence-stratigraphic controls on the distribution sand-bar facies. The study area was expanded to include adjoining Conoco Johnson and Cities Service Johnson Grayburg units and ARCO Johnson AB lease, where Prentice (1984) reported response to waterflood was poor because of "random anhydrite" flow barriers.

The Foster field was discovered in 1932; oil was first produced from the ARCO North Foster leases in 1939. Through 1963 recovery was by primary solution-gas drive, and 79 wells were averaging production of 6 bbl of oil per well per day (Gealy, 1966). Seventy-seven of these wells were drilled between 1939 and 1941. The ARCO North Foster leases were unitized as the North Foster unit for initiation of waterflood in 1962, and waterflood was implemented in 1963. Production and injection wells combined now total 152 in the unit area of 1,960 acres. Recovery efficiency with waterflood is only 29 percent (Galloway and others, 1983).

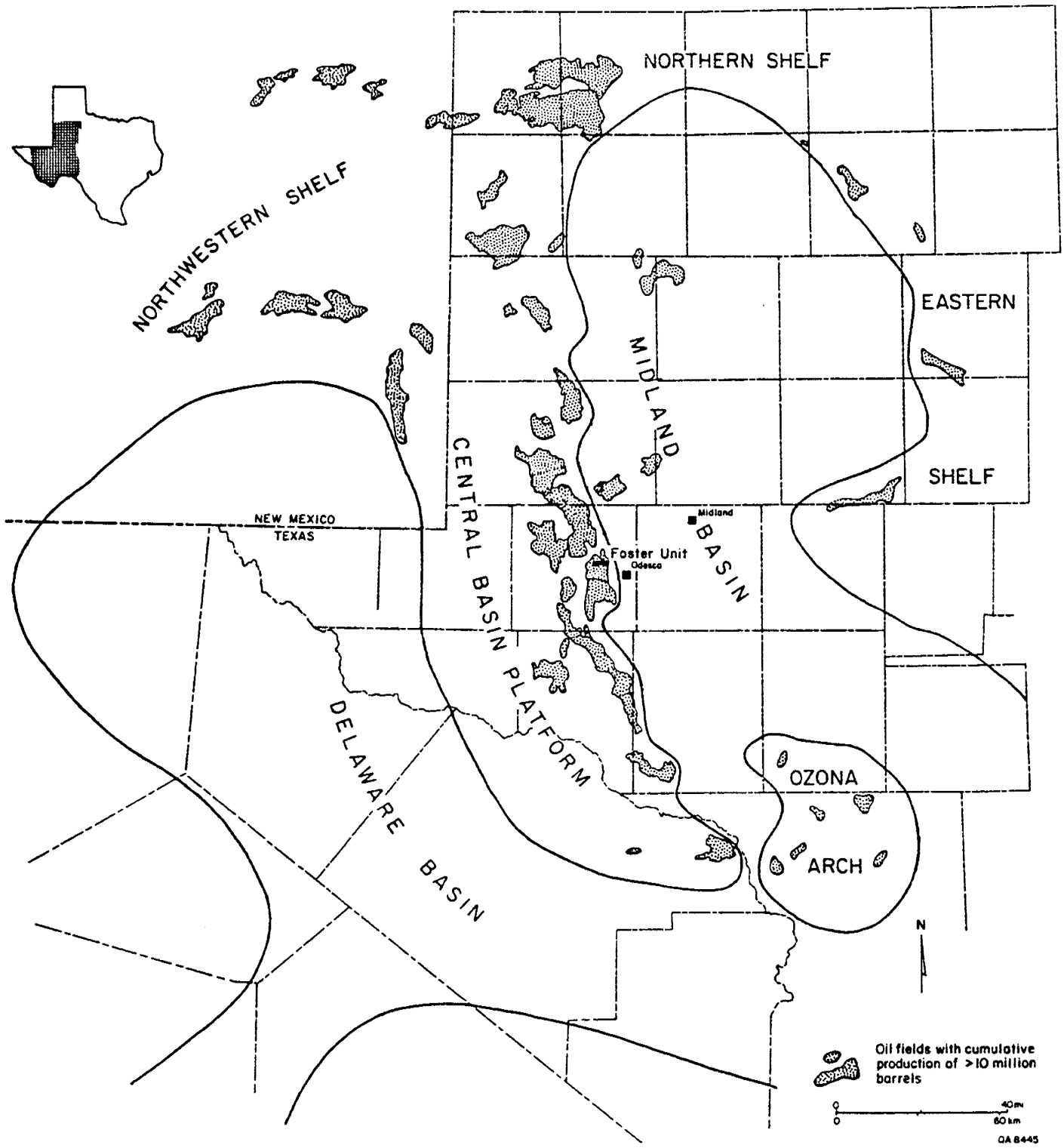


Figure IV-1. Index map of the Permian Basin showing the location of the ARCO North Foster unit on the eastern side of the Central Basin Platform, Ector County. The San Andres and Grayburg oil fields that have produced more than 10 million barrels of oil are also shown.

SYSTEM	SERIES	STRATIGRAPHIC UNIT	
PERMIAN	Ochoan	Dewey Lake	
		Rustler	
		Salado	
		Castile	
	Guadalupian	Capitan	Tansill
			Yates •
			Seven Rivers •
		Goat Seep	Queen •
			Grayburg •
	San Andres ●		
Leonardian	Clear Fork ●		
PENNSYLVANIAN		Spraberry •	
		Dean •	
		Wolfcamp •	
		Cisco •	
		Canyon •	
MISSISSIPPIAN		Horse-shoe Atoll •	
		Strawn •	
DEVONIAN		Bend •	
		Mississippian •	
SILURIAN		Devonian •	
		Fuselman •	
ORDOVICIAN	upper	Montoya •	
	middle	Simpson •	
	lower	Ellenburger ●	
CAMBRIAN			

Relative production • → ●

QA 8443

Figure IV-2. Stratigraphic section of the Paleozoic strata of the Central Basin Platform/Midland Basin showing relative distribution of produced oil. From Galloway and others (1983).

This reservoir study concentrated on the ARCO North Foster unit, from which the operator made available logs from 127 wells, continuous cores from 7 wells, and production, well-history, and test data from all wells (fig. IV-3). Cores were also examined from adjoining leases to gain insight into the lateral extent of the facies recognized in the North Foster unit. ARCO provided logs and cores from eight wells from its J. L. Johnson AB and D leases. Conoco provided logs and cores from two wells in its J. L. Johnson unit and one from its Gist unit. Cores and logs were also obtained from six wells in the Cities Service Johnson Grayburg/San Andres unit.

### Geological Setting

The North Foster unit, located on the eastern edge of the Central Basin Platform near the northern extent of the Midland Basin, during the time of deposition of the Grayburg section (fig. IV-1). The Midland Basin was only hundreds of feet deep, and a gentle slope or ramp descended from the shelf edge into the basin. Consequently, facies changes on the slope are subtle and gradational. As the basin was being filled and subsequently retreated to the south during deposition of the Grayburg, the relief from shelf to basin decreased; by the time the overlying Queen Formation siliciclastics and evaporites were being deposited, open-marine conditions were no longer present in the basin. Correlations within the Queen Formation show that this unit thickens only slightly basinward from the platform.

The Grayburg Formation represents the topmost depositional sequence of the Lower Guadalupian (fig. IV-2) and ranges in thickness from 250 to 300 ft at the shelf edge of the underlying San Andres sequence. The sequence boundary at the top of the San Andres is well defined by the presence of tidal-flat deposits consisting of thick siltstone units and pisolite facies (fig. IV-4). Karst features recognized locally on outcrop were not seen in core. The initial flooding over the San Andres is indicated by a thin marine grainstone over the tidal-flat section. The top of the fusulinid wackestone facies, which overlies the grainstone, indicates the position of the maximum flooding of the Grayburg sequence. The remaining upper part of the

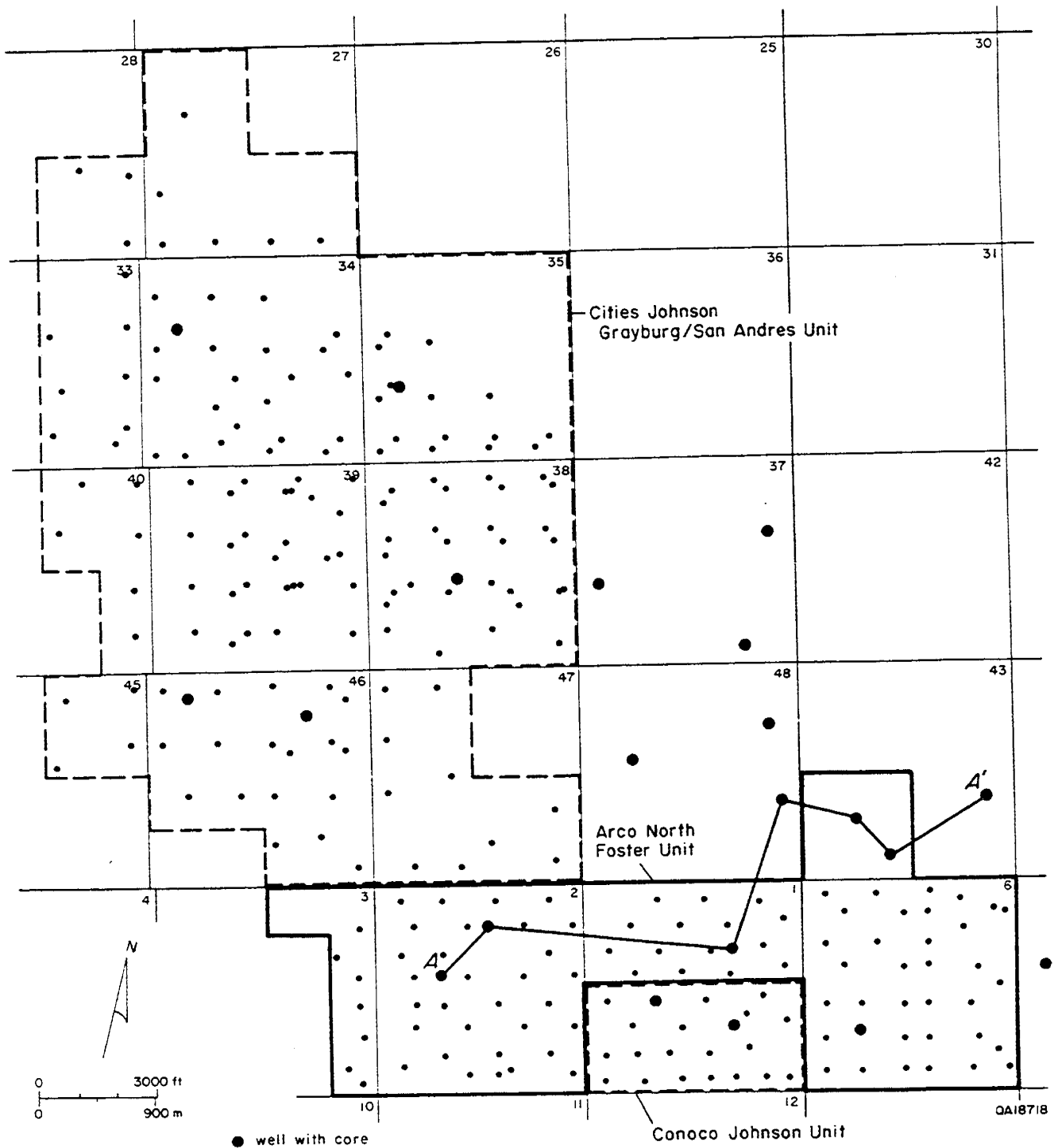


Figure IV-3. Well-location map of the study area showing location of the ARCO North Foster, Cities Service Johnson Grayburg, and Conoco Johnson units, and location of cross section A-A' (figs. IV-5 through IV-9).

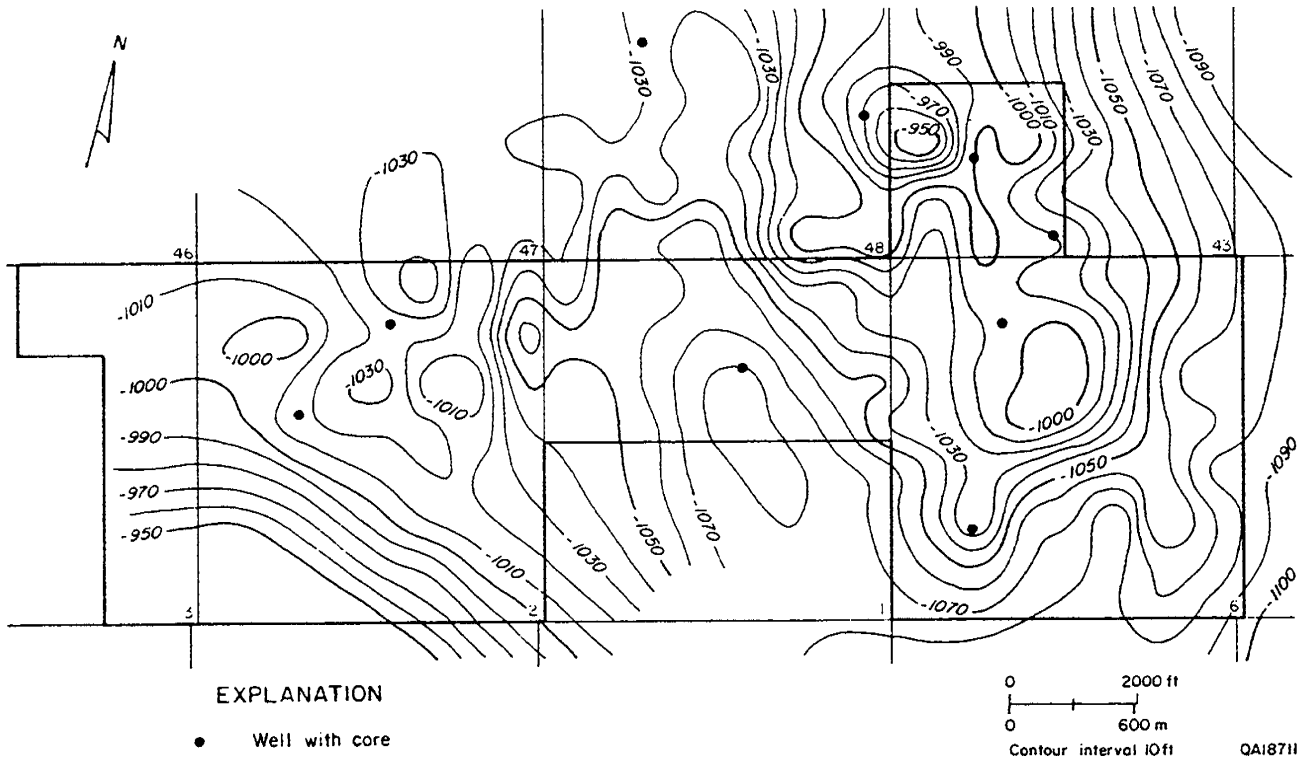


Figure IV-4. Structure map contoured on top of the Grayburg Formation.

Grayburg represents the high-stand systems tract, made up of 18 upward-shoaling cycles, or parasequences.

The present structure at North Foster is an asymmetrical anticline, with the crest of the anticline on the eastern side of the unit, just north of the center of section 6 (fig. IV-5). Relief is from -1,082 ft in the structural trough in the center of the unit, section 1, to -991 ft in section 6.

Long continuous cores from a number of wells provide a complete record of the vertical sequence of facies (table IV-1) through the Grayburg Formation in the ARCO North Foster unit. The lateral distribution of facies is illustrated by a cross section that includes wells with continuous cores of the Grayburg Formation in the ARCO North Foster unit (figs. IV-4 and IV-6 through IV-9).

### Grayburg Sequence Stratigraphy at North Foster

#### San Andres/Grayburg Sequence Boundary

The sequence boundary at the top of the San Andres Formation is well displayed in the core from the ARCO North Foster 125 (fig. IV-4); this core includes the upper 60 ft of the San Andres Formation. The top 15 ft of the San Andres consists of pisolite and lithoclast siltstone and silty pisolite grainstone; fenestral structures are common. The tidal flat and exposure surfaces at the top of the San Andres Formation are well documented in the cores. The contact of the top of the San Andres with the overlying Grayburg is sharp and possibly bored, but evidence of paleokarst as observed on the outcrop is lacking.

Below the pisolite and lithoclast siltstone and silty pisolite grainstone in the San Andres are three, approximately 10-ft-thick, upward-coarsening cycles, which grade from silty burrowed mudstone to packstone at the base to laminated and crossbedded, fine- to coarse-grained grainstone at the top. Grains are dominantly fine grained and not identifiable; however, coarse-grained parts are composed of intraclasts. Fusulinid wackestone occurs approximately

Table IV-1. Character and Interpretation of Grayburg facies at North Foster.

FACIES	STRUCTURES	ALLOCHEMS	DIMENSIONS THICKNESS (ft) DIP WIDTH (mi)	ENVIRONMENT	WATER DEPTH RANGE (ft)
Siltstone	Irregular laminations, small burrows, parallel laminations, and crossbedding	Silticlastic silt	3 to 40 ft Several miles	Shallow, quiet-water shelf	0-25
Mudstone	Even, parallel laminations, irregular laminations, small burrows, stylolites	—	2 to 10 ft Several miles	Shallow-water shelf	
Coarse-grained grainstone	Stylolites, vertical fractures, irregular laminations	Peloids, mollusks, rare lithoclasts	5 to 38 ft 0.5 to 1.0 mi	Shallow-water, flat with sand waves and troughs	5-15
Diagenetically altered fine-grained grainstone	Vertical-oriented large burrows	Mostly peloids, minor mollusks, crinoids	38 to 92 ft 1.5 to 2.0 mi	Open shelf	20-50
Fusulinid wackestone	Burrows, irregular laminations, stylolites	Dominantly fusulinid, crenous, mollusks, peloids	60 to 100 ft 2 to several mi	Upper slope	30-100
Fenestral/coated-grain packstone/grainstone	Fenestral, sheet cracks, small vertical burrows, mud erodes, stylolites	Mollusks	30 to 40 ft Several miles	Arid tidal flat	0-1.0

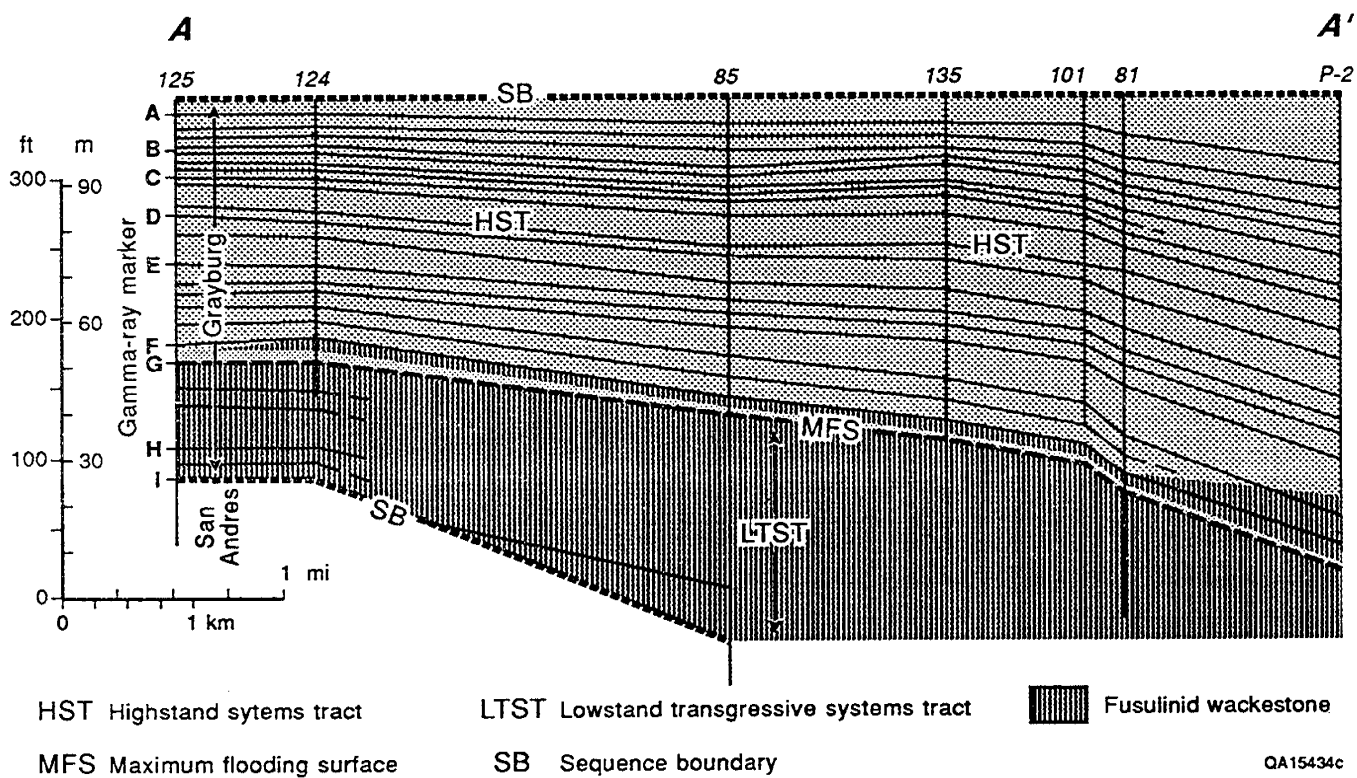


Figure IV-5. Generalized dip cross section A-A' across the ARCO North Foster and Conoco Johnson units showing the sequence-stratigraphic units of the Grayburg Formation and occurrence of the fusulinid-wackestone facies. Major gamma-ray markers that were used to develop a correlation grid throughout the study area area are also shown. Location of the cross section is shown in figure IV-3.

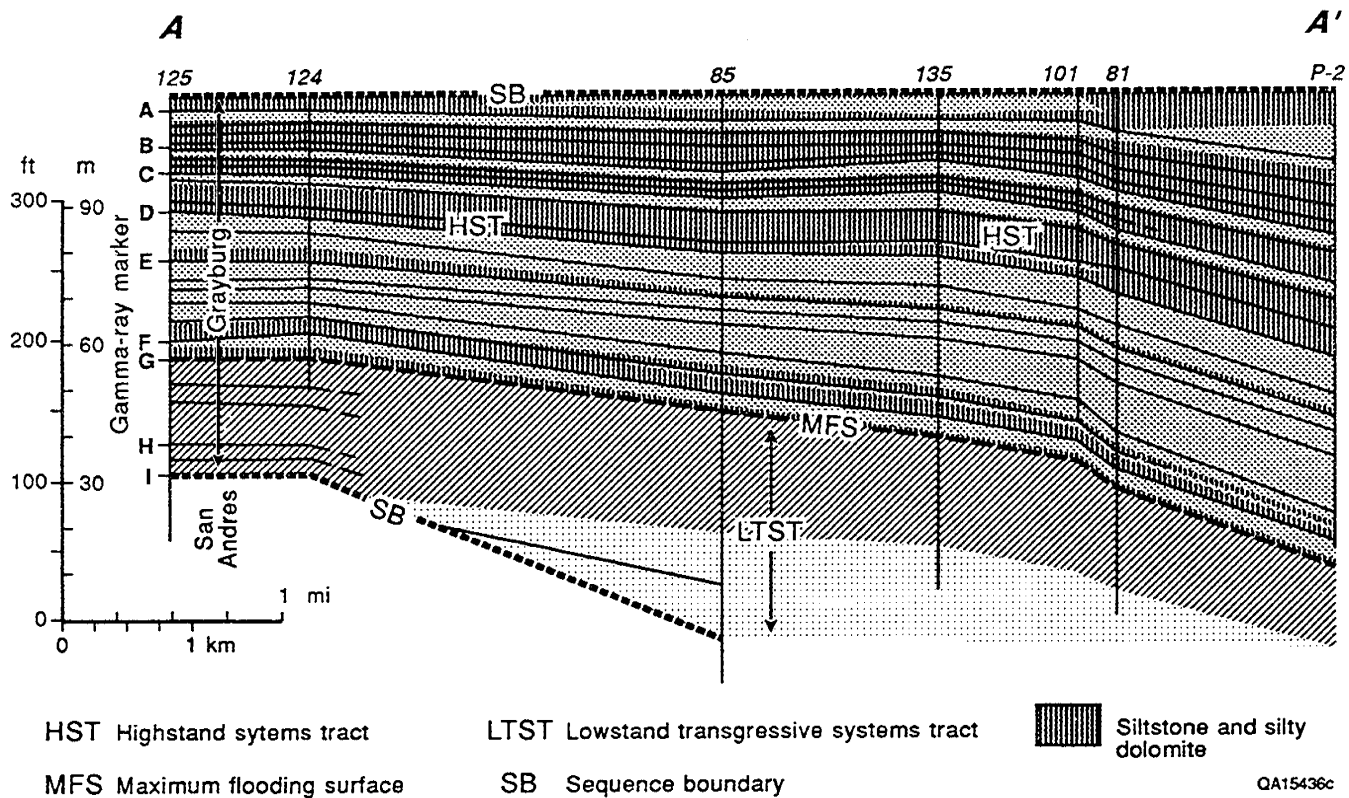


Figure IV-6. Generalized dip cross section A-A' across the ARCO North Foster and Conoco Johnson units showing the occurrence of the siltstone and silty dolostone facies. Location of the cross section is shown in figure IV-3.

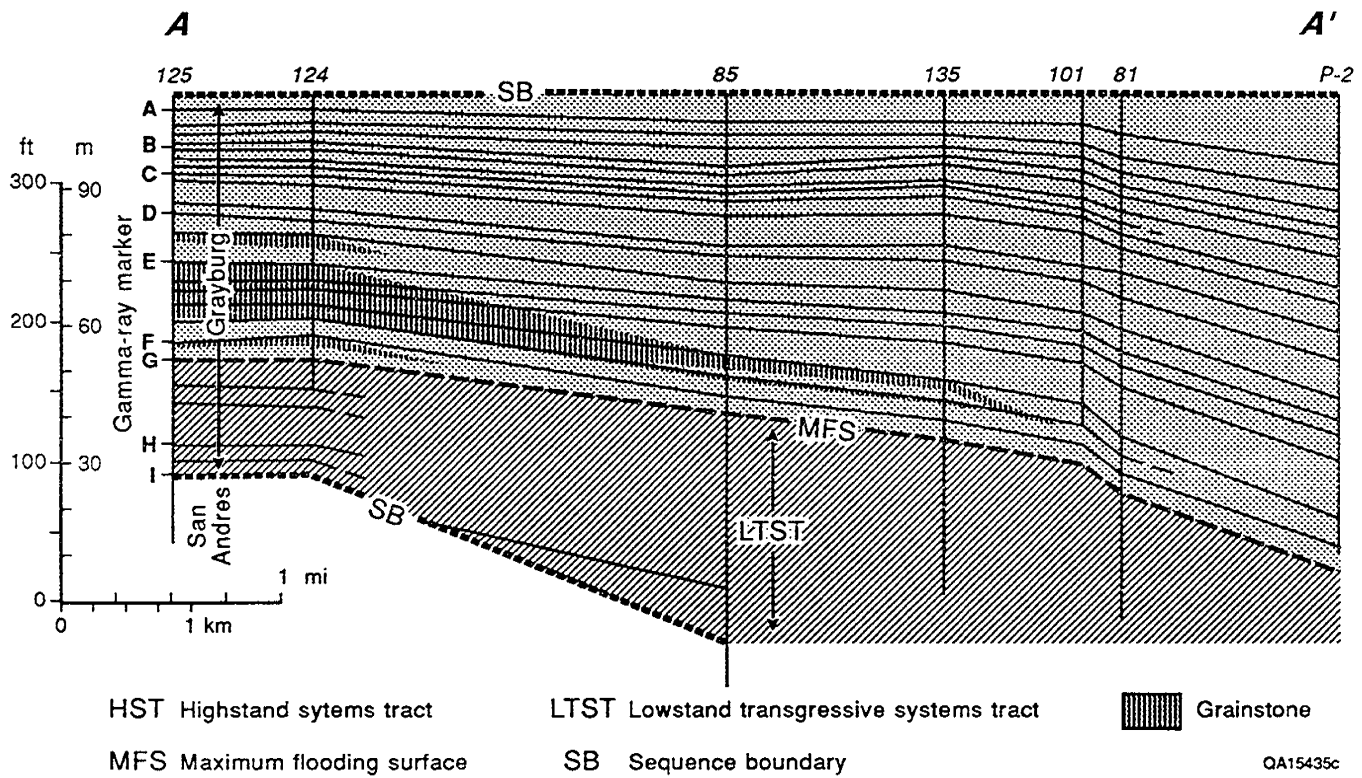


Figure IV-7. Generalized dip cross section A-A' across the ARCO North Foster and Conoco Johnson units showing the occurrence of the grainstone facies. Location of the cross section is shown in figure IV-3.

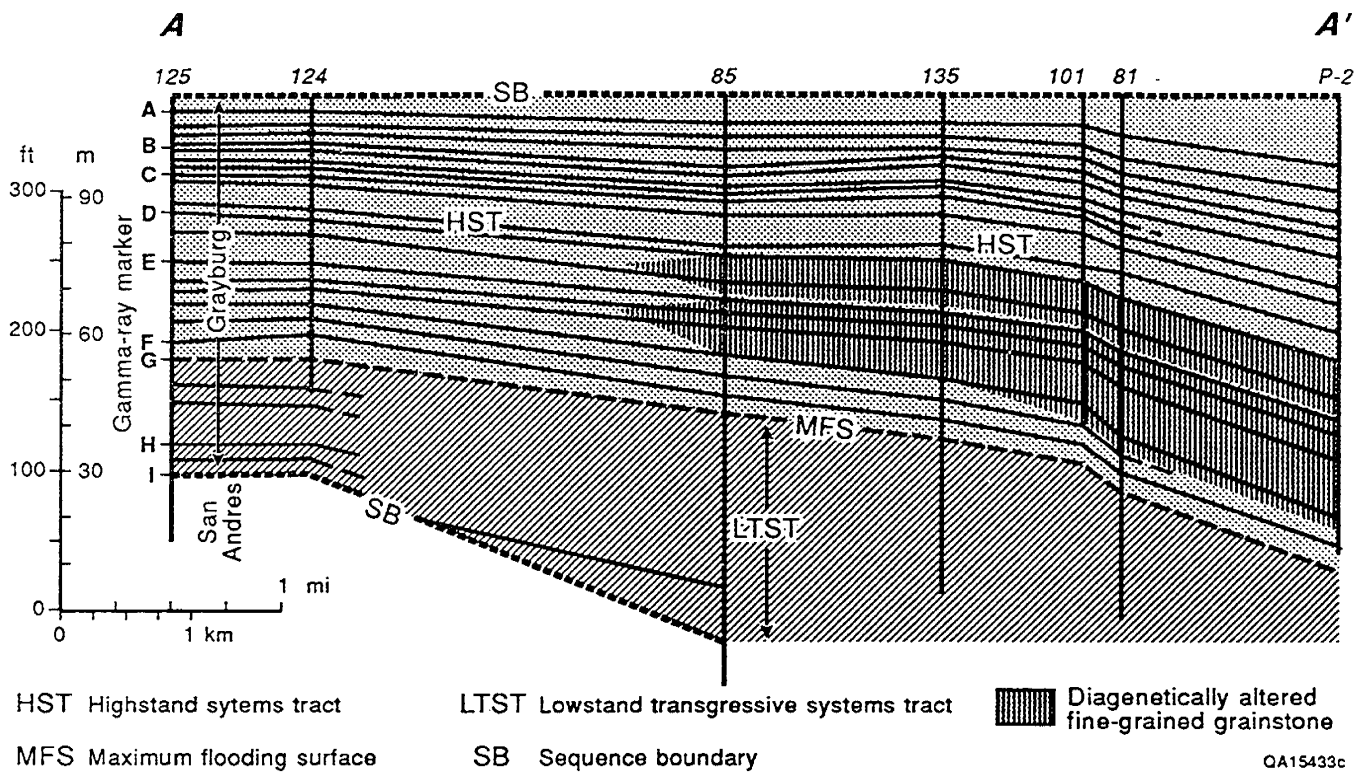


Figure IV-8. Generalized dip cross section A-A' across the ARCO North Foster and Conoco Johnson units showing the occurrence of the diagenetically altered dolostone facies. Location of the cross section is shown in figure IV-3.

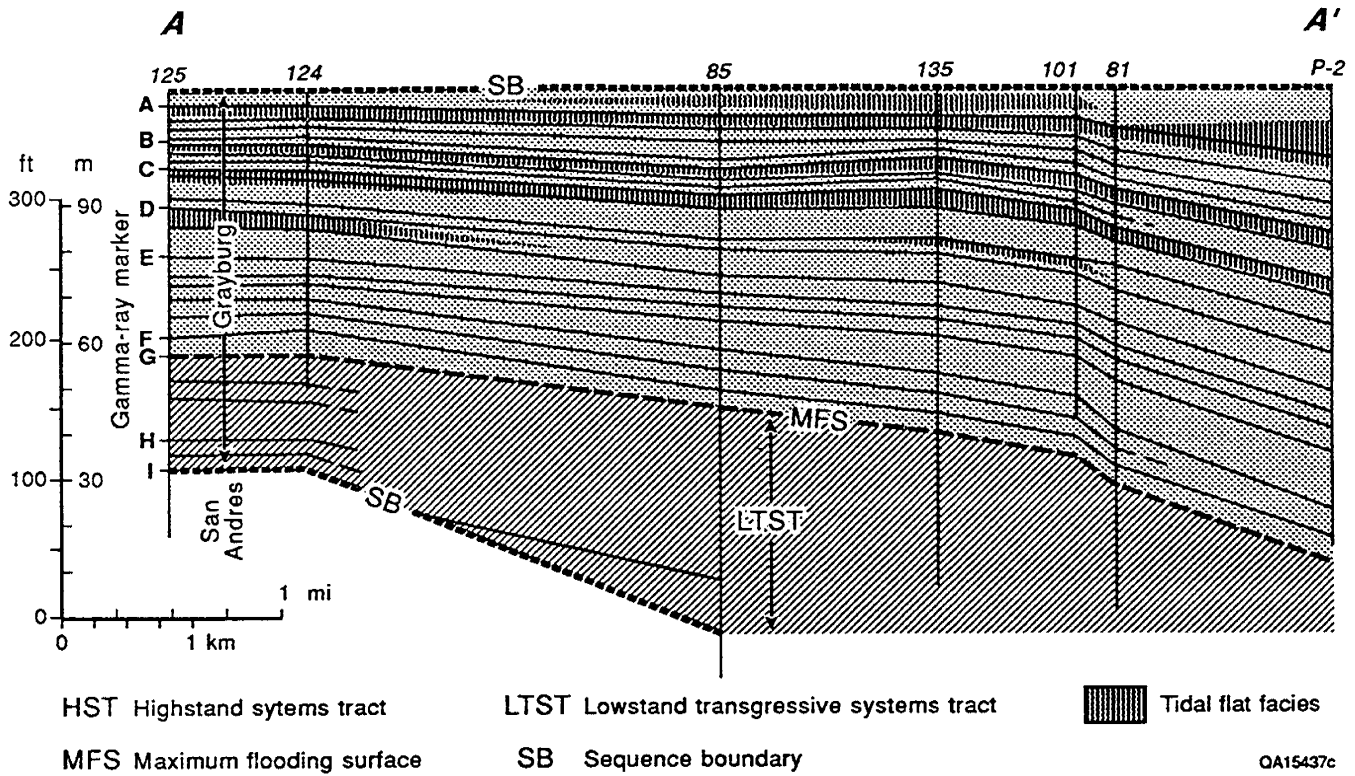


Figure IV-9. Generalized dip cross section A-A' across the ARCO North Foster and Conoco Johnson units showing the occurrence of the tidal-flat facies. Location of the cross section is shown in figure IV-3.

40 ft below the top of the San Andres Formation. The San Andres platform margin, documented by the tidal-flat siltstone and pisolite facies in the cores from these two wells to the east into the Midland Basin is believed to be just west of the ARCO North Foster 85 well because of the abrupt thickening of the lower two units of the basal Grayburg (GH and HI) on log correlations in the 85 well. No other wells in this area penetrate deeply enough to provide corroborating evidence for this shelf edge.

#### Lowstand/Transgressive Systems Tract (LTST)

The basal 20 to 40 ft of the Grayburg (correlation markers H to I), also cored by the ARCO North Foster 125 well (fig. IV-4), are represented by two approximately 10-ft-thick, upward-coarsening cycles. The lower part of the cycles is dominated by siltstone; the grainstone at the top of the cycles is fine grained and lacks lamination, suggesting relatively low-energy conditions. Fusulinids occur in wackestone parts of the lower part of both cycles. Up to 10 percent moldic and interparticle porosity occurs in the grainstone. These cycles are interpreted to represent transgressive onlap onto the San Andres sequence. Log correlations from North Foster 124, on the underlying San Andres shelf, to the North Foster 85, off the San Andres shelf margin, suggest that these grainstone-capped cycles thicken and extend at least this far basinward (fig. IV-4).

A thick section of fusulinid-wackestone facies overlies the lower grainstone cycles of the basal Grayburg. The fusulinid-wackestone facies is 95 ft thick in the core from the ARCO Johnson AB 135 well (fig. IV-4); however, this well did not penetrate the entire thickness of the formation, which is estimated to be approximately 155 ft. This facies attains a thickness of at least 135 ft, as indicated by log correlations to the nearby ARCO North Foster 85 well. The fusulinid wackestone facies varies in texture from dominantly wackestone to less common packstone. Fusulinids are the most common faunal constituent, but mollusks, dasycladacean algae, and crinoids are also present. The fusulinid wackestone facies represents the deepening of water over the flooded San Andres shelf—the transgressive systems tract—and is interpreted

to represent upper-slope environments. The transgressive systems tract, including the fusulinid wackestone and underlying thin upward-coarsening grainstone cycles, account for approximately one third of the Grayburg section.

Within the fusulinid-wackestone facies, as many as 12 upward-coarsening cycles have been identified. The upward change from wackestone to packstone textures is gradational in most cases and takes place over thicknesses ranging from a few feet to 20 ft. The change from packstone, at the top of a cycle, to the overlying wackestone is abrupt. Three to four feet of silty dolostone occur at the base of several of the cycles; these silty zones are correlatable from well to well.

#### Maximum Flooding Surface

The G correlation marker, located at the top of the fusulinid-wackestone facies at its maximum landward location, represents the maximum flooding surface for the Grayburg sequence (fig. IV-4). A 10- to 15-ft-thick section of fusulinid-wackestone facies occurs above the G marker (between the F and G markers) in more downdip wells and represents the deeper water part of the highstand systems tract.

#### Highstand Systems Tract

The overlying two thirds of the Grayburg is represented by sediments of the highstand systems tract, which includes a number of facies: diagenetically altered fine-grained grainstone, coarse-grained grainstone, mudstone, siltstone, and fenestral/coated-grain packstone/grainstone (figs. IV-6 through IV-9).

Above the fusulinid-wackestone facies and between correlation markers E to G, cores from wells on the western end of the cross sections (fig. IV-7), located over the buried San Andres platform, are characterized by up to 70 ft of repeated 10- to 15-ft thick upward-coarsening cycles, which are capped by coarse-grained grainstone. The lower two cycles, directly over the

fusulinid wackestone, are dominated by thick siltstone units at the base, just above the F and G correlation markers (fig. IV-6). Above the siltstone and up to the E marker are four grainstone-dominated cycles; the lower two cycles extend basinward farther than the remainder of the coarse-grained grainstone cycles (fig. IV-7). This grainstone-dominated part is present over the older San Andres shelf margin, and in this regard is similar to the grainstone facies on the outcrop in the Guadalupe Mountains. However, the subsequent depositional styles of these two areas differ in that the grainstone cycles in the North Foster unit demonstrate an aggradational stacking pattern, whereas those of the outcrop prograde basinward several miles. At North Foster the broad, shallow-water shoal complex that developed over the fusulinid wackestone on the western side of the study area remained essentially in that position (figs. IV-10 through IV-12). However, local migration of grainstone bars, which accumulated at least in part in the intertidal zone, across this approximately 1-mi-wide complex resulted in the formation of the upward-coarsening cycles (EG correlation unit).

Diagenetically altered, fine-grained grainstone occurs immediately above the fusulinid-wackestone facies in the expanding section of downdip wells located basinward of the underlying San Andres shelf margin (fig. IV-8). This facies is characterized by a vertical-mottled pattern of dark-brown dolostone with moldic porosity and light-brown dolostone with interparticle porosity. Mollusks and crinoids occur throughout. The texture of the dark-brown portion is difficult to discern but appears to be gradational into the light-brown portion, identified as dominantly fine-grained grainstone, and is thought to be also grainstone in texture. The vertical structures are presumed to represent large burrows, which altered the primary grainstone fabric sufficiently to affect subsequent diagenesis patterns. The pellet-sized grains accumulated in water depths of 20 to 30 ft; bottom currents were sufficient to remove the mud-sized sediment but left behind silt to fine-sand-sized grains, probably in low-relief, ill-defined bars. The presence of mollusks and crinoids supports the interpretation of a normal-marine setting, and the high grain content and general lack of lamination and cross-

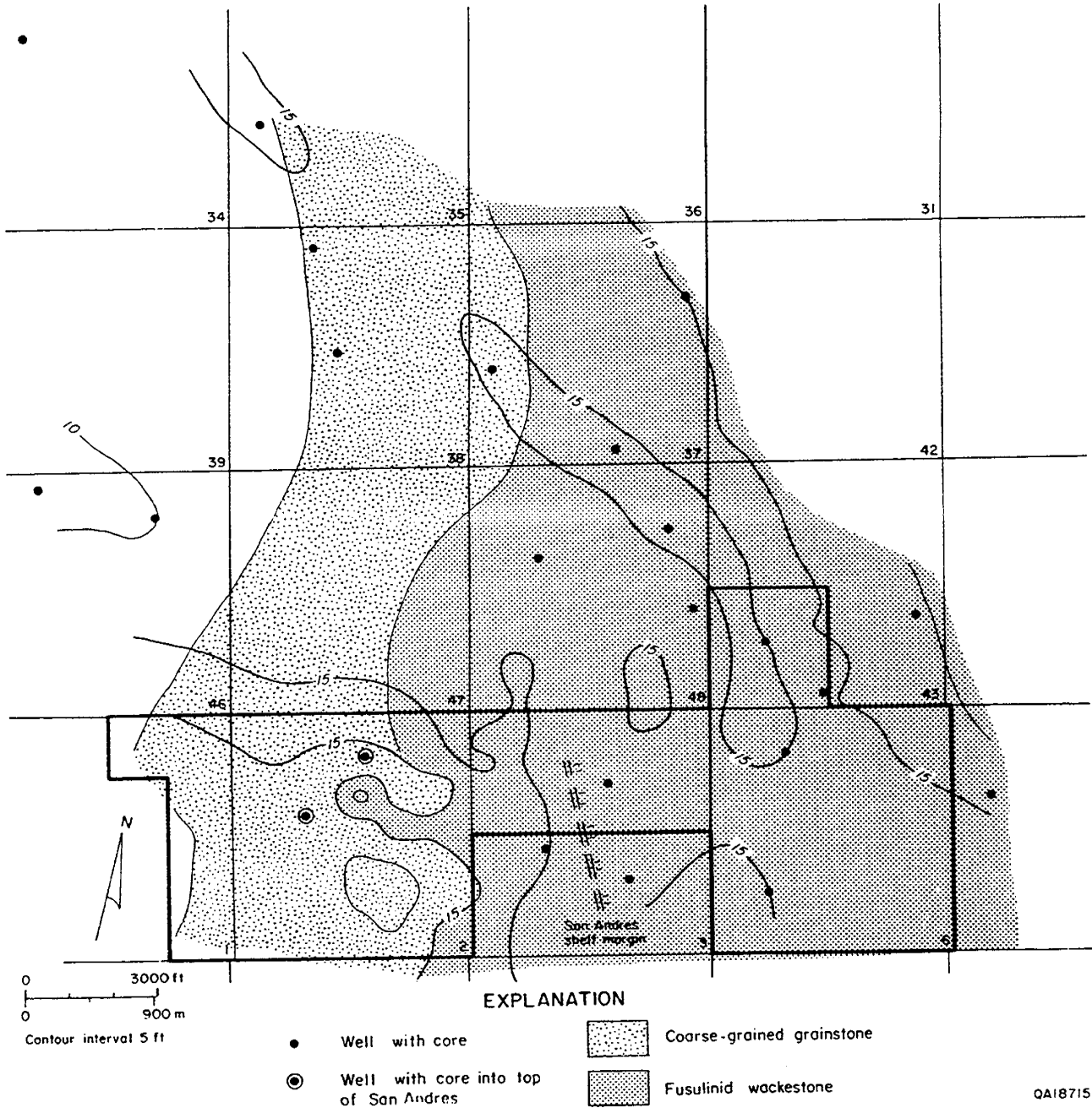


Figure IV-10. Isopach map of the FG correlation unit. The distribution of facies is from descriptions of cores from the wells on the cross sections. The location of the San Andres shelf margin was determined from core data from the wells on the western end of the A-A' and B-B' cross sections, as indicated by the larger circles, and log correlations to wells east of the shelf margin.

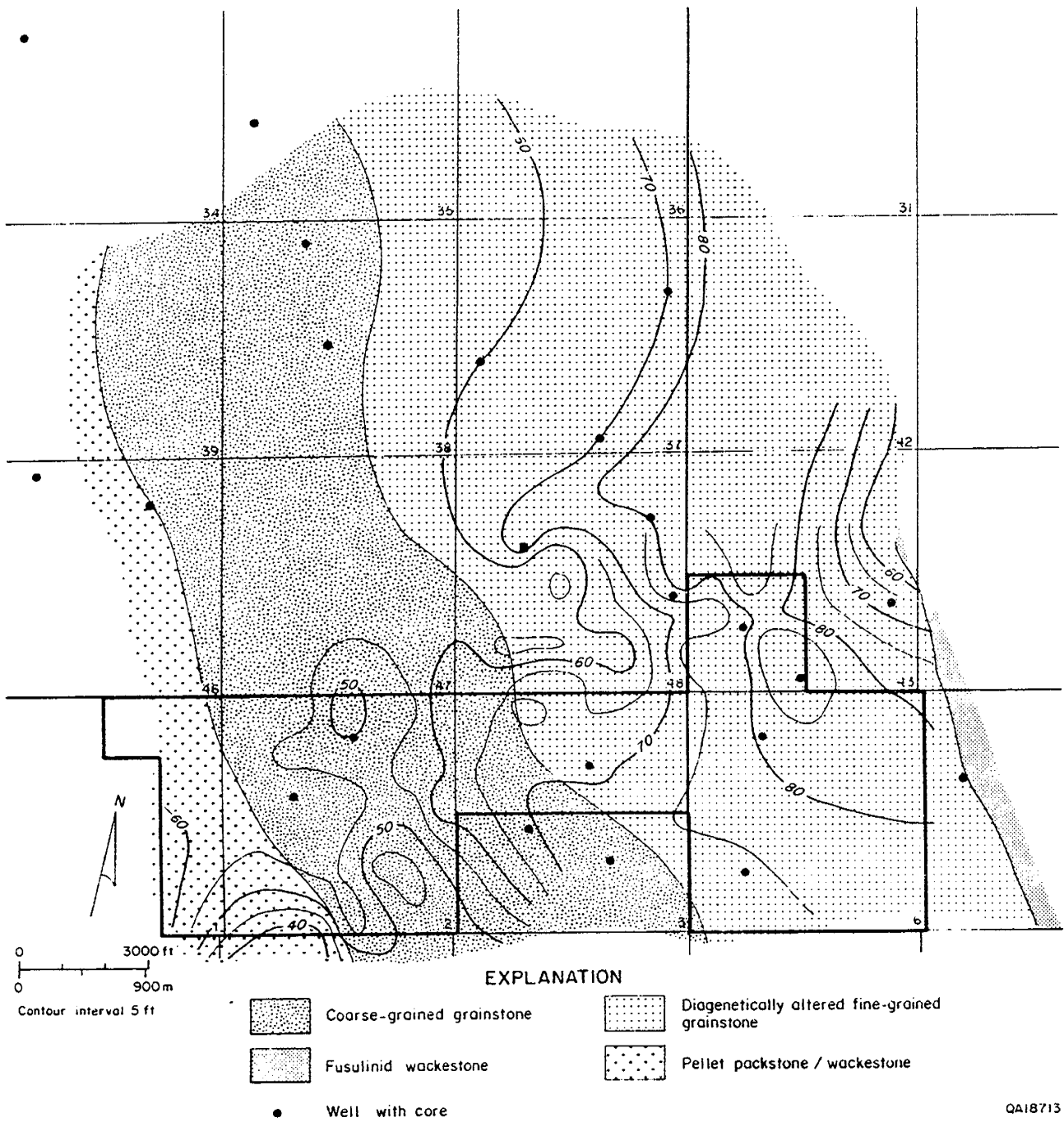


Figure IV-11. Isopach map of the EF correlation unit. The distribution of facies is from descriptions of cores from the wells on the cross sections.

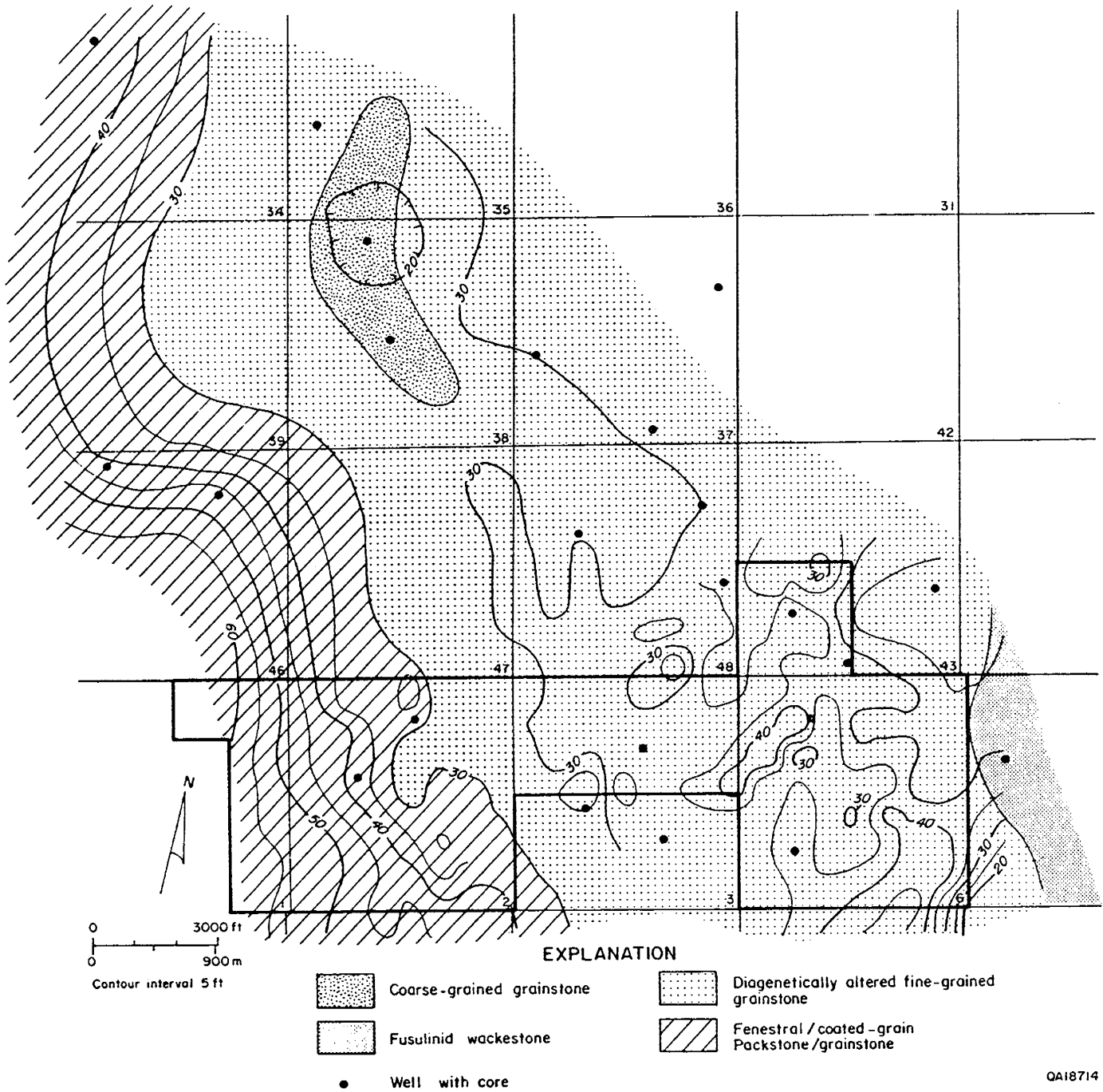


Figure IV-12. Isopach map of the DE correlation unit. The distribution of facies is from descriptions of cores from the wells on the cross sections.

lamination suggest that bottom currents may have been adequate to transport finer grained mud but were not high enough to produce laminations and cross-laminations. Burrowing organisms were abundant on these relatively stable grain bars, and vertical burrowing activity resulted in sufficient textural alteration of the original sediment to result in variations in subsequent diagenetic alteration—the diagenetically altered fine-grained grainstone. This low-energy grain flat was 1 1/2- to 2-mi wide and is replaced basinward by the fusulinid-wackestone facies of the upper slope (figs. IV-11 and IV-12).

The cyclic character of the Grayburg continues above the E marker to the top of the Grayburg Formation, but the nature of the cycles changes (figs. IV-6 and IV-9). Siltstone and mudstone occur at the base of each cycle, but the upper parts are composed of thick fenestral/coated-grain packstone/grainstone. The fenestral dolostone increases in thickness approximately 30 percent to the north in the Johnson unit. Thus, the shallowing trend continues above the shoal complex with the development of tidal-flat conditions indicated by the occurrence of the fenestral/coated-grain packstone/grainstone facies (DE correlation unit, fig. IV-12). The fenestral structures and sheet cracks indicate at least periodic exposure on the otherwise high-energy grain flat. The tidal-flat conditions were more persistent to the north in the Johnson unit where the DE correlation unit is up to 30 percent thicker and dominated by fenestral dolostone structures.

Above the D marker, siltstone is the dominant facies and the dolostone units are thinner and vary in texture from mudstone to grainstone and in structure from fenestrae to laminations and cross-laminations. These dominantly siltstone cycles above the D marker occur across the study area (figs. IV-6 and IV-9). The entire section from the top of the Grayburg to the D marker thickens basinward. The nature of the facies in these cycles suggests that the area was covered by very shallow-water to tidal-flat conditions. The siltstone units exhibit small burrows, laminations, cross-laminations, and fenestral structures. No fossils were found, indicating conditions were not normal marine. Likewise, the dolostone units are characterized by mudstone to grainstone textures with abundant small burrows and fenestral structures and no

marine fossils, suggesting very shallow water but not normal marine in character. Basinward of the North Foster unit, the dolostone contains mollusks, indicating a trend toward normal-marine conditions in this downdip position.

### Diagenesis

The major diagenetic event in the Grayburg sediments was dolomitization, and all the carbonates have been dolomitized. Bebout and others (1987) suggested that San Andres and Grayburg sediments were dolomitized early, during the Guadalupian, by downward-percolating hypersaline water originating from overlying arid tidal flats. The Guadalupian timing for dolomitization is based on strontium isotopic data reported by Leary and Vogt (1986), and the hypersaline nature of the fluids is based on oxygen- and carbon-isotope data of Leary and Vogt (1986), Naiman (1982), and Bein and Land (1982).

The dolomite crystals range in size from 2 to 60 microns. The finer crystals are typical of the tidal-flat facies, and the original textures and structures are best preserved in these dolostones. The tidal-flat carbonates are believed to have been dolomitized penecontemporaneously as a result of local salinity fluctuations on the arid tidal flat. Coarser crystals occur in the subtidal facies and probably resulted from the downward-percolating hypersaline brines of the subsequent younger Guadalupian tidal flats. The coarsest dolomite crystals are characteristic of the section below the hydrocarbon-bearing dolostone; corroded and hollow dolomite crystals, evidence of later dolomite dissolution, also occur locally below the hydrocarbon section.

Early submarine to intertidal aragonite cementation is clearly indicated on some ooid and pellet grainstones by thin rims of dolomite crystals, which are coarser than the crystals making up the grains. However, more of the grainstones are composed of uncoated, touching grains with porosity in the intergranular space or with anhydrite as the only recognizable cement.

The sulfate minerals anhydrite and gypsum are major components both as pore-filling cement in primary pores and in molds caused by leaching of skeletal grains and as a

replacement of the carbonates. Poikilotopic, anhydrite-filling primary pore space in very loosely packed ooid and pellet grainstones suggests very early cementation, probably as gypsum or anhydrite crusts at or near the surface of the tidal flat; these grainstones typically display no other preceding form of carbonate cement, indicating that they were uncemented, loose carbonate sand prior to cementation by the sulfate minerals.

Bebout and others (1987) interpreted the sulfates, particularly those replacing subtidal dolomite, as originating from the same hypersaline brines of the overlying tidal flats as those that dolomitized the carbonates, based on geochemical evidence by Bein and Land (1982). Bein and Land attributed the high strontium content of Palo Duro Basin sulfates to primary anhydrite precipitation from highly saline water.

Feldspar grains make up a minor component of the siltstone and silty dolostone facies. These grains are commonly leached, resulting in moldic porosity in the siliciclastic facies. Remnant lineations of the former feldspar cleavage are evidence of this diagenetic process.

#### Porosity and Permeability Distribution

Porosity and permeability in the North Foster field are strongly facies controlled. For this reason, the facies cross sections (figs. IV-5 through IV-9) and maps (figs. IV-10 through IV-12) are used to demonstrate their distribution vertically and laterally across the field.

Three types of porosity occur in the Grayburg dolostones: (1) primary intergranular, (2) secondary moldic, and (3) secondary intercrystalline. Intergranular porosity occurs within pores remaining between grains in both the coarse- and fine-grained grainstones. Some of the intergranular areas are rimmed with isopachous cement, which surrounds the grains, and others are defined solely by the edges of the grains themselves. Intergranular porosity also occurs between silt grains in the siltstone facies, particularly in those in which siliciclastic grain content is higher than 80 percent. Intergranular porosity in the coarse-grained grainstone facies (fig. IV-7) ranges from 3 to 15 percent, and permeability ranges from less than 1 to 70 md. Zones of higher porosity and permeability are 2 to 3 ft thick. Intergranular porosity in the

diagenetically altered fine-grained grainstone facies (fig. IV-8) ranges from 1 to 20 percent, and permeability ranges from <1 to 196 md.

Moldic porosity, the result of leaching of mollusk grains and fusulinids, occurs commonly in wackestone facies (fig. IV-5). However, it is also characteristic of the dark-colored portion (less altered) of the diagenetically altered, fine-grained grainstone facies, where it is the dominant porosity type because of the absence of leaching of the cement between the grains. Moldic porosity is best developed in the fusulinid-wackestone facies and ranges from 2 to 15 percent; permeability is low and ranges from 1 to 13 md. Moldic porosity also occurs in the siltstone facies (fig. IV-6) where feldspar grains are leached.

Intercrystalline porosity is present in low amounts throughout most of the Grayburg section; where intergranular and moldic porosity are developed, intercrystalline porosity goes unnoticed. This porosity type is best developed and recognized in the coarse-crystalline dolostone, where intercrystalline pores are easily visible.

#### RESERVOIR EXPLOITATION APPROACHES

Production in the North Foster Unit Grayburg reservoir is primarily from three facies: (1) coarse-grained grainstone, (2) fusulinid wackestone, and (3) diagenetically altered fine-grained grainstone. Each of these facies has a unique geographic location and vertical porosity/permeability distribution. Production from this unit has been highest on the eastern side just west of the center of section 6 (fig. IV-13).

The coarse-grained grainstone facies occurs in the western half of the unit (figs. IV-10 and IV-11) between the E and F correlation markers (fig. IV-7). This facies, which reaches a maximum of 40 ft thick, is represented in some wells as totally grainstone and in others as distinct upward-coarsening cycles with grainstone only at the top of each cycle. High porosity and permeability occur in thin zones 2 to 4 ft thick. Porosity in these zones is 16 to 17 percent, and permeability is as much as 70 md. These porous and permeable zones are separated by

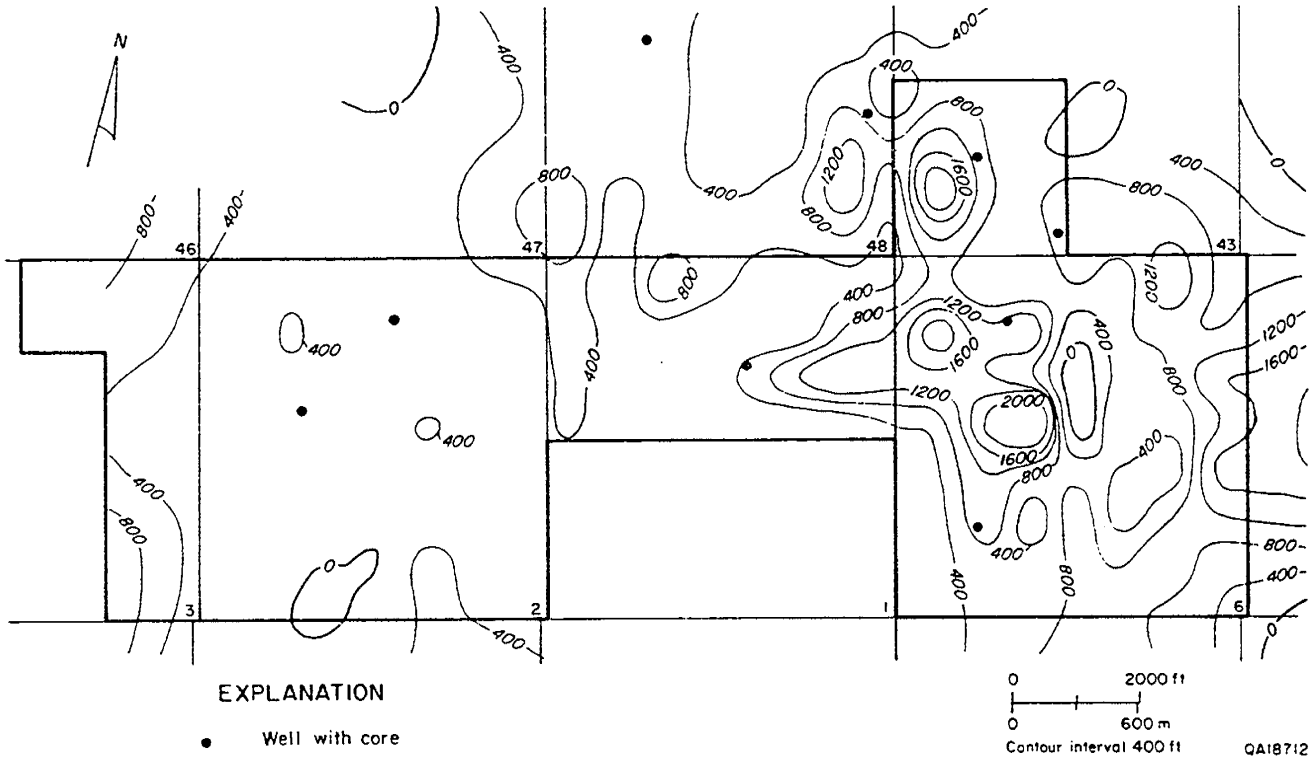


Figure IV-13. Rate of oil production from wells in the ARCO North Foster unit. The production rate has been normalized to barrels per month in order to take into account the widely varying ages of wells in the unit.

thicker zones of low porosity and permeability. Most of the production from the western side of the unit is from these thin, locally distributed porous zones. Infill wells drilled into this facies should be examined carefully in order to identify the thin reservoir zones to be perforated preferentially.

The fusulinid-wackestone facies occurs across the entire unit beneath the coarse-grained grainstone and diagenetically altered fine-grained grainstone facies (fig. IV-4); it is 50 to 60 ft thick on the western side and thickens to more than 90 ft on the eastern side. Intercrystalline and moldic porosity are generally less than 10 percent, and permeability rarely exceeds 1 md. Many wells penetrate this facies, but only a few are actually perforated in the fusulinid wackestone. This deeper zone should be tested, perhaps prior to perforating the shallower, commonly perforated zones.

The diagenetically altered fine-grained grainstone facies occurs in the eastern side of the unit (figs. IV-8, IV-11, and IV-12). The occurrence of this facies is coincident with the maximum production from the North Foster unit (fig. IV-13), and this fine-grained grainstone facies is the major reservoir component responsible for this production. Measured porosity varies from less than 5 to 15 percent; permeability has been recorded from 0.02 to more than 10 md. At least part of this range in porosity and permeability is due to the heterogeneous nature of the facies components on the scale of a core surface. To alleviate this problem, whole-core analyses are preferable to core-plug analyses in this facies in order to obtain representative results. The north-south trend of greatest production occurs within the boundaries of this facies, essentially along the crest of the structure (figs. IV-5 and IV-13). Infill drilling should target the diagenetically altered fine-grained grainstone facies, particularly where the occurrence of this facies and the highest structure coincide.

IMPLICATIONS OF OUTCROP ANALOG METHODOLOGY FOR IMPROVED RESERVOIR  
DESCRIPTION AT NORTH FOSTER GRAYBURG UNIT

This study of the Grayburg Formation reservoirs of the Permian Basin was designed to provide a comparative study of similar detail of a Grayburg reservoir in the subsurface and of Grayburg Formation outcrops in the Guadalupe Mountains with the goal of achieving a higher level of understanding of the architecture and spatial variation of reservoir properties of these complex shallow-water carbonate facies. The fundamental outcome of the outcrop study as it applies to the selected reservoir, the North Foster Grayburg unit, is the recognition that the Grayburg Formation is readily described in terms of vertically stacked depositional events, or parasequences; these parasequences have been found to have a consistent internal arrangement of rock fabrics that bear directly on petrophysical properties, hence providing predictability in terms of fluid flow behavior. Further, these parasequences are generally continuous for several thousand feet to several miles laterally and thus are useful at the reservoir scale to define a genetically based reservoir zonation. Comparing cross sections through the North Foster reservoir and the Grayburg outcrop demonstrates the parallel high-frequency cycle construction of these two geographically removed segments of the Grayburg shelf when viewed within this framework.

This outcrop-derived high-frequency cycle description approach provides a higher resolution to the correlation framework and a better description of facies continuity and, ultimately, fluid-flow stratification. In particular, the base and/or upper surface of a parasequence is commonly a low-flow zone or baffle. Accurate description of parasequences within the reservoir, therefore, provides a first step in generating a fluid-flow model by providing the critical layering scale needed for simulation. Numerical simulation of comparable San Andres Formation outcrops and reservoir analogs (Senger and others, 1991) has shown that thin mudstones that occur at the base of each parasequence separate more permeable intraparasequence lithologies and impart a strong control on fluid flow and, hence, recovery.

Previous San Andres and Grayburg reservoir description (Bebout and others, 1987; Ruppel and Cander, 1988) shows that without the higher resolution given by the parasequence framework, the continuity of these low-permeability carbonates may not be recognized. The high-resolution correlation framework now in place for the North Foster Grayburg provides an ideal starting point for development of a simulation grid because it can better guide the exercise of averaging petrophysical properties within, rather than across, the critical parasequence-bounding low-flow facies.

The outcrop-guided sequence stratigraphic model has also aided our understanding of the subsurface reservoir framework in placing the key productive facies at North Foster into their respective systems tracts and thus within the proper time-space context of the sequence framework. The dominant productive facies tracts in North Foster Grayburg in order of qualitatively estimated Kh ranking are (1) diagenetically altered fine-grained grainstone, (2) fusulinid wackestone, and (3) grainstone.

Examination of figures IV-5, IV-7 and IV-8 shows that each of the three main productive facies tracts occurs in a discrete region of the reservoir in terms of time and space. The fusulinid wackestone, which was deposited during the initial transgression of the platform, is restricted to a position beneath the maximum flooding surface within the lowstand transgressive systems tract. The maximum flooding surface here is capped by a laterally continuous parasequence-base siltstone that has a geometric mean permeability of 0.15 md, effectively removing it from communication with highstand facies.

The grainstone facies tract is developed preferentially directly above the shelf break of the precursor San Andres margin in the early highstand systems tract, whereas the altered fine-grained grainstone facies is situated in the early to mid highstand in a position some 2 km seaward of the main development of coarse grainstone. It can also be shown within this framework that highly laterally continuous, consistently low permeability parasequence-base siltstones separate the grainstone and diagenetically altered fine-grained grainstone facies tracts. Although degree of communication between these facies across the siltstone baffles can

only be quantified through pressure testing or numerical simulation, these relationships suggest that effective production strategies for these main productive zones should target each major facies individually to evaluate whether this zone is sufficiently contacted with injectors and producers.

The Grayburg Formation in outcrop and in the subsurface is pervasively dolomitized, but in general dolomite crystal size is sufficiently fine so that permeability characteristics still show a good relationship to depositional texture. The most extensive diagenetic overprint that alters depositional fabric is that observed in the altered fine-grained grainstone facies in more seaward (eastern) areas of North Foster. Enhanced intercrystalline porosity, intracrystalline moldic porosity, and some leached vuggy porosity combine to enhance total porosity and permeability of this facies beyond that expected for associated depositional textures. Although similar diagenetic textures were observed in outcrop, no detailed study of this diagenetic overprint was undertaken there.

Detailed diagenetic studies of the Grayburg outcrop at Stone Canyon demonstrated a selective distribution of separate-vug (moldic) porosity within a parasequence, particularly in areas of grainstone development. Similar separate vug development was observed in North Foster grainstones, but its distribution has not been quantified. Senger and others (1991) have shown that areas of high separate-vug porosity in grainstones can strongly affect the recovery of hydrocarbons from these zones. Such zones have a much higher residual oil saturation as a result of the poorly connected pore network, and recovery will be low in these zones relative to that anticipated from  $\phi/h$  mapping.

CHAPTER V: RESOURCE ASSESSMENT OF NONASSOCIATED GAS  
PRODUCTION IN FLUVIAL-DOMINATED DELTAIC RESERVOIRS, TEXAS

Mark Holtz

INTRODUCTION

An assessment of nonassociated gas (that is, gas-well-gas) production in Texas allowed quantification of cumulative production by geologic depositional system. The focus of this subtask was to determine the depositional reservoir type that has contributed the most significant portion of nonassociated gas production in the State. Attributes and volumetrics of the most productive reservoir group was then investigated in more detail. The assessment was conducted on 2,600 gas-well-gas reservoirs, all of which had a cumulative production of greater than 6 billion cubic feet (BCF) or 1 million barrels of oil equivalent (MMBOE).

DISTRIBUTION OF TEXAS GAS PRODUCTION BY GEOLOGIC DEPOSITIONAL SYSTEM

Classification of Depositional Systems

Clastic Depositional Systems

The depositional system classification scheme used for gas reservoirs in Texas has two large subsets, one for clastic depositional systems and the other for carbonate depositional systems. For the purpose of this analysis, we delineated eight major subdivisions within the clastic depositional systems: (1) alluvial fan, (2) fluvial, (3) deltaic, (4) shoreface, (5) eolian, (6) shelf, (7) submarine fan, and (8) shales. Each of these depositional systems were further divided by modifiers that describe major facies within the depositional system, additional geologic modifying processes, and sediment sources. This characterization resulted in 17 subdivisions.

## Carbonate Depositional Systems

Eight carbonate depositional systems were used in the classification scheme: (1) evaporitic flats, (2) restricted platform shoaling cycles, (3) open shelf, platforms and ramps, (4) shelf edge, (5) atolls, (6) oolitic bars and barriers, (7) karstic overprint, and (8) deep-water siliceous shales/cherts. Each of these depositional systems also has subdivisions associated with them based on either diagenesis, major facies within the depositional system, or tectonics.

## Distribution of Cumulative Production Sorted by Depositional System

Clastic gas reservoirs account for 94 trillion cubic feet (Tcf), or 53 percent of all the gas-well-gas production (fig. V-1) in Texas. Within this subset of clastic reservoirs, those classified as deltaic compose most of the production. Deltaic reservoirs account for 61 percent, or 57 Tcf, of all the clastic gas production. This amounts to 32 percent of the total Texas nonassociated gas production. There are five modifiers that characterize deltaic reservoirs in Texas: (1) wave-dominated, (2) wave-modified, (3) fluvial-dominated, (4) proximal delta front, and (5) distal delta front. Wave-dominated, wave-modified, and fluvial-dominated subdivisions are geologic modifying processes, whereas the proximal delta front and distal delta front are facies modifiers. Within the deltaic reservoir class, 77 percent, or 44 Tcf, of the cumulative production came from fluvial-dominated deltaic reservoirs. This volume is 25 percent of the total nonassociated gas production in Texas.

## PRODUCTION, DISCOVERY, DEPTH, AND TRAP CHARACTERISTICS OF FLUVIAL-DELTAIC RESERVOIRS

Fluvial-dominated deltaic reservoirs lie within the Tertiary Texas Gulf Coast, in the Cretaceous East Texas basin, and scattered in the Pennsylvanian formations of North-Central

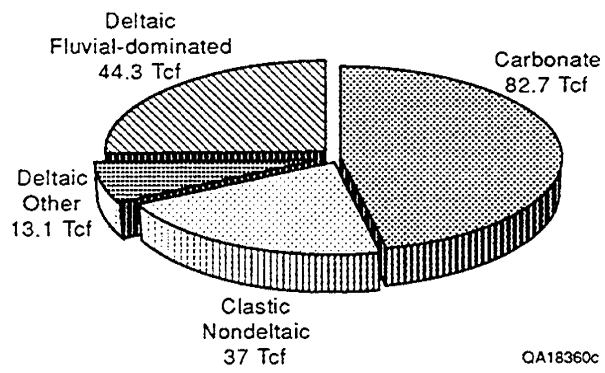


Figure V-1. Cumulative nonassociated gas production in Texas.

Texas and the Texas Panhandle. Figure V-2 displays the spatial distribution of these groups of reservoirs by geologic formation along with their cumulative production.

### Tertiary Texas Gulf Coast

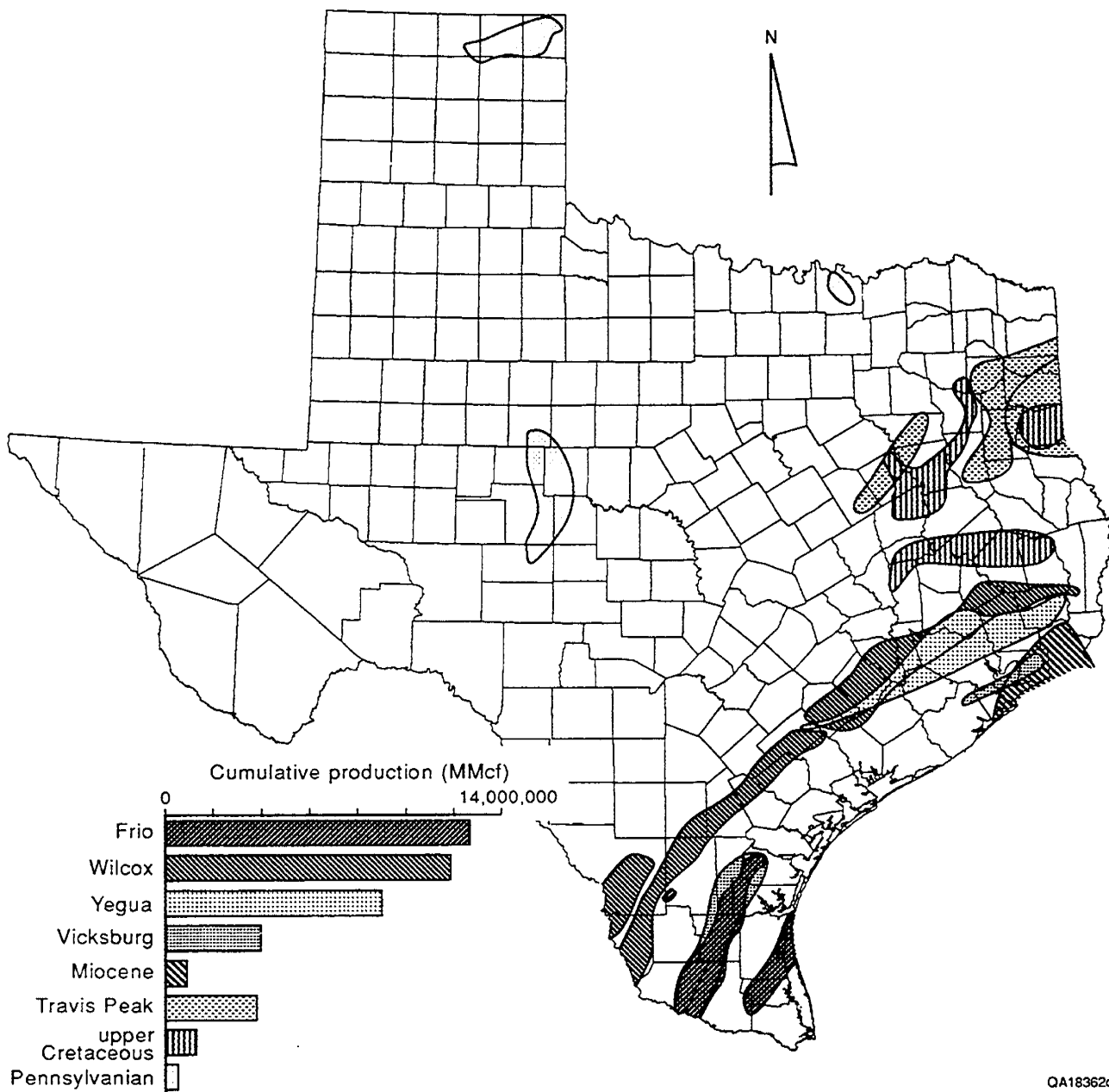
Tertiary Texas Gulf Coast nonassociated gas production is from the Wilcox, Frio, Yegua, Vicksburg Formations and from the Miocene. This subset of reservoirs has produced 38.2 Tcf, or 86 percent, of the total 44.3 Tcf from all fluvial-dominated deltaic reservoirs (fig. V-3). Production is dominantly from the Wilcox and the Frio. The Wilcox has produced 11.8 Tcf (27 percent), and the Frio 12.6 Tcf, or 28 percent (fig. V-4). The Yegua has produced 9.3 Tcf, or 21 percent, of the total Texas production from fluvial-deltaic reservoirs. The Vicksburg has produced 3.7 Tcf and the Miocene 0.8 Tcf.

#### Wilcox Fluvial-Deltaic Gas Reservoirs

There are 239 Wilcox fluvial-deltaic reservoirs discovered between 1938 through 1985 that have currently produced more than 1 MMBOE. By 1964, 51 percent of these reservoirs had been discovered, increasing to 66 percent by 1973 and to 75 percent by 1976. Peak years of discovery were the years 1979 to 1982, when 40 discoveries were made.

The Wilcox fluvial-deltaic reservoirs range in depth from 500 to 19,000 ft. The modal depth range is 8,000 to 8,500 ft with 34 reservoirs, or 14 percent of the total number of reservoirs. This is followed by 31 reservoirs, or 13 percent, at a depth range of 8,500 to 9,000 ft, and 30 reservoirs, or 13 percent at 9,500 to 10,000 ft.

Most of the Wilcox reservoirs are characterized as faulted anticlinal traps, with 113 occurrences, or 47 percent. The next most typical trap type is that of a combination trap facies change and faulted anticline, with 48 occurrences, or 20 percent. These two trap types constitute 67 percent of traps in the Wilcox fluvial-deltaic reservoirs.



QA18362c

Figure V-2. Distribution of gas-productive fluvial-dominated deltaic plays.

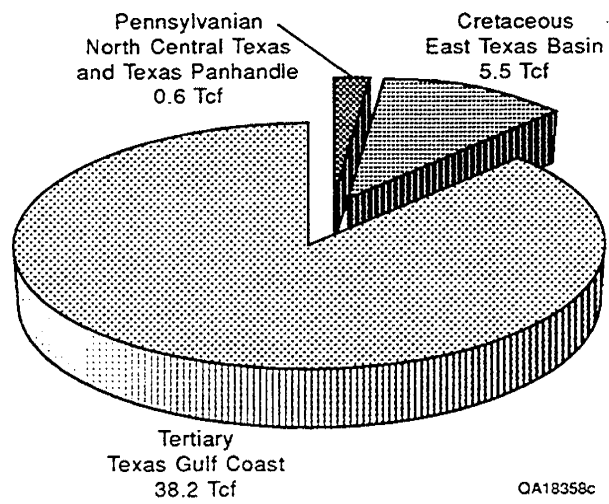


Figure V-3. The cumulative production of fluvial-deltaic reservoirs by region in Texas.

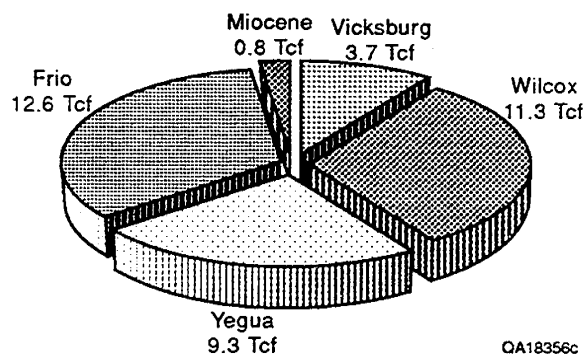


Figure V-4. The distribution of Tertiary cumulative fluvial-dominated deltaic gas production by formation in the Texas Gulf Coast.

## Frio Fluvial-Deltaic Gas Reservoirs

Frio fluvial-deltaic reservoirs were discovered from 1900 through 1986. A total of 239 reservoirs produced more than 1 MMBOE during that time. The major discovery years were from 1945 through 1965, accounting for 57 percent of all reservoirs. By 1956, 50 percent of these reservoirs had been discovered, increasing to 66 percent by 1961 and to 75 percent by 1964. The peak years of discovery were the years 1948 and 1949 (24 discoveries), and 1964 and 1965 (22 discoveries).

Reservoir depth ranges from 500 to 9,500 ft. The modal reservoir depth range lies between 5,500 and 6,000 ft in 35 of the reservoirs, or 15 percent of the total number of reservoirs. Thirty-three reservoirs, or 14 percent, lie between 6,000 and 6,500 ft and 30 reservoirs, or 13 percent, between 6,500 and 7,000 ft.

Major trap types are a combination of facies change and faulted anticlines, having 129 occurrences (54 percent of the total number of reservoirs). The next most abundant are rollover fault-bounded anticlines, with 44 occurrences (18 percent), and a combination of anticline and facies change with 10 occurrences (4 percent). These three trap types constitute 76 percent of traps in Frio fluvial-deltaic reservoirs.

## Yegua Fluvial-Deltaic Gas Reservoirs

Fifty-eight Yegua fluvial-deltaic reservoirs that have produced more than 1 MMBOE were discovered between 1933 and 1982. The major discovery years were from 1948 through 1960; during this period 50 percent of all reservoirs were discovered. By 1951, 50 percent of these reservoirs had been discovered, increasing to 66 percent by 1955 and to 75 percent by 1959. Peak years of discovery were the years 1948, 1953, and 1955, with four discoveries each.

Reservoir depth ranges from 4,000 to 11,500 ft and have a mode (14 reservoirs) of 6,500 to 7,000 ft. This is followed by 9 reservoirs, or 16 percent of the reservoirs at a depth range of

7,000 to 7,500 ft, and 8 reservoirs, or 13 percent, at 5,000 to 5,500 ft. These three depth intervals contribute 53 percent of the depth ranges.

Major trap types are a combination of facies changes coupled with faulted anticlines, with 18 occurrences, or 31 percent of the total number of reservoirs, followed by combination traps of combined facies changes over anticline structures, with 17 occurrences (29 percent), and faulted anticlines with 10 occurrences (17 percent). These three trap types constitute 77 percent of the traps.

#### Vicksburg Fluvial-Deltaic Gas Reservoirs

Vicksburg fluvial-deltaic reservoir discoveries were made from 1939 through 1986. A total of 125 discoveries, each of which have produced more than 1 MMBOE, were made during this time period. By 1965, 49 percent of these reservoirs had been discovered, increasing to 63 percent by 1971 and to 74 percent by 1975. The peak year of discovery was 1964, with 10 new reservoir discoveries.

Reservoir depths range from 4,500 to 14,000 ft, with a mode depth of 7,000 to 7,500 ft. This mode range accounts for 20 reservoirs, or 16 percent. Fifteen reservoirs, or 12 percent, have a depth range of 7,500 to 8,000 ft and another 15 reservoirs, or 12 percent, have a range of 8,500 to 9,000 ft.

The major trap type is a combination structural trap or faulted anticline, with 60 occurrences, or 50 percent of all Vicksburg fluvial-deltaic reservoirs. The next most common trap type is a combination of facies change and fault, with 54 occurrences, or 44 percent. The remaining reservoirs are characterized by a combination facies change over anticlinal structure, with 9 occurrences, or 6 percent.

## Miocene Fluvial-Deltaic Gas Reservoirs

Fifty-three Miocene fluvial-deltaic reservoirs have produced more than 1 MMBOE between 1900 and 1986. By 1971, 51 percent of these reservoirs had been discovered, increasing to 66 percent by 1975 and to 77 percent by 1977. Sixteen reservoirs were discovered during the peak years between 1969 and 1971.

Reservoir depth ranges widely between 1,000 and 13,500 ft, with mode depth range of 8,000 to 8,500 ft accounting for 9 reservoirs, or 17 percent. Seven reservoirs, or 13 percent, range between a depth of 8,500 and 9,000 ft, and 5 reservoirs, or 9 percent, range between 9,000 and 9,500 ft. The principal trap type is a faulted anticline.

## Cretaceous East Texas Basin

Fluvial-deltaic gas production from the Cretaceous East Texas Basin is from the Travis Peak Formation of the Cotton Valley Group and from the Upper Cretaceous on the Sabine Uplift, in salt-related structures and in downdip shelf-margin sandstones. The total cumulative production within this area is 5.5 Tcf, (fig. V-3), with 4.1 Tcf attributable to the Travis Peak and 1.4 Tcf attributable to the Upper Cretaceous.

## Travis Peak Fluvial-Deltaic Gas Reservoirs

Forty-nine reservoirs within the Travis Peak have produced more than 1 MMBOE each. This group of reservoirs was discovered between 1940 and 1982. By 1969, 50 percent of these reservoirs had been discovered, increasing to 63 percent by 1975 and to 80 percent by 1977. Peak years of discovery were between 1976 and 1979, with 13 discoveries.

Reservoirs range in depth between 6,000 and 12,000 ft. The depth range is bimodal at depth ranges of 7,000 to 7,500 ft and 10,000 to 10,500 ft. Each of these depth ranges accounts for 7 reservoirs, or 14 percent of the total. Six reservoirs, or 12 percent, lie within the depth range of 7,500 to 9,000 ft.

Most reservoirs (65 percent) are formed by combination of facies change over faulted anticlines. The next most prevalent trap type (35 percent) is a combination of facies change over anticline or structural nose.

#### Upper Cretaceous Group Fluvial-Deltaic Gas Reservoirs

Seventy-seven Upper Cretaceous fluvial-deltaic reservoirs, discovered between 1936 and 1980, have each produced greater than 1 MMBOE. By 1959, 50 percent of these reservoirs had been discovered, increasing to 66 percent by 1972 and to 75 percent by 1974. The major discovery years were from 1972 through 1980; during this period 37 percent of all discoveries were made. The peak year of discovery was in 1957, when three reservoirs were discovered.

Reservoir depth ranges between 3,000 and 13,000 ft. The mode depth range is 5,500 to 6,000 ft, accounting for eight reservoirs, or 30 percent. The next most frequent depth range is between 8,500 to 9,000 ft with four reservoirs, or 15 percent. The remaining reservoirs are scattered at depths throughout the entire range.

Stratigraphic facies changes account for most of the traps. Nine reservoirs (33 percent) display this trap type, and the next most common trap type is a combination of stratigraphic facies change and faulted anticline, accounting for six reservoirs, or 22 percent. Three reservoirs, or 11 percent, display faulted anticlinal traps. These three trap types constitute 66 percent of the reservoirs analyzed.

#### Pennsylvanian North-Central Texas and Texas Panhandle

Pennsylvanian fluvial-deltaic reservoirs produce from the Strawn Formation in North-Central and West Texas and from the Morrow Formation in the Texas Panhandle. This set of reservoirs has produced 0.6 Tcf of gas (fig. V-3).

Sixteen Pennsylvanian fluvial-deltaic reservoirs that have each produced more than 1 MMBOE were discovered between 1949 through 1983. By 1958, 38 percent of these

reservoirs had been discovered, increasing to 63 percent by 1959 and to 88 percent by 1961. Most of the reservoirs were discovered between 1958 and 1961, when 50 percent of all reservoirs were discovered.

Reservoir depth range between 4,000 ft to 8,500 ft with a mode depth range of 7,000 to 7,500 ft. Major trap type is a stratigraphic up-dip porosity pinchout accounting for 6 reservoirs, or 38 percent. The next most common trap is a combination stratigraphic trap of updip porosity pinchout on a structural nose, which accounts for 5 reservoirs, or 31 percent. Combination stratigraphic and anticlinal traps account for four reservoirs, or 25 percent.

## ASSESSMENT OF THE REMAINING RESOURCES IN WILCOX FLUVIAL-DELTAIC GAS RESERVOIRS

### Methodology of Gas-in-Place Calculation

Original gas-in-place (MMSCF) is calculated by the volumetric method. In this method the gas pore volume is related to reservoir bulk volume, average porosity, and irreducible water saturation. The reservoir volume of gas is converted to standard volume of gas by applying the gas formation volume factor of Smith (1983):

$$\text{OGIP (MSCF)} = 43.560 Ahf (1-S_{wc})/ B_g + R_s N \quad (1)$$

where

- OGIP = original gas in place (MSCF),
- A = reservoir area (acres),
- h = net pay thickness (ft),
- f = porosity (fraction),
- S<sub>wc</sub> = connate water saturation (fraction),
- B<sub>g</sub> = gas formation volume factor (reservoir cubic feet [CF]),
- R<sub>s</sub> = solution gas oil ratio (cubic feet per stock tank barrel [CF/STB]), and
- N = original oil in place (in thousand stock tank barrels).

Retrograde gas condensate reservoirs and associated gas reservoirs are the only types that have a non-zero  $R_{SN}$  term. Reservoir acreage and net pay is determined from subsurface contour and isopach maps. Porosity and irreducible water saturations are generally obtained from publicly reported values. The gas formation-volume factor is a complex function of the reservoir pressure, temperature and fluid composition. The gas formation-volume factor (Smith, 1983) is given by equation (2):

$$B_g = (P_{sc}Z_{res}T_{res}) / (T_{sc}P_{res}) \quad (2)$$

where

- $P_{sc}$  = pressure at standard conditions (14.7 psi),
- $T_{sc}$  = temperature at standard conditions (60°F),
- $P_{res}$  = reservoir pressure (psi)
- $T_{res}$  = reservoir temperature (°F), and
- $Z_{res}$  = gas compressibility factor at reservoir conditions.

The gas compressibility factor (Z factor), is a function of the fluid composition and reservoir temperature and pressure. Reservoir temperature and pressure were obtained from Koster and others (1989) and Bebout and others (1982). The Z-factor can be calculated as a function of pseudo-reduced temperature and pressure of the reservoir gases from the Standing and Katz correlations (Beggs, 1984). However, a slightly modified equation of Brill and Beggs (1974) yields values accurate enough for many engineering calculations and is used here.

$$Z = A + (1-A)/e^B + C (P_{pr})^D \quad (3)$$

where

- $A = 1.39(T_{pr} - 0.92)^{0.5} - 0.36T_{pr} - 0.101,$
- $B = (0.62 - 0.23T_{pr})P_{pr} + [0.066/(T_{pr} - 0.86) - 0.037] (P_{pr})^2$   
 $+ 0.32(P_{pr})^6/10^9(T_{pr} - 1),$
- $C = 0.132 - 0.32 \text{ Log } T_{pr},$
- $D = \text{antilog}(0.3106 - 0.49T_{pr} + 0.1824(T_{pr})^2)$
- $T_{pr} = T_{res}/T_{pc},$  pseudo-reduced temperature,

$P_{pr} = P_{res}/P_{pc}$ , pseudo-reduced pressure, and

$P_{pc} (T_{pc})$  = pseudo-critical pressure (temperature)

To calculate pseudo-reduced pressure and temperatures, it is necessary to calculate the pseudo-critical temperature and pressure of the gas. The most accurate method to calculate the pseudo-critical pressure and temperature is to use gas composition, but because the composition is not available an indirect method of estimating these parameters from the reservoir gas gravity is used. The correlations of Brown and others (1948) are used to estimate these parameters (equations 4 through 7). The surface, or "California," gas curves are fit by the equations:

$$P_{pc} = 677 + 15.0 g_r - 37.5 (g_r)^2 \quad (4)$$

$$T_{pc} = 168 + 325 g_r - 12.5 (g_r)^2 \quad (5)$$

and the "condensate" gas curves, has the following relationship:

$$P_{pc} = 706 - 51.7 g_r - 11.1 (g_r)^2 \quad (6)$$

$$T_{pc} = 187 + 330 g_r - 71.5 (g_r)^2 \quad (7)$$

where

$g_r$  = reservoir gas gravity (air = 1),

$P_{pc}$  = pseudo-critical pressure, and

$T_{pc}$  = pseudo-critical temperature.

Reservoir fluids that remain single phase (gas) at reservoir conditions can enter the two-phase envelope at surface conditions. Thus, the composition of the separator gas is not the same as reservoir gas unless the condensate production is zero. Hence, the reservoir gas gravity is a function of the separator gas gravity and the specific gravity of the produced oil. From a calculation of apparent molecular weight of gas/oil mixture, the wet gas gravity in the reservoir ( $g_r$ ) can be calculated from equation (8):

$$g_r = (g_s + 4600 g_o / Rg) / (1 + 133,000 g_o / MoRg) \quad (8)$$

where

- $R_g$  = gas/oil ratio (SCF/STB),  
 $g_s$  = separator gas gravity (air = 1),  
 $g_o$  = condensate gravity (water = 1), and  
 $M_o$  = molecular weight of condensate.

The condensate gravity is calculated from condensate API gravity, as shown in equation (9). The molecular weight of the condensate is calculated by applying equation (10). The gas oil ratios are reported from the reservoir.

$$g_o = 141.5 / (\text{API} + 131.5) \quad (9)$$

$$M_o = 6084 / (^\circ\text{API} - 5.9) \quad (10)$$

Reserves within the Wilcox fluvial-deltaic reservoirs were estimated from regional production and reserve trends. Annual gas-well-gas production and reserve values are reported by the U.S. Department of Energy, Energy Information Administration (1989). In Texas these values are reported for districts set up by the Texas Railroad Commission. To calculate the reserves within the Wilcox, the ratio of reserves to production for the district were applied to annual production in the Wilcox, allowing the calculation of the reserves from the district ratio.

#### Remaining Gas Resource

There are 9.2 trillion cubic feet (Tcf) of remaining gas resource within the 178 Wilcox fluvial-deltaic reservoirs analyzed (fig. V-5). Originally they contained 18 Tcf. Of this original volume, 8.8 Tcf has been produced; thus, just under 50 percent of this resource has been produced. The current estimated proved producible reserves are 560 BCF, leaving 8.5 Tcf as potential for reserve growth. An ultimate recovery efficiency of 90 percent would allow a total of 16.2 Tcf of production, whereas the abandoned gas volume will be 1.8 Tcf.

The 52 Wilcox fluvial-deltaic reservoirs in the Houston embayment which have produced over 1 MMBOE originally contained 6 Tcf (OGIP) of gas. Of this OGIP 2.7 Tcf has been

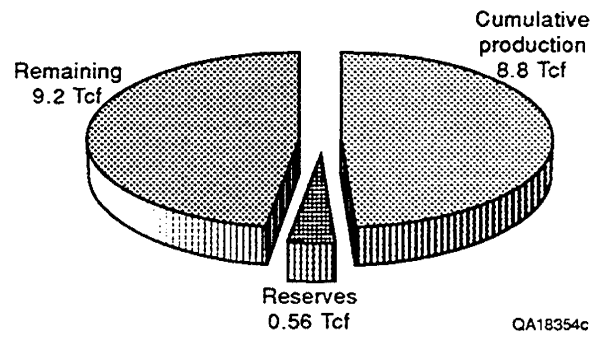


Figure V-5. Current status of the gas resource in Wilcox fluvial-deltaic reservoirs displaying the breakdown of the 18.56 Tcf original gas in place.

produced, 500 MMSCF is proved producible reserves and 3 Tcf is a target for reserve growth. This play contains 23 percent of the reserves and 36 percent of the remaining reserve growth target contained in the 178 reservoirs analyzed.

Wilcox fluvial-deltaic reservoirs within the Rio Grande Embayment currently have 126 reservoirs which have produced over 1 MMBOE. OGIP was 12 Tcf, of this 6 Tcf has been produced, 503 MMSCF are estimated to be proved producible reserves, and 5.4 Tcf is the target for reserve growth. This subset of reservoirs accounts for 67 percent of the total OGIP, 77 percent of the reserves and 64 percent of the reserve growth target.

## CHAPTER VI: QUANTIFICATION OF FLOW UNIT AND BOUNDING ELEMENT

### PROPERTIES AND GEOMETRIES, FERRON SANDSTONE, UTAH:

#### IMPLICATIONS FOR HETEROGENEITY

#### IN GULF COAST TERTIARY DELTAIC RESERVOIRS

R. Stephen Fisher, Noel Tyler, and Mark D. Barton

### INTRODUCTION

In this chapter we address the predictability of reservoir and intrareservoir seal properties and the spatial distribution of permeability in deltaic reservoirs—a reservoir class that accounts for 64 percent of total gas production from Texas Gulf Coast reservoirs. On the basis of similar depositional and diagenetic histories, we have selected the Cretaceous Ferron delta system in central Utah as an analog for these prolific Gulf Coast reservoirs. This chapter discusses the permeability characteristics of a single pulse of this deltaic system (Ferron unit 5) deposited during overall base-level rise.

This chapter addresses research on the controls of sedimentary architecture on permeability structure in a superbly exposed and cored delta/distributary-channel complex and describes how this permeability structure would affect gas mobility in a sandstone reservoir. The project aimed to (1) document and quantify the geometric, petrophysical, and petrographic attributes of flow units and their associated flow baffles on the outcrop, and (2) quantify directional attributes and properties of flow barriers bounding flow units on the outcrop. The approach was to establish the depositional architecture and diagenetic modification of fluvial-deltaic sandstones within the context of a well-defined sequence-stratigraphic framework, and then to determine how these factors affect the spatial distribution of permeability. The steps in this characterization of heterogeneity are (1) the determination of facies architecture, (2) delineation of the position, continuity, and causes of both permeable zones and barriers to gas flow, and (3) the establishment of predictable permeability trends common to fluvial-deltaic

sandstones. Ultimately, the goal is to translate this understanding of outcrop architecture to a reservoir model that can be used to test hypotheses concerning the most efficient methods for recovery of incremental gas reserves in a heterogeneous, compartmented sandstone.

### Study Area

Extensive discussions of the geology of the Ferron Sandstone are presented by Ryer (1981a, b; 1982; 1983) and Gardner (1991). This well-documented geological framework allowed us to focus rapidly on a single pulse of the Ferron deltaic system (unit 5) that is representative of the styles and scales of heterogeneity that exemplify Gulf Coast deltaic reservoirs.

Three-dimensional exposures of the Ferron Sandstone exist where canyons dissect the western limb of the San Rafael Swell, east-central Utah (fig. VI-1). Sparse vegetation and the absence of structural complexity allow continuous examination and sampling of outcrops both parallel and perpendicular to the direction of sediment transport. Outcrops of Ferron deltaic unit 5 expose a wide range of depositional facies that include fluvial through coastal-plain and marine strata. In the area of study, the upper Ferron includes facies that were deposited in several closely associated deltaic environments including fluvial point bar, straight and sinuous distributary channels, distributary mouth bar, delta-front, and transgressive sandstones.

### Approach

The approach utilized was to establish the depositional framework using color photomosaics of the outcrop to map the distribution and interrelations of component architectural elements of Ferron deltaic sandstones. Within this stratigraphic framework, the spatial distribution of permeability was investigated and petrographic analyses were conducted to relate reservoir properties to sandstone composition. The steps in characterizing

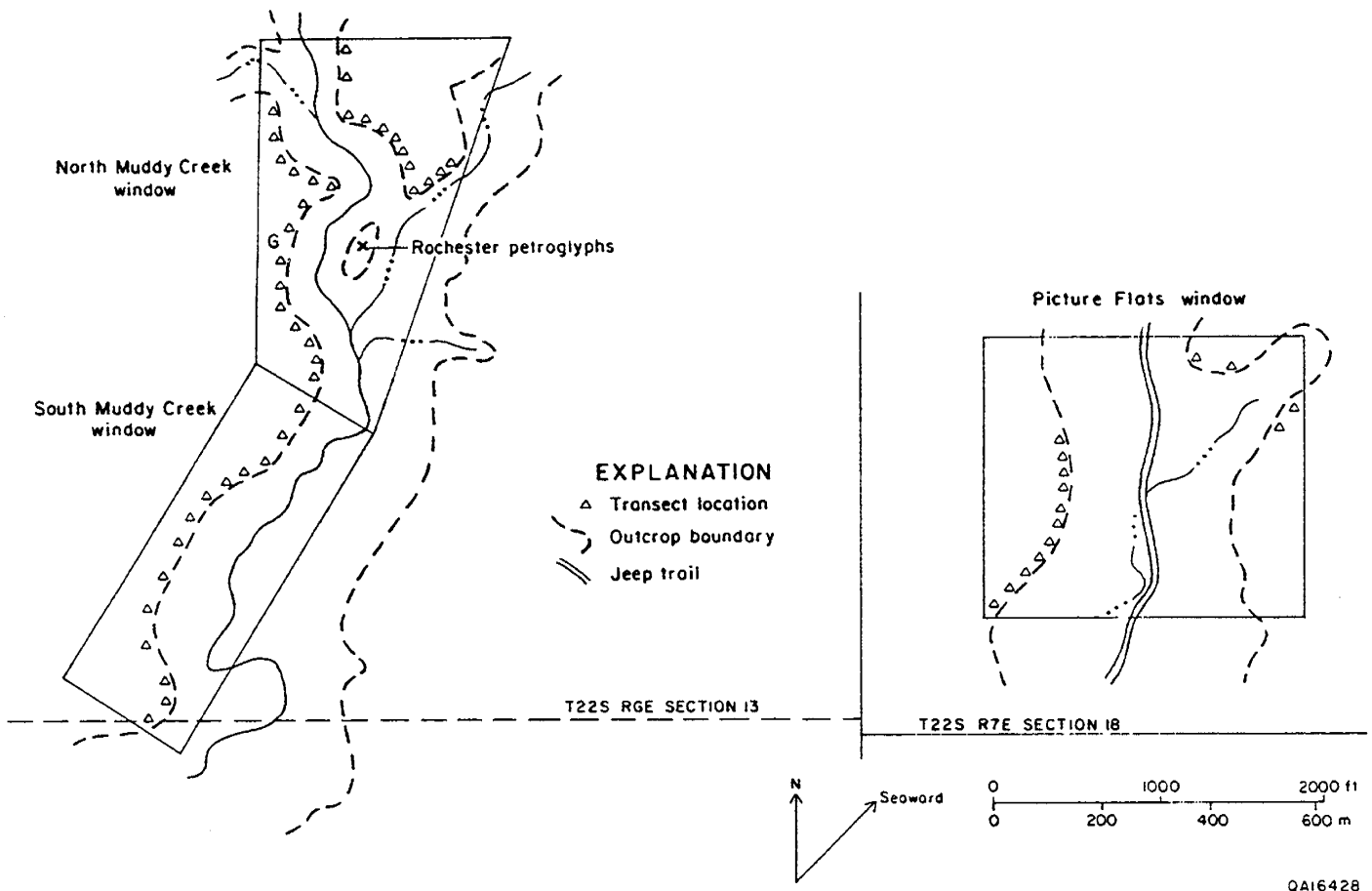


Figure VI-1. Location map of measured sections in Muddy Creek and Pictured Flats canyons. Study area is approximately 3 mi east of Emery, Utah. Location of grids for detailed permeability measurements is indicated by G in the North Muddy Creek window. Measured sections of the South Muddy Creek window provide data for the cross-section panel (fig. VI-3).

heterogeneity are (1) determination of facies architecture, (2) identification of detrital and diagenetic components of the sandstones, (3) delineation of permeable zones, (4) determination of continuity of permeable zones, (5) identification of barriers and baffles to flow, and ultimately, (6) the establishment of predictable permeability trends.

Permeability was measured using a portable minipermeameter, a gas-flow measuring system that is ideal for quickly making a large number of permeability determinations on the outcrop with minimal sample preparation. Effects of outcrop weathering are reduced by choosing relatively fresh surfaces and then chipping away the weathered surface of the rock. Numerous studies have demonstrated the accuracy of the minipermeameter measurements in comparison with conventional measures of permeability (Weber, 1982; Goggin, 1988; Kittridge, 1988). In general, good correspondence between minipermeameter and conventional measurements is reported over the range of approximately one to several thousand millidarcys. The minipermeameter used in this investigation has a detection range of about 0.1 to 3,000 md. Comparison of measured and accepted permeability values for 60 specimens over the range of 5 to 1,000 md showed agreement to be within 5 percent. Repeated permeability measurements collected from a single sample point showed that precision is better than 5 percent over the range of one to several hundred millidarcys.

Detailed vertical transects were measured at spacings of 100 to 200 ft, and permeability measurements were taken at 1-ft spacings on each measured section. Additionally, sample grids were constructed in order to examine the small-scale (inches to feet) spatial variability of permeability within lithofacies. Two sampling grids were constructed to comprise a 40- by 40-ft grid wherein permeabilities were measured at 2-ft intervals and a 6- by 6-ft grid (nested within the larger grid) with a 4-inch sampling interval. The sampling grids were located on a vertical exposure to minimize the effects of surface weathering and to ensure that profiles were truly vertical. Almost 4,000 minipermeameter measurements have been taken on the outcrop.

Petrologic investigations were conducted in conjunction with outcrop characterization to determine what mineralogic, textural, and diagenetic properties characterize flow units, baffles,

and barriers, and to relate these properties to depositional processes and burial history so that general criteria for predicting permeability structure can be developed. The major goals of this work are (1) to establish the initial mineralogic composition of Ferron sandstones from various facies and environments so that similarities and differences between the outcrop and various analogous gas reservoirs can be evaluated, (2) to quantify the physical and chemical changes that have occurred during burial and diagenesis and the accompanying effects on porosity, pore structure, and permeability, and (3) to establish relations between lithofacies type, cement and pore types, and permeability.

## RESULTS

### Architecture of Unit 5 Ferron Sandstones

#### Delta-Front Sandstones

In the landward parts of the delta platform, Ferron deltaic unit 5 consists of basal delta-front sandstones that are erosionally overlain by distributary-channel and associated sandstones. Thickness and geometries of the delta-front sandstones have thus been influenced by both depositional and erosional processes. Thicknesses of the delta-front sands range from 0 (where erosionally removed) to 35 ft.

The delta-front sandstone interval is a composite of at least four subintervals (fig. VI-2). Grain size in each of the subintervals is very fine and does not appreciably increase vertically. The basal subinterval contains relict, locally preserved, hummocky cross-stratification; however, intense bioturbation is the dominant characteristic of this sandstone. This zone is interpreted to be the maximum flooding surface that marks the base of Ferron deltaic unit 5.

Overlying the bioturbated zone are three discrete subintervals. Bedding in the subintervals is largely hummocky, cross-stratified, and to a lesser extent planar, trough, and ripple cross-

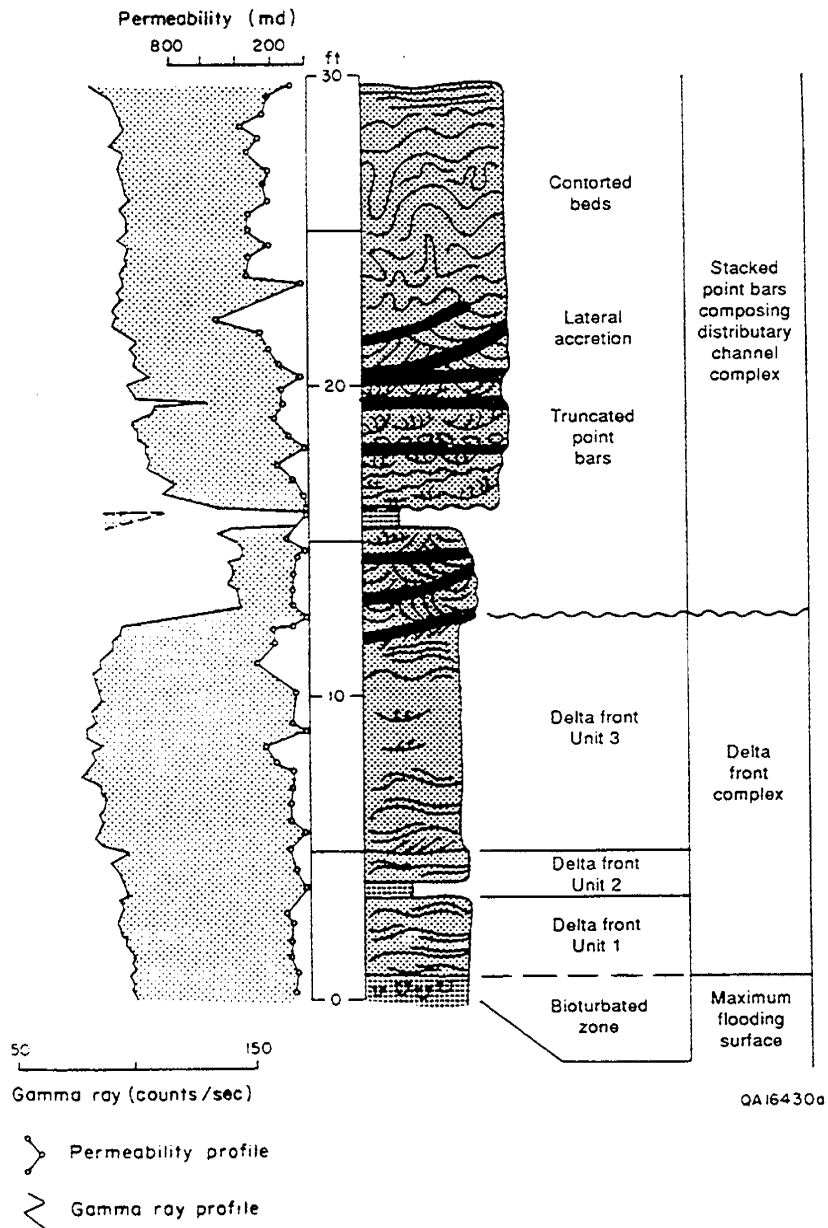


Figure VI-2. Vertical profile through typical delta-front and distributary-channel sandstones showing vertical changes in depositional environment, lithofacies, permeability, and gamma-ray response.

stratified. Lateral facies variation in the subintervals is subtle, and no well-defined facies boundaries have been detected.

Each of the tabular subintervals extends downdip for at least 1 mi. Thus, the dominant style of heterogeneity in the delta-front sandstones is vertical layering, with subintervals ranging between 3 and >10 ft in thickness. Lateral heterogeneity resulting from depositional processes in the subintervals is minimal, and component lateral variability of the delta-front sandstones is more a product of the erosive processes associated with the deposition of the superposed distributary sandstones. Vertical variation, in contrast, is pronounced. The lower bounding surface of each delta-front subinterval is erosional; upper bounding surfaces are composed of laterally continuous interbedded siltstone and mudstone layers. The uppermost of the subintervals is the thickest. Its basal surface is strongly erosional into the underlying subinterval.

#### Distributary-Channel and Associated Sandstones

Sandstones deposited in the distributary system have a high degree of both lateral and vertical heterogeneity. Three stages of channel formation are recognized in the distributary system: (1) early, down-cutting channels are followed by (2) a second stage of channel sedimentation that was dominated by lateral migration, and then (3) the final stage of channel sedimentation, which is characterized by deep, relatively narrow channels. Each stage of channel sedimentation is characterized by distinctive internal and external geometries.

##### *Basal channels*

At the base of the distributary complex, and erosive into the underlying, tabular delta-front sandstones, are a series of relatively narrow and laterally isolated channel sandstones. The channels are mostly small features that have similar width-to-thickness ratios (average of 9.5; table VI-1). One of the channels is considerably larger than the other three, with an apparent

Table VI-1. Apparent dimensions of distributary-channel macroforms in amalgamated Ferron unit 5 distributary-channel sand bodies.

Laterally Migrating Channels—Muddy Creek Canyon: Sand-Body Dimensions

Sand body	Thickness	Width	W/T
1	9.5	430	45.3
2	6	447	74.5
3	11	640	58.5
4	5	227	45.4
5	7.5	418	55.7
6	2.5	100	40
7	7	119	17
8	6.5	83	12.8
9	7.5	74	9.9
10	9.3	204	21.9
11	6.5	563	86.6
12	6.8	629	92.5
13	17	681	40.1
14	6.5	510	78.5
15	8.5	589	69.3
16	9	332	36.9
17	4.5	140	31.1
Average	7.7	363.9	48.0

Laterally Migrating Channels—Picture Flats: Sand-Body Dimensions

Sand body	Thickness	Width	W/T
1	15.5	192	12.6
2	27	353	13.1
3	16.5	610	37
4	19	636	33.5
5	15.5	262	16.9
6	20.5	430	21
7	16	278	17.4
8	12.5	308	24.6
9	12.5	250	20
10	16.5	195	11.8
11	10.5	200	19
12	11	71	6.5
13	4	83	20.5
14	13	612.6	47.1
15	10.5	133	12.7
Average	14.7	307.5	20.9

Tidally Influenced Channels—Muddy Creek Canyon: Sand-Body Dimensions

Sand Body	Thickness	Width	W/T
1	7	120	17.1
2	7.5	152	20.3
3	3.5	82	23.4
4	25	200	8
Average	10.8	138.5	17.2

Late-Stage Distributaries—Muddy Creek Canyon: Sand-Body Dimensions

Sand Body	Thickness	Width	W/T
1	57	580	10.2
2	35	400	11.4
Average	46.0	490.0	10.8

width of 200 ft and a maximum thickness of 25 ft; the other channels have apparent widths of several tens of feet and thicknesses of less than 10 ft (table VI-1). Bedding in these channels is varied. Large avalanche foresets are locally present in the main axis of the channel. Herringbone crossbedding may be present on the shallower flanks of the channels. Paleocurrent directions are bimodal.

#### *Laterally migrating distributary channels*

These channel sandstones are much more laterally extensive than the subjacent channel deposits. Two distributary-channel complexes exposed in Muddy Creek are 1,200 and 1,320 ft wide. The channels are strongly erosional into the underlying channels and into the delta-front sands and locally erode completely through the delta-front sandstones. The channel complexes shale out laterally into overbank muds and silts, or they are truncated by superjacent distributary-channel sandstones.

A typical vertical sequence contains three stratal types, beginning with a basal zone of clay-clast-bearing trough crossbeds that overlie a sharp erosional base. These mud clasts typically deform into pseudomatrix during compaction. As will be shown later, these mud-clast-rich zones display substantially lower permeabilities than do the mid- to upper distributary sediments and may provide effective baffles to fluid flow. Scale of trough crossbeds decreases upward from 1–2.5 ft to 0.5–1 ft. Grain size decreases upward, ranging from very coarse to medium fine. Planar crossbeds with minor amounts of horizontal stratification abruptly overlie trough crossbeds and also display an upward-decreasing trend in stratification and grain size, from medium to small scale and medium to fine grained, respectively. The sequence is capped by fine- to very fine grained, moderately to highly contorted strata or less commonly by very fine grained ripple-laminated sandstones.

The dominant characteristic of this lithofacies is well-defined lateral accretion surfaces (fig. VI-3) that dip gently toward the channel base. Angles of dip of the accretion surfaces are

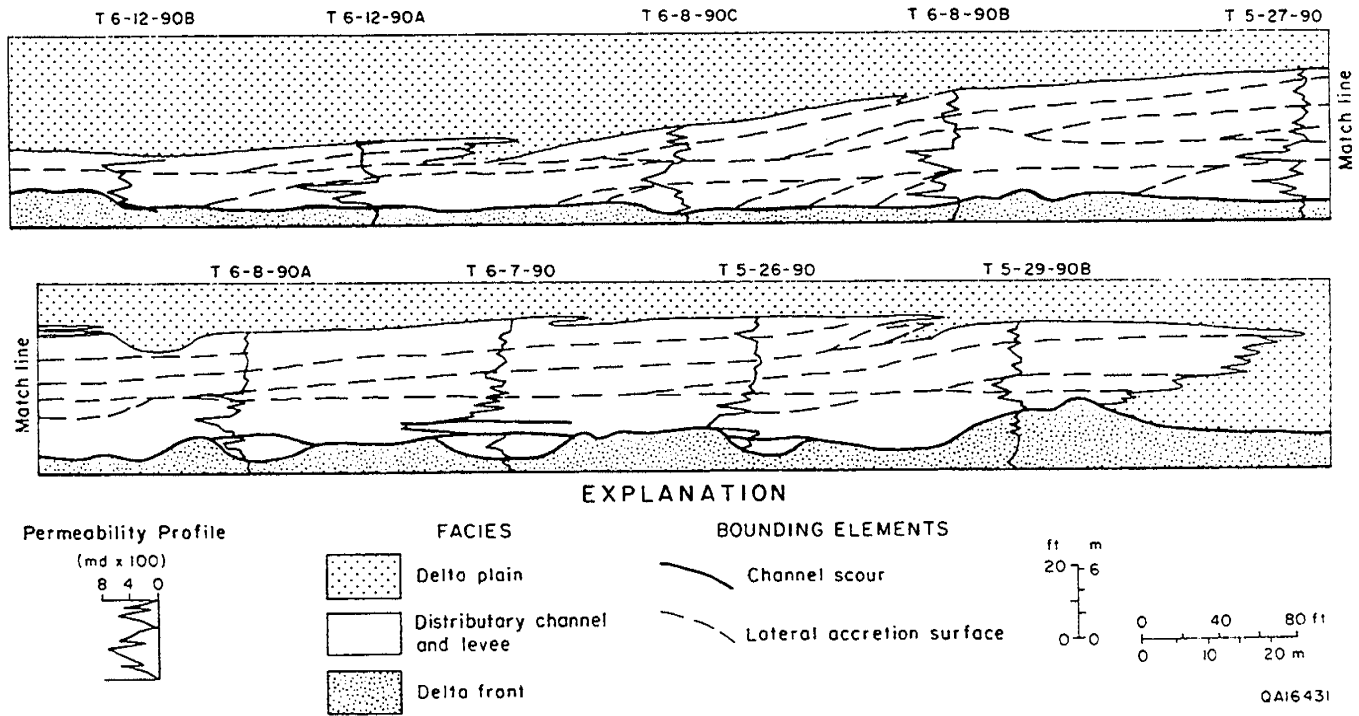


Figure VI-3. Cross section of outcrop panel, South Muddy Creek window, showing geometry of major facies and bounding elements, and permeability profiles at each measured section.

between 4° and 80°. There is considerable variability in the dimensions of the sandstone packages bounded by the accretion surfaces (table VI-1). Updip in the distributary system, widths of the sigmoid-shaped bodies average 360 ft but range from 75 to almost 700 ft. Individual lenses are 3 to 15 ft thick (average 7.7 ft; table VI-1) and erosionally overlap to form multilateral sand bodies with cumulative thicknesses of 15 to 40 ft. Individual sand lenses are 100 to 400 ft wide; belt width is as much as 1,320 ft. There are also substantial differences between the lateral-accretion-bounded sandstones updip and those 1 mi farther seaward, where the sigmoidal bodies have narrowed slightly (average of 308 ft) but are twice as thick as the equivalent units in Muddy Creek. These assemblages compose two distinct populations (fig. VI-4). Width-to-thickness ratios decrease seaward from 481 ft landward to 211 ft 1 mi seaward (table VI-1).

Laterally across the complex in the direction of accretion, the three main stratal types (as discussed earlier) are not continuous but pinch out over the underlying stratal type. The lower trough crossbedded facies is 5 to 18 ft (averaging about 15 ft) thick and has the greatest lateral dimensions, extending 1,000 to 1,200 ft across the sand belt. The planar crossbedded facies is 5 to 15 ft thick and extends approximately 750 to 800 ft. The upper contorted facies is about 5 ft thick and has a width of approximately 500 ft.

#### *Late-stage distributary channels*

Channel deposits formed during the final stage of distributary-channel sedimentation are narrower than those in the underlying distributary complex but are considerably thicker (table VI-1). Typically, these late-stage point bars are perched above and erode deeply into the subjacent sandstones. The basal point-bar contacts are typically rich in intraformational mud clasts. Because lateral-accretion surfaces in the late-stage distributaries are not accentuated by abundant mudchips, they are less well defined than those of the early meandering distributaries. Landward, remnant-accretion surfaces are mainly preserved at the base of the

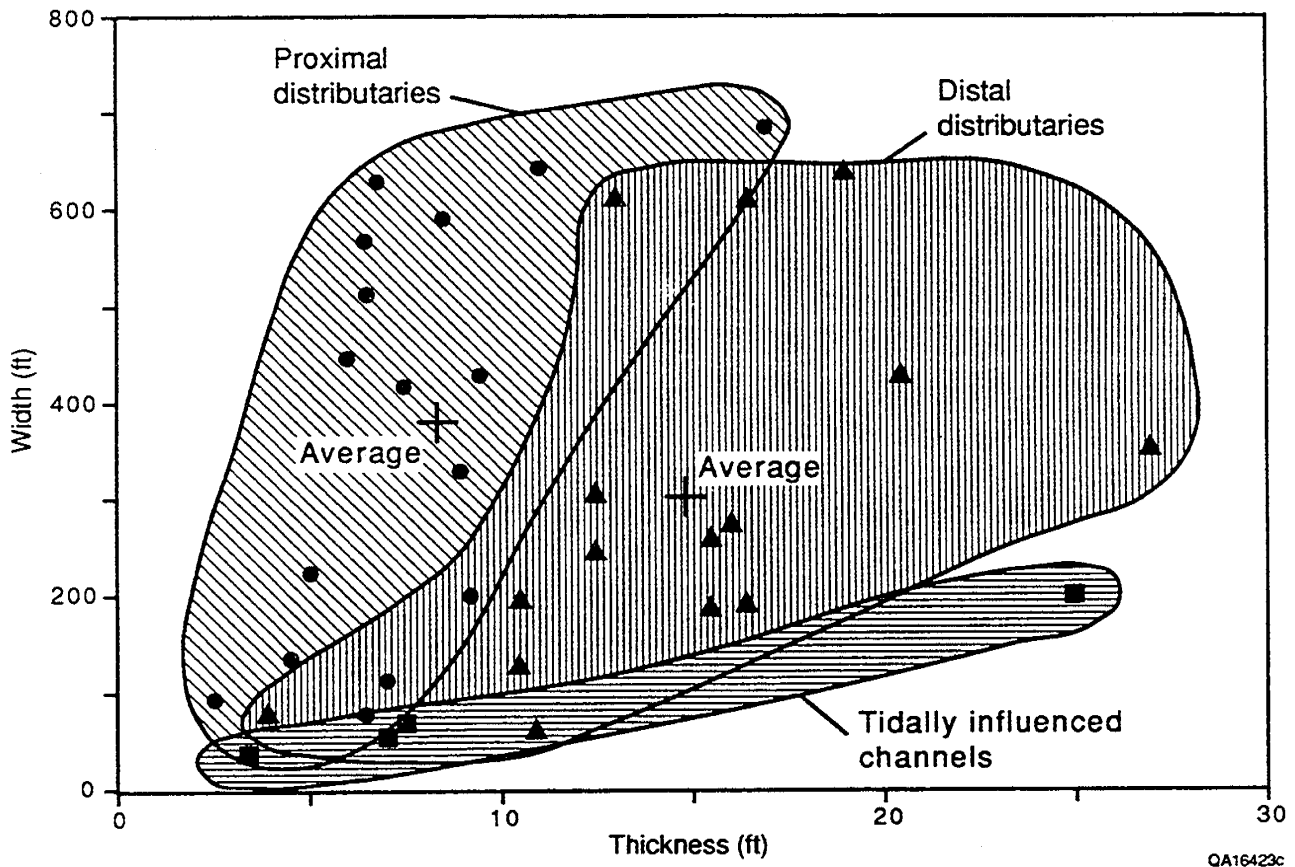


Figure VI-4. Plot of apparent width and thickness dimensions of distributary-channel and tidal channel sandstones.

channel sandstones, the upper part of the point bar being characterized by intense contortion of the fine-grained sandstones.

### Bounding Element Hierarchy

A five-level hierarchy of bounding elements and flow baffles has been delineated, each with characteristic properties and dimensions. At the megascale (the scale of depositional systems), the transition from deltaic sandstones to delta-front or delta-plain mudstones provides primary sealing surfaces. Bounding surfaces are planar and span three to four orders of (absolute) permeability magnitude. Multiple levels of bounding surface occur at the macro, or interwell, scale. Facies variation, coupled with changes in lithology, is the dominant heterogeneity at the second level of magnitude. Distributary-channel to interdistributary bay and channel-abandonment facies provide linear flow barriers that span three orders of (absolute) permeability magnitude. Sand-on-sand facies changes (channel/channel, channel/levee, channel/delta front) compose the third level of bounding surface and can display permeability variation of up to two to three orders of magnitude. Bounding surfaces of this type are inclined planar with a large areal extent. Irregular interfacies boundaries such as channel-on-channel contacts provide the dominant heterogeneity in amalgamated distributary-channel sandstones. In retrogradational deltaic systems, reworking of floodplain mudstones results in mudclast-lag accumulations along the floor and flanks of the channel (that through differential compaction of the coarse mudflakes into pseudomatrix) result in dramatic (often two-to-three orders of magnitude) permeability reduction. Intrafacies boundaries such as planar-inclined lateral accretion surfaces and planar-horizontal boundaries between stratal types compose levels four and five of the hierarchy and span two-to-three and one-to-two orders of permeability magnitude, respectively.

## Petrography of Unit 5 Ferron Sandstones

Framework grain mineralogy, intergranular material, and cement compositions of Ferron sandstones from Muddy Creek vary systematically between fluvial, transgressive and delta-front, and distributary-channel sandstones. Transgressive and delta-front sandstones of Ferron unit 5 are the most quartz-rich samples examined, averaging approximately 90 percent quartz, 5 percent feldspar, and 5 percent rock fragments (fig. VI-5a). Distributary-channel sandstones average approximately 80 percent quartz, 10 percent feldspar, and 10 percent rock fragments. Fluvial sandstones of Ferron unit 4 contain more feldspar minerals than do unit 5 sandstones; fluvial sandstones average approximately 65 percent quartz, 20 percent feldspar, and 15 percent rock fragments. The general increase in amount of quartz from fluvial to distributary-channel to transgressive and delta-front sandstones corresponds to an increase in the amount of reworking in the depositional environment. In all sandstones examined, the most abundant lithic components are metamorphic rock fragments and chert. Where abundant, these grains significantly reduce porosity and permeability because they are deformed around more rigid framework grains during burial and compaction.

Intergranular material is predominantly cement, pore space, and pseudomatrix (clay clasts and shale fragments, which deform around rigid detrital grains). Delta-front and transgressive sandstones contain little or no pseudomatrix, whereas most distributary-channel sandstones contain relatively little cement (fig. VI-5b). Fluvial sandstones contain approximately equal amounts of cement, pseudomatrix, and pore space. Pseudomatrix affects porosity and permeability in the same manner as rock fragments—compaction during burial squeezes pseudomatrix between rigid framework grains, reducing both porosity and pore throat dimensions. Most porosity is well-connected intergranular void space. However, microporosity (micron-sized voids within kaolinite cement or leached grains) is common in fluvial sandstones,

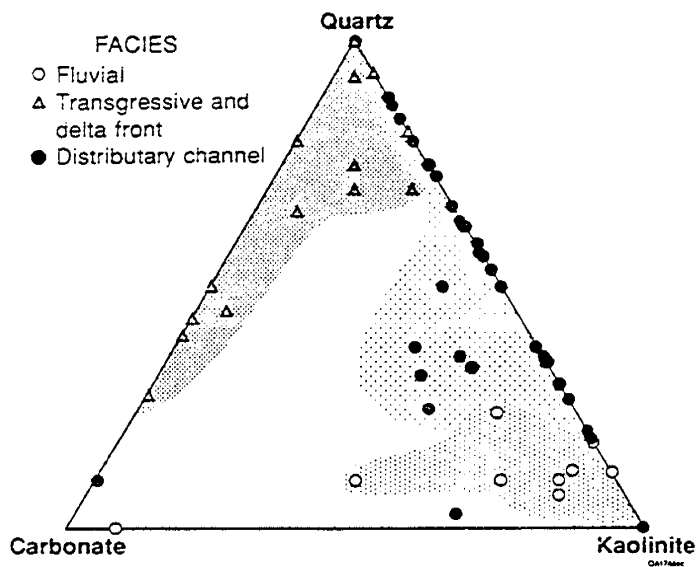
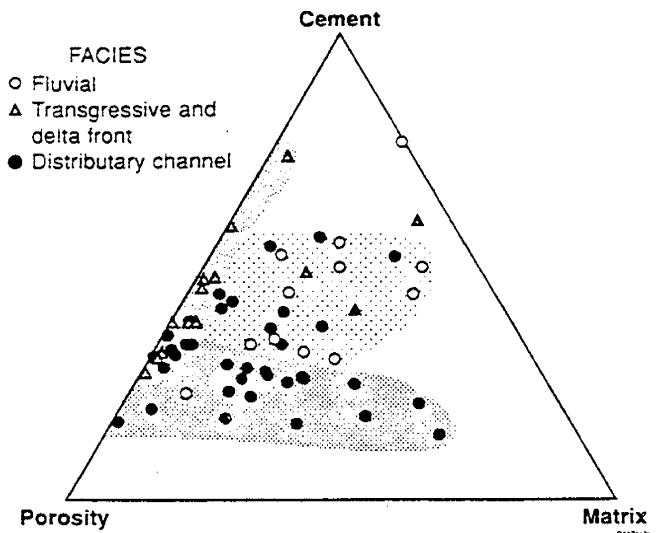
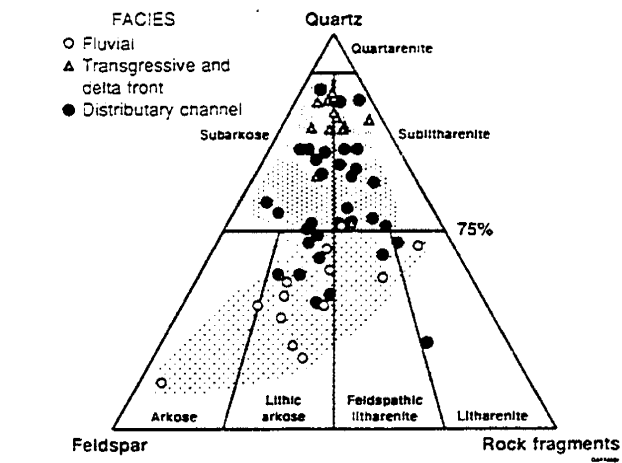


Figure VI-5. Trilinear plots of Ferron unit 5 sandstone compositions: (a) framework grain composition as percent quartz, feldspar, and rock fragments of total grains, (b) composition of intergranular material as percent cement, porosity, and matrix of total intergranular volume, and (c) cement composition as percent quartz, carbonate, and kaolinite of total cement.

and isolated pores (secondary porosity within pseudomatrix) is common in distributary sandstones.

Quartz, kaolinite, and carbonate are the volumetrically important authigenic phases in Ferron sandstones. Delta-front and transgressive sandstones typically contain both quartz (about 70 percent of total authigenic material) and carbonate cement (about 30 percent), with only traces of kaolinite (fig. VI-5c). Fluvial sandstones typically contain approximately 75 percent kaolinite, 15 percent carbonate, and 10 percent authigenic quartz. Distributary-channel sandstones contain approximately equal amounts of quartz cement and kaolinite, with only minor amounts of carbonate. Carbonate cement is typically associated with pseudomatrix; consequently, carbonate-cemented sandstones generally have low permeability. Likewise, the microporosity associated with kaolinite significantly reduces permeability. Quartz cement rarely fills intergranular pores, and quartz cement has relatively smooth surfaces; therefore, the presence of quartz cement has minimal effect on permeability.

The compositional trends exhibited by sandstones in the proximal part of the delta sandstones generally correspond to systematic differences in permeability between facies. Distributary-channel sandstones have the highest mean permeability (337 md) and, except where occluded by pseudomatrix, relatively high porosity compared with matrix and cement (fig. VI-5b), and subequal amounts of kaolinite and quartz cement (fig. VI-5c). Fluvial sandstones have the lowest mean permeability (29 md), subequal amounts of cement, matrix, and porosity (fig. VI-5b), and relatively large amounts of kaolinite cement, which fills intergranular voids and retards fluid flow. Delta-front and transgressive sandstones have intermediate values of mean permeability (54 md and 129 md, respectively), small amounts of pseudomatrix (fig. VI-5b), and large amounts of quartz cement, which results in smooth grain surfaces and little resistance to fluid flow.

## PERMEABILITY STRUCTURE OF UNIT 5 FERRON SANDSTONES

### Permeability Characteristics of Facies and Stratal Types

Permeability characteristics of the principal facies and their dominant stratification types and associated bounding surfaces were investigated. The following were measured to characterize the different groups: (1) distribution type as estimated by the coefficient of skewness, (2) central tendency as estimated by the arithmetic mean, and (3) variance as estimated by the coefficient of variation.

Each of the facies that compose the Ferron unit 5 have characteristic permeability distributions (table VI-2). Comparison by facies shows the mean permeability of the distributary-channel facies (363 md) to be almost an order of magnitude higher than that of delta-front (54 md) and fluvial facies (29 md) (fig. VI-6). Somewhat surprising is the relatively low permeability of the fluvial facies, even though its grain size is much greater than that of the distributary-channel facies.

Within the distributary-channel facies, permeability corresponds well to grain size and stratification type. F- and t-tests indicate that, although the permeability class of each stratal group overlaps considerably, they are significantly different. Much of the overlap between groups can be associated with grain size, sorting, and mineralogical variation. Permeability shows a predictable increase with increasing grain size from very fine through medium-grained sandstone. However, average permeability decreases as grain size increases beyond medium-grained sandstone. This trend is probably due to the poor sorting and an increase of mud clasts associated with these sediments. Clay rip-up clasts, particularly within the trough crossbedded stratal type, cause a dramatic decrease in permeability. In planar crossbedded sandstones, however, grain size ranges from fine to medium, and we observe within this stratal type an increase in permeability with increasing grain size. Thus, within each stratal type, permeability varies depending on the grain-size distribution.

Table VI-2. Statistical characterization by depositional classification and scale.

<u>Classification</u>	<u>Mean (md)</u>	<u>Cv</u>	<u>Csk</u>	<u>N</u>	<u>Distribution</u>
<b>Facies</b>					
Dist. Channel	337	0.60	0.39	889	square root
Delta Front	54	0.57	0.11	126	square root
Transgressive	129	0.58	0.60	27	square root
Fluvial	29	0.81	-0.54	210	log normal
<b>Channel Complexes</b>					
South Muddy Creek	220	0.57	0.73	371	square root
Picture Flats	436	0.50	0.08	518	square root
<b>Stratification Type (South Muddy Creek Laterally Migrating Channel)</b>					
Contorted	88	0.17	-0.05	37	log normal
Planar	145	0.17	-0.42	61	log normal
Trough	311	0.14	-0.30	101	log normal
Bounding Elements	44	0.35	-0.35	55	log normal
<b>Scale</b>					
40 × 40 ft grid	308	0.37	0.30	319	square root
6 × 6 ft grid	299	0.59	0.28	361	normal

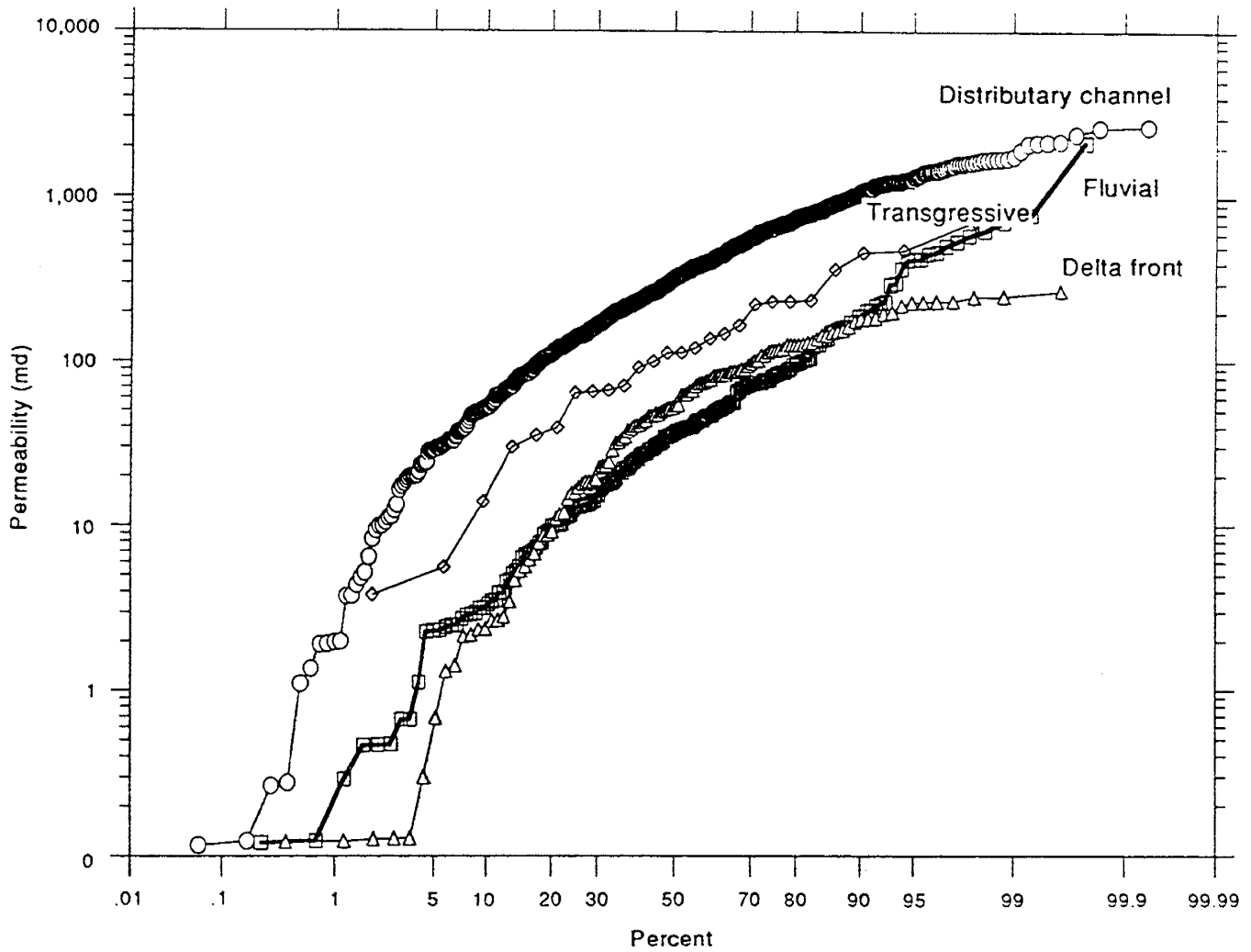


Figure VI-6. Facies cumulative-frequency plot for Ferron unit 5 sandstones from South Muddy Creek and Picture Flats.

A comparison by stratification type shows average permeability to increase from 88 md in contorted strata, to 145 md in the planar crossbedded strata, to 308 md in the trough crossbedded strata (fig. VI-7). Although the base of the channel displays relatively low permeabilities, highest permeabilities are located within the lower part of the channel fill, and overall permeability displays an upward-decreasing trend. Erosional discontinuities and bounding surfaces between stratal types display the lowest permeabilities within the distributary-channel facies (average permeability 44 md) and disrupt the overall upward-decreasing trend of the distributary-channel sediment. The permeability histogram for the entire distributary-channel complex approaches a lognormal distribution, with a range of permeability greater than four orders of magnitude.

Within each stratal type, permeability variation is partitioned according to individual bedded units. The coefficient of variation ( $C_v$ , defined as the ratio of the sample standard deviation to the sample mean) is used as an indicator of variability that is not sensitive to the sample mean. Table VI-2 compares the  $C_v$  of permeability groups of different scales and shows that  $C_v$  decreases significantly when permeability measurements are disaggregated, first according to stratification type and then according to individual bedded units within stratal types. This decrease indicates that the variability between lithological units is greater than within lithological units. Additionally, the  $C_v$  is relatively constant for the contorted, planar crossbedded, and trough crossbedded units, suggesting that sample standard deviation increases with sample mean. Permeability data further indicate that, of the distributions examined, aggregate populations at the channel-belt-facies scales approach a distribution that falls between normal and lognormal (approximated by a square-root distribution (table VI-2). Unmixed or disaggregated populations may approach lognormal (at the stratal level) or normal distributions (data subsets within stratal types).

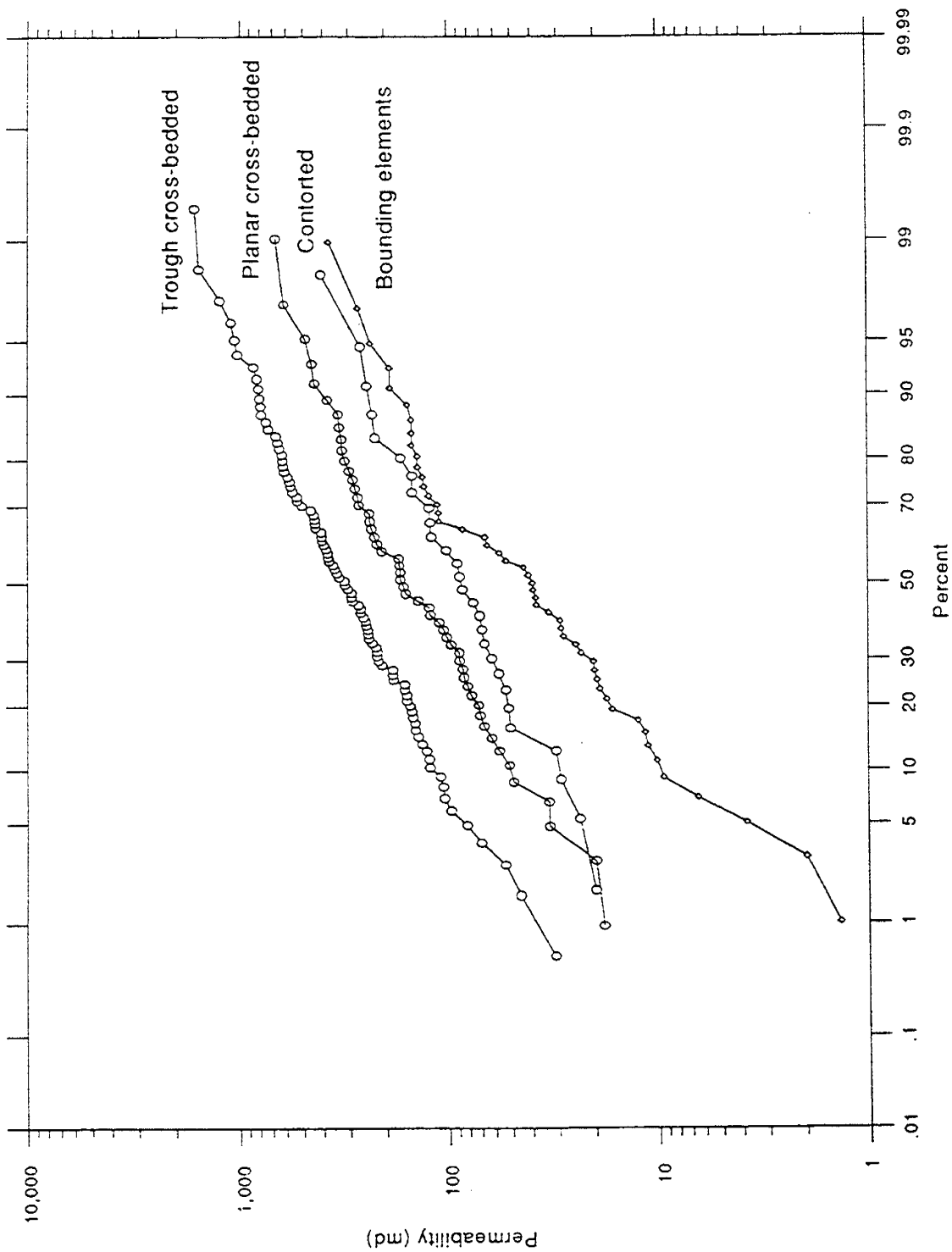


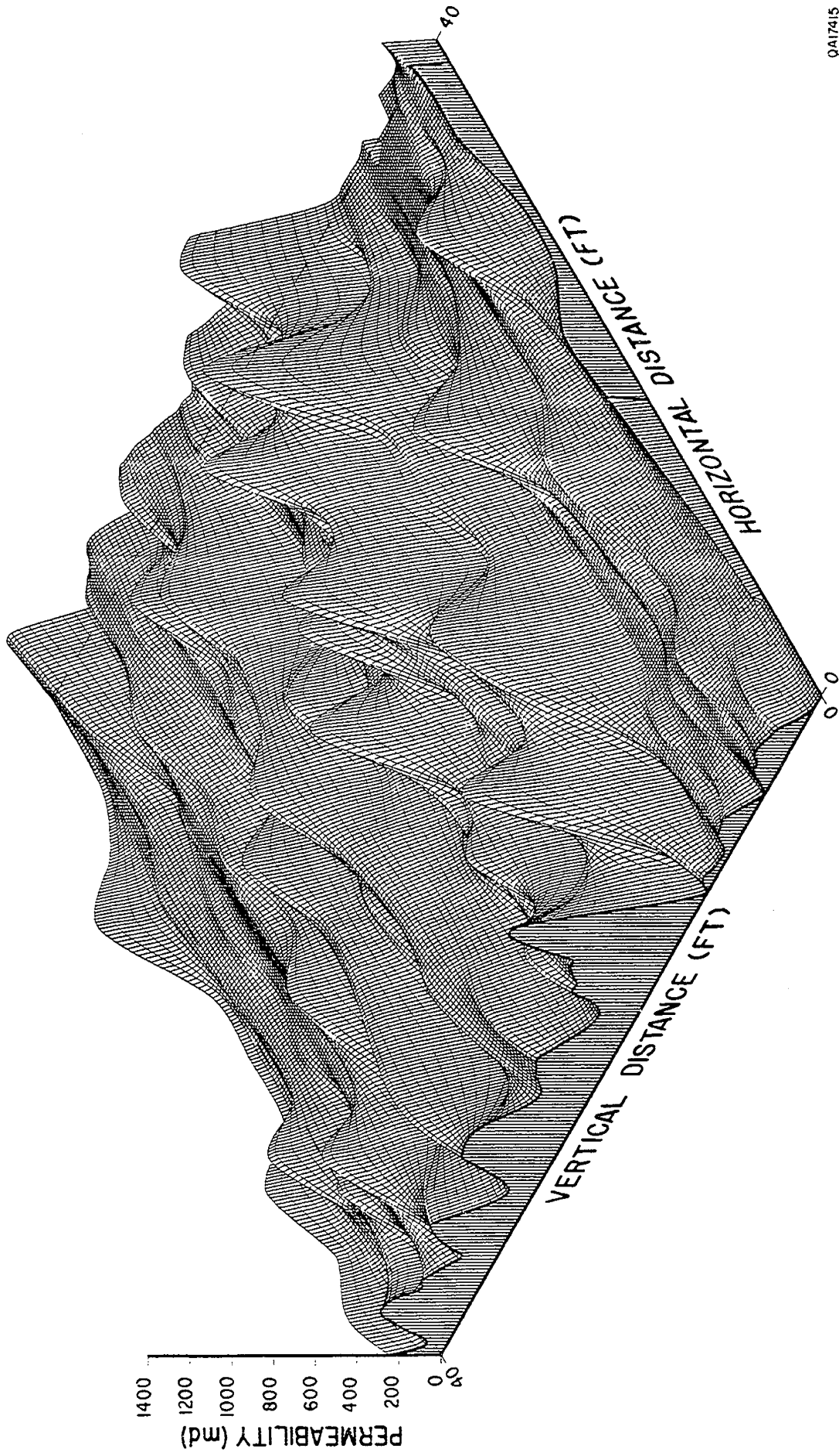
Figure VI-7. Stratal-type cumulative-frequency plot for Ferron unit 5 sandstones from South Muddy Creek.

### Small-Scale Permeability Structure

Two grids were constructed in the distributary-channel deposits in Muddy Creek to determine the spatial distribution of permeability according to stratification type and the nature of small-scale permeability variation. The largest grid (40 by 40 ft [12 by 12 m]; 2-ft [0.6-m] sample interval) was located in order to sample the three dominant stratification types contorted bedding at the top, planar crossbedding in the middle, and trough crossbedding at the base. A smaller grid (6 by 6 ft [2 by 2 m]; 0.33-ft [0.1-m] sample interval) was located entirely within the planar crossbedded facies.

Permeability structure within the distributary-channel deposits is highly stratified (fig. VI-8). The lower one-third of the 40-ft (12-m) grid sampled lower permeability delta-front sandstones overlaid by distributary-channel sandstones that have much higher permeabilities. The upper two-thirds of the grid sampled trough and planar crossbedded sandstones overlaid by contorted bedding. The dominant characteristic in the upper part of the grid is the alternation of low and high permeabilities reflecting the interbedding of trough and planar crossbedded sandstones and mudflake-rich bounding surfaces. These inclined bounding surfaces provide reservoir discontinuities that would clearly influence paths of fluid migration in reservoir analogs.

The 6-ft (2-m) grid provides high-resolution information on permeability variation within a stratal type and across its associated bounding surfaces. Permeability values within the tabular crossbedded sandstone are similar, and little variation is evident. In contrast, major decreases in permeability are evident across the adjacent bounding surfaces.



QA17415

Figure VI-8. Kriged permeability structure of distributary-channel sandstones as indicated by a 40-ft<sup>2</sup> (12-m<sup>2</sup>) sample grid with measurements at 2-ft (0.6-m) intervals. Pronounced layering results from alternation of sand-rich distributary-channel sandstones with associated bounding surfaces.

## Spatial Correlation of Permeability

### Permeability Correlation Using Vertical Profiles

Stalkup and Ebanks (1986) and Dreyer and others (1990) used permeability profiles to evaluate the lateral continuity of permeability zones. This method can be used visually to compare the continuity of permeability profiles and to see whether any correlation with adjacent profiles exists.

Figure VI-3 shows the lateral and vertical extent of stratal types, bounding elements, and permeability from the South Muddy Creek window. Permeabilities were measured at 1-ft (0.3-m) intervals along vertical transects spaced 120 to 160 ft (37 to 49 m) apart. At this spacing, stratal-type intervals displayed good correlation between profiles, indicating that different stratal types are distinguished by characteristic gross permeability layering. These permeability units are continuous over distances of 500 to 1,200 ft (152 to 366 m).

Crosscutting elements, such as lateral-accretion surfaces, display good correlation across the cross section and disrupt lateral continuity within stratal types. Vertical profile trends indicate that the stratal types are composed of permeability subintervals on the order of 1 to 5 ft (0.3 to 1.5 m) thick. However, these subintervals display a poor correlation between profiles. The limited degree of correlation among these subintervals indicates that permeability zones within stratal type are lenticular. Laterally, permeability displays an increasing trend toward the center of the channel, particularly within the trough crossbedded stratal type.

### Permeability Correlation Using Variograms

Permeability variation in permeable media can be described by two components, correlation and randomness (Goggin, 1988). The variogram is a statistical tool used to estimate the spatial variability of a property such as permeability, that is, how laterally or vertically

correlatable a given permeability measurement may be. It expresses the similarity or dissimilarity, on average, between data pairs a distance (h) apart. In particular, a variogram provides an estimate of the distance over which permeabilities are correlated, or alternatively, an indication of the absence of correlation in the data. A variogram is calculated by summing the squares of the differences of all data pairs separated by the distance (h) and dividing this sum by the number of pairs. This value is then plotted on the ordinate of a graph, and the distance between pairs is plotted on the abscissa.

In this model the range of influence of a property is the distance at which the variogram function becomes constant (correlation ceases), and the sill is the value at which the function levels off (approximates the global sample variance). When  $h=0$  the variogram should approach zero, but when h is so large that the data are not correlated, the variogram approaches the sample standard deviation. In general, experimental variograms do not go through the origin, an effect known as the nugget effect, which may be attributable to either measurement error or correlation on a distance smaller than the smallest lag distance.

Within the laterally migrating distributary-channel facies, permeability displays several scales of correlation that relate to the hierarchy of constructional elements composing the deltaic systems tract. Horizontally, permeability displays correlation ranges of 600 ft (183 m) to less than 4 ft (1.3 m) and is related to the lateral extent of the accretionary deposits that compose the distributary-channel complex.

Horizontal variograms for the contorted, planar, and trough crossbedded stratal types based on the 40- by 40-ft (12- by 12-m) sampling grid indicate that the range at which permeability is spatially correlated depends on the stratification type. At the small scale within the distributary-channel complex, lateral continuity of permeability is greatest in the lower part of the channel fill (18 ft [5.5 m]) and least in the upper part (less than 4 ft [1.3 m]) (fig. VI-9). Nearly all ordinate values in this facies approximate the total variance of the population, indicating that primary depositional features that influence the permeability distribution have been highly disrupted.

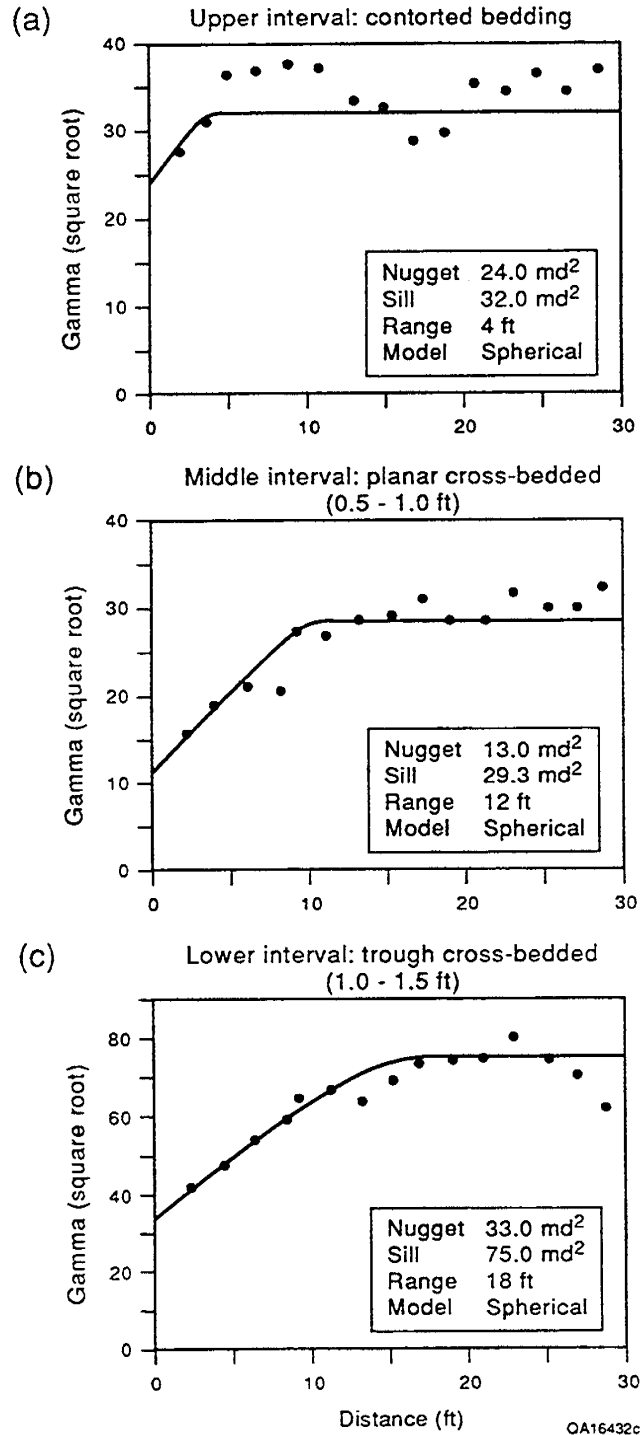


Figure VI-9. Horizontal semivariograms for permeability measurements on the 40-ft<sup>2</sup> grid classified by stratal type: (a) contorted bedding at the top of the distributary-channel complex, (b) planar crossbedding in the middle, and (c) trough crossbedding at the base.

Much unexplained variation (nugget effect) exists within the experimental variograms; therefore, the nature of this variation was analyzed by reducing the sample interval. At the smallest point spacing measured (4 inches [10 cm]), the range of influence is reduced to 2 ft (0.6 m). Given that the detailed grid was analyzed entirely within the boundaries of a planar crossbedded unit, this abrupt decrease in range indicates that the permeability distribution is scale dependent.

Vertically, three types of correlation were observed, having ranges of 2 ft (0.6 m), 6 ft (2 m), and 20 ft (6 m). The 2-ft (0.6-m) correlation fits a spherical model and is related to the average distance between discontinuities. The 6-ft (2-m) range fits a spherical model and is related to the average distance between stratal-type boundaries. The 20-ft (6-m) correlation fits a Gaussian model and is related to the upward-decreasing trend in permeability associated with grain size.

At Picture Flats, trends in average permeability, variation, and distribution type at the facies level are similar to those described at Muddy Creek (with the distributary-channel facies having much higher permeabilities than the delta-front facies). Additionally, within the distributary-channel facies, permeability corresponds to grain size and stratification type in the same manner that it does at Muddy Creek, although average permeability is nearly twice as high at Picture Flats (436 md versus 220 md). Erosional discontinuities also display low permeabilities and serve to disrupt permeability trends. Zones of highest permeability are more evenly distributed throughout the channel fill and not concentrated in the lower part, as seen in Muddy Creek. Figures VI-10 through VI-13 summarize the horizontal and vertical permeability structure of distributary-channel sandstones at Muddy Creek and Picture Flats. Permeability displays correlation over a range of scales that can be related to the depositional architecture. The differing architectures of the channel types contained in the distributary-channel system are reflected in different correlation structures, as estimated by the semivariogram, although permeability is controlled by similar factors in each case.

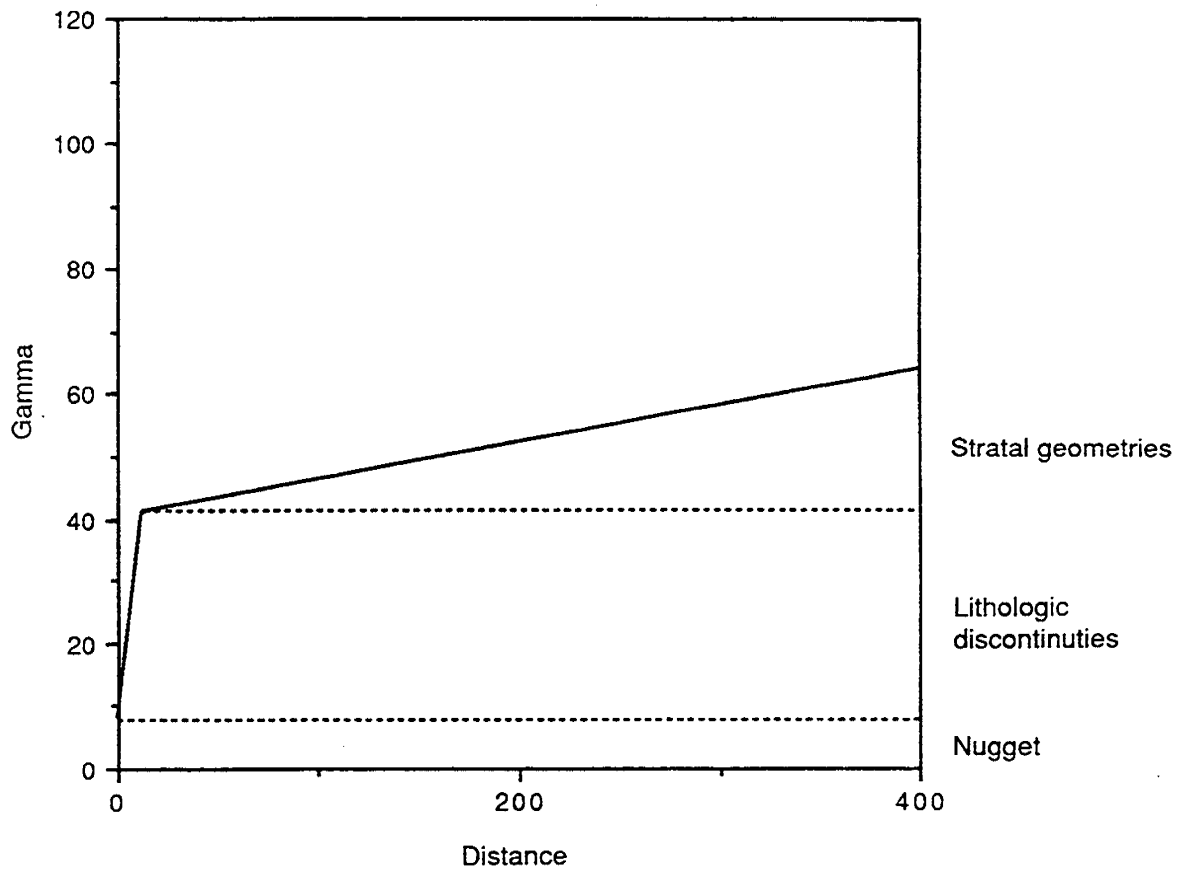


Figure VI-10. Horizontal variogram structure of laterally migrating distributary channel and geologic interpretation.

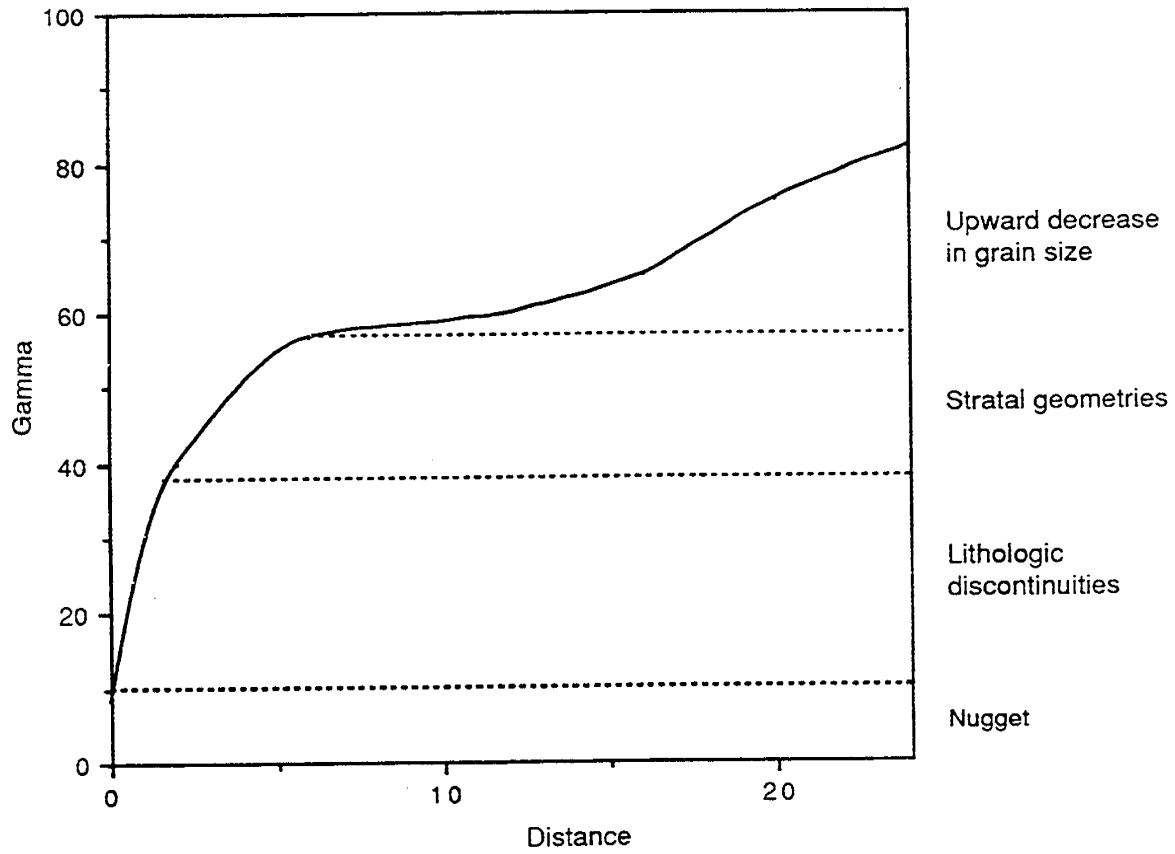


Figure VI-11. Vertical variogram structure from laterally migrating distributary channel and geologic interpretation.

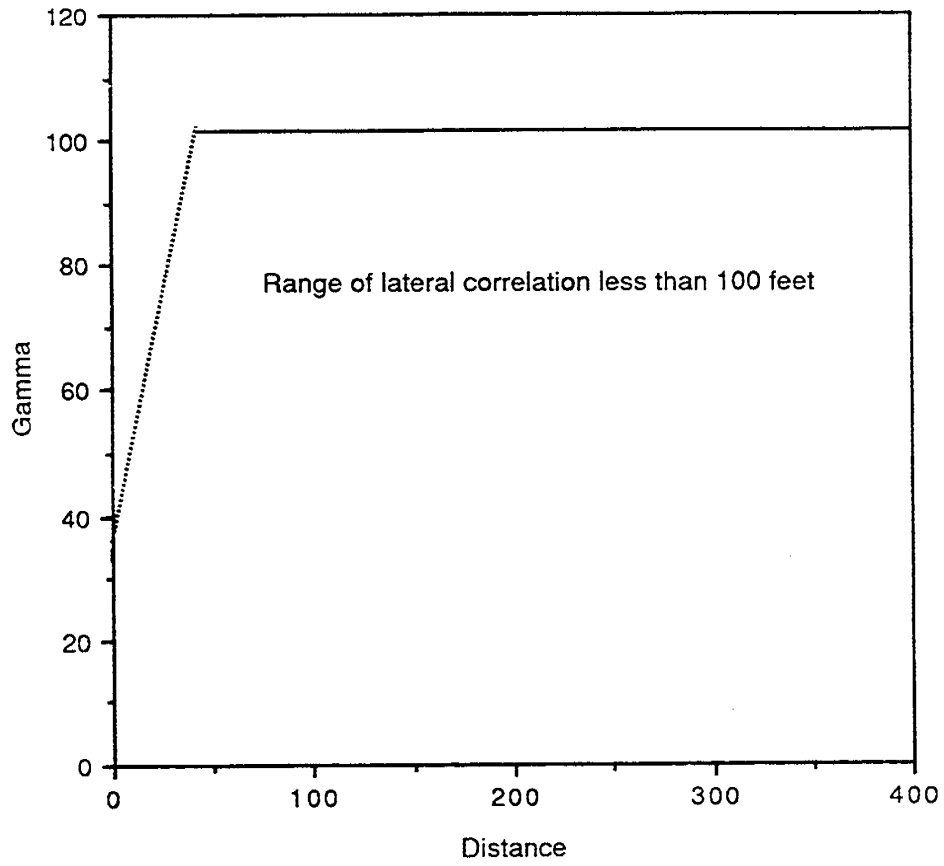


Figure VI-12. Horizontal variogram structure of late-stage distributary channel and geologic interpretation.

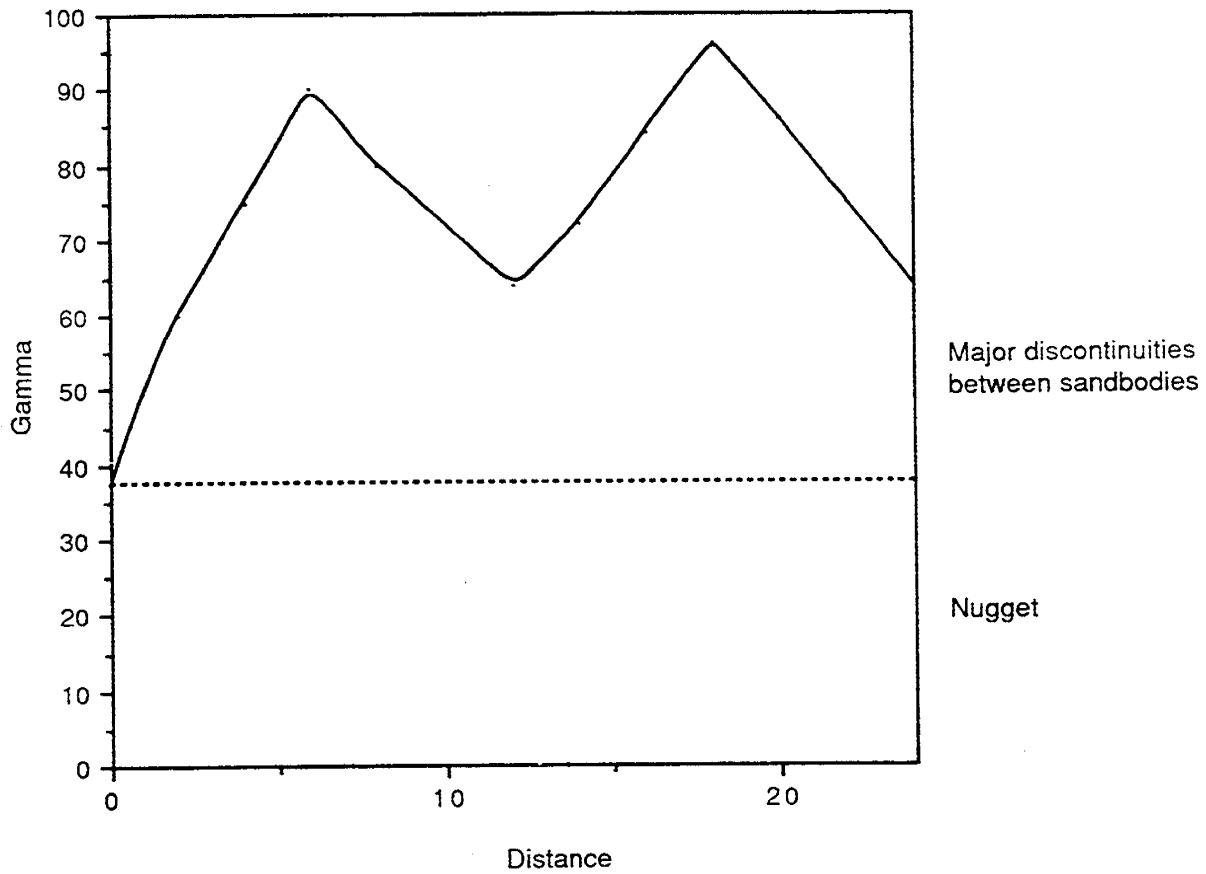


Figure VI-13. Vertical variogram structure of late-stage distributary channel and geologic interpretation.

## CONCLUSIONS

Outcrop studies provide high resolution information on facies architectural controls on the spatial distribution of petrophysical attributes in reservoir analogs. One of the sandstones in the Ferron delta system in central Utah has been selected for detailed analysis as an analog for Gulf Coast deltaic reservoirs. Unit 5 of the Ferron, a wave-modified deltaic sandstone, consists of a meandering distributary system that fed stratified delta-front deposits. Lateral migration, coupled with rising base level, resulted in horizontally and vertically heterogeneous distributary sandstones, in contrast to the delta front where vertical heterogeneity is dominant and lateral complexity minimal.

Analysis of the architecture of distributary and delta-front sandstones in this wave-modified deltaic system has demonstrated that heterogeneity patterns can be defined on the outcrop. Delta-front sandstones are vertically heterogeneous but laterally continuous over typical gas-well spacings. In contrast, the distributary system is characterized by both lateral and vertical heterogeneity and by spatial variation in geometric and dimensional attributes. Distributary sand belts are composite sand bodies composed largely of amalgamated, laterally accreted sandstones that rest on younger tidally modified channels, and are overlaid by late-stage distributary channels. Landward in the distributary system, sand belts display similar widths and are internally composed of thin and wide, laterally accreted, sigmoidally shaped sandstones. Seaward in the distributary system, accretion-foreset-bounded sand bodies are comparatively narrower but are twice as thick.

The compositions of framework grains, intergranular material, and authigenic material vary systematically with facies. These variations appear to correlate well with general differences in mean permeability between facies, suggesting that relations between fundamental sedimentary processes and permeability can be established. An understanding of such relations will allow

construction of more detailed, formation-specific reservoir models for other fluvial-deltaic sandstones.

Permeability distribution and structure are strongly related to facies composition, stratal type, and grain size. Distributary-channel sandstones have the highest mean permeability; delta-front sandstones the lowest. Within the distributary system the trough crossbedded stratal type has the highest mean permeability. Variogram analysis indicates correlation at several scales. Largest correlation lengths are 600 ft (180 m) in the distributary-channel sandstones. At the stratal level, horizontal correlation lengths are less than 20 ft (6 m) and relate to erosional discontinuities and bed size.

Permeability disparity between juxtaposed facies typically results from a combination of factors, including contrasting physical properties of the sediment coupled with disparate diagenetic overprints. However, flow barriers and baffles can also be physical barriers, such as calichified lateral accretion surfaces and mudflake-coated erosion surfaces at the base of channels. Quantification of permeability characteristics suggests a hierarchy of bounding surface types with attendant geometric and permeability characteristics. Hierarchical levels one and two compose flow barriers, and levels four and five probably are more likely to be semipermeable at reservoir conditions. That is, levels four and five probably compose flow baffles during production of gas. Sparse evidence from the literature suggests that level-three bounding surfaces can act as either flow boundaries or flow baffles. Infill wells or recompletions targeting reservoir compartments defined by level-three boundaries have tapped into a spectrum of pressures ranging from original reservoir conditions to depleted sands. Frequently however, the targeted compartment is only partially depleted, suggesting that level-three boundaries can compose dynamic flow barriers that become increasingly effective as a result of compaction as reservoir pressure decreases.

Several generalizations can be made regarding permeability values measured in Ferron sandstones.

1. Permeability characteristics display a close correspondence to stratification type. Highest permeabilities occur in the trough crossbedded stratal type. Lowest permeabilities are associated with bounding elements.
2. Within each stratal type, permeability variation is related to grain size, sorting, and mineralogy. Within a homogeneous lithology, permeability is further partitioned between bedding units.
3. Vertical trends in permeability are predictable. Where associated with intraformational lags, the trough crossbedded stratal type displays an upward-increasing trend; lower permeabilities are associated with mudflake conglomerates typically found at the base of trough crossbedded strata. The planar crossbedded stratal type displays an upward-decreasing trend, and the contorted stratal type displays no trend.
4. Comparison of permeability profiles shows that permeability groups based on stratal types are correlatable over hundreds of feet. Variogram analysis confirmed long-range correlation attributes of the vertical profiles. However, permeability subzones within stratal groups display little correlation at this scale.
5. Analysis of permeability structure at the small scale (6 ft [2 m]) shows that permeability distribution within macroforms is relatively uniform. Discontinuities within permeability distribution at this scale are provided by the bounding elements (in this case mud-rich accretion surfaces) that separate individual macroforms.
6. At an intermediate scale (40 ft [12 m]), permeability variability within macroforms becomes more apparent and is probably a result of grain size and diagenetic variation. Permeability variability within macroforms, however, is not as pronounced as variation between beds.
7. Variogram analysis demonstrates that permeability structure is dependent on stratal type and sampling scale. At a sampling interval of 2 ft (0.6 m), the trough crossbedded sandstone showed the greatest lateral correlation length (18 ft [5.5 m]) and the

contorted beds the least (less than 4 ft [ $<1.2$  m] [correlation length was dependent on the sampling scale]). At a sampling interval of 2 ft (0.6 m) the correlation length was 12 ft (4 m), whereas at a sampling interval of 0.33 ft (0.1 m) the correlation length was 2 ft (0.6 m). This difference demonstrates the scale dependency of the correlation length and suggests that the permeability structure may be fractal.

8. Highest permeabilities occur toward the center of the channel and decrease toward the channel margins.

CHAPTER VII: OUTCROP-CONSTRAINED DELINEATION OF STRATIGRAPHIC  
ARCHITECTURE AND RESERVOIR PROPERTIES  
OF WILCOX GROUP DELTAIC DEPOSITS,  
LAKE CREEK FIELD, TEXAS

Edgar H. Guevara, Jeffry D. Grigsby, and Raymond A. Levey

INTRODUCTION

Lake Creek field (fig. VII-1a) is part of the Wilcox Deltaic Sandstone (Houston Embayment) gas play (WX-1, Kosters and others, 1989). Fifty-four major reservoirs (each having produced more than 10 Bcf) in the Wilcox WX-1 gas play reservoirs have produced more than 3.8 Tcf of gas through January 1987 (Kosters and others, 1989). In this gas play, hydrocarbons (mostly gas) are trapped in roll-over anticlines along the Wilcox growth-fault zone. Reservoirs are distributary-channel, channel-mouth-bar, and delta-front sandstone facies of the Paleocene to lower Eocene Wilcox Group, which represents the first major Tertiary progradational episode into the north part of the Gulf Coast Basin (fig. VII-2).

Both oil and gas were discovered in Lake Creek field in 1941. The major control on hydrocarbon production within the field is a fault-bounded rollover anticline (fig. VII-3). Reservoirs are fluvial and deltaic sandstones in the Wilcox Group. The Lake Creek unit (LCU) contains 47 wells over 4.3 mi<sup>2</sup> (fig. VII-1b). The unit was created in 1944 as a pressure-maintenance, gas-cycling operation to maximize recovery of liquid hydrocarbons. Gas cycling extended through the mid-1950's. Cumulative gas production through January 1990 from the LCU was 120 Bcf of gas and 15.7 MMbbl of condensate.

The objective of this subtask was to develop strategies to maximize recovery of natural gas in established fields using known, state-of-the-art technologies calibrated to findings on the architecture of analogous reservoir types developed on the outcrop (chapter VI). Investigations

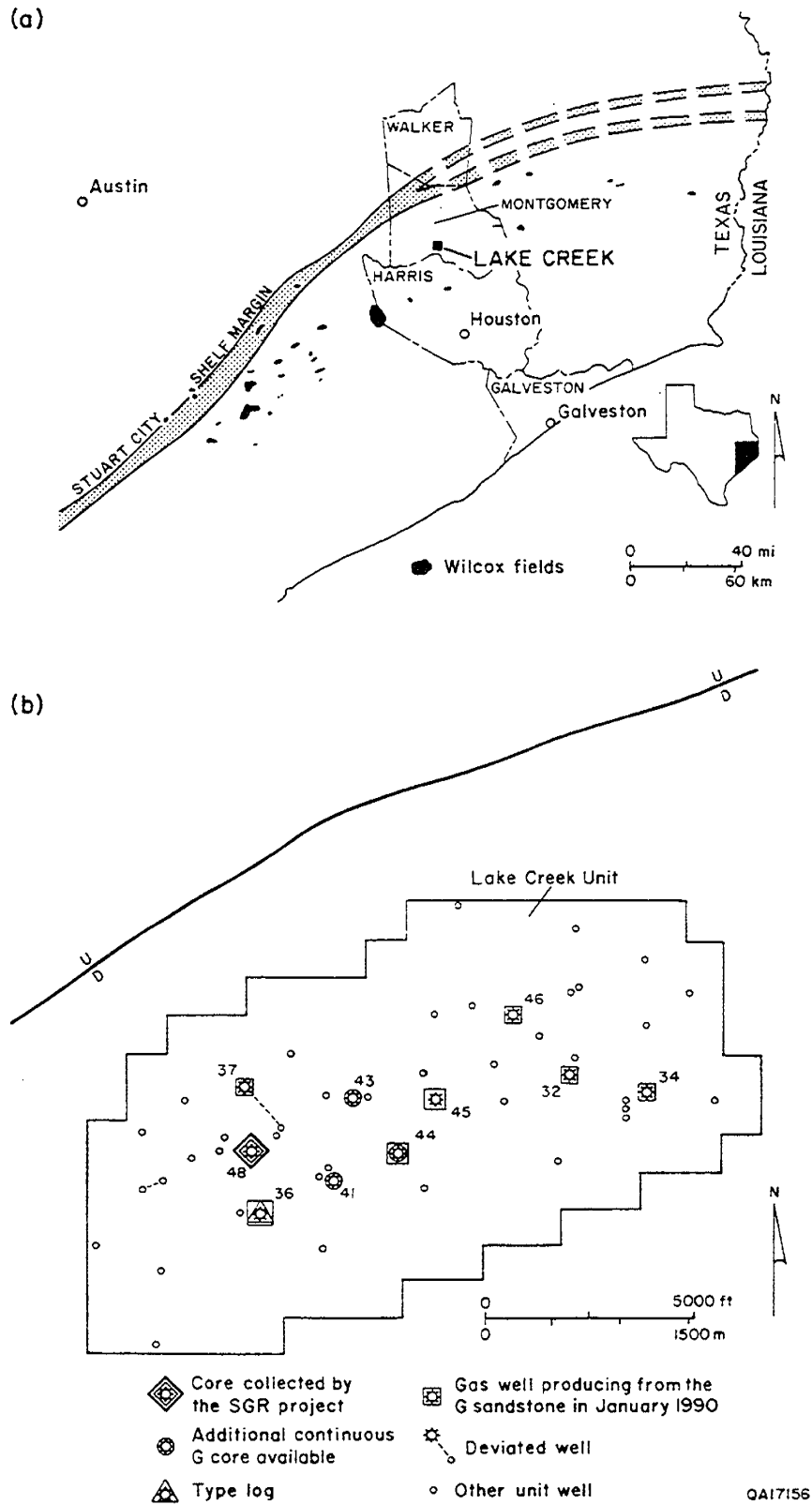


Figure VII-1. (a) Location map of the Lake Creek unit (LCU) in the Wilcox WX-1 gas play (modified from Kusters and others, 1989); (b) index map of wells in the LCU.

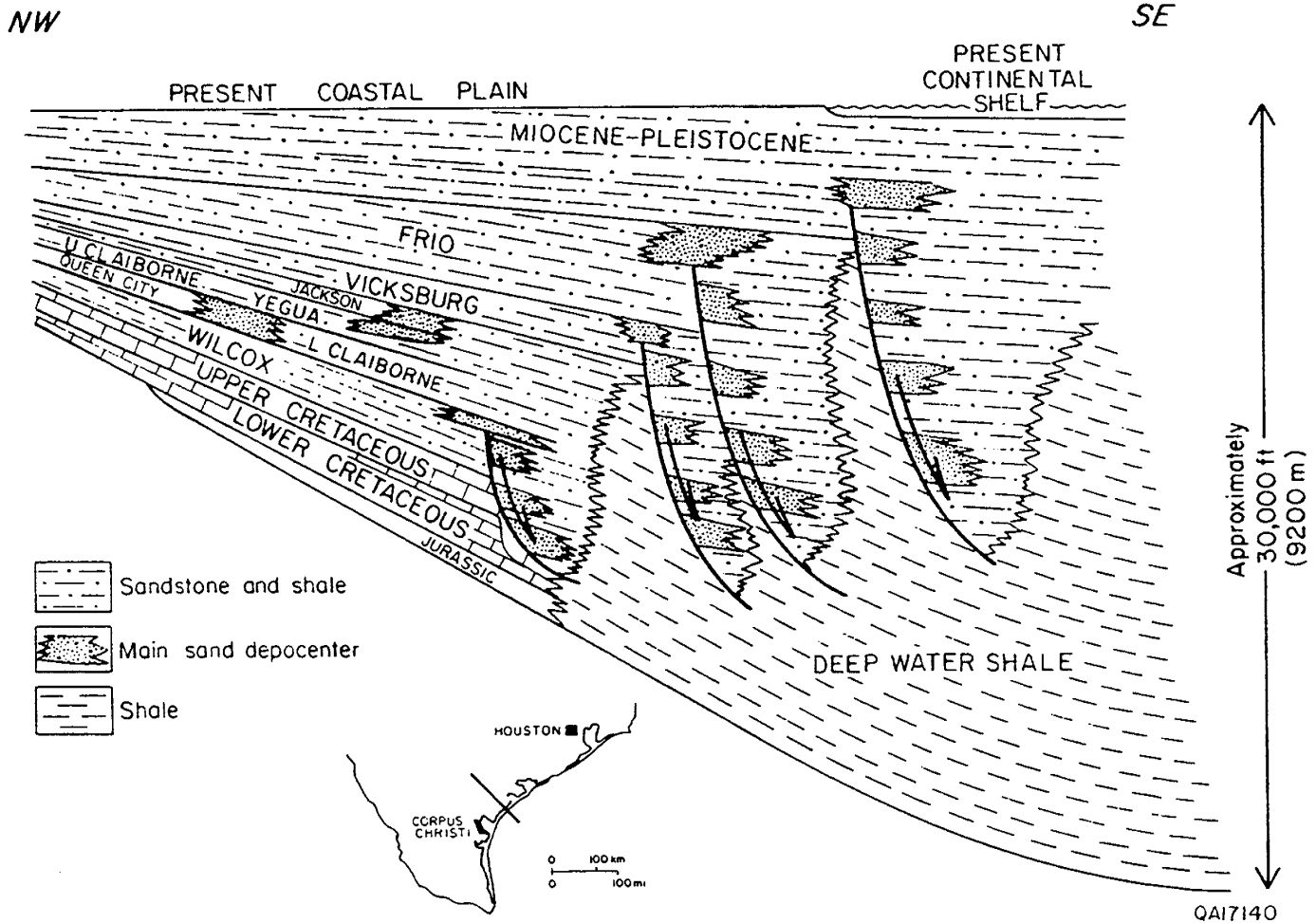


Figure VII-2. Schematic depositional dip-oriented cross section through the central Texas Gulf Coast Basin, illustrating the relative position of major sand depocenters (after Bebout and others, 1982).

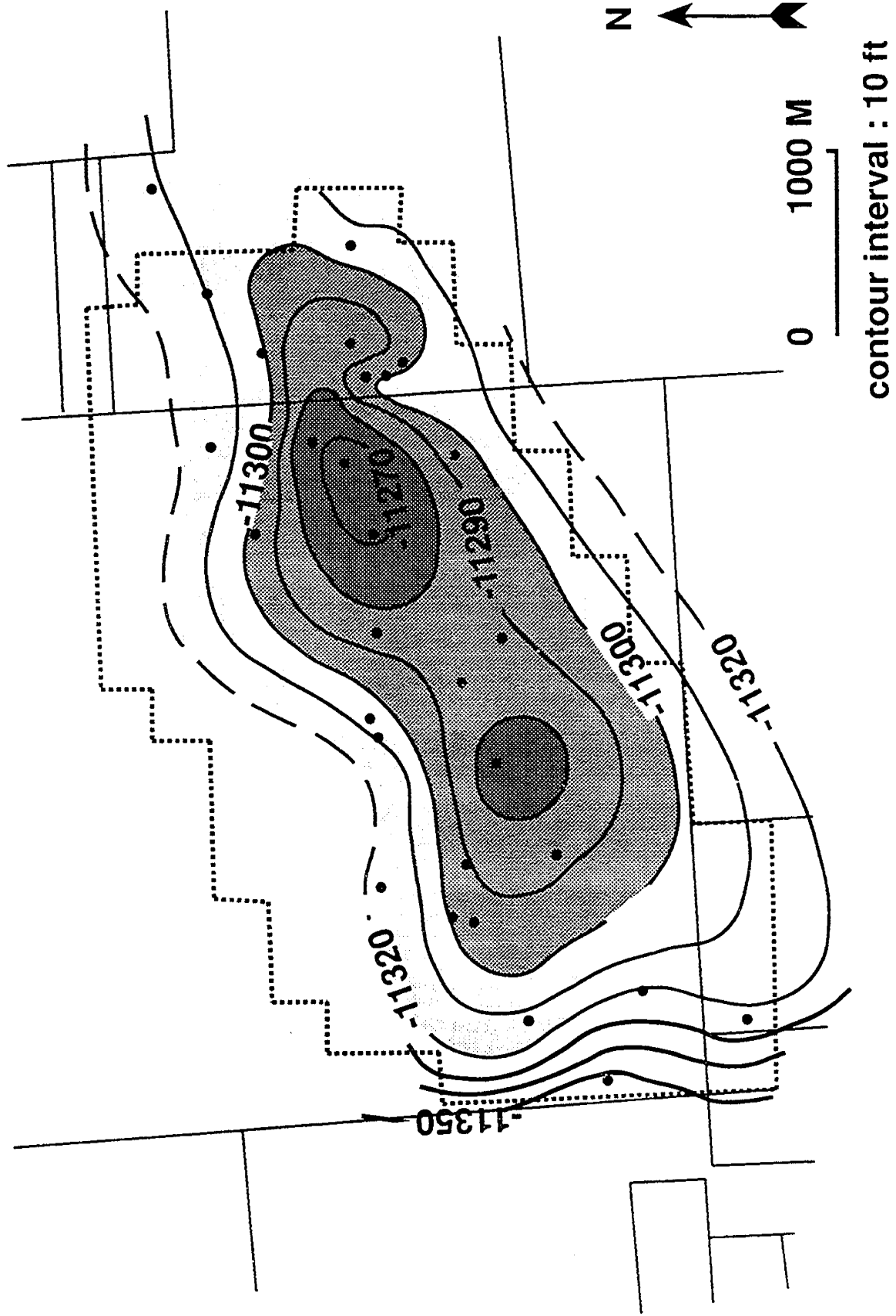


Figure VII-3. Structure map showing the top of G-1 across the Lake Creek unit.

aimed at the recognition and assessment of untapped and incompletely drained reservoir compartments containing additional gas resources. This subtask was co-funded by the Gas Research Institute and the State of Texas.

This chapter of the report addresses the architecture of the G sandstone in LCU. The G sandstone, analogous to unit 5 of the Ferron, was the target of a successful infill well drilled by Mobil Exploration and Producing U.S., Inc. Data collected from this new well afford an opportunity to test architectural and advanced-recovery models developed using outcrop-constrained subsurface information.

Hydrocarbon reservoirs at the LCU are sandstones of the Wilcox Group. Gas-condensate reservoirs (A through Q sandstones) underlie the oil-gas reservoirs named the La Gloria and 1 through 5 sandstones (Fig. VII-4). Porosities range from 12 to 20 percent. Permeabilities are often less than 1 md but locally exceed 100 md. The gas-condensate reservoirs are geopressed below approximately 13,000 ft below mean sea level (generally, K sandstone and deeper reservoirs). Only the A, B, D, and E reservoirs underwent gas-cycling operations (Fig. VII-5).

## DEPOSITIONAL ENVIRONMENTS OF THE G SANDSTONE

### Vertical and Areal Facies Development

Studies within the Lake Creek Unit have focused on gas reservoirs in the G sandstone, one of 18 gas-condensate reservoirs ranging in depth from 9,200 to 14,500 ft. The G sandstone, composed of individual, multistoried, stratigraphically heterogeneous reservoirs, is one of several 150- to 500-ft-thick upward-coarsening intervals forming part of the fluvial-dominated Brazos deltas of the lower Wilcox Rockdale delta system delineated by Fisher and McGowen (1967). In the area of the LCU-36 and LCU-48 well, the G sandstone is approximately 300 ft thick and comprises repetitive, mostly upward-coarsening and upward-thickening intervals separated by mud-rich intervals in an overall retrogradational interval similar to the upper Ferron (Ferron units 3-7). Deltaic sandstones separated by intervening bay/shelf shales result

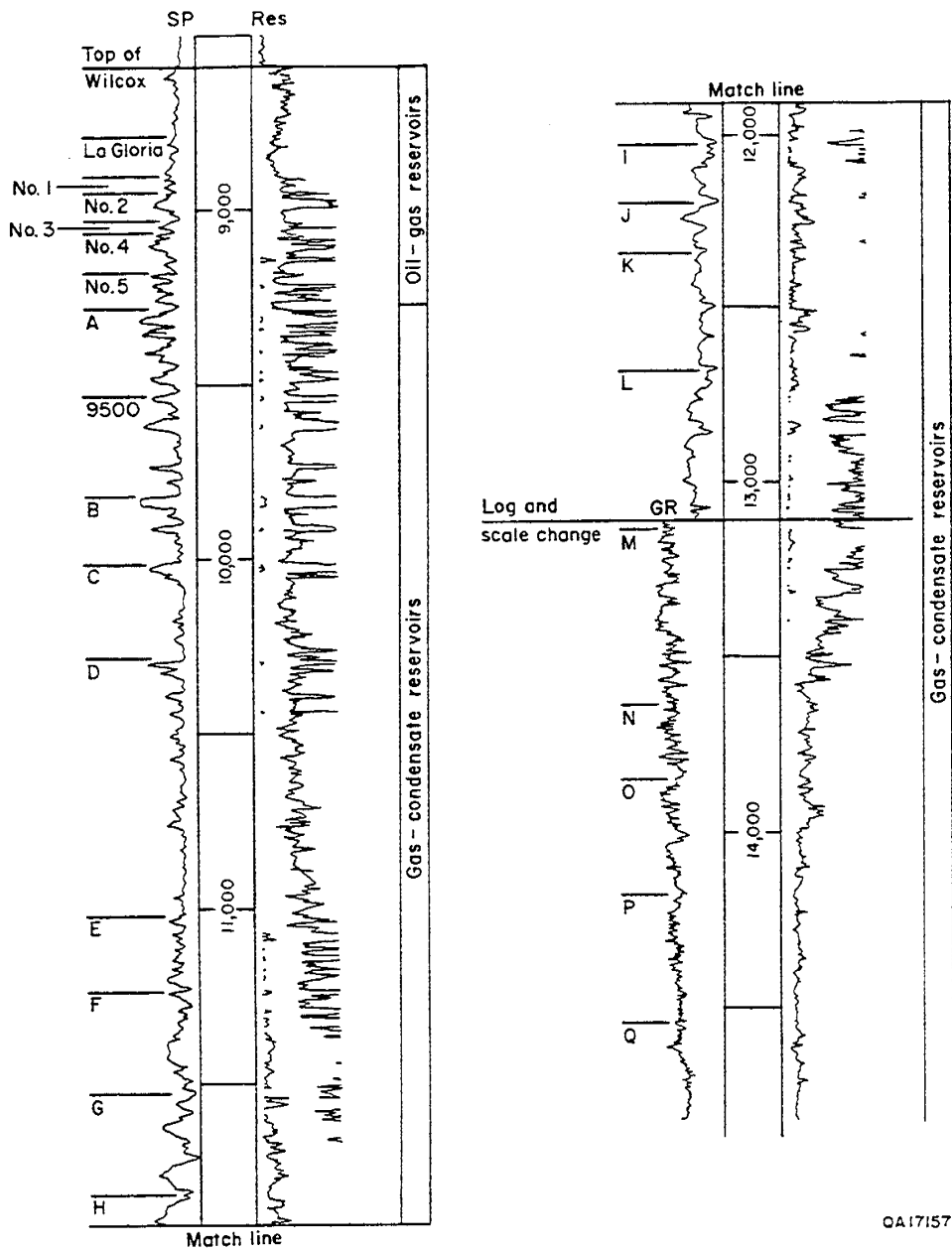


Figure VII-4. Type well log showing the oil reservoirs at the top and gas and condensate reservoirs in the lower stratigraphic intervals of the Wilcox Group at LCU.

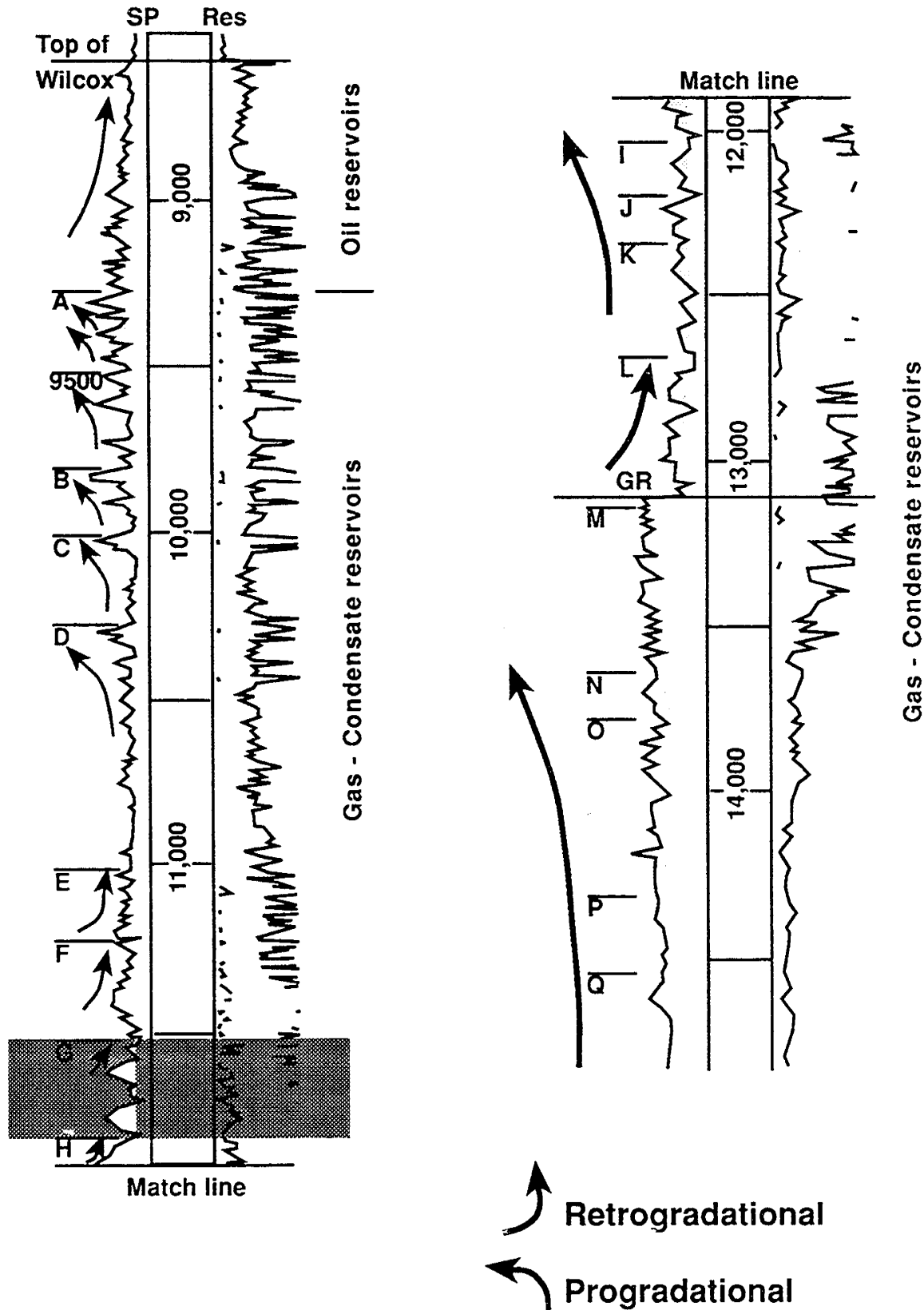


Figure VII-5. Spontaneous potential gamma-ray-resistivity log of the Mobil LCU-36 well showing oil-gas reservoirs (La Gloria and 1 through 5 sandstones) and underlying gas-condensate reservoirs (A through Q sandstones) of the Wilcox Group in the Lake Creek unit. Well location shown in figure 1b.

in stratified reservoirs. Lateral facies variations within reservoir sandstones result in reservoirs that are compartmentalized along facies boundaries. The thickest and most laterally persistent of the mud-rich intervals were used to subdivide the G sandstone into four operational units that from youngest to oldest are named G-1 through G-4 (fig. VII-6). Each of these subintervals or parasequences is equivalent in scale to individual deltaic units of the Ferron. Cores of the LCU-48 well are from G-1, G-2, and the upper part of G-3. Thin, commonly widespread beds of lignite and carbonaceous shales, occurring mostly in the G-1 through G-3 units, are excellent markers on density and neutron logs (fig. VII-6). Within these four operational units or parasequences, the G-1 has been the most frequently perforated.

#### Shelf/Interdistributary Bay/Prodelta Mud Facies

Shelf, interdistributary bay, and prodelta mud-rich facies compose the lower part of the operational units. Basal shelf/bay facies are overlain by prodelta facies. Shelf/bay facies consist of mostly bioturbated shales interbedded with laminae and thin beds of siltstone and sandstone, commonly bioturbated, massive and rippled. Generally, siltstones and sandstones are thicker and more abundant, and bioturbation is less intense in the prodelta facies. Sandstones displaying parallel bedding, hummocky cross-stratification, and current and wave ripples are locally interbedded with shelf/bay mud facies. They represent shelf sandstones and crevasse splays in interdistributary and delta-margin embayments.

#### Delta-Front Facies

Relatively thick sand-rich intervals in the middle of the operational units consist of delta-front facies overlying the shelf/bay/prodelta mud-rich facies. They consist of laterally extensive, massive to crossbedded, locally burrowed sandstones interbedded with shales in mostly upward-coarsening and upward-thickening intervals. Locally, the upper part of these

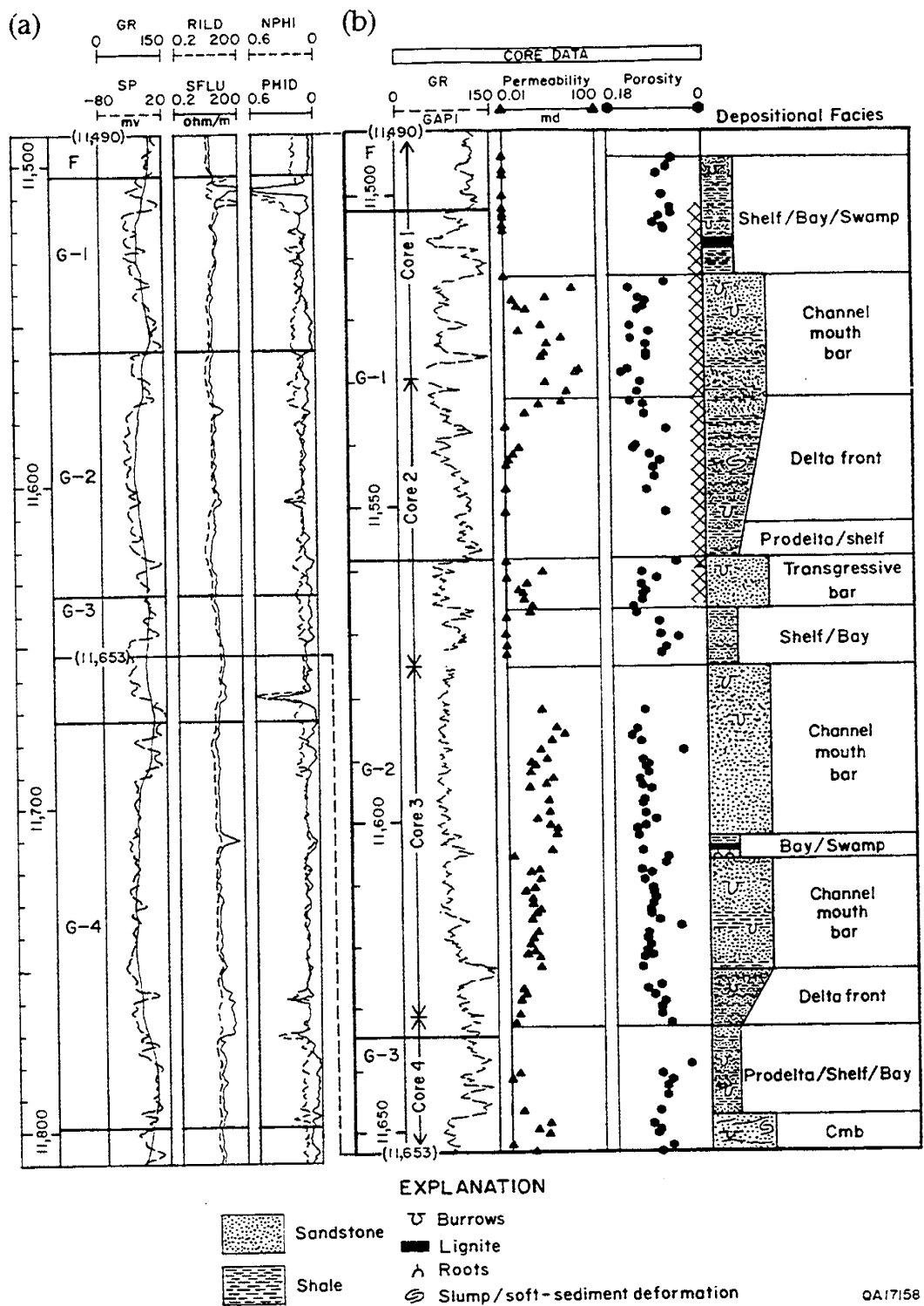


Figure VII-6. (a) Well log showing subdivisions of the G sandstone; (b) core graph and petrophysical data of cores of the G sandstone in the LCU-48 well, Lake Creek unit, Montgomery County. Laterally extensive, relatively thick, mud-rich intervals allow delineation of operational units (parasequences) G-1 through G-4. Sharp deflections to the left of the density and neutron logs correspond to carbonaceous shales and thin beds of lignite. The operational units comprise delta-front facies and locally overlying delta-plain facies in the middle part; shelf/bay/prodelta mud-rich facies and associated crevasse-splay and delta-destructural sandstones compose the lower and upper parts. Hatched interval between 11,501 and 11,566 ft represents cored interval.

intervals is aggradational (blocky-serrate log shapes), suggesting proximity to the distributary channel.

Two main parts are distinguished in the delta-front facies. The lower part, comprising shales interbedded with generally thin sandstones are bar-front and distal-bar deposits that grade downward into shelf/bay/prodelta mud facies. Locally, these deposits display soft-sediment deformation characteristic of fluviially dominated deltaic deposits produced by sudden sand loading on the underlying, undercompacted muds. The upper part, comprising massive, crossbedded, and parallel-bedded, locally rippled and burrowed sandstones interbedded with shales, represents the proximal delta front and distributary mouth bar. These delta-front deposits are analogous to the laterally continuous delta-front sandstones of Ferron unit 5 (fig. VI-2).

#### Distributary-Channel Facies

Distributary-channel facies examined from available core control in the Lake Creek Unit are characterized by sand-rich intervals containing massive to crossbedded sandstones that fine upwards. SP and gamma-ray log suites are typically blocky in character. Abundant rip-up (clay) clasts are common at the base of individual channels. These rip-up clasts occur as pebble conglomerates that strongly affect the gamma-ray log by creating an above-normal GR-API response within the basal part of the channel system. Individual distributary-channel fill facies range from 15 to 38 ft in thickness and average 27 ft among 13 well logs interpreted to penetrate this facies. Planimetric view of the G sandstone facies maps (figs. VII-7 through VII-11) indicate that the widths of these distributary channels range from 1,200 to 3,500 ft. These channels are oriented parallel to depositional dip and are generally aligned in a northwest-to-southeast direction. In the lower part of the G sandstone interval, distributary-channel sandstones are mostly adjacent to channel-mouth-bar and delta-front facies. In the upper part of the G sandstone, the distributary-channel facies are also adjacent to channel-

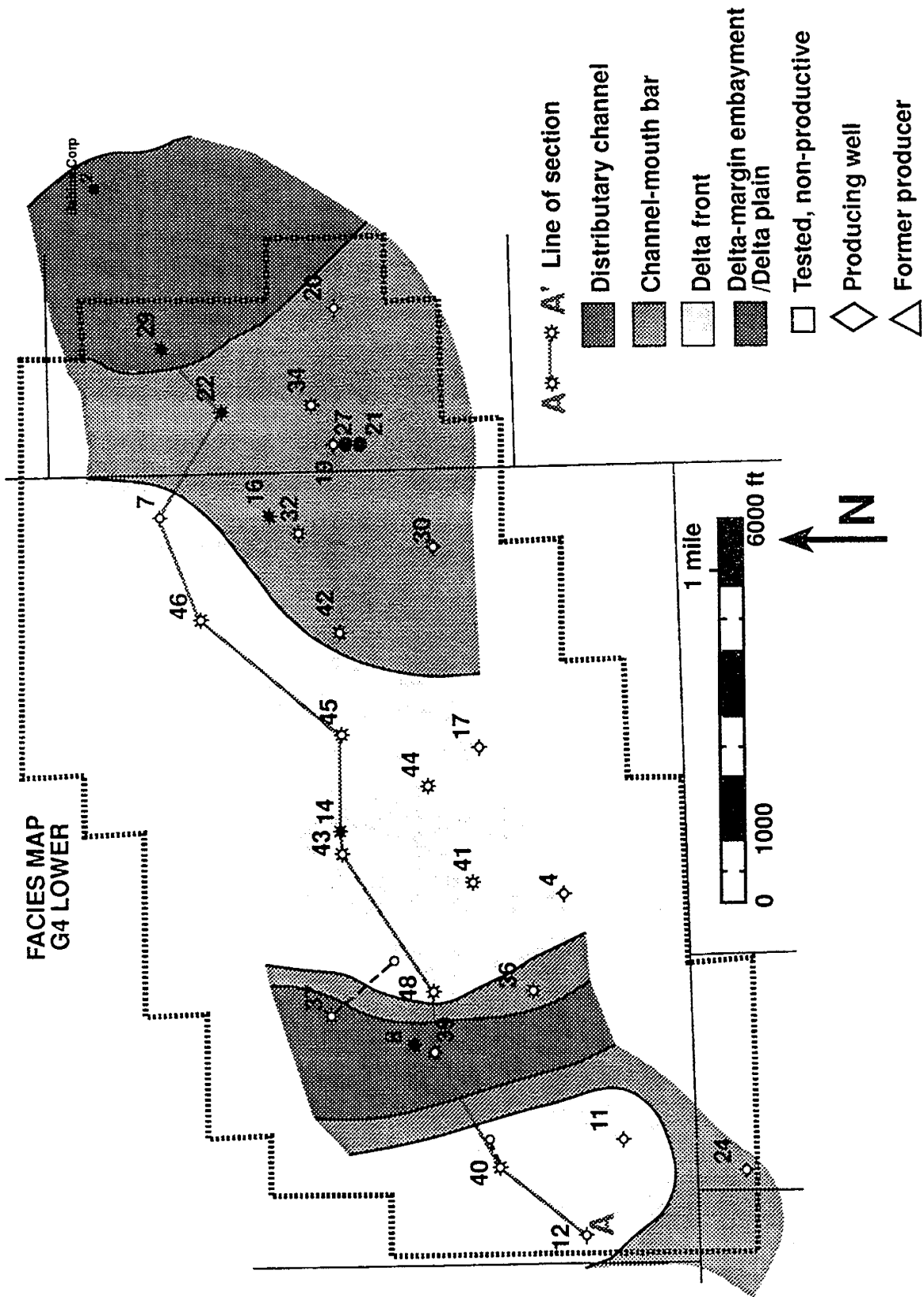


Figure VII-7. Facies map of the G-4 lower interval illustrating the lowest parasequence in the G sandstone.

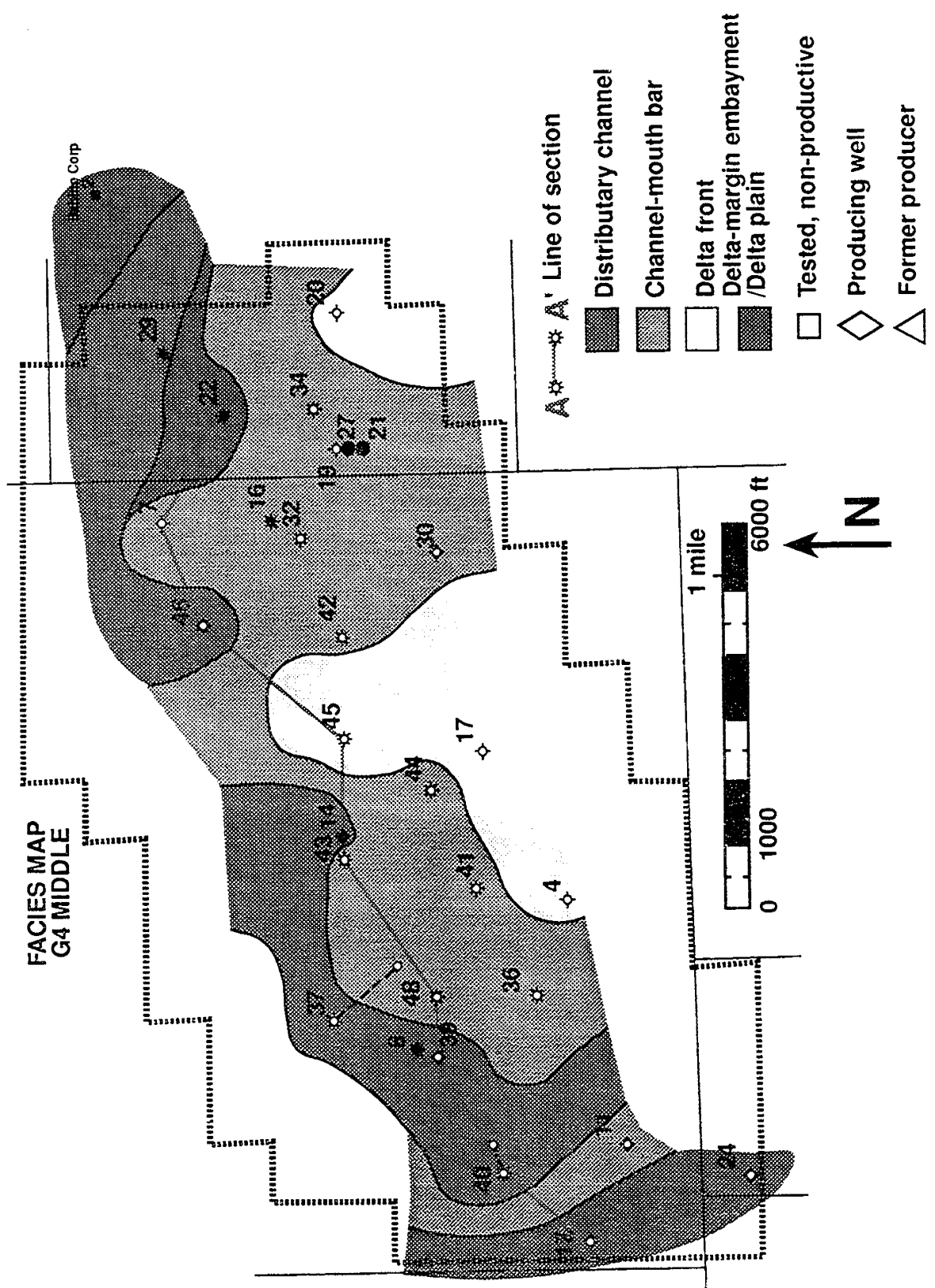


Figure VII-8. Facies map illustrating the G-4 middle interval in the G sandstone.

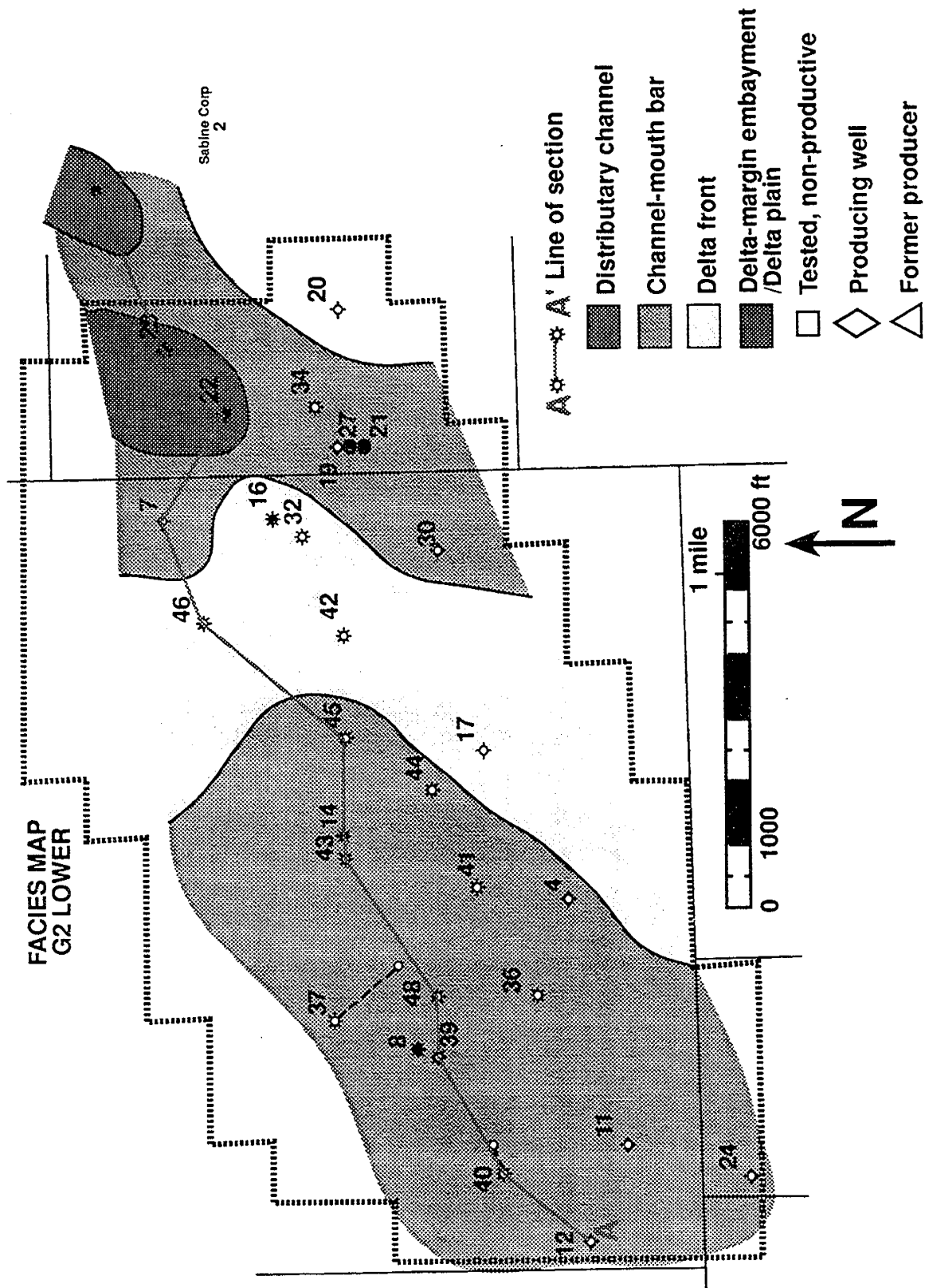


Figure VII-9. Facies map illustrating the G-2 lower interval in the G sandstone.

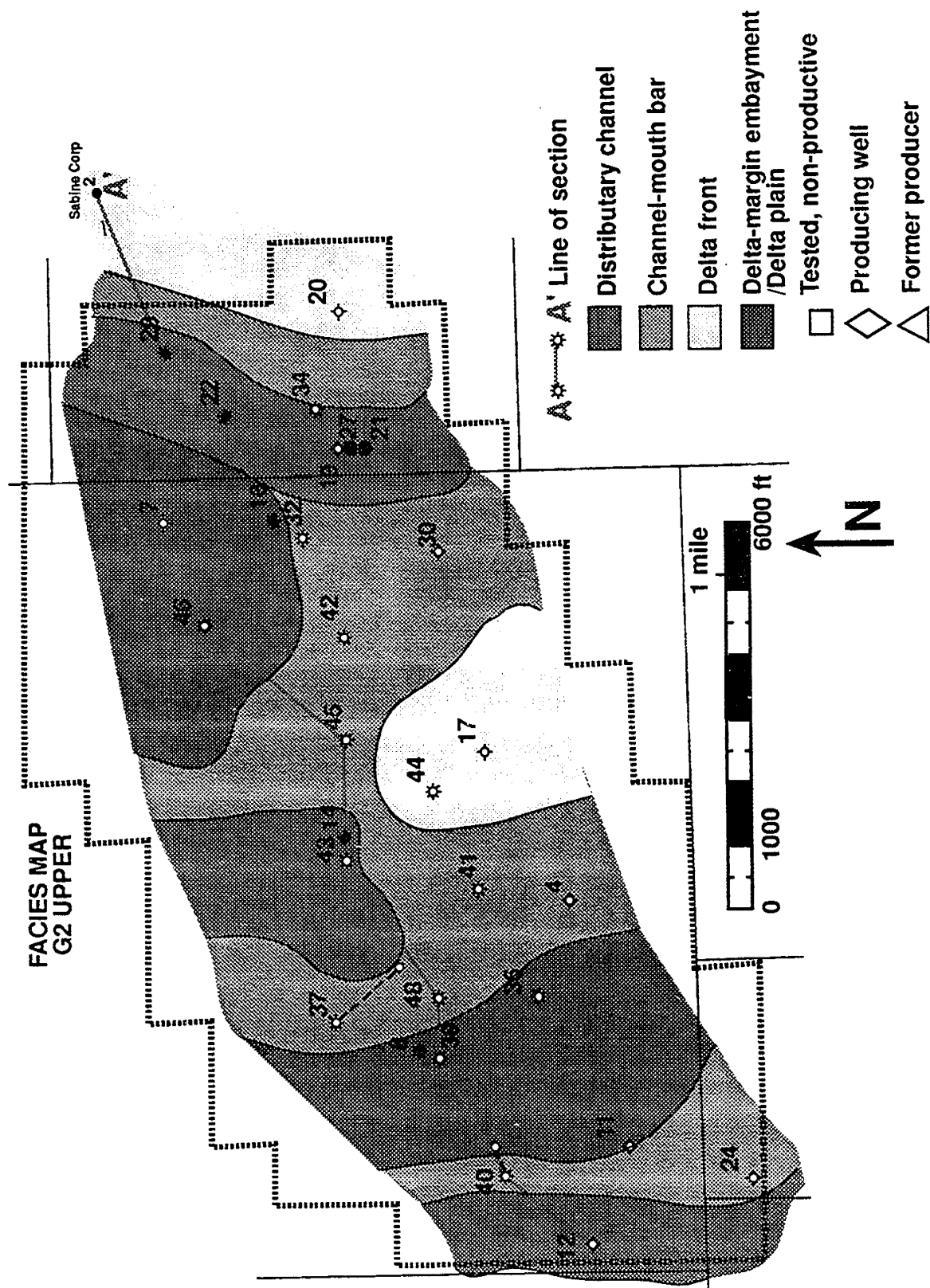


Figure VII-10. Facies map illustrating the G-2 upper interval in the G sandstone.

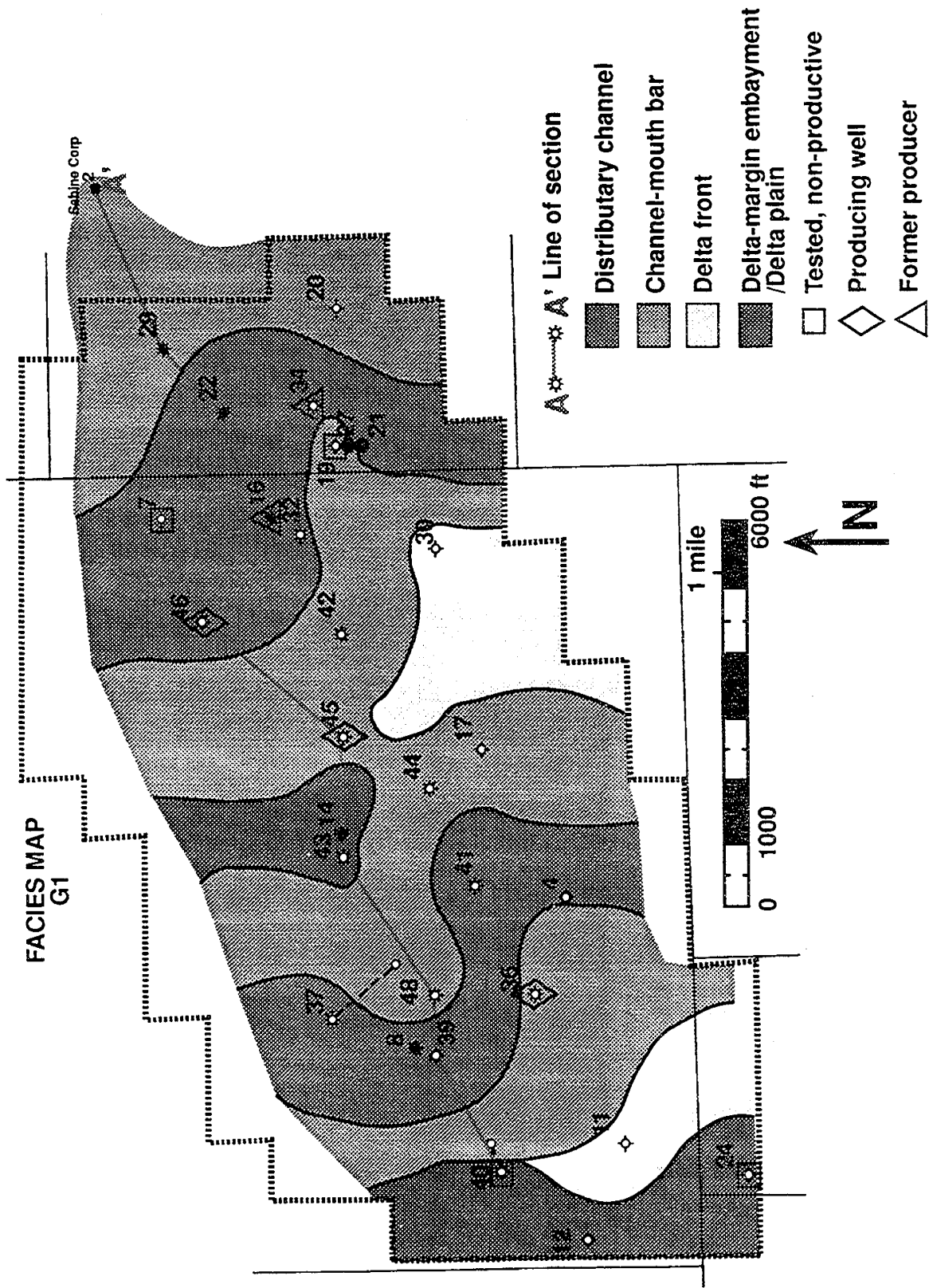


Figure VII-11. Facies map of the G-1 interval illustrating the uppermost parasequence in the G sandstone. G-1 has the greatest number of completions.

mouth-bar and delta-front facies but locally replace delta-margin embayment and delta-plain facies.

#### Delta-Plain Facies

Mud-rich facies, commonly rich in organic matter and locally displaying root molds, represent delta-plain deposits. Delta-plain muds, overlying interbedded with delta-front facies, locally grade into interdistributary bay facies.

#### Transgressive, Delta-Destructional Facies

Thin, bioturbated sandstones locally occurring in the upper parts of the operational units represent delta-margin, barrier-island, and sheet sandstones comprising transgressive, delta-destructional facies. They result from reworking of the delta-front and delta-plain facies of the underlying, abandoned, foundering delta, and grade up into and are interbedded with shelf/bay mud facies and are analogous to the maximum flooding surfaces defining the base of progradational Ferron deltaic sandstones (fig. VII-2).

### STRATIGRAPHIC ARCHITECTURE OF THE G SANDSTONE

#### Vertical and Areal Facies Development

Subsurface characterization of stratigraphic architecture is dependent on use of well-log profiles constrained by sparse information from cored holes to define depositional facies and their three-dimensional extent and geometries. This approach formed the basis for the characterization of the G sandstone parasequences; however, information developed on the Ferron outcrop was used to more rigorously constrain facies limits and internal structure. Spontaneous potential (SP) and gamma-ray (GR) logs of the operational units of the G sandstone generally display funnel-shaped log traces in the lower part and blocky-serrate log shapes

in the middle part. The upper part of each operational unit is a thin interval generally showing funnel-shaped log curves. Slabbed cores indicate that these log shapes reflect thick upward-coarsening and upward-thickening intervals (funnel log traces and overlying blocky-serrate log shapes) that are commonly overlain by a thin, upward-coarsening interval.

Lithologically, each operational unit generally comprises three parts. A basal interval is composed of mostly bioturbated shales interbedded with generally thin, locally parallel-laminated, rippled, and hummocky crossbedded sandstones. The middle part typically consists of massive, locally crossbedded and rippled sandstones interbedded with thin shales. The upper part is a generally thin interval comprising rippled and bioturbated sandstones bounded by bioturbated, locally carbonaceous and lignitic shales. Because the operational units are stacked, the upper, shale-rich interval is also the base of the overlying unit.

The tripartite division of operational units discussed above is interpreted as follows: (1) The lower part of the operational units comprises mostly shelf/bay and prodelta mud-rich facies. (2) The middle part is a thick interval of sand-rich, delta-front facies locally interbedded with delta-plain and bay muds. (3) The upper part is composed of mud-rich, shelf/bay facies locally associated with crevasse-splay and transgressive, delta-destructive, sheet sandstones (fig. VII-6).

Cores and wireline logs of the G sandstone in the LCU No. 48 well and vicinity illustrate deltaic progradation and subsequent local, transgressive flooding of the abandoned deltas. Each operational unit (G-1 through G-4, fig. VII-6) corresponds to a period of deltaic progradation, units G-2 and G-4 representing relatively major progradations, each overlain by smaller progradations (G-1 and G-3). Delta-front facies are locally overlain or replaced by channel-mouth bar facies, in turn locally overlain and truncated by distributary-channel facies. This variation in stratigraphic architecture is illustrated in the series of facies maps showing the progression of facies development in the G-4 through the G-1 operational units (figs VII-7 through VII-11).

The effects of progradation on reservoir architecture are well represented in the operational unit G-4 lower and middle intervals (figs. VII-7 and VII-8). The more distal deposits of the lower interval of G-4 show laterally continuous delta-front deposits to be volumetrically more important than they are in the middle interval. Conversely, sand-rich, but more heterogeneous, mouth-bar and distributary-channel deposits dominate in the middle interval of operational unit G-4. This pattern is repeated in the vertical succession of operational units G-2 (lower), G-2 (upper), and G-1 (figs. VII-9 through VII-11). Retrogradation (progradation during overall sea-level rise), analogous to that displayed in the upper Ferron (chapter VI), is well represented by the G sandstone, wherein operational units G-4, G-2, and G-1 progressively become thinner vertically in the section. Thus, the stratigraphic architecture of the G sandstone in the Wilcox at LCU shows a strong parallel to the interpretation of stratigraphic variability documented within the Ferron Sandstone outcrops of central Utah.

#### Styles of Between-Well Heterogeneity

The style of between-well heterogeneity in the G sandstone becomes readily predictable in the context of outcrop-constrained reservoir characterization and is well displayed in strike cross section A-A' across the crest of the field (fig. VII-12a, b). The parasequences that compose the G sandstone compose a multistoried reservoir suite separated by shelf-deposited flooding surfaces. The mud-rich flooding surfaces provide the primary barriers to vertical gas flow in the section and effectively provide vertical compartments within the G sandstone.

Lateral heterogeneity is also pronounced and is a response to deep incision by distributary channels into associated mouth-bar and delta-front sandstones. Delta-front facies are the most laterally persistent (on the order of several miles); mouth-bar facies have intermediate continuities (maximum lateral extents of 1-2 mi); and channel deposits are the most areally restricted (less than 6,000 ft in strike section). Outcrop characterization of analogous deltaic deposits in the Ferron has demonstrated that mud-clast-rich zones compose the fringes of the channel sandstones and that these zones compose low permeability barriers that effectively

segment the reservoir (chapter VI). This facies mosaic of amalgamated channel, mouth-bar, and delta-front facies provides a highly heterogeneous reservoir interval that historically has largely been perforated in the G-1 parasequence.

#### RESERVOIR COMPOSITION AND QUALITY

Lower Wilcox sandstones are poorly to moderately well sorted, fine-grained quartzose subarkoses to arkoses. Plutonic and metamorphic rock fragments are the major lithics; volcanic rock fragments are minor constituents. The major authigenic minerals are quartz (as overgrowths), illite, and chlorite, with variable amounts of kaolinite, siderite, ankerite, calcite, and feldspar (as overgrowths).

G sandstones are low porosity ( $10.5 \pm 3$  percent) and low permeability ( $1.33 \pm 5$  md, mostly less than 1 md) reservoirs. Although permeabilities are mostly less than 1 md, the best values generally correspond to channel-mouth bar and distributary-channel sandstones in the G-1, G-2, and G-4 parasequences. The generally weak correlation between porosity and permeability is at least partly due to diagenesis. Initial petrographic data suggest that, in addition to quartz overgrowths, authigenic fibrous illite may reduce reservoir permeability.

Progradational delta-front and transgressive sheet sandstones generally form laterally extensive gas reservoirs. Heterogeneity in these reservoirs results from the juxtaposition of lithologically different facies. For example, barriers or baffles to gas flow may locally develop along boundaries between distributary-channel mouth bar and delta-plain facies, along progradational delta-lobe margins, and between delta-margin-island sandstones, tidal inlets, and shelf/bay facies. Additionally, the low permeability of the reservoirs and the corresponding limited radius of drainage of the wells result in heterogeneous reservoirs. Unrecovered gas resources may thus remain in the interwell areas, in sectors of the field having relatively widely spaced wells.

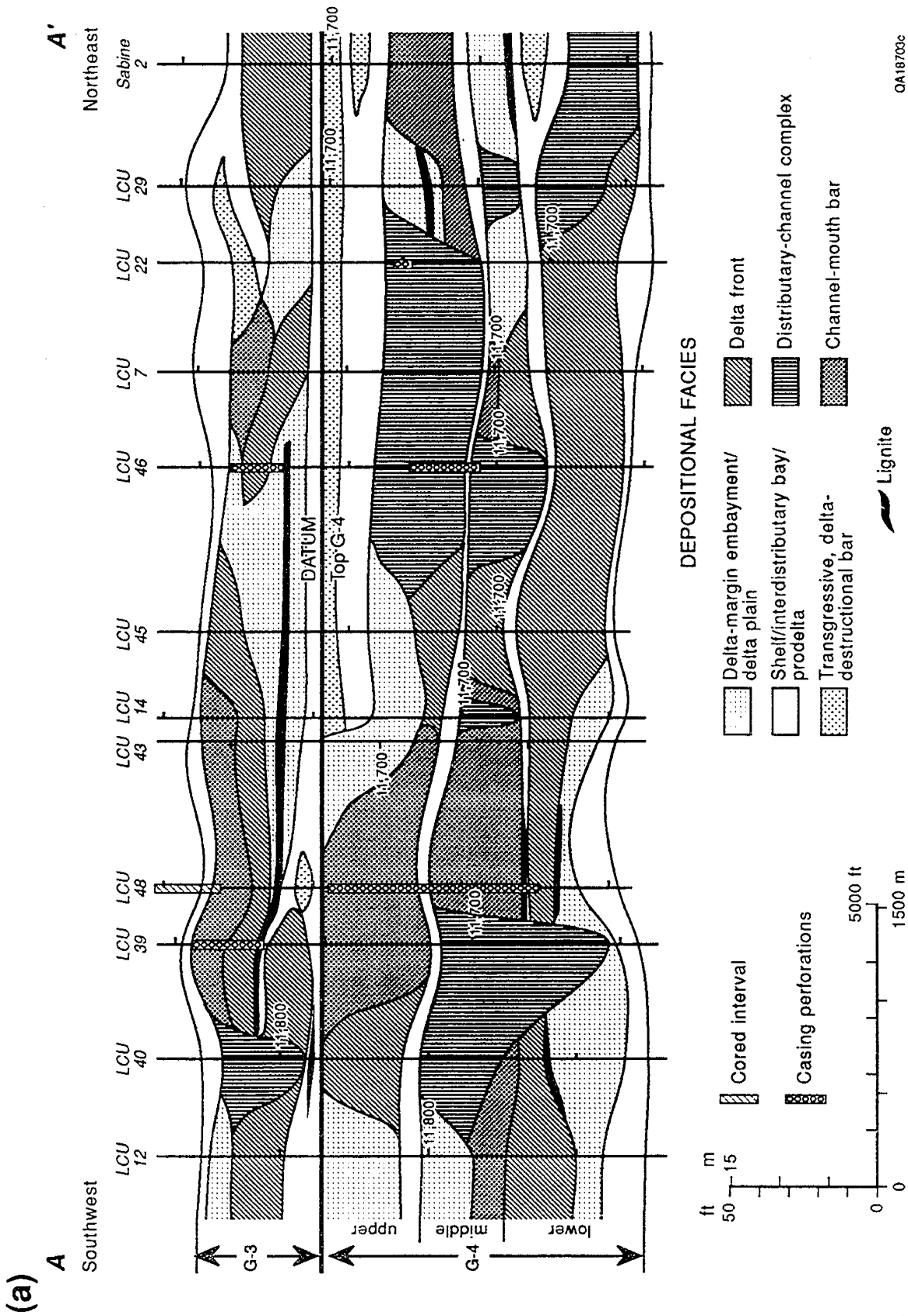


Figure VII-12. Depositional strike-oriented cross section A-A' showing the four parasequences in the G sandstone interval across the Lake Creek unit; (a) shows the G-4 and G-3 parasequences; (b) shows the overlying G-2 and G-1 parasequences.



IMPLICATIONS FOR GAS RESERVE GROWTH  
IN WILCOX DELTAIC RESERVOIRS

Analysis of well logs and cores indicates that gas reserve growth within sandstone reservoirs of the Wilcox Group is a function of both diagenesis and depositional facies variation. Because of the lateral continuity of the delta-front sandstones in Lake Creek field, these reservoirs, in general, contain fewer well-defined compartments than do fluvial sandstones, which are part of the laterally adjacent updip facies tract. Up depositional dip the potential for compartmentalization will increase as discontinuous distributary-channel sandstones become more abundant.

Diagenesis is important in restricting gas flow within both the Wilcox deltaic reservoir examples. In the Wilcox Group the major pore-filling cements are quartz (as overgrowths) and fibrous pore-bridging illite. These cements decrease permeability, and gas flow is confined to limited radii around wells.

Within the deltaic environments of Lake Creek field, the delta-front facies form laterally extensive sandstone reservoirs. However, low permeabilities and corresponding limited radii of drainage may locally result in unrecovered gas reserves at wide completion spacings. Infill and recompletion targets are based on poor drainage radii and diagenetic heterogeneity. In contrast, in the more proximal facies infill drilling and recompletion opportunities result from the complex style of vertical and lateral heterogeneity. Optimized recovery efforts will target facies-based heterogeneity where, for example, barriers or baffles to gas flow along facies boundaries adversely affect hydrocarbon recovery. Typical infill targets are fluvial or distributary-channel sandstones encased in mud-rich delta-plain or bay facies and distributary-channel sandstones lying in erosive contact with delta-front sandstones. Therefore, determination of the facies composition and extent in deltaic gas sandstones is essential for adequate reservoir description aimed at additional gas recovery.

## CONCLUSIONS

Deep Wilcox gas reservoirs of the G sandstone at the LCU comprise low-porosity and low-permeability reservoirs that were deposited in fluvial-dominated deltas during early retrogradational (landward-stepping) deposition of the lower Wilcox Rockdale delta system. Four main deltaic progradations are recognized (operational units G-1 through G-4), two of which (G-2 and G-4) are relatively major progradations. The reservoirs comprise repetitive intervals of deltaic deposits (prodelta, delta-front, and locally delta-plain facies) bounded by mud-rich shelf/bay facies locally associated with sand-rich splays and delta-destructive facies. Sand-rich progradational and transgressive deltaic facies form laterally extensive reservoirs. Reservoir heterogeneity in more proximal reservoirs is related to facies boundaries and to the limited radius of drainage of the wells due to low permeability. Initial flow rates from the LCU-48 (infill well) in the G-4 parasequence indicate production of 1.7 MMcf/d following a fracture completion in June 1991. This production is primarily from the G-4 lower and middle, which are interpreted to represent the channel-mouth-bar complex within the G-4 parasequence. Permeability analyses indicate that these channel-mouth-bar and adjacent distributary-channel sandstones are potential "sweet spots" and may represent the best opportunity for incremental gas reserves in similar stratigraphically controlled parts of the deltaic complex. Studies of Wilcox gas reservoirs at Lake Creek field allow testing of facies-architecture and flow-unit models constructed using data from comparable facies in outcrops of the Ferron Sandstone.

## CHAPTER VIII: CONCLUSION

Noel Tyler

An enormous resource of conventionally recoverable hydrocarbons remains, in addition to proved reserves, in mature and complex Lower 48 States' reservoirs. Nationwide, this resource amounts to 100 billion barrels (Bbbl) of mobile oil (Fisher, 1987) and 180 Tcf gas (Finley and others, 1988) and composes a low-cost, low-risk target for advanced oil and gas recovery. In Texas, restricted platform carbonates and fluvial-deltaic reservoirs collectively contain the vast bulk of the oil resource—a volume that amounts to more than two-thirds of the unrecovered mobile oil in this state.

As has been discussed in this report, internal discontinuities in reservoirs serve to constrain the between-well flow of hydrocarbons including oil, gas, and condensate. Advanced understanding of the architectural attributes of these internal discontinuities is requisite for implementation of advanced recovery strategies. It is at the macro (or between-well) scale that physical and mineralogic bounding surfaces exist between lithofacies and diagenetic facies that serve to *compartmentalize* the reservoir. Compartments adjacent to that penetrated by a well will not be drained by the existing production infrastructure, and additional wells that are geologically targeted must be drilled to capture the *uncontacted* oil remaining in the reservoir. It also follows that if the existing well was converted to injection of water for secondary recovery or injection of chemicals for tertiary recovery, the adjacent compartments would remain isolated from the introduced fluids. These compartments are described as being *areally bypassed* by the flood (fig. VIII-1). Thus, the models developed in attempting to improve recovery of remaining mobile oil are a critical step toward ensuring maximum efficient recovery of the residual oil as well. Yet this step has often received inadequate attention in the design of advanced recovery projects.

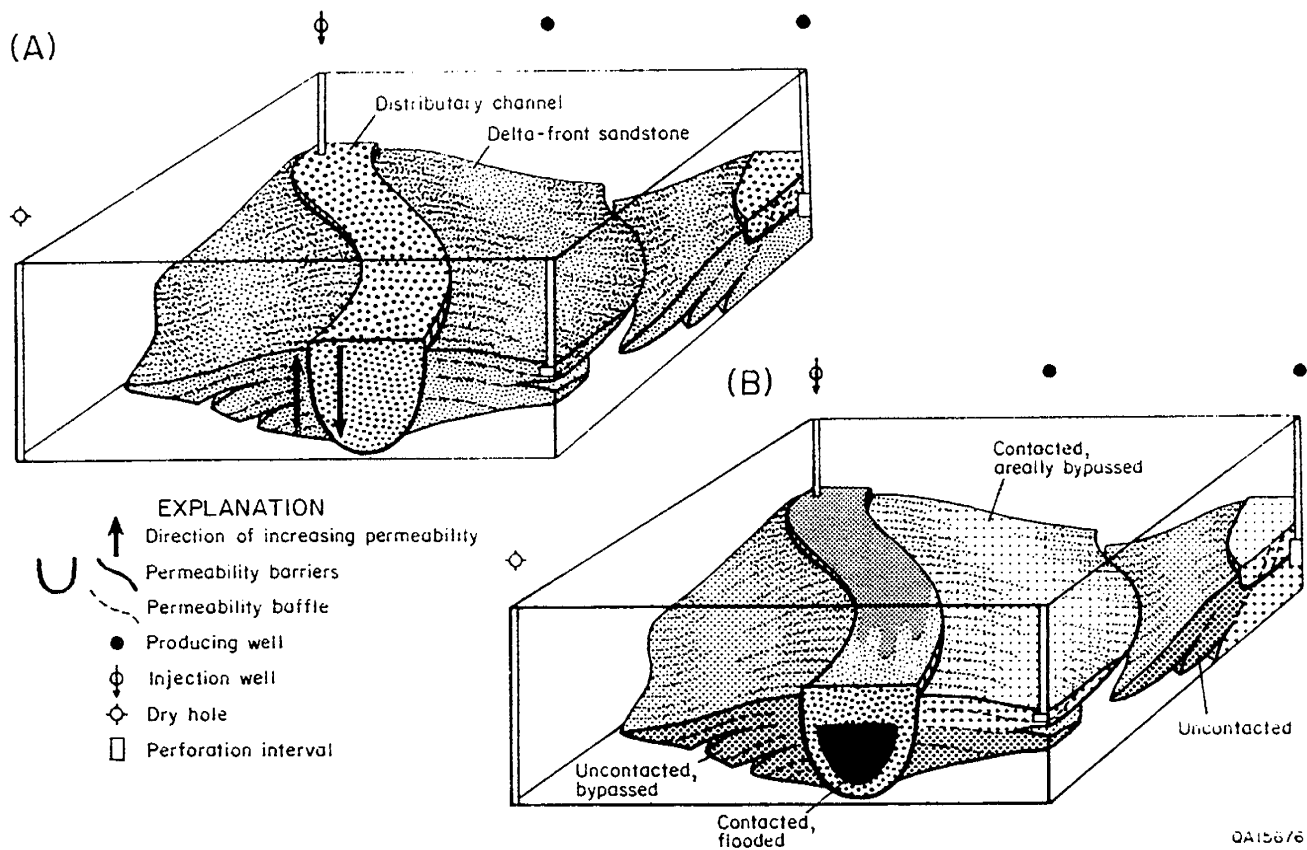


Figure VIII-1. Schematic fluvial-dominated delta (a) drilled on 40-acre spacing. Conventional development practice (b) allows only partial contact and flooding of reservoir compartments. After Tyler and Finley (1991).

In addition to the uncontacted oil compartments in reservoirs, a second component of unrecovered mobile oil is particularly important in thicker and highly stratified reservoir intervals that display vertical permeability variations as well as lateral variability. Highly aggradational sandstone systems and thick carbonate reservoirs, such as those of the Permian Basin in West Texas, typically display these characteristics. Water injected into these reservoirs during secondary recovery preferentially focuses into the higher permeability units and does not contact or mobilize the oil in lower permeability intervals. This *vertically bypassed* oil becomes the target for improved secondary recovery through modification of injection profiles, temporary and nondestructive sealing of the more permeable stringers, and to some extent, geologically targeted infill drilling. Delineation of bypassed oil resources, as in the case of uncontacted compartments, requires detailed geological characterization of the internal structure, or architecture, of the reservoir to map and quantify paths of fluid movement.

RESERVOIR ARCHITECTURAL CONTROLS ON  
UNRECOVERED MOVABLE OIL—THE  
APPLICATION OF PREDICTIVE GEOLOGY

As discussed in this report, reservoir architecture exerts a fundamental control on hydrocarbon recovery efficiency. Wave-dominated deltaic and shore-zone systems are characterized by high mobile oil recovery efficiencies; mixed-load channelized systems are characterized by much lower recovery efficiencies. This predictable trend largely reflects the style of heterogeneity in the reservoir. Much attention has been focused on heterogeneity at the scale of micrometers to a few meters. Saturation characteristics, capillarity, and local flow pathways around well perforations are controlled at this scale of pore structure and sedimentary structure. However, heterogeneity style at the scale of one to a thousand meters is more important in controlling fluid flow pathways and access to the unrecovered mobile oil and residual oil remaining in the reservoir.

Because heterogeneity style, the geometric component of reservoir compartmentalization, is a product of depositional process, it is predictable. Conventional production response, then, may also be predictable, because characteristic locations of both uncontacted and bypassed oil can be defined on the basis of depositional system. Depositional systems, and the processes by which the large-scale reservoir architectural elements are laid, therefore become a fundamental basis for the extrapolation of research results from key reservoirs to larger groups of similar reservoirs for which less data exists. For example, aggradational reservoirs are typically bottom-flooding or they have multiple flood fingers and poor vertical conformance. Laterally, the flood is strongly confined to paleochannels, and hydrocarbons in adjacent facies are bypassed (fig. VIII-1). Progradational reservoirs are top-flooding and recovery efficient; however, boundaries between accretion wedges can provide flow baffles. Lateral accretion in fluvial and tidal sandstones also can produce such flow baffles (Tyler and others, 1991).

The preceding discussion has emphasized that reservoirs display varying degrees of lateral and vertical heterogeneity. Because internal heterogeneities in a reservoir are the product of the processes responsible for the formation of that reservoir, by developing an understanding of those processes the styles and scales of heterogeneity that typify the reservoir type become predictable. Furthermore, with this understanding it becomes possible to classify reservoir types into a heterogeneity matrix according to the intensity of vertical and lateral complexity.

The heterogeneity matrix for major sandstone reservoir types is shown in table VIII-1. Systems displaying minimal internal heterogeneity are those associated with strong nearshore marine processes, such as the axis of barrier islands, sand-rich strandplains, and wave-dominated deltas. At the other end of the spectrum are systems characterized by intense internal heterogeneity. These deposits are typically characterized by well-developed channel networks, such as in submarine fan cones, stacked fluvially dominated deltas, and some back-barrier island sediments. The other end members in the matrix are systems with pronounced complexity in one dimension and minimal variability in the other, such as basin-flooring turbidites (good

Table VIII-1. Heterogeneity matrix wherein depositional systems are classified according to vertical and lateral heterogeneity.

		LATERAL HETEROGENEITY		
		LOW	MODERATE	HIGH
VERTICAL HETEROGENEITY	LOW	Wave-dominated delta Barrier core Barrier shore face Sand-rich strand plain	Delta-front mouth bar Proximal delta front (accretionary) Tidal deposits Mud-rich strand plain	Meander belt* Fluvially dominated delta* Back barrier*
	MODERATE	Eolian  Wave-modified delta (distal)	Shelf bars Alluvial fan Fan delta Lacustrine delta Distal delta front Wave-modified delta (proximal)	Braided stream  Tide-dominated delta
	HIGH	Basin-flooring turbidites	Coarse-grained meander belt Braid delta	Back barrier* Fluvially dominated delta* Fine-grained meander belt* Submarine fans*

- \* single units
- stacked systems

lateral continuity but a high degree of stratification) and meanderbelts (highly variable laterally but with minimal internal vertical heterogeneity).

The utility of the heterogeneity matrix is that it allows prediction of primary and secondary recovery efficiencies and of the location of the movable oil remaining in the reservoir after conventional recovery (table VIII-2). Furthermore, we can now design the appropriate advanced secondary recovery strategy based on the nature of geological heterogeneity of the reservoir. In systems with a low degree of internal heterogeneity most of the movable oil is recovered. Because of their internal homogeneity these reservoirs compose ideal candidates for enhanced oil recovery (EOR). Systems with a high lateral heterogeneity component are characterized by low to moderate recoveries; the remaining movable oil is contained in uncontacted or poorly drained compartments that typically are areally bypassed by injectants. Targeted infill drilling by vertical or horizontal wells, together with strategic placement of injection wells, is the optimum recovery strategy in these reservoirs. Vertically complex reservoirs also display low to moderate recoveries. In these reservoirs, advanced recovery applications must focus on strategic recompletion of bypassed zones and waterflood optimization, including modification of injection profiles to seal off high permeability stringers. Finally, in those systems of great vertical and lateral complexity, conventional recovery is very low, and the entire spectrum of advanced recovery options must be considered and strategically applied on the basis of the results of detailed geoscience characterization of the candidate reservoirs.

#### ADVANCED SECONDARY RECOVERY—A NEW APPROACH TO ADVANCED RECOVERY

Most of the mature fields of Texas have passed through the stage of primary production (where oil is recovered via the indigenous energy of the reservoir) and are in secondary recovery (where energy of the reservoir, that is, pressure, is being maintained through

Table VIII-2. Projected recovery efficiency, residency of unrecovered mobile oil, and appropriate recovery strategies, as a function of reservoir heterogeneity, to target remaining mobile-oil saturations.

		LATERAL HETEROGENEITY	
		LOW	HIGH
VERTICAL HETEROGENEITY	LOW	<ol style="list-style-type: none"> <li>1. Very high to total</li> <li>3. Excellent EOR candidates</li> </ol>	<ol style="list-style-type: none"> <li>1. Low mobile-oil recovery efficiency</li> <li>2. Compartmentalized, uncontacted, and laterally bypassed</li> <li>3. Targeted infill drilling</li> </ol>
	HIGH	<ol style="list-style-type: none"> <li>1. Low</li> <li>2. Vertically bypassed mobile oil</li> <li>3. Profile modification, waterflood redesign, recompletions</li> </ol>	<ol style="list-style-type: none"> <li>1. Very low mobile-oil recovery efficiency</li> <li>2. Both uncontacted and bypassed</li> <li>3. Targeted infill drilling, waterflood redesign, profile modification, and recompletions</li> </ol>

1. Mobile-oil recovery efficiency
2. Residency of mobile oil
3. Appropriate recovery strategy

injection of gas or water). Historically, as reservoirs approached the latter stages of secondary recovery, they became candidates for tertiary or enhanced recovery to extract residual oil. It was the commonly held view that primary and secondary production effectively recovered the majority of the conventionally recoverable oil. Texas' experience illustrates that this is not the case and that substantial volumes of movable oil (on average between 40 and 50 percent and up to three quarters of the original movable oil in place) may remain in these mature reservoirs following conventional primary and secondary recovery. The aggregate volume of unrecovered movable oil across the state is 35 Bbbl (Fisher and Galloway, 1983; Fisher and Finley, 1986a, b), or more than half of this state's historic production. On a national basis, almost 100 Bbbl of unrecovered movable oil awaits advanced recovery applications (Fisher, 1987).

In addition to the sheer magnitude of this resource, several other factors serve to make unrecovered movable oil a key near-term research, development, and recovery objective. First, we know in a general sense where the oil is. It resides within the confines of existing fields. Second, the oil is mobile and does not require the costly injection of physical or chemical additives to implement mobilization and recovery. Third, because the oil is located within existing field boundaries, the field infrastructure, such as holding tanks for storage and pipelines for transportation, is already established. The cumulative effect is that movable oil remaining in inefficiently drained reservoirs nationwide composes a resource that is immediately available for infield reexploration and development at low to moderate cost.

The nation's unrecovered movable oil resource lies in established, mature reservoirs that are typically in declining conventional secondary recovery. Translation of this resource to reserves will require application of advanced recovery strategies guided by a thorough understanding of reservoir complexity. It is proposed that these strategies be collectively categorized as advanced secondary recovery (ASR).

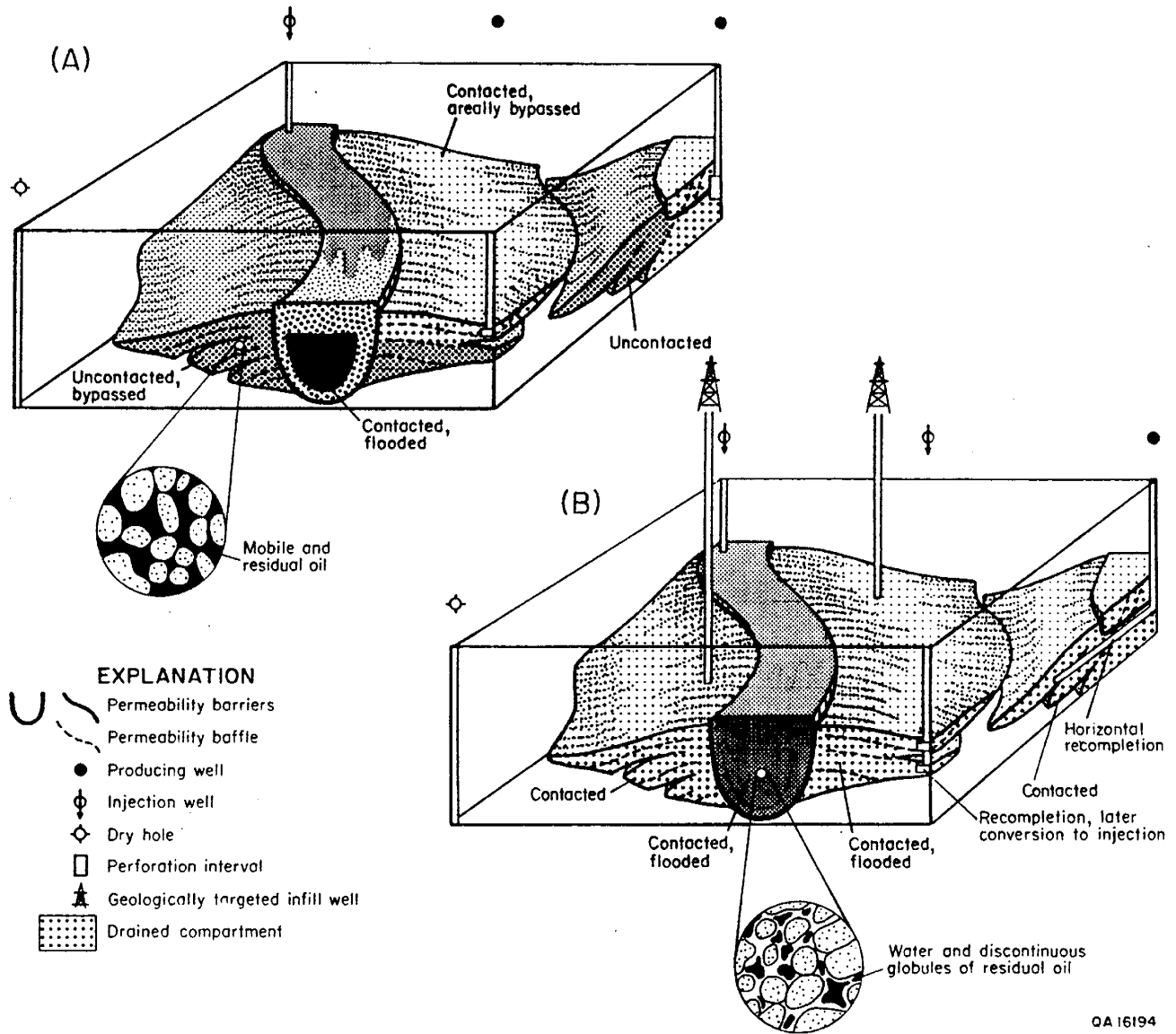
ASR as currently defined includes four techniques that would be optimized according to the style of reservoir complexity. The techniques are (1) geologically targeted infill drilling, (2) horizontal drilling, (3) selective recompletions of previously unrecognized and bypassed

pools or zones, and (4) strategic cross-reservoir flooding with water, commonly assisted by polymer injection.

*Geologically Targeted Infill Drilling.* Conventional oil field practice allows for infill drilling (subject to regulatory approval) in existing fields as long as it follows set geometric patterns. Infill wells are placed between existing wells and are separated from the existing wells by set distances defined by regulatory agencies. This procedure results in a regular grid of wells that may not capture internal variability and thus may miss significant portions of oil remaining in the reservoir.

In contrast, geologically targeted infill wells are drilled on the basis of a thorough understanding of the internal character of the reservoir. This strategy is based on information derived from existing wells, supplemented by production engineering data and advanced geophysical information, to target poorly drained or uncontacted areas of the reservoir. New wells are unevenly distributed across the field but are clustered in areas of greatest potential (fig. VIII-2). In this way, the number of subeconomic or uneconomic wells is reduced to a minimum, which is critical to the economic success of the project and therefore to ultimate recovery. Geologically targeted infill drilling typically occurs at well spacings of 20 acres or less.

*Horizontal Drilling.* Horizontal wells offer the potential for increased recovery in reservoirs where lateral or areal variability is great. The higher the degree of lateral variability in a reservoir, the smaller the area that will be contacted and drained by a given well drilled vertically. Horizontal wells allow penetration of the flow barriers that separate the compartments in a reservoir (fig. VIII-2). They also allow contact with vertical fractures that may be conduits for flow in low-permeability reservoirs—a strategy that has been extremely effective in the Austin Chalk in South Texas and the Bakken Formation of North Dakota. Targeting of horizontal wells to obtain maximum yield requires detailed characterization of the reservoir. Although horizontally drilled wells have applicability in EOR efforts, they are largely drilled to capture difficult-to-recover, remaining movable oil and are thus classed as an advanced secondary recovery technique. The production response of horizontal wells is expected to be



QA 16194

Figure VIII-2. Advanced secondary recovery strategies applied to (a) a hypothetical (compare with fig. VIII-1) fluvial-dominated delta to (b) tap uncontacted compartments and to optimize injection profiles to waterflood zones bypassed by the flood. Appropriate advanced secondary recovery strategies include infill drilling of vertical or horizontal wells targeted to penetrate uncontacted compartments and waterflood optimization to effectively flood bypassed zones. After Tyler and Finley (1991).

substantial because nearly 25 Bbbl of unrecovered movable oil exists in reservoirs specifically amenable to horizontal drilling.

*Selective Recompletions.* Many reservoirs display a high degree of vertical complexity, especially vertical variability in permeability. Thus, oil may flow much more easily through some layers than through others, resulting in bypassed zones. Detailed geological and geophysical characterization of these reservoirs to delineate bypassed zones can guide recompletions of wells to target layers containing large volumes of bypassed movable oil.

*Strategic Cross-Reservoir Flooding.* Many reservoirs with weak drive mechanisms require the injection of water to move hydrocarbons to the well. In reservoirs with a high degree of vertical variability, ensuring that injected water contacts oil in zones less capable of producing hydrocarbons becomes a major problem, particularly during the later stages of a water injection program. Injected water tends to follow the easiest path of flow; thus, over time, the effectiveness of this procedure decreases. ASR strategies, based on detailed geological and engineering analysis, seek to maximize recovery by optimizing waterflood design through relocating injection in intervals that have been bypassed (fig. VIII-2), perhaps coupled with introducing chemicals (polymers) that help seal off the high-flow zones.

#### CONCLUSION—TRANSLATION FROM RESOURCE TO RESERVES

The recent analysis of Bookout and others (1990) indicates that approximately 50 Bbbl, a volume equivalent to half of the nation's unrecovered movable oil resource, should be the goal for incremental recovery from existing reservoirs during the next 50 yr. Annual reserve additions from this level of activity would be a billion barrels per year, a substantial amount but less than half of the annual United States reserve growth achieved from 1977 to 1988. A similar conclusion was reached by an American Association of Petroleum Geologists (1989) analysis, which suggested that at prices of less than \$25 per barrel applying advanced technology and efficiency could recover an incremental 45 Bbbl of unrecovered movable oil over the middle to

long term. At higher prices, in the \$25 to \$50 range, recovery of 65 Bbbl of remaining movable oil is within reach.

Advanced secondary recovery offers increasing potential as the nation's reservoirs approach the latter stages of secondary production. As emphasized in this report, the successful application of ASR depends on integration of geoscience, engineering disciplines, and data. In short, ASR requires maximum information retrieval and examination, followed by integration into the reservoir model. Furthermore, accepted theories and beliefs regarding the origin and drainage mechanisms of the reservoirs or plays in question should be closely scrutinized and challenged because of geoscience's constantly evolving understanding of reservoir genesis and behavior.

#### ACKNOWLEDGMENTS

Research undertaken for this report was funded by the U.S. Department of Energy (contact number DE-FG22-89BC-14403).

Research undertaken in subtask 6 (the Ferron outcrop study, chapter VI) was cofunded by the Gas Research Institute (contract number 5089-260-1902). Ted Angle is thanked for his able assistance in the field on this part of the project.

Research undertaken in subtask 7 (the Lake Creek study, chapter VII) was cosponsored by the Gas Research Institute (contract number 5088-212-1718), the U.S. Department of Energy (contract number DE-FG21-88MC25031), and the State of Texas through the Bureau of Economic Geology as part of an ongoing research program entitled "Secondary Natural Gas Recovery: Targeted Technology Applications for Infield Reserve Growth." We are grateful for cooperation from Mobil Exploration and Producing U.S. Inc., and from Mobil Research and Development Corporation for the opportunity to share existing data and acquire new core and well log data.

We would also like to thank the following individuals, who helped us secure permission to borrow cores and also provided us with core analyses and well-history information: Larry Lofton of ARCO in Midland, Texas; Charles Ways of Conoco in Midland, Texas; and James Landrum of OXY in Tulsa, Oklahoma.

## REFERENCES

- American Association of Petroleum Geologists, 1989, Data support need for exploration: American Association of Petroleum Geologists Explorer, v. 10, no. 4, p. 42.
- Archie, G. E., 1952, Classification of carbonate reservoir rocks and petrophysical considerations: American Association of Petroleum Geologists Bulletin, v. 36, no. 2, p. 278–298.
- Ball, M. M., 1967, Carbonate sand bodies of Florida and the Bahamas, Journal of Sedimentary Petrology, v. 37, p. 556–591.
- Bathurst, R. G. C., 1975, Developments in sedimentology 12: carbonate sediments and their diagenesis: Amsterdam, Elsevier, 658 p.
- Bebout, D. G., and Loucks, R. G., 1984, Handbook for logging carbonate rocks: The University of Texas at Austin, Bureau of Economic Geology Handbook 5, 43 p.
- Bebout, D. G., Lucia, F. J., Hocott, C. R., Fogg, G. E., and Vander Stoep, G. W., 1987, Characterization of the Grayburg reservoir, University Lands Dune field, Crane County, Texas: The University of Texas at Austin, Bureau of Economic Geology Report of Investigations No. 168, 98 p.
- Bebout, D. G., Weise, B. R., Gregory, A. R., and Edwards, M. B., 1982, Wilcox sandstone reservoirs in the deep subsurface along the Texas Gulf Coast, their potential for production of geopressured geothermal energy: The University of Texas at Austin, Bureau of Economic Geology Report of Investigations No. 117, 125 p.
- Beggs, H. Dale, 1984, Gas production operations: Tulsa, Oklahoma, OGCI Publications, Oil & Gas Consultants International Inc., p 22–30.

- Bein, Amos, and Land, L. S., 1982, San Andres carbonates in the Texas Panhandle: The University of Texas at Austin, Bureau of Economic Geology Report of Investigations No. 121, 48 p.
- Bookout, J. F., Fisher, W. L., Moncrief, C. B., 1990, Oil and gas recovery research—a recommended program: Austin, Texas, Governor's Energy Council, Committee on Research and Development, 6 p.
- Boyd, D. W., 1958, Permian sedimentary facies, central Guadalupe Mountains, New Mexico: New Mexico Bureau of Mines and Mineral Resources Bulletin 49, 100 p.
- Brill, J. P., and Beggs, H. D., 1974, Two-phase flow in pipes: University of Tulsa, INTERCOMP Course, The Hague.
- Brown, C. G., Katz, D. L., Oberfell, G. B., and Alden, R. C., 1948, Natural gasoline and volatile hydrocarbons: Tulsa, Oklahoma, NGAA.
- Budd, D. A., and Vacher, H. L., 1991, Predicting the thickness of fresh-water lenses in carbonate paleo-islands: *Journal of Sedimentary Petrology*, v. 61, no. 1, p. 43–53.
- Chandler, M. A., Kocurek, G. A., Goggin, D. J., and Lake, L. W., 1989, Effects of stratigraphic heterogeneity on permeability in eolian sandstone sequence, Page Sandstone, northern Arizona: *American Association of Petroleum Geologists Bulletin*, v. 73, no. 5, p. 658–668.
- Dickey, R. I., 1940, Geologic section from Fisher County through Andrews County, Texas to Eddy County, New Mexico: *American Association of Petroleum Geologists Bulletin*, v. 24, p. 37–51.
- Dreyer, T. A., Scheie, A., and Walderhaug, O., 1990, Minipermeameter-based study of permeability trends in channel sand bodies: *American Association of Petroleum Geologists Bulletin*, v. 74, no. 4, p. 359–374.

- Dunham, R. J., 1962, Classification of carbonate rocks according to depositional texture, *in* Ham, W. E., ed., Classification of carbonate rocks—a symposium: American Association of Petroleum Geologists Memoir 1, p. 108–121.
- Dunnington, H. V., 1954, Stylolite development post-dates rock induration: *Journal of Sedimentary Petrology*, v. 24, p. 27–49.
- Ewing, T. E., 1991, The tectonic framework of Texas: text to accompany *The Tectonic Map of Texas*, The University of Texas at Austin, Bureau of Economic Geology, 36 p.
- Fekete, T. E., Franseen, E. K., and Pray, L. C., 1986, Deposition and erosion of the Grayburg Formation (Guadalupian, Permian) at the shelf-to-basin margin, western escarpment, Guadalupe Mountains, Texas, *in* Moore, G. E., and Wilde, G. L., eds., Lower and middle Guadalupian facies, stratigraphy and reservoir geometries, San Andres-Grayburg Formations, Guadalupe Mountains, New Mexico and Texas: Society of Economic Paleontologists and Mineralogists, Permian Basin Section, Publication No. 86-25, p. 69–81.
- Finley, R. J., 1984, Geology and engineering characteristics of selected low-permeability gas sandstones: a national survey: The University of Texas at Austin, Bureau of Economic Geology Report of Investigations No. 138, 220 p.
- Finley, R. J., Fisher, W. L., Seni, S. J., Ruppel, S. C., White, W. G., Ayers, W. B., Jr., Dutton, S. P., Jackson, M. L. W., Banta, Nancy, Kuuskraa, V. A., McFall, K. S., Godec, Michael, and Jennings, T. V., 1988, An assessment of the natural gas resource base of the United States: The University of Texas at Austin, Bureau of Economic Geology Report of Investigations No. 179, 69 p.
- Fisher, W. L., 1987, Can the U.S. oil and gas resource base support sustained production?: *Science*, v. 236, p. 1631–1636.

- Fisher, W. L., and Finley, R. J., 1986, Future trends in Texas oil and gas: presentation to Texas House Committee on Energy, January 23, 1968, 23 p. Reprinted in part as Texas still has big hydrocarbon resource base: *Oil and Gas Journal*, v. 84, no. 22, p. 57–69.
- Fisher, W. L., and Finley, R. J., 1986, Recent production trends and outlook for future oil and gas supplies in Texas: The University of Texas, Bureau of Economic Geology Geological Circular 86-4, 31 p.
- Fisher, W. L., and Galloway, W. E., 1983, Potential for additional oil recovery in Texas: The University of Texas at Austin, Bureau of Economic Geology Geological Circular 83-2, 20 p.
- Fisher, W. L., and McGowen, J. H., 1967, Depositional systems in the Wilcox Group of Texas and their relationship to occurrence of oil and gas: *Gulf Coast Association of Geological Societies Transactions*, v. 17, p. 105–125.
- Franseen, E. K., Fekete, T. E., and Pray, L. C., 1989, Evolution and destruction of a carbonate bank at the shelf margin: Grayburg Formation (Permian), western escarpment, Guadalupe Mountains, Texas, *in* Crevello, P. D., Wilson, J. L., Sarg, J. F., and Read, J. F., eds., Controls on carbonate platform and basin development: Society of Economic Paleontologists and Mineralogists, Special Publication No. 44, p. 289–304.
- Friedman, G. M., Ghosh, S. K., and Urschel, Stephen, 1990, Petrophysical characteristics related to depositional environments and diagenetic overprint: a case study of the San Andres Formation, Mabee field, West Texas, *in* Bebout, D. G., and Harris, P. M., eds. Geologic and engineering approaches in evaluation of San Andres/Grayburg hydrocarbon reservoirs—Permian Basin: The University of Texas at Austin, Bureau of Economic Geology, p. 125–144.

- Galloway, W. E., and Cheng, E. S., 1985, Reservoir facies architecture in a microtidal barrier system—Frio Formation, Texas Gulf Coast: The University of Texas at Austin, Bureau of Economic Geology Report of Investigation No. 144, 36 p.
- Galloway, W. E., Ewing, T. E., Garrett, C. M., Tyler, Noel, and Bebout, D. G., 1983, Atlas of major Texas oil reservoirs: The University of Texas at Austin, Bureau of Economic Geology Special Publication, 139 p.
- Gardner, M. H., 1991, Siliciclastic facies architecture in a foreland basin clastic wedge—field guide to the Ferron Sandstone Member of the Mancos Shale, east-central Utah: Colorado School of Mines, unpublished report, 35 p.
- Gealy, R. D., Jr., 1966, North Foster unit—evaluation and control of a Grayburg–San Andres waterflood based on primary oil production and waterflood response: Society of Petroleum Engineers, SPE Paper 1474, 8 p.
- Goggin, D. J., 1988, Geologically sensible modeling of the spatial distribution of permeability in eolian deposits Page Sandstone (Jurassic), northern Arizona: The University of Texas at Austin, Ph.D. dissertation, 418 p.
- Goggin, D. J., Chandler, M. A., Kocurek, G. A., and Lake, L. W., 1986, Patterns of permeability in eolian deposits: Society of Petroleum Engineers/U.S. Department of Energy Paper 14893, p. 181–188.
- Haldorsen, H. H., and Damsleth, E., 1990, Stochastic modeling: *Journal of Petroleum Technology*, v. 42, p. 404–412.
- Halley, R. B., and Harris, P. M., 1979, Fresh-water cementation of a 1,000-year-old oolite: *Journal of Sedimentary Petrology*, v. 49, no. 3, p. 969–988.

Harris, P. M., 1979, Facies anatomy and diagenesis of a Bahamian ooid shoal, *in* Ginsburg, R. N., ed., *Sedimenta VII: Miami, Florida, The Comparative Sedimentology Laboratory, Division of Marine Geology and Geophysics, University of Miami, and the Rosentiel School of Marine and Atmospheric Science*, 164 p.

Harris, P. M., Dodman, C. A., and Bliefnick, D. M., 1984, Permian (Guadalupian) reservoir facies, McElroy field, West Texas, *in* Harris, P. M., ed., *Carbonate sands—a core workshop: Society of Economic Paleontologists and Mineralogists Core Workshop No. 5*, p. 136–174.

Hayes, P. T., 1959, San Andres limestone and related Permian rocks in Last Chance Canyon and vicinity, southeastern New Mexico: *American Association of Petroleum Geologists Bulletin*, v. 43, p. 2197–2213.

\_\_\_\_\_ 1964, *Geology of the Guadalupe Mountains, New Mexico: United States Geological Survey Professional Paper 446*, 69 p.

Hayes, P. T., and Adams, J. E., 1962, Permian of the central Guadalupe Mountains, Eddy County, New Mexico: 1962 Field Trip Committee, Hobbs, Roswell, and West Texas Geological Societies, Publication 62-48, 115 p.

Hinrichs, P. D., Lucia, F. J., Mathis, R. L., 1986, Permeability distribution and reservoir continuity in Permian San Andres shelf carbonates, Guadalupe Mountains, New Mexico, *in* Bebout, D. G., and Harris, P. M., eds., *Hydrocarbon reservoir studies, San Andres/Grayburg Formations, Permian Basin: Permian Basin Section, Society of Economic Paleontologists and Mineralogists, Special Publication No. 86-26*, p. 31–36.

Humphrey, J. D., Ransom, K. L., and Matthews, R. K., 1986, Early meteoric diagenetic control of Upper Smackover production, Oaks field, Louisiana: *American Association of Petroleum Geologists Bulletin*, v. 70, no. 1, p. 70–85

- Jones, J. R., Scott, A., and Lake, L. W., 1987, The geological aspects of reservoir characterization for numerical simulation, Mesaverde meanderbelt sandstone, northwestern Colorado: Society of Petroleum Engineers, Formation Evaluation, March, p. 97–107.
- Kerans, Charles, 1988, Karst-controlled reservoir heterogeneity in Ellenburger Group carbonates of West Texas: American Association of Petroleum Geologists Bulletin, v. 72, p. 1160–1183.
- Kerans, Charles, Lucia, F. J., Senger, R. K., Fogg, G. E., Nance, S. H., Kasap, Ekrem, and Hovorka, S. D., 1991, Characterization of reservoir heterogeneity in carbonate-ramp systems, San Andres/Grayburg, Permian Basin: final report, Reservoir Characterization Research Laboratory, The University of Texas at Austin, Bureau of Economic Geology, 245 p.
- Kerans, Charles, and Nance, H. S., 1991, High frequency cyclicity and regional depositional patterns of the Grayburg Formation, Guadalupe Mountains, New Mexico, *in* Meader-Roberts, Sally, and others, eds., Sequence stratigraphy, facies, and reservoir geometries of the San Andres, Grayburg, and Queen Formations, Guadalupe Mountains, New Mexico and Texas: Society of Economic Paleontologists and Mineralogists, Permian Basin Section, Publication 91-32, p. 53–69.
- King, P. B., 1948, Geology of the southern Guadalupe Mountains, Texas: United States Geological Survey Professional Paper 215, 183 p.
- Kittridge, M. G., 1988, Analysis of areal permeability variations—San Andres Formation (Guadalupian): Algerita Escarpment, Otero County, New Mexico: The University of Texas at Austin, Master's thesis, 361 p.
- Kosters, E. C., Bebout, D. G., Seni, S. J., Garrett, C. M., Jr., Brown, L. F., Jr., Hamlin, H. S., Dutton, S. P., Ruppel, S. C., Finley, R. J., Tyler, Noel, 1989, Atlas of major Texas gas reservoirs: The University of Texas at Austin, Bureau of Economic Geology, 161 p.

- Lang, W. B., 1937, The Permian formations of the Pecos Valley of New Mexico and Texas: American Association of Petroleum Geologists Bulletin, v. 21, p. 833–898.
- Leary, D. A., and Vogt, J. N., 1986, Diagenesis of the Permian (Guadalupian) San Andres Formation, Central Basin Platform, West Texas, *in* Bebout, D. G., and Harris, P. M., eds., Hydrocarbon reservoir studies—San Andres/Grayburg Formations, Permian Basin: Permian Basin Section, Society of Economic Paleontologists and Mineralogists, Publication No. 86-26, p. 67–68.
- Lewis, J. J. M., 1988, Outcrop-derived quantitative models of permeability heterogeneity for genetically different sand bodies: Society of Petroleum Engineers, SPE Paper 18153, p. 449–463.
- Lindsay, R. F., 1991, Grayburg Formation (Permian–Guadalupian): comparison of reservoir characteristics and sequence stratigraphy in the northwest Central Basin Platform with outcrops in the Guadalupe Mountains, New Mexico, *in* Meader-Roberts, Sally, and others, eds., Sequence stratigraphy, facies, and reservoir geometries of the San Andres, Grayburg, and Queen Formations, Guadalupe Mountains, New Mexico and Texas: Society of Economic Paleontologists and Mineralogists, Permian Basin Section, Publication 91-32, p. 111–118.
- Longacre, S. A., 1980, Dolomite reservoirs from Permian biomicrites, *in* Halley, R. B., and Loucks, R. G., eds., Carbonate reservoir rocks: Society of Economic Paleontologists and Mineralogists Core Workshop No. 1, p. 105–117.
- Loucks, R. G., and Longman, M. W., 1985, Cities Service No. 1 J. B. Kitchens core, Lower Cretaceous Ferry Lake Anhydrite, Fairway Field, East Texas, *in* Bebout, D. G., and Ratcliff, Doug, eds., Lower Cretaceous depositional environments from shoreline to slope—a core workshop: Annual meeting of the Gulf Coast Association of Geological Societies and Gulf

- Coast Section, Society of Economic Paleontologists and Mineralogists, Austin, Texas, October 16, p. 119–128.
- Lucia, F. J., Senger, R. K., Fogg, G. E., Kerans, Charles, and Kasap, Ekrem, 1991, Scale of heterogeneity and fluid flow response in carbonate ramp reservoirs: San Andres outcrop, Algerita Escarpment, New Mexico: Society of Petroleum Engineers Annual Technical Conference and Exhibition, Dallas, Paper 22744, p. 839–840.
- Major, R. P., and Holtz, M. H., 1989, Effects of geologic heterogeneity on waterflood efficiency at Jordan field, University Lands, Ector and Crane Counties, Texas: Transactions of the 1989 Annual Technical Conference and Exhibition of the Society of Petroleum Engineers, Formation Evaluation and Reservoir Geology, p. 633–640.
- Major, R. P., Vander Stoep, G. W., Holtz, M. H., 1990, Delineation of unrecovered mobile oil in a mature dolomite reservoir: East Penwell San Andres Unit, University Lands, West Texas: The University of Texas at Austin, Bureau of Economic Geology Report of Investigations No. 194, 52 p.
- Mitchum, R. M., Vail, P. R., and Thompson, S., III, 1977, Seismic stratigraphy and global changes of sea level, part 2: the depositional sequence as a basic unit for stratigraphic analysis, *in* Payton, C. E., ed., Seismic stratigraphy—applications to hydrocarbon exploration: American Association of Petroleum Geologists, Memoir 26, p. 53–62.
- Moore, C. H., 1989, Developments in sedimentology 46: carbonate diagenesis and porosity: Amsterdam, Elsevier, 338 p.
- Moore, C. H., Chowdhury, A., and Chan, L., 1988, Upper Jurassic Smackover platform dolomitization, northwestern Gulf of Mexico: a tale of two waters, *in* Shukla, V., and Baker, P. A., eds., Sedimentology and geochemistry of dolostones: Society of Economic Paleontologists and Mineralogists, Special Publication No. 43, p. 175–189.

Moran, W. R., 1954, Proposed type sections for the Queen and Grayburg Formations of Guadalupe age in the Guadalupe Mountains, Eddy County, New Mexico (abs.): Geological Society of America Bulletin, v. 65, p. 1288, and Guidebook of Southeastern New Mexico, New Mexico Geological Society, p. 147-150.

\_\_\_\_\_ 1962, Surface type localities of the Queen and Grayburg Formations in the Guadalupe Mountains: West Texas, Roswell, and Hobbs Geological Societies, p. 76-86.

Naiman, E. R., 1982, Sedimentation and diagenesis of a shallow marine carbonate and siliciclastic shelf sequence: the Permian (Guadalupian) Grayburg Formation, southeastern New Mexico: The University of Texas at Austin, Master's thesis, 197 p.

Nance, H. S., 1988, Interfingering of evaporites and red beds: an example from the Queen/Grayburg Formation, Texas: Sedimentary Geology, v. 56, p. 357-381.

Newell, N. D., Rigby, J. K., Fischer, A. G., Whiteman, A. J., Hickox, J. E., and Bradley, J. S., 1953, The Permian Reef Complex of the Guadalupe Mountains region, Texas and New Mexico: W. H. Freeman and Co., San Francisco, 236 p.

Pingitore, N. E., Jr., 1976, Vadose and phreatic diagenesis: processes, products and their recognition in corals: Journal of Sedimentary Petrology, v. 46, no. 4, p. 985-1006.

\_\_\_\_\_ 1982, The role of diffusion during carbonate diagenesis: Journal of Sedimentary Petrology, v. 52, no. 1, p. 27-39.

Prentice, R. S., 1984, Waterflooding the Grayburg Formation on the J. L. Johnson AB lease—experience in the Johnson field: Journal of Petroleum Engineering, v. 36, no. 11, p. 1773-1780.

- Ravenne, C., Eschard, R., Galli, A., Mathieu, Y., Monadert, L., and Rudkiewicz, J. L., 1989, Heterogeneities and geometry of sedimentary bodies in a fluvio-deltaic reservoir: Society of Petroleum Engineers, Journal of Formation Evaluation, June, p. 239–246.
- Ross, C. A., and Ross, J. R. P., 1986, Paleozoic paleotectonics and sedimentation in Arizona and New Mexico, *in* Peterson, J. A., ed., Paleotectonics and sedimentation in the Rocky Mountain region, United States: American Association of Petroleum Geologists, Memoir 41, p. 653–668.
- \_\_\_\_\_ 1987, Late Paleozoic sea levels and depositional sequences, in Ross, C. A., and Haman, D. eds., Timing and depositional history of eustatic sequences, constraints on seismic stratigraphy: Cushman Foundation for Foraminiferal Research, Special Publication 24, p. 137–149.
- Ruppel, S. C., and Cander, H. S., 1988, Effects of facies and diagenesis on reservoir heterogeneity: Emma San Andres field, West Texas: The University of Texas at Austin, Bureau of Economic Geology Report of Investigations No. 178, 67 p.
- Ryer, T. A., 1981a, Deltaic coals of Ferron Sandstone Member of Mancos Shale—predictive model for Cretaceous coal-bearing strata of western interior: American Association of Petroleum Geologists Bulletin, v. 65, no. 11, p. 2323–2340.
- \_\_\_\_\_ 1981b, The Muddy and Quitcupah Projects—a project report with descriptions of cores of the I, J, and C coal beds from the Emery coal field, central Utah: U.S. Geological Survey Open-File Report 81-460, 34 p.
- \_\_\_\_\_ 1982, Possible eustatic control on the location of Utah Cretaceous coal fields: Utah Geological and Mineralogical Survey, Bulletin 118, Proceedings, 5th ROMOCO Symposium, p. 89–93.

- \_\_\_\_\_ 1983, Transgressive-regressive cycles and the occurrence of coal in some Upper Cretaceous strata of Utah: *Geology*, v. 11, p. 207–210.
- Sarg, J. F., 1986, Facies and stratigraphy of upper San Andres basin margin and lower Grayburg inner shelf, *in* Moore, G. E., and Wilde, G. L., eds., Lower and middle Guadalupian facies, stratigraphy and reservoir geometries, San Andres-Grayburg Formations, Guadalupe Mountains, New Mexico and Texas: Society of Economic Paleontologists and Mineralogists, Permian Basin Section, Publication No. 86-25, p. 83–93.
- Sarg, J. F., and Lehmann, P. J., 1986, Lower-middle Guadalupian facies and stratigraphy, San Andres-Grayburg formations, Permian Basin, Guadalupe Mountains, New Mexico, *in* Moore, G. E., and Wilde, G. L., eds., Lower and middle Guadalupian facies, stratigraphy and reservoir geometries, San Andres-Grayburg Formations, Guadalupe Mountains, New Mexico and Texas: Society of Economic Paleontologists and Mineralogists, Permian Basin Section, Publication No. 86-25, p. 1–36.
- Senger, R. K., Lucia, F. J., Kerans, Charles, Ferris, M. A., and Fogg, G. E., 1991, Dominant control on reservoir-flow behavior in carbonate reservoirs as determined from outcrop studies (preprint 3RC-58) *in* Burchfield, T. E., and Wesson, T. C., chairpersons, Proceedings, Third International Reservoir Characterization Technical Conference (preprints), IIT Research Institute, National Institute for Petroleum and Energy Research, and U.S. Department of Energy, v. 1, unpaginated.
- Sharma, D., Honarpour, M. M., Jackson, S. R., Schatzinger, R., and Tomutsa, L., 1989, Determining the productivity of a barrier island sandstone deposit from integrated facies analysis based on log and core data and fluid production: SPE Paper 19584, p. 133–148.
- Shinn, E. A., and Robbin, D. M., 1983, Mechanical and chemical compaction in fine-grained shallow-water limestones: *Journal of Sedimentary Petrology*, v. 53, no. 2, p. 595–618.

- Skinner, J. W., 1946, Correlation of Permian of West Texas and southeastern New Mexico: American Association of Petroleum Geologists Bulletin, v. 30, no. 11, p. 1857-1874.
- Smith, R.V., 1983, Practical natural gas engineering: Tulsa, Oklahoma, PennWell Publishing Company, 252 p.
- Sonnenfeld, M. D., 1991, High-frequency cyclicity within shelf-margin and slope strata of the upper San Andres sequence, Last Chance Canyon, *in* Meader-Roberts, Sally, Candelaria, M. P., and Moore, G. E., eds., Sequence stratigraphy, facies and reservoir geometries of the San Andres, Grayburg, and Queen Formations, Guadalupe Mountains, New Mexico and Texas: Permian Basin Section, Society of Economic Paleontologists and Mineralogists, Publication 91-32, p. 11-51.
- Stalkup, F. I., and Ebanks, W. J., Jr., 1986, Permeability variation in a sandstone barrier island-tidal delta complex, Ferron Sandstone (Lower Cretaceous), central Utah: Society of Petroleum Engineers, SPE Paper 15532, p. 1-8.
- Tait, D. B., Ahlen, J. L., Gordon, A., Scott, G. L., Motts, W. S., and Spitler, M. E., 1962, Artesia group of New Mexico and West Texas: American Association of Petroleum Geologists Bulletin, v. 46, no. 4, p. 504-517.
- Tye, E. N., 1986, Stratigraphy and formation of tepee structures in the Guadalupian Grayburg Formation, southeast New Mexico, *in* Moore, G. E., and Wilde, G. L., eds., Lower and Middle Guadalupian facies, stratigraphy and reservoir geometries, San Andres-Grayburg Formations, Guadalupe Mountains, New Mexico and Texas: Society of Economic Paleontologists and Mineralogists, Permian Basin Section, Publication No. 86-25, p. 95-105.
- Tyler, Noel, and Ambrose, W. A., 1986, Depositional systems and oil and gas plays in the Cretaceous Olmos Formation, South Texas: The University of Texas at Austin, Bureau of Economic Geology, Report of Investigations No. 152, 42 p.

- Tyler, Noel, and Banta, N. J., 1989, Oil and gas resources remaining in the Permian Basin: targets for additional hydrocarbon recovery: The University of Texas at Austin, Bureau of Economic Geology Geological Circular 89-4, 20 p.
- Tyler, Noel, Barton, M. D., and Finley, R. J., 1991, Outcrop characterization of flow unit and seal properties and geometries, Ferron Sandstone, Utah: Society of Petroleum Engineers, SPE Paper 22670, p. 127–134.
- Tyler, Noel, and Finley, R. J., 1991, Architectural controls on the recovery of hydrocarbons from sandstone reservoirs, *in* Miall, A. D., and Tyler, Noel, eds., The three-dimensional facies architecture of terrigenous clastic sediments and its implications for hydrocarbon discovery and recovery: Society of Economic Paleontologists and Mineralogists (Society for Sedimentary Geology), *Concepts in Sedimentology and Paleontology*, v. 3, p. 1–5.
- Tyler, Noel, Galloway, W. E., Garrett, C. M., Jr., and Ewing, T. E., 1984, Oil accumulation, production characteristics, and targets for additional recovery in major oil reservoirs of Texas: The University of Texas at Austin, Bureau of Economic Geology Geological Circular 84-2, 31 p.
- Tyler, Noel, Holtz, M. H., Garrett, C. M., and White, W. G., 1990, Atlas of major Texas oil reservoirs data base: The University of Texas at Austin, Bureau of Economic Geology, 1 disk.
- U.S. Department of Energy, Energy Information Administration, 1989, Annual report, U.S. crude oil, natural gas, and natural gas liquid reserves: Washington, D.C., U.S. Government Printing office, DOE/EIA.
- Vail, P. R., 1987, Seismic stratigraphy interpretation using sequence stratigraphy. Part 1: seismic stratigraphy interpretation procedure, *in* Bally, A. W., ed., Atlas of seismic stratigraphy, v. 1: American Association of Petroleum Geologists studies in Geology 27, p. 1–10.

- Van Wagoner, J. C., 1985, Reservoir facies distribution as controlled by sea-level change (abs.): Society of Economic Paleontologists and Mineralogists, midyear meeting, p. 91-92.
- Van Wagoner, J. C., Mitchum, R. M., Campion, K. M., and Rahmanian, V. D., 1990, Siliciclastic sequence stratigraphy in well logs, cores, and outcrops: American Association of Petroleum Geologists, Methods in Exploration Series, No. 7, 55 p.
- Van Wagoner, J. C., Posamentier, H. W., Mitchum, R. M., Jr., Vail, P. R., Sarg, J. F., Loutit, T. S., and Hardenbol, J., 1988, An overview of the fundamentals of sequence stratigraphy and key definitions, *in* Wilgus, C. K., Hastings, B. S., Kendall, C. G. St. C., Posamentier, H. W., Ross, C. A., and Van Wagoner, J. C., eds., Sea-level changes: an integrated approach: Society of Economic Paleontologists and Mineralogists, Special Publication No. 42, p. 39-46.
- Wagner, P. D., and Matthews, R. K., 1982, Porosity preservation in the upper Smackover (Jurassic) carbonate grainstone, Walker Creek field, Arkansas: response of paleophreatic lenses to burial processes: *Journal of Sedimentary Petrology*, v. 52, no. 1, p. 3-18.
- Wanless, H. R., 1979, Limestone response to stress: pressure solution and dolomitization: *Journal of Sedimentary Petrology*, v. 49, no. 2, p. 437-462.
- Ward, R. F., Kendall, C. G. St. C., and Harris, P. M., 1986, Upper Permian (Guadalupian) facies and their association with hydrocarbons—Permian Basin, West Texas and New Mexico: *American Association of Petroleum Geologists*, v. 70, p. 239-262.
- Weber, K. J., 1982, Influence of common sedimentary structures on fluid flow in reservoir models: *Journal of Petroleum Technology*, March, p. 665-672.

\*U.S.GPO:1992-661-026/60053

